# ADVANCED TECHNIQUES FOR THE IMPROVEMENT OF OPTICAL TRANSMISSION SYSTEMS

NEIL JOSEPH MURRAY

Doctor of Philosophy

ASTON UNIVERSITY

April 2014

Aston University

# Advanced Techniques for the Improvement of Optical Transmission Systems

Neil Joseph Murray
Doctor of Philosophy

April 2014

## Summary

This thesis presents the experimental investigation into two novel techniques which can be incorporated into current optical systems. These techniques have the capability to improve the performance of transmission and the recovery of the transmitted signal at the receiver. The experimental objectives are described and the results for each technique are presented in two sections:

The first experimental section is on work related to Ultra-long Raman Fibre lasers (ULRFLs). The fibre lasers have become an important research topic in recent years due to the significant improvement they give over lumped Raman amplification and their potential use in the development of system with large bandwidths and very low losses. The experiments involved the use of ASK and DPSK modulation types over a distance of 240km and DPSK over a distance of 320km. These results are compared to the current state-of-the-art and against other types of ultra-long transmission amplification techniques.

The second technique investigated involves asymmetrical, or offset, filtering. This technique is important because it deals with the strong filtering regimes that are a part of optical systems and networks in modern high-speed communications. It allows the improvement of the received signal by offsetting the central frequency of a filter after the output of a Delay Line Interferometer (DLI), which induces significant improvement in BER and/or Q-values at the receiver and therefore an increase in signal quality.

The experimental results are then concluded against the objectives of the experimental work and potential future work discussed.

**Keywords:** asymmetric filtering, nonlinear optics, Raman amplification, offset filtering, ultra-long Raman fibre laser

# Acknowledgements

I would like to express my thanks and gratitude to members of the Aston Institute of Photonic Technologies for their advice, help and guidance with my study towards a PhD degree, with special thanks to Dr Paul Harper whose support, direction and knowledge has been invaluable during my time carrying out research at AIPT.

I would also like to thank those who have helped me with my work and given me advice within the laboratory, namely Dr Atalla El-Taher, Dr Mercedes Alcon Camas, Dr Hua Wang, and Lee Barker; all of whom were more like friends than just colleagues.

I would like to separately acknowledge and thank Dr Olugbenga Olubodun for the use of his offset filtering simulations in this thesis.

I acknowledge my co-authors Dr Paul Harper, Dr Olugbenga Olubodun, Prof Nick Doran, Pawel Rosa and Dr Juan Diego Ania-Castanon.

Finally I thank my parents for their on-going encouragement, love, motivation and support at all times during my research and in everything beyond.

# Contents

# List of Figures

# List of Tables

# Abbreviations

| | |
|---|---|
| AMI | Alternate Mark Inversion |
| ASE | Amplified Spontaneous Emission |
| ASK | Amplitude Shift Keying |
| AWG | Arrayed Waveguide Gratings |
| BER | Bit Error Rate |
| BPG | Bit Pattern Generator |
| BW | Bandwidth |
| CSRZ | Carrier Suppressed Return to Zero |
| CW | Continuous Wave |
| DB | Duo-binary |
| DC | Direct current |
| DCF | Dispersion Compensated Fibre |
| DEMUX | Demultiplexer |
| DFB | Distributed Feedback Laser |
| DLI | Delay Line Interferometer |
| DPSK | Differential Phase Shift Keying |
| DRBS | Double Rayleigh Backscattering |
| DSF | Dispersion Sifted Fibre |
| DSP | Digital Signal Processor/Processing |
| EDFA | Erbium Doped Fibre Amplifier |
| ESA | Electrical Spectrum Analyser |
| FBG | Fibre Bragg Grating |
| FEC | Forward Error Correction |
| FPL | Fabry-Perot Laser |

| | |
|---|---|
| FSR | Free Spectral Range |
| FWM | Four Wave Mixing |
| IF | Intermediate Frequency |
| LEAF | Large Effective Area Fibre |
| LO | Local Oscillator |
| MUX | Multiplexer |
| MZI | Mach-Zehnder Interferometer |
| NRZ | None Return to Zero |
| NZDSF | None-Zero Dispersion Shifted Fibre |
| OADM | Optical Add-Drop Multiplexers |
| OOK | On-Off Keying |
| OBPF | Optical Bandpass Filter |
| OSA | Optical Spectrum Analyser |
| OSNR | Optical Signal-to-Noise Ratio |
| OTDM | Optical Time Division Multiplexing |
| OTDR | Optical Time Domain Reflectometer |
| OXC | Optical Cross-connects |
| PC | Polarisation Controllers |
| PG | Pattern Generator |
| PMD | Polarisation Mode Dispersion |
| PRBS | Pseudorandom Binary Sequence |
| PSK | Phase Shift Keying |
| Q(D)PSK | Quadrature (Differential) Phase Shift Keying |
| RFL | Raman Fibre Laser |
| RF | Radio Frequency |
| RIN | Random Intensity Noise |

| | |
|---|---|
| ROPA | Remote Optically Pumped Amplifier |
| RZ | Return to Zero |
| SBS | Stimulated Brillouin Scattering |
| SDH | Synchronous Data Hierarchy |
| SMF | Single Mode Fibre |
| SPM | Self-Phase Modulation |
| SRS | Stimulated Raman Scattering |
| TDCM | Tuneable Dispersion Compensation Module |
| ULLF | Ultra Low Loss Fibre |
| ULRFL | Ultra Long Raman Fibre Laser |
| WDM | Wavelength Division Multiplexing |
| WSS | Wavelength Selective Switch |
| XPM | Cross-Phase Modulation |

# Chapter 1

# Introduction

## 1.1. Introduction

In today's world of readily increasing demand for the transmission of large amounts of data at high-speed, optical communications has become the backbone of the infrastructure of a highly connected global community. With an increase in the use of cloud computing networks to store the data of millions of individuals and companies, along with heavy usage services such as video and TV streaming services on the rise, the push for higher data rates and larger bandwidths is consequential, but also improved data quality has become imperative.

When optical fibre was first considered for data transmission it had very high loss and the light sources which were used, such as LEDs, had very broad-linewidths, this meant that the distance the light could travel before being absorbed was only a few kilometres.
With the invention of the laser by Theodore Maiman [1], plus significant enhancements by Don F. Nelson and Willard S. Boyle at Bell laboratories [2], and further significant improvements led by Charles K Kao in optical waveguides and the manufacture and design of optical fibres, for which he won the Nobel Prize for Physics in 2009 [3, 4]; led to an upsurge in the late 1960s and early 1970s into how light travelling through an optical fibre could be successfully used and commercialised [5].

One of the first commercial silica fibres was SMF-28 by Corning, which gave an attenuation of 0.2dB/km. There are now a range of different fibres, from low absorption fibre to those with large effective areas (LEAF and TW) [6, 7, 8, 9, 10].

Later developments came within the area of optical amplifiers with the invention of Erbium-doped Fibre Amplifiers (EDFAs) [11], which meant low loss and low noise optical transmission was available and would lead to an increase in the lengths light could be transmitted.

Raman amplification is based on Raman scattering, a type of inelastic radiative effect discovered by Sir Chandrasekhara V. Rāman and Sir Kariamanickam S. Krishnan in liquids [12], and by Grigory Landsberg and Leonid Mandelstam in crystals [13]; both discoveries were in 1928. This effect allows the amplification of light over long distances without the need for repeatered sections, although Raman amplifiers can be used to reduce the number of repeatered sections, as it allows almost lossless transmission up to 250km [14, 15], where EDFA is repeatered typically every 70km [16].

One of the major constraints for ultra-long haul transmission is cost. To build or replace transmission network infrastructure is very costly, so it is intended that these networks, once built, can be used for many decades. With the need for high data rates and larger bandwidth requirements some of the older systems cannot cope and will need replacing, but a lot of these are of a repeatered design [16, 17], which means there are amplifier sections stationed every few kilometres within the transmission network.

In more modern transmission spans unrepeatered techniques can be used. Examples of this are remote optically pumped amplifiers (ROPA) which are mainly based on Erbium-doped Silica fibres [18, 19, 20, 21, 22, 23, 24, 25], but techniques using Raman are increasingly being considered as they do not require specially doped fibre but can use normal silica fibres such as SMF-28. These techniques can be used in either repeatered or unrepeatered transmission designs.

Ultra-long Raman fibre lasers are a good example of an amplification method with relatively low loss, flat gain, and low power difference over the transmission span [26, 14, 15, 27, 28, 29, 30, 31].

In submarine spans repeatered techniques are still used; this is due to the extremely long distances needed for intercontinental communications, and the fact that fibre passes through a medium that is very difficult to access i.e. at oceanic depths [16], so reliable tried and tested technology is required.

## 1.2. Thesis Overview

This thesis explores the following specific areas: The first area to be explored was the potential improvements within long-haul transmission by using Raman amplification techniques. The second area explored was to confirm simulated improvements at the receiver using offset filtering in DPSK modulated signals. By using specific types of Raman amplification, in this case ultra-long Raman fibre lasers, a comparison with the current state-of-the-art can be made to find which technique gives the best overall improvement. This comparison is made with EDFA as well as with other Raman amplification techniques, plus the difference between repeatered and unrepeatered amplification.
Offset filtering improvements depend on the configuration and the number of filters, as the strongly filtered regime is in effect a cascade of devices that have filtering effects on the signal. Using DPSK requires a Delay Line Interferometer (DLI) and it is the effect on the outputs from this device, by using filters, which is investigated.

This thesis contains the following chapters:

- Chapter 1 is a general introduction to the topic of optical systems and states the objectives of the experimental work within this thesis.

- Chapter 2 gives background information on optical systems, including optical fibres, optical noise mechanisms, linear effects such as dispersion, non-linear effects such as SPM, XPM, FWM, Rayleigh scattering, Brillouin scattering and Raman scattering. Also discussed are transmitter and receiver types and their advantages and disadvantages along with amplification techniques; for instance EDFA and Raman amplification. Different modulation techniques are also considered.

- Chapter 3 is an experimental chapter with more specific background on ultra-long transmission using Raman amplification, specifically ultra-long Raman fibre lasers (ULRFL), with comparisons against lumped Raman amplification and other amplification techniques. The experimental results and conclusions are contained after the discussion.

- Chapter 4 is mainly an experimental chapter, with a small amount of background on offset filtering and it's applications in optical systems. The experiments consist of placing filters in different combinations to compare with previously simulated results [32]. The results of the different experimental configurations are then summarised and concluded.

- Chapter 5 is the culmination of the thesis and is where the overall conclusions, based on the experimental results, are given and compared to the initial objectives of the thesis.

My contribution to the state of the art consist of setting up the dispersion compensation for use with the ULRFL experiment; altering the time delays between the different photodiodes used for balanced receiving; splicing together of the Raman fibre spans used in the experiments; the characterisation of the pre and post compensation amplifiers for 240km and 320km distances, and the recording of BER measurements for the 240km distance for ASK and DPSK modulation types.

For the offset filtering, my contribution was the setup of the experiments, making the correct length of fibre for the delay between the Constructive and Destructive ports, adjusting the losses so that both filters had the same loss, measuring the BER with respect to offset wavelengths and making sure the measurements were optimised. The recording of all measurements relating to the process of offset filtering using the DLI and the Waveshaper, and the analysis of those results.

# Chapter 2

# Optical Communication Systems

## 2.1. Introduction to Optical Systems

Optical systems are simply those systems which deploy light to transmit data in comparison to electrical or RF systems which use RF frequencies to do the same.

A typical optical system uses many connections to route transmitted signals to their expected receive points. These systems consist of components such as Optical Crossconnects (OXC) for wavelength switching, Add/Drop Multiplexers, Filters and Regenerators.

OXC's allow the coupling of signals to different paths; this is usually via different wavelengths being switched. Most OXC's consist of an Arrayed Waveguide Grating (AWG) which conjugates multiple wavelengths together or separates them, these are also known as wavelength cross-connects or WXC's. These can either be static or dynamic; the difference being that dynamic WXC has optical switches between the multiplexer and the demultiplexer [33].

Multiplexers are a major part of optical networks and are used to switch between 2 or more inputs or outputs thus allowing multiple signals to be passed through a system, demultiplexers do exactly the opposite. Alternatively multiplexers can be used as a type of wavelength switching device, and are used in the modulation of signals for Wavelength Division Multiplexing (WDM) as well as Time Division Multiplexing (TDM). They can also be used in a filtering device as they will reject some wavelengths but not others, they also help in equalising the gain from optical amplifiers and filtering out noise and this is what we are simulating in the experimental setups.

There are different kinds of multiplexer; most common are Wavelength Add/Drop Multiplexers, they are used to change the bit-rate of the incoming signals to a higher or lower bit-rate, depending on what is required [34]. An example of the above devices in a network is shown in Figure 2.1.1.

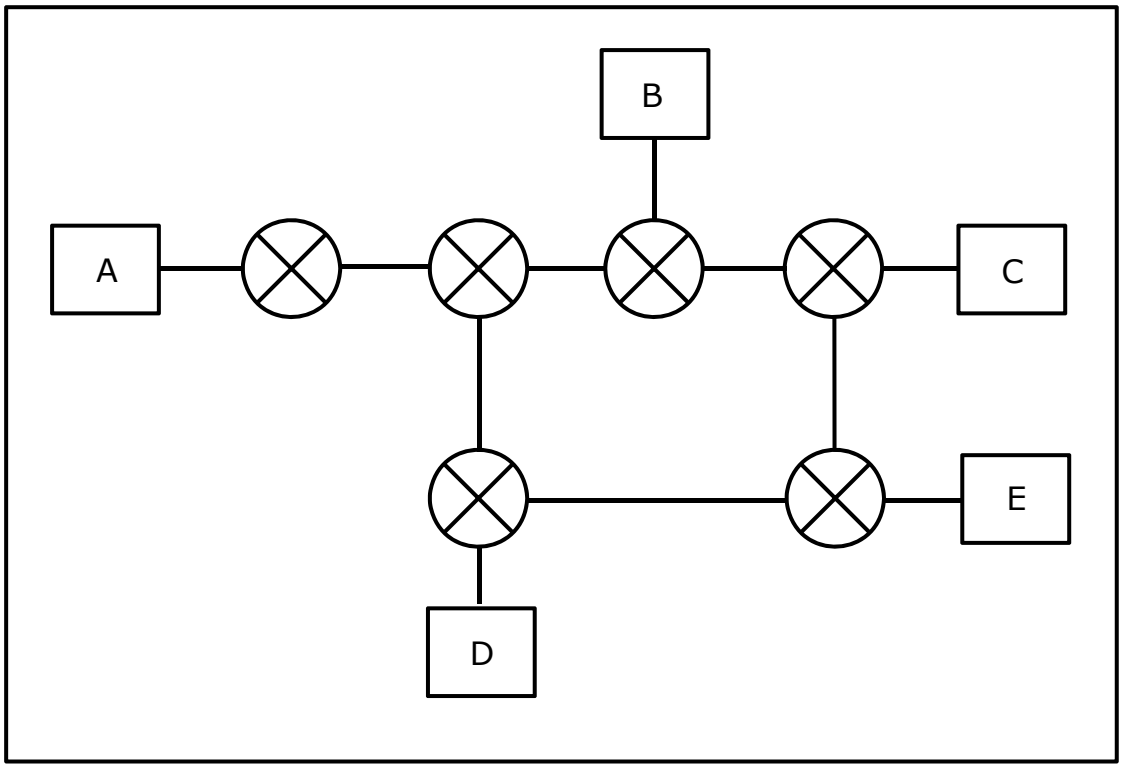


*Figure 2.1.1 – Typical network with Optical Cross-connects (OXCs) and Optical Add-Drop Multiplexers (OADMs) and connecting Fibres.*

There are many different techniques that allow signals to be regenerated purely by optical means without using techniques involving electrical-optical-electrical conversion. The main types of repeatered techniques are in the realm of using amplification with a physical presence in the network such as EDFA's and Hybrid MZI's, the latter use Silicon Optical Amplifiers (SOAs) in their design. The Unrepeatered fibre techniques use a number of amplification technologies; some have laser sources based just after the transmitter and/or just before the receiver in the network, such as with Raman amplification, whilst others use doped fibre within the transmission span. Unrepeatered amplification based on Raman scattering is also used to create a Supercontinuum, which is a flat gain broadband technique that is useful for WDM signals.

Some unrepeatered techniques involve the use of a piece of Erbium-doped fibre, called a ROPA (Remote Optically Pumped Amplifier), which is placed around 100km from the receiver to boost the signal [25, 35]. This process involves sending a pump laser with a wavelength around 1480nm from the receive end of the transmission span. The 1480nm laser pumps the ROPA in a counter-propagating direction when compared to the direction the signal is travelling in the fibre. The use of 1480nm as the pump wavelength rather than 980nm is due to 1480nm having a lower loss when travelling through silica fibres, and the availability of lasers at this wavelength with higher output powers when compared to 980nm pumps. These advantages outweigh the issues of 1480nm pumps being less efficient and generating more noise comparative to 980nm pumps. Although ROPA is a successful technique, it involves the addition of Erbium Doped Fibre (EDF) within the transmission fibre span, which adds costs to the network. More on EDFAs can be found in Section 2.6.

A list of recent unrepeatered experiments is shown in [17], while an example of an Erbium-Doped Fibre (EDF) Repeatered experiment is summarised in [25]. A review of the current literature on repeatered and unrepeatered transmission can be found in Chapter 3 Section 3.1.

The design of the receiver is important; these can be either of Coherent or Direct-Detection design. The Coherent receiver is much more complex as it needs information relating to the modulation format being used, as with phase or frequency modulations where the phase or frequency needs to be known at the receiver so the signal can be demodulated. Polarisation, phase and frequency tracking are usually used so the receiver can identify how to correctly demodulate the signal. For Direct-Detection the receivers are much simpler, not needing any prior information for demodulation they can use purely optical means, such as Mach-Zehnder Interferometers and photodiodes.

This does mean that in general these types of receiver are less sensitive as the information about the signal is unknown and ambiguous, so polarisation and phase will not be known. It also means that the transmitter and transmission span need to be controlled in the way they affect the phase and polarisation as

it emerges and then travels down the fibre, as any changes may corrupt the data and effect the received signal. Optical noise such as ASE is not filtered out automatically, as with Coherent designs, as the Coherent receiver mixes the signal with a Local Oscillator (LO) which reduces the effect of optical noise [36, 37]. More on these types of receiver can be found in Section 2.5.

Special fibres can also be used, such as True Wave (TW), Large Effective Area Fibre (LEAF), both types of Non-Zero Dispersion Shifted Fibres (NZDSF), and Ultra-Low Loss (ULL) fibres, but using these means replacing current network infrastructure and therefore adds cost [33]. For more information on these types of fibres see Section 2.2.

Electrical dispersion compensators are also used; these can be placed before or after transmission spans to create pre or post-compensation for known chromatic dispersion. An Electrical dispersion compensator was used in some of the experiments presented in this thesis and compared with dispersion compensation using fibre [36]. The results and analysis relating to this can be found in Section 3.4 and Dispersion management can be found in Section 2.7.1.1.

Modulation is also a key issue in optical communication systems, as the modulation chosen will depend on many factors, such as how many WDM channels are used, how much data needs to be sent, the quality of the resulting signal and the complexity of the transmitter and receiver. Common types are On-Off Keying (OOK), which is the simplest type of Amplitude Shift Keying (ASK), Phase Shift Keying (PSK), Differential Phase Shift Keying (DPSK) and Differential Quadrature Phase Shift Keying DQPSK. More on Modulation can be found in Section 2.4.2.

Linear and Non-linear impairments are major issues in optical communication. Linear effects are those such as Dispersion, which broadens optical pulses in time as they travel through the fibre; see Section 2.7. For Non-Linear impairments such as Brillouin Scattering and Rayleigh scattering, which reduce the signal quality and power, will be discussed in Section 2.8.

## 2.2. Optical Fibre Types

The most common optical fibre in use in optical fibre networks and transmission spans is SMF-28 which is a single mode fibre that has been around commercially since the 1970s. It has become ubiquitous due to its cost per km and fairly low loss of 0.2dB/km. Although Single Mode Fibres (SMFs) were around prior to Multi-Mode fibres, MMFs have larger Numerical Aperture (NA) and so can couple more light, this was important when using LED light sources where it was difficult for the diffuse light to couple into SMFs with their low NA. When semiconductor lasers were invented this marked a sea-change as it was now easier to couple light into SMFs, so their higher bandwidth and use at longer wavelengths could be taken advantage of. Since then however SMF has been increasingly used in many applications, especially long-haul applications. MMFs are still used for low power short-links. Other advantages of SMF over MMF include smaller loss per km and attenuation consistency, as MMFs loss depends on the mode profiles travelling through the fibre, plus dispersion is a major issue which precludes its use at longer lengths [7]. Although SMF-28 is the main fibre type in use today, there are many other types that have important advantages, as well as disadvantages, when comparisons are made.

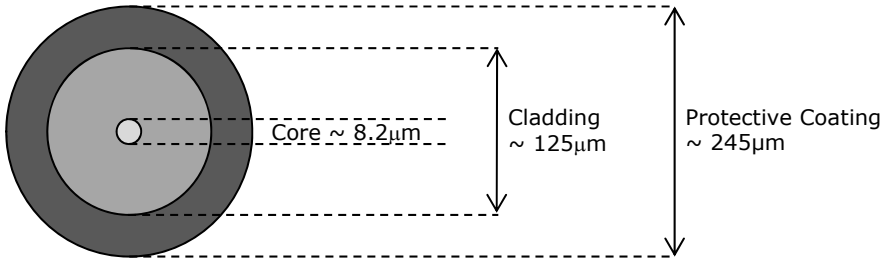


*Figure 2.2.1 – Typical structure of an SMF-28 optical fibre.*

Large Effective Area Fibre (LEAF) and True-Wave (TW) fibres are types of Non-Zero Dispersion Shifted Fibre (NZDSF).

Due to the $\frac{1}{\propto}$ relationship larger $A_{eff}$ has with non-linearities, where $\propto$ is the fibre loss, the $A_{eff}$ for NZDSF can be smaller than for SMF-28 type fibres; this is due to balancing the reduction in dispersion, a linear effect, with non-

linearities, as fibres with larger $A_{eff}$ suffer from an increase in dispersion while the non-linearities are decreased.
The larger effective area of the fibre core means that LEAF has an advantage over SMF-28, but in practice this balancing effect depends on the wavelength of light passing through the fibre, as there is some wavelength dependency for both dispersion and non-linear effects which can reduce this advantage [6, 7, 33, 38, 39, 40, 41].

NZDSF were designed to minimise Four-Wave Mixing (FWM) (see Section 2.8.3), as FWM occurred when the dispersion in the fibre was at zero. It made sense to create a fibre where the dispersion was non-zero to minimise FWM, this also minimises other non-linear effects, but the dispersion inherent in the fibre must be small so as not to significantly increase the overall dispersion in a system; typically the dispersion figure is somewhere between 3ps/km/nm and 8ps/km/nm [7] of either normal or anomalous dispersion, with the zero dispersion wavelength outside of the EDFA bandwidth.

NZDSF can also be useful in pre-chirping a signal before transmission, or post-chirping before a signal reaches a receiver, and therefore correcting the known amount of dispersion either before or after transmission.

In summary, the design of LEAF gives an advantage over fibre such as SMF-28 by allowing more light into the fibre core because its acceptance angle is larger, this means the loss can be reduced and the effects from non-linearities are smaller when the signal power is high [42]. The reduction in the effect of non-linearities which occurs in LEAF is due to a larger effective area having an inversely proportional relationship with non-linear regimes [7]. A disadvantage is the increase in chromatic dispersion, which although small can build up over ultra-long distances. When used with distributed Raman Amplification LEAF reduces the efficiency as it is based on non-linear effects [1].

Ultra-Low Loss (ULL) fibres are fibres made to produce very low attenuation over long distances by doping to supress Rayleigh scattering (see Section 2.6), for example Corning SMF-28 ULL fibre and Sumitomo Pure Advance SE-12 fibre both have an attenuation of 0.18dB/km [8, 43], while the Corning

Vascade EX2000 has an attenuation factor of 0.16dB/km [9] and the Sumitomo Z-Fiber has an attenuation factor of 0.17dB/km [10]; both of these fibres are suitable for submarine transmission spans. There are lower attenuation fibres but they are usually specifically made to order and can reach as low as 0.1484dB/km (at 1570nm) [7].

ULL fibres are usually low attenuation versions of SMF-28, NZDSF or LEAF, so you have the advantages those types of fibre bring, along with low loss [8, 9, 43].

## 2.3. Optical Loss and Noise Mechanisms

Two major issues for long and ultra-long transmission are loss and noise. An example of loss is in a silica optical fibre where signal attenuation occurs at approximately 0.2dB/km. This loss is due to the absorption of light within the fibre and the refracting of light from the core and into the cladding, where most of it is either totally refracted out of the fibre or absorbed in the cladding. The loss, although small, can over thousands of kilometres have a significant impact on the transmitted signal and receive errors can be huge.

One of the regimes found to overcome this problem is using optical amplifiers to amplify the signal and increase the eventual receive power, the problem here is that whilst the signal is amplified so is the noise associated with the signal, and this adds up as each amplifier, as well as amplifying the original transmission noise, adds its own noise to the signal. The noise from amplifiers is known as Amplified Spontaneous Emission or ASE, and is discussed in more detail in Section 2.3.1.

Other types of noise that are important in optical systems are:

- Relative Intensity Noise transfer: RIN transfer is where the noise of the laser is transferred to the signal within the laser cavity. This is similar to Signal-Spontaneous Beating but occurs mainly in high power Raman

pumps. RIN transfer is a major issue in Raman amplification and is covered in more detail in Chapter 3 Section 3.3.

- Signal-Spontaneous Beating: This type of noise is caused by the mixing of the signal frequencies with frequencies that are contained within the noise caused by spontaneous emission; this creates a frequency difference of $\Delta f$ which is seen as additional noise at the output. Also the amount of ASE transferred is only half as the signal is polarised while the noise is not polarised at all.

- Spontaneous-Spontaneous Beating: this is the different noise frequencies within the ASE mixing with each other causing a frequency difference of $\Delta f$ which then interacts in the system as additional noise.

- Shot Noise: this is produced by the current created by the uneven flow of electrons caused by their random distribution within the gain medium, and the timing difference in the arrival of photons due to this distribution.

- Thermal Noise: this type of noise is caused by the vibration of electrons within the gain medium. This is similar to how molecules behave. As the temperature of the gain medium increases, the vibrations of the electrons intensify and therefore the noise increases. This type of noise is also known as Johnson or Nyquist noise.

There is also beat-noise relating to the beating of shot noise and the signal, and shot noise and ASE; this type of noise is small compared to the other signal and ASE beat noises considered previously, and can therefore generally be neglected when using laser sources and high gain amplifiers. Shot noise is a greater problem with LEDs and related light sources and low gain amplifiers due to their lower output powers. Thermal noise can also be an issue, but for temperature controlled lasers and amplifiers, for example those using a Thermo-Electric-Controller (TEC), it is usually relatively stable and it can be ignored.

The noise output from an amplifier such as an EDFA can be given by the following equations, assuming a narrow bandpass filter is used. If a filter is not used the optical bandwidth of the amplifier should be used instead and added as a term in the equations.

The output power of the amplifier with noise in Watts is:

$$\langle P_{out} \rangle = GP_s + P_{ASE} \qquad \text{Eq. 2.3.1}$$

Where $GP_s$ is the amplified signal and $P_{ASE}$ the ASE noise developed in the amplifier. Then the noise power can be written as:

$$P_{ASE} = 2\rho_{ASE}B_o \qquad \text{Eq. 2.3.2}$$

Where the term $\rho_{ASE}$ is the noise spectral density in a single polarisation and $B_o$ is the bandwidth of the narrow bandpass filter at the central wavelength of the signal. The ASE terms are made up of Shot noise, Signal-Spontaneous beating and Spontaneous-Spontaneous beating [44].

The signal-spontaneous beating is caused by the interference between the signal and ASE noise and is therefore additional to the ASE. As the signal light is polarised the ASE is not, thus the ASE only interferes with one polarisation of the signal-spontaneous beating, which means that only half of the ASE noise power will contribute to signal-spontaneous beating noise.
The spontaneous-spontaneous beating can be classed as the intensity noise of the ASE, and so, unlike signal-spontaneous beating, it is not an addition to ASE but a part of it. The separate noise terms can be calculated using the following.

The signal-spontaneous beating can be given by:

$$\sigma^2_{Sig-Spon} = 4r^2\, GP_s\rho_{ASE}B_e \qquad \text{Eq. 2.3.3}$$

Where $\sigma^2_{Sig-Spon}$ is the variance of the photocurrent due to the signal-spontaneous beating while $r$ is the responsivity and $B_e$ is the electrical bandwidth of the filter.

For the spontaneous-spontaneous beating we have:

$$\sigma^2_{Spon-Spon} = 2r^2\rho^2_{ASE}B_e(2B_o - B_e) \qquad \text{Eq. 2.3.4}$$

Where $\sigma^2_{Spon-Spon}$ is the again variance of the photo current due to the beating noise, this time spontaneous-spontaneous, all the other terms have been identified previously.

The output SNR can be calculated using the equation Eq. 2.3.5. The noise term takes into account only signal-spontaneous beat noise. Spontaneous-spontaneous and shot noise can usually be neglected due to the signal-spontaneous beat noise being much larger in magnitude.

Therefore it can be shown that:

$$SNR_{out} = \frac{(rGP_s)^2}{4r^2\,GP_s\rho_{ASE}B_e} \qquad \text{Eq. 2.3.5}$$

With $I = rGP_s$, Eq. 2.3.5 can simplify to:

$$SNR_{out} = \frac{I^2}{\sigma^2_{Sig-Spon}} \qquad \text{Eq. 2.3.6}$$

An example of how loss and noise in optical systems effects how they are transmitted and received is given here:

Amplifiers are placed at intervals along the transmission span, which is determined by the point at which any additional attenuation would make it very difficult for amplification to recover the OSNR sufficiently, as amplification of the noise floor occurs by the same amount as amplification of the signal. If the signal is at low levels then the ratio of signal to noise is much lower, hence lower OSNR, whilst if the signal is amplified at a higher power then the OSNR is much larger. There is a balancing point for when the OSNR is at its minimum and can still have the signal data recovered at the receiver without any errors. This states that the loss in the fibre plus the noise mechanisms such as ASE create a position that, if not managed, will make a signal become unrecoverable, hence why loss and noise management are important factors in optical systems [33, 40, 44, 45].

### 2.3.1. Amplified Spontaneous Emission (ASE)

Amplified Spontaneous Emission, or simply Spontaneous Emission, is the process where atoms drop energy states without any need for additional energy being available via electrical or optical means, but because it happens at random and the photons released travel in a multitude of different directions, it cannot be classed as amplifier gain. This means that ASE can be classed as "noise" in optical systems as it is a totally random process (see Section 2.6 for an explanation of stimulated emission in EDFAs and Section 3.2. in Raman Amplification).

Looking at it in more detail, we have different energy levels available for electrons to travel between. As an example there are 2 levels, $E_1$ and $E_2$, available for electrons to change between, so when an electron drops from $E_2$ to $E_1$ there is a photon released with the energy $hf_p$. The rate at which the electrons change between these levels is based on the Planck Hypothesis and is instantaneous; any time delay is due to other interactions occurring within the energy level or band, slowing the total emission/absorption process.

The population inversion is dependent on the number of atoms that have electrons at those levels and is defined by:

$$N_{sp} = N_{21} = \frac{N_2}{N_2 - N_1} \qquad \text{Eq. 2.3.7}$$

Where the electron densities are represented by $N_1$ and $N_2$, and the overall state of the population inversion is represented by $N_{sp}$ [45, 46, 47, 48].

Also the rate of spontaneous emission is the inverse of the spontaneous emission lifetime, so that:

$$N_{21} = \frac{1}{\tau_{21}} \qquad \text{Eq. 2.3.8}$$

From all of the previous equations it can be shown that the spontaneous emission is equal to $N_2/\tau_{21}$ and the power of the spontaneous emission is $hf_pN_2/\tau_{21}$.

The overall effect is an incoherent emission over a wide range of frequencies, which appears as noise at the output of the amplifier. An increase in the ASE from the amplifier is realised when the amplifier output power is increased and eventually reaches its saturation point. As the amplifier becomes saturated, the amount of ASE generated rises due to an escalation in the rate of wideband spontaneous emissions, which overtakes the production of narrowband stimulated emission by the light from the input signal; hence at this point ASE becomes almost self-generating and thus the ASE overwhelms the signal and the output from the amplifier is noisy. The overwhelming of the signal by ASE is represented by a lowering of the signal to noise ratio. This lowering of SNR can be mitigated by using filters and isolators to control the ASE [45, 46, 47, 48].

Another aspect of ASE is called ASE Beat Noise, which is made up of two separate components. These components are the beat noise between the signal frequency and the frequency of the ASE, and are known as the signal-ASE beat noise. Secondly there are the frequency components of the ASE acting against themselves; this is called the ASE-ASE beat noise. The signal-ASE beat noise is channel dependent, while the ASE-ASE beat noise is not. The beat noise itself is caused by minute vibrations between frequencies that are very close to each other, causing addition and subtraction to occur, in turn creating a "beat" between the frequencies [49].

## 2.4. Optical Transmitters

Optical transmitters turn information in the electrical domain into information in the optical domain using the manipulation of light. In general there are two main types of transmitter, those where the light is modulated within the laser, called internal or direct modulation, and those that use external modulation.

The direct modulation uses the input current to the laser itself to adjust the output power, above threshold, to indicate a 1 or a 0. This type of modulation is fine for simple modulation techniques such as On-Off Keying (OOK) and is cheaper, but it is limited for use with more complex modulation techniques. One exception to this is semiconductor lasers due to the material that they are made from. These can incorporate a modulator called a semiconductor electro-absorption (EA) modulator; this uses the Stark Effect to reduce the band gap within the modulator when an electrical field is present, thus allowing greater absorption of photons. This creates a compact transmitter which can be used up to fairly high transmit rate such as 10Gbps, at higher data rates external modulation becomes the better choice [33].

External modulation allows much more freedom as external modulator can change the amplitude, the phase, or the timing of the light pulses. These can be EA or, most usually, Lithium-Niobate ($LiNbO_3$) modulators. The Lithium-Niobate modulator use the electro-optic effect where the refractive index of the waveguides inside the modulator, which are made of lithium niobate crystal, can be altered by a voltage applied to the surface. They are usually based on thin-film technology. The designs of the Lithium Niobate modulator are based on a Mach-Zhender Interferometer which is more flexible when compared to an EA modulator, plus induces less chirp on the optical pulses [33].

### 2.4.1. ITU 100GHz and 50 GHz DWDM Grids

The ITU 50GHz and 100GHz Dense Wavelength Division Multiplex (DWDM) Grids are the standard channel spacing set by the International Telecommunications Union for all telecommunications across the globe [50].

A standardised set of channels is important as there is a need for the knowledge that a channel, for example Channel 27, is set at 1550.52nm in the C-Band in the 50GHz grid, or 1550.92nm in the 100GHz grid. If these channels are not adhered to then communication between continents would be impossible, as one country could use 1550.34nm whilst another might use

1550.62nm. This alone would create incompatibility, but it would also create problems when data from other countries using the grid tried to use a receiver from a non-compatible country, plus if data using grid Channels, and those that are not, are passed through a network, ISI and crosstalk would become a major problem possibly degrading data beyond recognition and thus undermining global communications. An ITU grid at 200GHz is also available.

### 2.4.2. Modulation Formats

There are a number of different modulation formats, the simplest being On-Off Keying (OOK) which is an example of Amplitude Shift Keying (ASK).

Firstly there are two ways of converting a train of electrical pulses by modulating the lightwave. These are Return-to-Zero or RZ and Non-Return-to-Zero or NRZ. These relate to the way the light is transformed from a Continuous Wave (CW) to a modulated one.

The NRZ is the simpler of the two as it only requires a single modulator to convert light to on or off over the bit slot of the clock rate being used, which is equal to 1 and 0 respectively and could be said to have a duty cycle of 100%, where the duty cycle is the percentage of the bit slot that is used during modulation. One disadvantage of using NRZ is when there is a train of 1's in a row they become a block where transitions between the bits is indistinguishable, this is the same with 0's; this can make it difficult to recover the clock rate. One of the advantages is that a much smaller bandwidth is occupied due to $f = \frac{1}{T}$ where a larger temporal pulse means a smaller spectral pulse and visa-versa.

RZ only uses part of the bit slot which is where the comparison to duty cycle comes in. NRZ can be said to have a duty cycle of 100% as it fills the bit slot, while RZ can have numerous different duty cycles which can be calculated by $\rho = \frac{T_{on}}{T_{on} - T_{off}}$, although the most common are 33%, 50% or 67%. This duty cycle is created by using a second modulator to alter the amount of time the light

occupies the bit slot. This is done by having a pulse carver which can be adjusted to provide the correct duty cycle.

Since RZ has a gap between pulses, i.e. the transitions between pulses can be seen, the clock rate can be recovered more easily, but the same issue as NRZ applies with a train of 0's. This also limits Inter-Symbol Interference (ISI) and it is therefore more of an issue with NRZ. A downside is that a higher peak power is required per bit for RZ than the equivalent NRZ pulse to keep the overall energy of the bit slot the same [33, 45].

An example of the differences between RZ and NRZ can be seen in Figure 2.4.1.

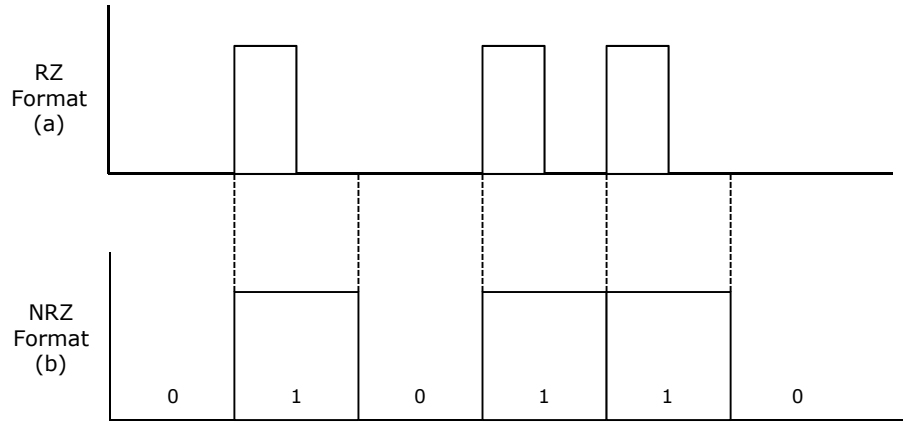


*Figure 2.4.1 – Diagram showing difference between RZ (a) and NRZ (b) formats.*

A summary of some of the most commonly used modulation formats are as follows:

- RZ: Return to Zero is where the pulse bit 1 occupies only a fraction of the bit period, this is usually a 50% duty cycle, but can be varied to other duty cycles such as 67% and 33%. The 0 bit is not represented by a pulse, but by the lack of one, so therefore the noise floor. One advantage is that it is easier to get a clock recovered due to the pulses not joining up, but this means a larger bandwidth, up to double compared to NRZ, and a higher peak power at the transmitter to maintain the same energy per bit as NRZ [33].
  Examples of RZ spectra can be seen in Figure 2.4.3 (b) and (d).

- NRZ: Non-Return to Zero is a format that uses the whole of the bit period for 1, and no pulse in the bit period for 0. The advantage here is the smaller Bandwidth used to transmit NRZ data, however, if the bit rate clock needs to be recovered it is very difficult to do without additional information, as a string of 1's or 0's means there are no pulse transitions for the clock recovery to latch on to [33].

- CSRZ: Carrier Supressed Return to Zero is the same as RZ, but the signal carrier is supressed, just leaving the sidebands with the data encoded in them.

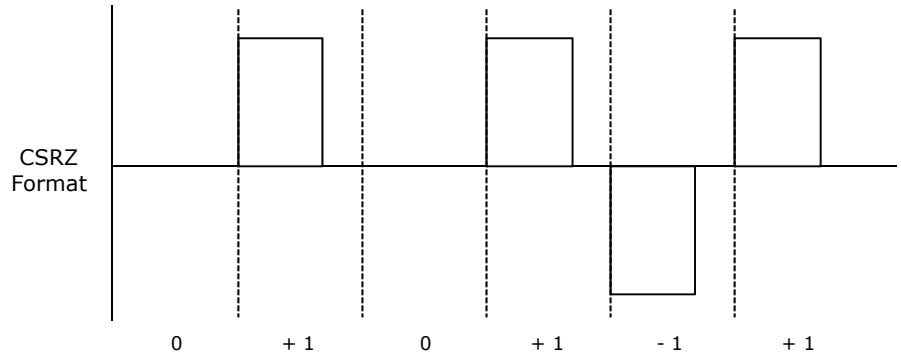


*Figure 2.4.2 – Diagram showing CSRZ modulation format.*

Due to the broad spectrum of CSRZ, caused by its generation using MZI and half-bit rates, the resultant effect on the temporal pulse is the same as having an RZ 67% duty cycle. The half-bit rates used in the generation of CSRZ cause the spectrum to show peaks at $\pm B_R/2$ from the centre of the spectrum, as shown in Figure 2.4.3 (b), which means there is no central peak present when compared to RZ [51].

CSRZ can be classed as a pseudo-multilevel modulation, which is a type of "memory modulation", which when the data is transmitted an additional bit is present, in this case the transmitted bits are +1, 0, -1, where 0 = 0 while +1 and -1 = 1. This is caused by using a MZM to modulate the signal, where the peak relating to 1 is seen alternately on each arm of the MZM, this in turn causes the resulting total phase to be 0 which cancels out the carrier, hence the name. The difference in the sign is a phase shift, but in the context of the transmitted data the phase information is not used, but as the phase stays the same it has

"memory". However, the additional symbol can be harnessed to improve the performance against non-linear impairments [51].

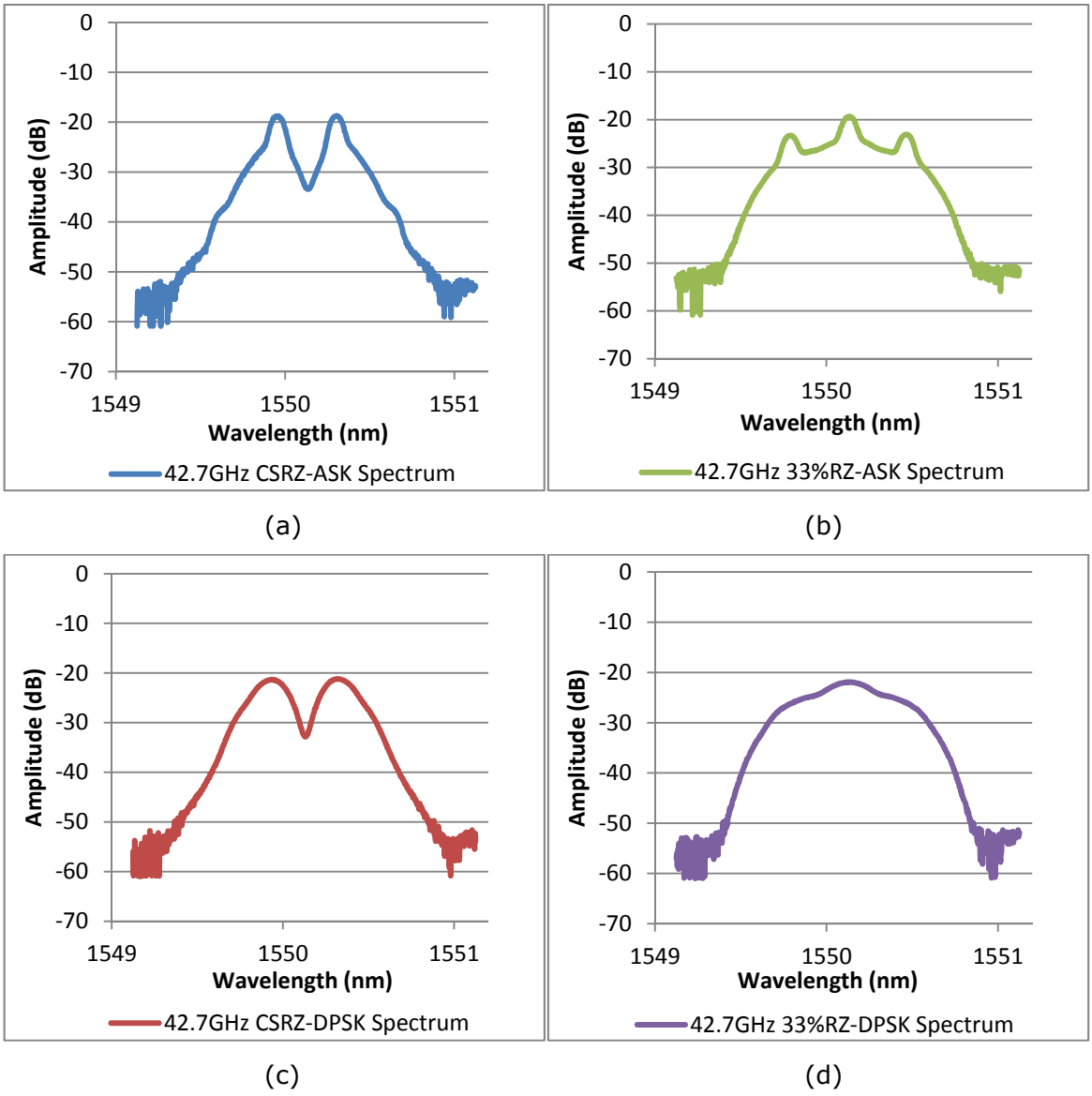


*Figure 2.4.3 – Graphs showing Spectral responses of (a) CSRZ-ASK, (b) 33%RZ-ASK, (c) CSRZ-DPSK and (d) RZ-DPSK formats.*

The phase shifts in CSRZ reduce the potential for Intersymbol Interference (ISI), and therefore the effects of dispersion; they also make the signal more robust to non-linear impairments as the π phase changes at every bit, reducing the potential of Self Phase Modulation (SPM) and Cross-Phase Modulation (XPM) through concurrent pulses interfering, i.e. destructive interference; this can also reduce Intrachannel Four-Wave Mixing (IFWM).

Examples of CSRZ spectra can be seen in Figure 2.4.3 (a) and (b).

- ASK: Amplitude shift keying, an example of which is On-Off Keying or OOK, is the simplest type of modulation, as it involves either turning the light source on or off, or using an external modulator to do the same thing [33]. Examples of ASK spectra can be seen in Figure 2.4.3 (a) and (b).

- PSK: Phase Shift Keying involves the use of the phase of the light source carrying information. An external phase modulator is driven by an electrical signal that uses the absolute phase to encode data, usually giving a phase of either $0^{o}$ or $180^{o}$. The biggest issue is that once the phase drifts off then it is difficult to retrieve and errors can occur [52].

- DPSK: Differential Phase Shift Keying, like PSK, uses phase to carry information. In this case it is the relative difference between the phases of two adjacent pulses, rather than absolute phase of a pulse that is encoded with information, for example 0 can equal $0^{o}$ and 1 can equal $90^{o}$ changes. This can only be carried out by coding an already created signal, such as an RZ pulse train, which is synchronised with the modulator to allow the phase information to be "added" to the RZ signal. This requires the data to be prepared at the transmitter by going through an XOR gate which has a feedback loop; hence a differential in the phase is created.

  For a receiver all that is needed is a MZI with a known delay in one of its arms; this allows simple demodulation of the phase information when the two outputs from the MZI are connected to a balanced receiver (see section 2.5). In effect this can double the useful data rate by doubling the number of symbols per bits, which means that the efficiency per bit increases compared to PSK, also using phase transitions means that it doesn't matter if the actual phase drifts off as long as the phase difference stays the same [52].
  Examples of DPSK spectra can be seen in Figure 2.4.3 (c) and (d).

- QPSK: Quadrature Phase Shift Keying is a level modulation technique which quadruples the amount of data one optical pulse can carry by the

way it is encoded, in this case 4 symbols per bit, where the change in the actual phase needs to be known. The downside to this is the same as PSK that if the phase isn't constant over the transmitted distance then errors will occur [52].

- DQPSK: Differential Quadrature Phase Shift Keying is similar to DPSK in that is uses transitions in phase rather than absolute. It uses 4-symbols instead of 2, but uses 2-bits to encode information rather than one as with DPSK. An example of using DQPSK is a simple 2 bit code, which would have 4 positions, 00, 01, 10, 11, which can be read as 0, 1, 2, 3. When these bits are encoded they can have 90$^{o}$ phase shifts for each bit, so 0$^{o}$, 90$^{o}$, 180$^{o}$, 270$^{o}$, so a change from 00 to 10 would equal a change of 180$^{o}$ in phase. As with DPSK, the information being encoded within the phase transitions rather than the absolute phase gives greater protection against errors [52].

- DB: Duobinary is a type of Correlative-Level Coding, which is in effect the process of creating ISI to get the correct data output. When coded DB uses a three level signal, 1, 0 and -1 of which 0 always has to follow 1 or -1, which leads to some resilience to dispersion.
  In this case DB is not generated but is a consequence of DPSK being used, as after demodulation the output from the DLI is DB. This occurs as the DLI is setup to introduce a 1 bit delay, in effect automatically converting any signal to DB. The downside is that if one error is transmitted, then that error cascades through the data until another error occurs. For these experiments it is only used just before the receiver to help create the building block for improved balanced receiving. It initially occurs on the Constructive port, but using offset filtering means it can be in effect transferred to the Destructive port [51, 53].

- AMI: Alternate Mark Inversion modulation format is a Line Code and is also known as BRZ or Bipolar Return to Zero modulation. As with DB, it uses three levels, except that positive and negative pulses are

recognised as 1, whilst no pulse is a 0 and so requires no additional encoding, but has a higher bandwidth requirement than DB.
In a DLI, or an MZI, this is the output usually seen on the Destructive Port, or alternative port to where the DB output is found [51, 53].

Modulation techniques using Amplitude are the simplest as it involves the laser being switched on or off, whilst this is effective it is limited by the optical noise build-up as well as dispersion. However those systems that use ASK with coherent receivers must use external modulation, as the phase still needs to be kept nearly the same even though it is not actually used to encode data [45]. Another advantage is it is cheap to create transmitters and receivers using this type of modulation.

Phase modulation is more complex in that the phase information has to stay unaltered as it travels through the fibre, which is a specific requirement for PSK, as the data is modulated using actual phase. The receiver must be coherent for PSK as the phase information would otherwise be lost. For Differential Phase modulation this is not the case, as it is changes in phase that need to be recovered, not the absolute phase. The changes in phase should be recognised at the receiver as long as the actual phase is stable over 2 bit slots [45]. The advantages are that they can be coded for use as multi-symbol modulation which increases the spectral efficiency per bit [33].

Details of some modulation formats which were used or involved in the Offset Filtering experiments can be found in Chapter 4 Section 4.4.

### 2.4.3. Forward Error Correction (FEC)

Forward Error Correction (FEC) is a type of coding used at the beginning of data to improve the error rate at the receiver.

There are two types of FEC, Hard-decision and Soft-decision; hard–decision FEC is where the error checking gives a probability and chooses either a 1 or a 0, while with soft-decision FEC gives an output that is a probability of the

original symbol plus a confidence level in that probability. This is given as a quantised code that usually has more levels than symbol values in the data stream, Soft-decision FEC can have a 1.5dB improvement on hard-decision, but the receivers are more complex [54, 55].

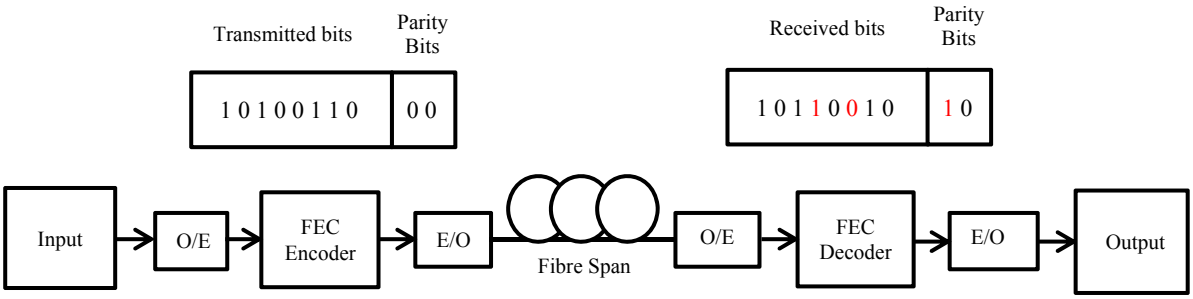


*Figure 2.4.4 – System with Forward Error Correction (FEC) coding showing bit errors in an (8,2) block code.*

An example of how FEC works is shown in Figure 2.4.2. An overhead of 2 bits is added to the data being sent, which when checked by the FEC decoder indicates errors in the data by flagging up one of the parity bits. If a block code is used such as in Figure 2.4.2, the FEC encoder adds *k* dummy check bits in front of the data bits which gives a total of *n* bits to construct an n-bit code-word, in this case k=2 bits and n=10 bits, therefore the *n-k* bits are 8. The parity bits indicate the checksum of the data which is encoded as 00, a 1 appearing in either parity bit indicates an error has been received.

The terms 1st generation, 2nd generation and 3rd generation refer to the data rate that the FEC will be used with; 2.5Gbps and above for 1st Generation which gives an improvement of 5.8dB for 7% overhead; 10Gbps and above for 2nd Generation which gives an improvement of 8dB for 7% overhead, but can give a 9.5dB improvement with a 20% overhead, although this can increase bandwidth significantly; 100Gbps and above for 3rd Generation can give 10dB+ improvement with a 20% overhead.

FEC does not continuously improve with ever higher overhead because with higher overheads the data rate has to be increased. An increase in errors could be caused in two ways; first by employing higher data rates which affects latency when receiving data, plus higher data rates usually mean an increase in the complexity of the transmitter and receiver, and therefore a rise in the potential for data errors.

The overhead for a specific data transmission is calculated using the ratio of the number of parity or check bits to the number of data bits. So for our example in Figure 2.4.2, this would be $R = k/n - k$ which is then $2/8 = 0.25$ or 25% [55]. For real systems, increasing the overhead doesn't necessarily give a relative increase in the systems error correction performance.
The reason for these differences is that with high data rates more errors are likely, plus adding a small amount of redundancy in the data will not make a huge difference when increasing the bandwidth, which is a major factor for lower data rates.

The FEC limit is based on the Shannon limit, which is defined as the ratio of the energy per bit $E_b$ over the noise power spectral density $N_0$ which is $E_b/N_0$, this gives errorless transmission when the bandwidth has no limitations at full channel capacity. This limit in decibels is -1.6dB [54, 55]. Obviously for real systems there are many factors that determine that actual Shannon limit for that particular system.

## 2.5. Optical Receivers.

Optical receivers are devices that can receive light signals and covert them to RF signals, allowing electrical processing of the data.

The receiver design is another aspect that can improve the quality of the received signal, but it is a balance of complexity versus actual improvement.

Comparing Direct-Detection and Coherent detectors we see that Coherent receiving requires a Local Oscillator (LO) and sometimes a Frequency Lock Loop (FLL) which adds design complexity for DPSK receiving, which Direct-Detection does not. An increase in receiver noise can occur due to ASE noise from the LO laser and also noise from the LO beating frequency, although this is only small. Due to increased use of amplifiers in these systems, ASE has a greater effect on Direct Detection. When compared to Direct Detection, Coherent receiver has between 0.4-0.8dB less SNR penalty [52] but the simplicity of Direct-Detection needs to be taken into account.

### 2.5.1. Direct Detections Receivers

Direct-detection receivers are comparatively simple receivers in that they consist of a photodiode which "detects" the light of the incoming signal and converts the signal from optical intensity to RF power.

Direct-detection receivers can be joined with Delay Line Interferometers, also known as Asymmetric Mach-Zehnder Interferometers, to demodulate incoming DPSK signals. This happens by the way of two paths, one with a 1 bit delay, which interferes and results in two outputs that are out of phase by 90°, thus when detected by the photodiodes at the receiver the signal amplitude is doubled and the BER is significantly improved.
The DLIs, as part the Direct-Detection receiver, improves the quality of the received signal by using interferometry in place of an LO mixer to recover phase information [52].

Disadvantages relate to issues with noise and polarisation, both of which are of a random state unless actively controlled using polarisers and filters.

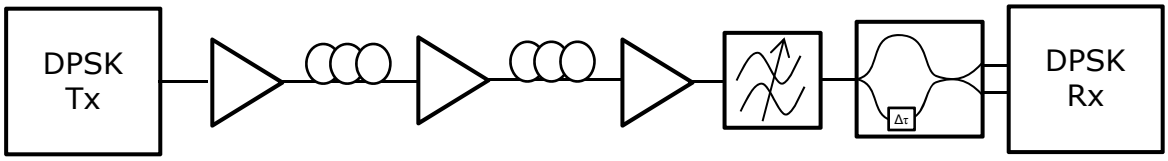


*Figure 2.5.1 – Schematic of single path DPSK direct-Detection link.*

A Direct-Detection DPSK receiver consists of a MZI, where the split signals interfere, and the resultant outputs have a $2/\pi$ difference in phase. This is also known as a DLI, (section 2.5.3). These outputs are known as "Constructive" and "Destructive" and are passed to two photodiodes which convert the optical signal to an RF signal; once converted the total signal then becomes differential in nature and are passed through an RF amplifier and an ELPF (Electrical Low Pass Filter) and are then measured for their error rate per bit, which is known as the BER.

### 2.5.2. Coherent Receivers

A more complex receiver than Direct-detection is a Coherent Receiver, which requires mixing of a Local Oscillator (LO) frequency to demodulate data correctly. For instance a Coherent detector will be able to receive a lower quality signal, but it must be able to detect the phase of the signal using phase tracking and therefore be synchronous. A Local Oscillator for frequency locking may be used depending on whether the receiver is homodyne or heterodyne [52].

In general Heterodyne Receivers have the advantage of having greater sensitivity than Direct-Detection receivers, but the disadvantages can outweigh this with greater complexity than with Direct-Detection receivers. One example is of the complexity is that both the transmit source and the LO source have to have their frequencies stabilised to be kept from drifting, otherwise the Intermediate Frequency (IF) will be incorrect and the demodulation will have errors because both the phase and polarisation information need to be exactly the same.

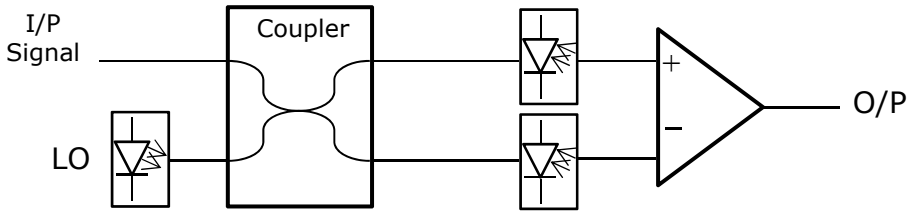


*Figure 2.5.2 – Schematic of a Heterodyne Coherent Receiver.*

If the LO and the transmitted frequency are the same in a Heterodyne receiver, this will in effect be a Homodyne receiver. In a purpose designed Homodyne the frequencies of both transmitted signal and the LO must be locked together otherwise demodulation will not occur. For both Homodyne and Heterodyne types of receiver the LO, which is mixed in a 90 degree optical hybrid with the signal, acts as a signal amplifier [56].

Coherent receivers can give advantages over direct-detection when WDM systems are involved, the use of an IF means instead of using a demultiplexer

or filter to pick out channels it could be done electronically. Instead of using demultiplexers or tuneable filters the IF is adjusted electronically to pick out channels which can be done rapidly. On the downside is the issue of complexity where controllable lasers with highly stable wavelengths would be needed [33].

Using a Balanced receiver is also advantageous for use in coherent or direct-detection receiver as it reduces noise and increases the amount of signal power received [52].

A major issue when using phase modulation is Nonlinear Phase Noise, this is caused by the Kerr Effect [49] and its interaction with the intensity of optical noise such as ASE, this produces SPM and XPM which can cause issues with phase modulation, hence the term phase noise. It can also trigger an increase in issues related to Relative Intensity Noise (RIN). Two such sources of phase noise are the transmitter laser and the local oscillator in coherent receivers. The phase noise can be reduced by laser design and also by using phase-diversity receivers [45].

There are also techniques using Digital Signal Processing (DSP) which corrects signals after they have been received, and these can be used for the outputs of either repeatered or unrepeatered configurations. These techniques will not be discussed in this thesis.

### 2.5.3. Delay Line Interferometer (DLI)

Delay Line Interferometers (DLI) are basically Mach-Zehnder Interferometers except that they have an inherent delay in one arm of the MZI. This design is useful in the demodulated of optical DPSK modulation.

In one arm of the Delay Line Interferometer there is a time delay, $\Delta\tau$, which is equal to one bit slot. This time delay is created either via an additional bit of fibre, or via a voltage controlled thin-film device which alters the length of the

fibre minutely by heating it, this leads to only a few picoseconds (ps) change, but it is enough to cause a delay.
The delay needs to be chosen for the data rate which is being used, for instance, at 10.664Gbps the delay of 1-bit would need to be 93.77ps, while at 42.656Gbps it would have to be 23.44ps.

An example is as follows. A MZI is used to modulate the signal phase wise using a precoded data pattern. An example is a data pattern of 110010, you will have [53]:

| | |
|---|---|
| Original Data: | • 1 1 0 0 1 0 |
| Precoded Data: | 1 1 1 0 1 1 0 |
| Phase Mod: | 0 0 0 π 0 0 π |

For a demodulator the incoming DPSK signal is split 50:50 so that equal amplitudes appear on each arm of the delay line. A time delay, Δτ, is also present in one of the arms of the MZI.
The expected output is shown below [53]:

| | |
|---|---|
| Arm A: | • 0 0 0 π 0 0 π |
| Arm B: | -π -π -π 0 -π -π 0 • |
| Output 1: | • 0 0 1 1 0 1 |
| Output 2: | • 1 1 0 0 1 0 |

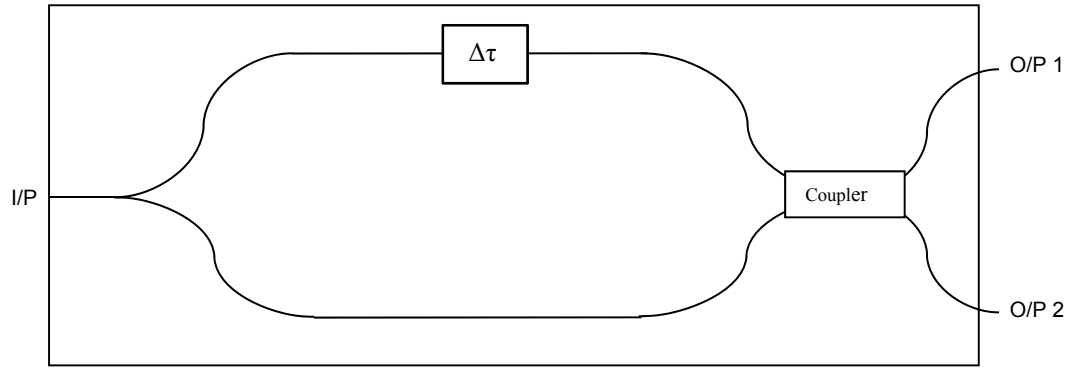


*Figure 2.5.3 – Basic diagram of an MZI with phase changes.*

For more complex modulation techniques, such as DQPSK, DLI's are used at the transmitter to add relative phases of 0°, 90° 180° and 270°, as the data

passes through to allow four state, or two bit per symbol, therefore increasing the data rate.

For a detailed explanation of Mach-Zehnder Interferometers, see Chapter 4 Section 4.3.

### 2.5.4. Probability of Error in Digital signals

The number of errors in received signals is one of the most important factors to measure as they indicate issues within a transmission system or network, and by looking at additional data such as eye diagrams, their cause can be surmised. Linear effects such as dispersion cause ISI and crosstalk, which is shown as widened vertical elements of an eye diagram, while with non-linear effects such as SPM and XPM the horizontal elements are affected. From this we can calculate the effect of these issues on the signal by calculating the probabilities that a 1 or 0 will be received. The basic equations for this are shown and explained below.

Probability of error for the 0|1 threshold can be defined as:

$$P_e = aP_1(v_{th}) + bP_0(v_{th}) \qquad \text{Eq. 2.5.1}$$

The weighting factors *a* and *b* refer to the probabilities that a 1 or 0 occurs, this depends on the data modulation, but for unbiased data, *a* and *b* both equate to 0.5 or 50% chance of either being received. The problem then becomes finding the decision threshold ($v_{th}$) where $P_e$ is at a minimum.

The complementary error function or erfc is a useful statistical formula that allows the calculation of the difference between the normal Gaussian distribution and the statistical error of the measured signal, which can indicate noise mechanisms within the measured system affecting the signal. The erfc is the basis of the Q-Value measurements. It can be defined by.

$$\mathrm{erfc}(x) = \frac{2}{\sqrt{\pi}} \int_x^\infty e^{-y^2} dy \qquad \text{Eq. 2.5.2}$$

Noise variance is calculated by using the statistical variance calculation:

$$\sigma^2 = \sum_{i=1}^{N} P(x_i)\,(x_i - \mu)^2 \qquad \text{Eq. 2.5.3}$$

It also needs to take into account the standard deviation, which is the square root of variance, as it covers the total width of the probability distribution at 1/e of the maximum amplitude.

$$\sigma = \sqrt{\sum_{i=1}^{N} P(x_i)\,(x_i - \mu)^2} \qquad \text{Eq. 2.5.4}$$

Where, $\mu$ is the expected value and $x$ is the actual value. The next section goes into more detail in how these formulas are applied.

### 2.5.5. Bit Error Rate (BER) and Q-Value

Calculating BER can be done, using the techniques shown, by using the threshold value of the decision circuits in the receiver.

$$BER = p(1)P(0|1) + p(0)P(1|0) \qquad \text{Eq. 2.5.5}$$

Where p(1) and p(0) are the probabilities of having transmitted a 1 bit or a 0 bit, respectively, with P(0|1) being the probability of 0 occurring when a 1 is received, and P(1|0) being the probability of a 1 occurring when a 0 is received. In general the probability of either a 1 or a 0 being received is 0.5, so p(1) = p(0) = 0.5 (or ½), and the BER becomes

$$BER = \frac{1}{2}[P(0|1) + P(1|0)] \qquad \text{Eq. 2.5.6}$$

In reality the probability is not exactly ½ and can be skewed towards either 1 or 0 being more likely, this depends on many external factors affecting the received signal, as well as factors relating to the actual receiver.

The probabilities for 1 and 0 rely on the sampled Intensity value, $I$, of the received signal, of which a probability density function can be calculated, $p(I)$. This value depends on statistical properties of the noise sources causing

current fluctuations, in the main these factors are Thermal noise and Shot noise.

Thermal noise can be represented by $i_T$ which when described by Gaussian statistics gives a zero mean and a variance of $\sigma_T^2$. The Shot noise can also be described through Gaussian statistics, but only for a *p-i-n* receiver, however an Avalanche Photodiode (APD) cannot be described in this way. To get around this problem the variance is assumed to be different for *p-i-n* and APD's, which allows a Gaussian approximation for both types of receivers.

The variance for a *p-i-n* receiver is given by:

$$\sigma_s^2 = 2q(I_p + I_d)\Delta f \qquad \text{Eq. 2.5.7}$$

Whilst for an APD receiver the variance is:

$$\sigma_s^2 = 2qM^2F_A(RP_{in} + I_d)\Delta f \qquad \text{Eq. 2.5.8}$$

where $F_A$ is the excess noise factor of the APD, $\Delta f$ is the effective noise bandwidth, $I_d$ is the dark current, $I_p = RP_{in}$ is the average current, *M* is the multiplication factor that relates to the internal gain improvement over *p-i-n*, and *q* is related to the spectral density given by $2qI_p$ which relates to the positive side of the spectrum only, where $qI_p$ is the double sided spectrum for the shot noise, which is also a description of White Noise.

The sampled value $I$, mentioned previously, has a Gaussian probability density function with a variance of $\sigma^2 = \sigma_s^2 + \sigma_T^2$. In addition the average current $I_p$ and the variance are different for 1 and 0, because $I_p$ in equation 2.5.9 can be equal to either of the currents, $I_1$ or $I_0$, depending on the received bit.

$$I(t) = I_p + i_s(t) + i_T(t) \qquad \text{Eq. 2.5.9}$$

Where $i_T(t)$ is the current fluctuation due to thermal noise and $i_s(t)$ the current fluctuation due to shot noise.

If $\sigma_1^2$ and $\sigma_0^2$ are the corresponding variances, the conditional probabilities are given by

$$P(0|1) = \frac{1}{\sigma_1\sqrt{2\pi}}\int_{-\infty}^{I_D}\exp\left(-\frac{(I-I_1)^2}{2\sigma_1^2}\right)dI$$

$$P(0|1) = \frac{1}{2}\mathrm{erfc}\left(\frac{I_1-I_D}{\sigma_1\sqrt{2}}\right) \qquad \text{Eq. 2.5.10}$$

$$P(1|0) = \frac{1}{\sigma_0\sqrt{2\pi}}\int_{I_D}^{\infty}\exp\left(-\frac{(I-I_0)^2}{2\sigma_0^2}\right)dI$$

$$P(1|0) = \frac{1}{2}\mathrm{erfc}\left(\frac{I_0-I_D}{\sigma_0\sqrt{2}}\right) \qquad \text{Eq. 2.5.11}$$

Where, erfc stands for the complimentary error function, as defined by.

$$\mathrm{erfc}(x) = \frac{2}{\sqrt{\pi}}\int_x^{\infty} e^{-y^2}dy \qquad \text{Eq. 2.5.12}$$

Using Eq. 2.5.11 and 2.5.12 and substituting them into Eq. 2.5.6, the BER can be calculated by

$$BER = \frac{1}{4}\left[\mathrm{erfc}\left(\frac{I_1-I_D}{\sigma_1\sqrt{2}}\right) + \mathrm{erfc}\left(\frac{I_D-I_0}{\sigma_0\sqrt{2}}\right)\right] \qquad \text{Eq. 2.5.13}$$

This equation shows that the BER depends on the decision threshold, $I_D$, at the receiver, where it is optimised to minimise the BER, the expression of this is

$$\frac{(I_D-I_0)^2}{2\sigma_0^2} = \frac{(I_1-I_D)^2}{2\sigma_1^2} + ln\left(\frac{\sigma_1}{\sigma_0}\right) \qquad \text{Eq. 2.5.14}$$

Although $ln\left(\frac{\sigma_1}{\sigma_0}\right)$ can be neglected for most purposes. $I_D$ can be approximately found from:

$$\frac{I_D-I_0{}^2}{\sigma_0} = \frac{I_1-I_D{}^2}{\sigma_1} \equiv Q \qquad \text{Eq. 2.5.15}$$

The term $I_D$ is given by:

$$I_D = \frac{\sigma_0 I_1+\sigma_1 I_0}{\sigma_1+\sigma_0} \qquad \text{Eq. 2.5.16}$$

When $\sigma_1 = \sigma_0$ then $I_D = (I_1 + I_0)/2$, this is equal to setting the decision threshold to half way. This is the status for most *p-i-n* receivers as their noise figure is

mostly due to the Thermal noise within the receiver, this confirms the noise is independent from the average current noise of the received signal.
Shot noise however is different for received bits 1 and 0, with 1 having a larger shot noise, since the variance $\sigma_s^2$ is linear with respect to the average current.

For APD receivers, the decision threshold should be set to a value pertaining to Eq. 2.5.16.

The optimum setting for the decision threshold for the minimum BER is calculated by combining Eqs. 2.5.13 and 2.5.15, and depends on the Q factor, which can be found by

$$BER = \frac{1}{2}\mathrm{erfc}\left(\frac{Q}{\sqrt{2}}\right) \qquad \text{Eq. 2.5.17}$$

$$BER \approx \frac{exp\left(-\frac{Q^2}{2}\right)}{Q\sqrt{2\pi}} \qquad \text{Eq. 2.5.18}$$

Where, the parameter Q is obtained from Eqs. 2.5.15 and 2.5.16 and is then given by

$$Q = \frac{I_1 - I_0}{\sigma_1 + \sigma_0} \qquad \text{Eq. 2.5.19}$$

The above equations are from [45].

Another way that BER and Q Value can be defined is:

$$BER = \frac{N_e}{N_t} = \frac{N_e}{Bt} \qquad \text{Eq. 2.5.20}$$

Where $B = \frac{1}{T_b}$ is the bit rate, $N_e$ is the number of errors and $N_t$ is the number of pulses and $t$ is the time interval over which the measurements takes place [40].

The Q-value can be found by

$$Q = \frac{v_{th} - b_{off}}{\sigma_{off}} = \frac{b_{on} - v_{th}}{\sigma_{on}} \qquad \text{Eq. 2.5.21}$$

Where for a binary 1 $b_{on}$ is the mean signal level and $\sigma_{on}$ the variance, for a binary 0, $b_{off}$ and $\sigma_{off}$ are the mean and variance, while $v_{th}$ is the threshold voltage [40].

## 2.6. Optical Amplifiers

In optical systems there are two common types of optical amplifier; Semiconductor Optical Amplifiers (SOAs) and Erbium Doped Fibre Amplifiers (EDFAs) which are used extensively throughout optical systems worldwide. A third type of amplifier is the Raman Amplifier; this type is currently used less widely than the previous two, but is increasingly being used in long and ultra-long distance transmission [14, 15, 18, 19, 20, 21, 22, 23, 24, 25, 35, 57, 58, 59, 60, 61, 62, 63, 64].

A small summery of SOAs are mentioned here as SOAs were not used in any experiments contained within this thesis.

More detail on the operation and usage of EDFAs and Raman Amplifiers are in the next two sections.

### 2.6.1. Erbium Doped Fibre Optical Amplification

Erbium Doped Fibre Amplifiers (EDFAs) are used regularly in optical networks as an effective amplifier which is transparent to modulation formats, has high gain over a wide bandwidth, has a low noise figure and amplifies at wavelengths in the C-Band with a centre wavelength at around 1550nm [56].

The actual physical layer of a basic EDFA design, shown in Figure 2.6.1, includes an Erbium-doped Fibre loop connected to WDMs at either end that multiplex the pumps lasers at 980nm and 1480nm wavelengths with the incoming signal. The reason for two different pump wavelengths being used is described further on in this section.

There are three ways to pump EDFAs, these are: Co-propagating and Counter-propagating, both of which use a single pump laser; and Dual-pumping, which uses two pumps, one in co-propagating direction usually at 980nm wavelength and one counter propagating using 1480nm. The advantage of co-propagation is the improved noise performance, so therefore less ASE, whilst counter-propagation has a higher potential gain. Using Dual-pumping therefore gives you high gain and lower noise when compared to individual pumping in either direction. The potential gain for single pumping is +17dB while dual pumping is +35dB [40]. The reasons for using these wavelengths are described in more detail further on in this section.

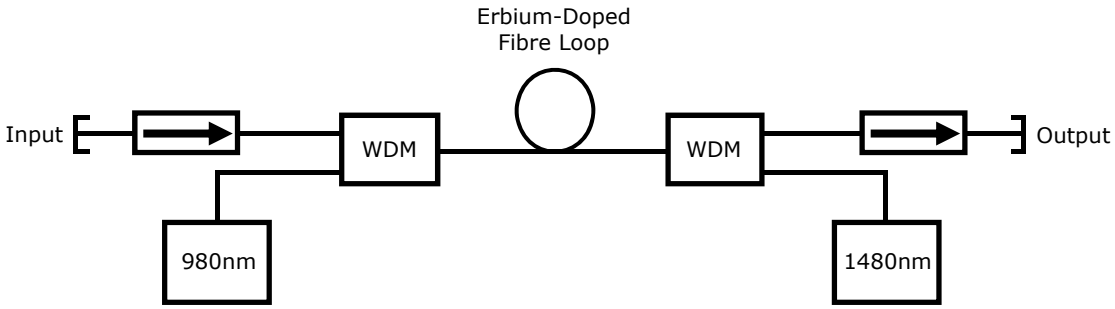


*Figure 2.6.1 – Schematic of Erbium Doped Fibre Amplifier (EDFA).*

An isolator is placed at each end of the amplifier to limit back reflected wavelengths propagating within the EDFA in the reverse direction to the signal, as these reflections can increase amplifier noise and decrease the amplifiers efficiency by reducing gain. The isolators also reduce the probability of laser oscillation by supressing the reflected laser and therefore limiting the feedback mechanism.

An EDFA used in transmission spans would have to deal with many wavelengths at the same time at different powers, plus the spectral gain profile is un-uniform so different channels would receive differing amounts of gain. To deal with these issues the EDFAs are more complex and would have additional elements such as filters, gratings and taps.

The taps are placed at either end of the amplifier to compare the input power and the output power; these taps have a ratio of 99:1 or 95:5 and take a small percentage of the overall power which is then fed back for comparison to

calculate the amount of gain. This information can then be used externally to see whether the amplification process is working as designed.

Optical filters are used to add loss at specific bands to flatten the gain profile; this reduces the need for external techniques such as pre-emphasising individual channels prior to them passing through the EDFA, therefore giving a more uniform gain over all channels. There are different types of filters which can be used [45], such as thin-film interference filters [65, 66] and Mach-Zehnder filters [67], which both work by using phase changes to achieve cancellation within high-gain areas and enhancement of low-gain areas to create a flattened gain, although with thin-film filters there does not have to be the exact inverse for cancellation or enhancement to occur. Acousto-optical filters [68] work by using a structure that can vibrate, such as a crystal, to change the optical properties of the light passing through it, the interaction is through phonons which build into a shear wave, this then either diffracts or retards the optical wave and changes the polarisation. Using polarisers this can reduce the gain through amplitude reduction due to non-orthogonal polarisation loss.

There are also Long-period Fibre Gratings [69] which are used in EDFAs for fixed gain flatness. These LPFGs are different to Fibre Bragg Gratings (FBGs) in two main ways; The LPFGs have a much longer wavelength period of between 200μm and 700μm [70], whilst a FBGs period is around 0.1μm [70]. LPFGs have low insertion loss and back reflections when compared to other techniques, but are limited to only one specific wavelength. The way around this is to use a combination of lots of LPFGs of different wavelengths and phase-shifted LPFG which would cover the C-band and lower the main gain peaks more than using a phase-shifted LPFG on its own. [69].

#### 2.6.1.1. EDFA - Principle of Operation

The amplifiers work by using Silica fibre doped with Erbium to enable the fibre to create additional photons when a pumped laser beam is passed through the fibre, this is caused by the absorption of photons in the Erbium-doped fibre,

this in turns creates an excitation of the atoms which causes what is known as a population inversion, this is where more atoms are at higher energy levels than at lower energy levels. This causes the stimulated atom to emit photons at long wavelengths; hence they emit photons around 1550nm.

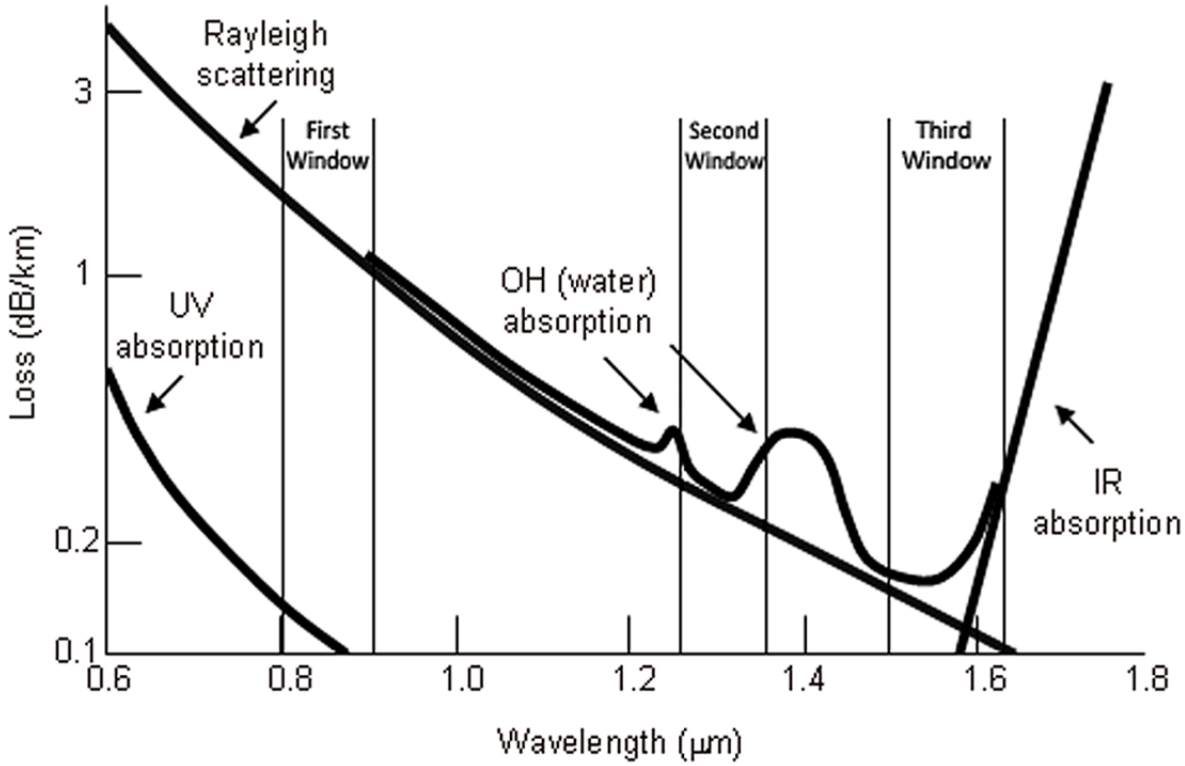


*Figure 2.6.2 – Graph showing the typical wavelength ranges of the causes of attenuation within Optical fibres. The first (800-900nm), second (1250-1360nm), and third (1530-1625nm) optical windows are also shown [72].*

The result is, as explained above and in Figure 2.6.3, the signal wavelength at around 1550nm gets a boost by using lower wavelength pumps to excite the erbium to give additional photons at 1550nm, and hence signal amplification. The advantage here is that 1550nm lies in the lowest point of the absorption spectra of silica due to OH molecules [40, 71, 72].

The signal beam and the 980nm pump travel in the same direction which depletes the pump power in the Erbium-doped fibre loop, whilst at the other end the 1480nm pump enters in the opposite direction to the signal and 980nm pump and induces amplification at that end, this compensates for the pump depletion at 980nm giving less amplification further along the Erbium-doped fibre loop.

How this occurs is that the 980nm pump excites ions from the ground state up to the pump energy level, which is at a higher energy than the energy band needed for signal amplification. Ions are atoms or molecules with either missing electrons which give an overall positive charge, $e^+$, or an additional electron that gives a negative charge, $e^-$, in this case they are missing an electron and are positive ions or $e^+$.

The ions in an EDFA are $Er^{3+}$ which means there are three electrons missing on the outer shell of the Erbium atom, this gives the potential for high gain by photons being absorbed by electrons in lower energy bands moving up into the holes available in the outer shell of the atom. These electrons are only at these higher energy levels of the 980nm pump for a short period of time and decay within 1μs, this decay releases phonons which are absorbed and scattered within the fibre material. When the ions are excited by signal photons the resulting photons emitted are of the same wavelength, polarisation and orbital momentum as the original signal photons, which will be in the 1530-1560nm band.

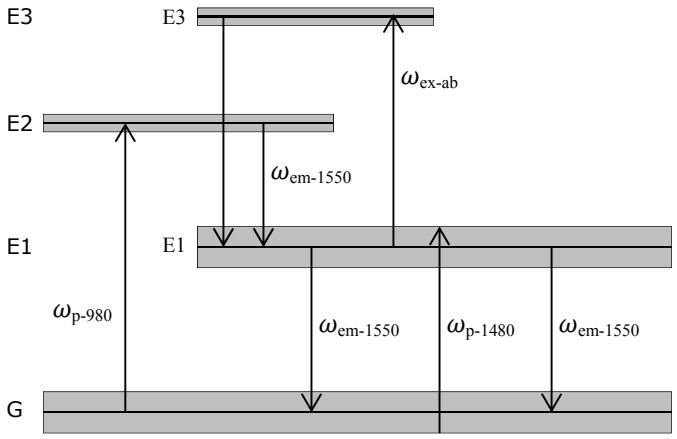


*Figure 2.6.3 – Energy transitions in Erbium Doped Fibre.*

The use of the 980nm wavelength is due to the fact that population inversion occurs at an energy level of 1.27eV [40] which relates to wavelengths around 980nm. The 1480nm wavelength relates to energies at the high end of the energy gap between the ground state (G) and the metastable band (E1) which has an energy level of 0.841eV [40]. Because 1480nm is limited to the metastable band, the population inversion is not as great as with 980nm.

The 1480nm pump raises ions to the top of the metastable band from the bottom of the ground state. 980nm is less efficient at exciting those ions at the lowest ground energy states than the 1480nm wavelength. These ions, once in the metastable band, then slowly move down towards the lower energies within the band. This is where most of the ions are found. As with 980nm pumping, once a signal photon is absorbed by one of these ions it decays releasing photons with the same information as the original photons. This process is known as stimulated emission.

The metastable band is the term for the energy band at which electrons stay for a relatively long period of time before decaying to the ground state, this time period is greater than that at the pump energy band, and is therefore >1μs and usually in the 10ms region. The metastable band energy is in the region relating to 1520-70nm and is one of the reasons for Erbium's use in optical amplification.

Also shown in Figure 2.6.3 is the excited-state absorption (E3) which causes a reduction in amplifier gain and therefore a loss. As pump photons are absorbed by the already high energy atoms, this increases their energy even more and thus reduces the available population. These electrons will then emit spontaneously at wavelengths outside of those useful for telecommunication purposes and will be seen purely as ASE.
The effect of excited-state absorption is minimised at 980nm and 1480nm wavelengths as they are more efficient when used in Erbium doped silica fibres than other wavelengths. The selection of the Erbium doping arrangement can also minimise the effect of excited-state absorption. An example of the Erbium dopant content in a Silica fibre is 1000ppm for light doping [40].

The energy changes shown in Figure 2.6.3 are generalised as higher energy level can be made available by higher pump powers, but this leads to an increase in amplifier inefficiency due to gain saturation and an increase in ASE. Saturation occurs when the population inversion is at its maximum, i.e. most electrons are at the higher energy levels, and there is no more space for other elections at lower energies to move up, this leads to a flattening out of the

gain when the pump power is increased past this point as only lower energy states are available.

The energies that the electrons inhabit are not purely discrete but are bands of energy levels. This phenomenon is caused by Stark Splitting, which is due to the area surrounding the Erbium ions being made from silica. Silica does not have a crystalline structure but is classed as an amorphous material and this leads to each Erbium ion having its own energy level separate from all other Erbium atoms. This means discrete energy levels do not exist alone but are part of a collection of energy levels. In other words where normally an individual energy level is seen an energy band is present instead, giving a range of energy levels that are being occupied.
This "banding" of the energy levels gives an advantage in that a larger range of wavelengths can be amplified with one amplifier rather than a narrow band of wavelengths. Therefore bandwidths of EDFAs can be large and can amplify many WDM channels at the same time over a 40 to 50nm bandwidth, as shown in Figure 2.6.4 [26].

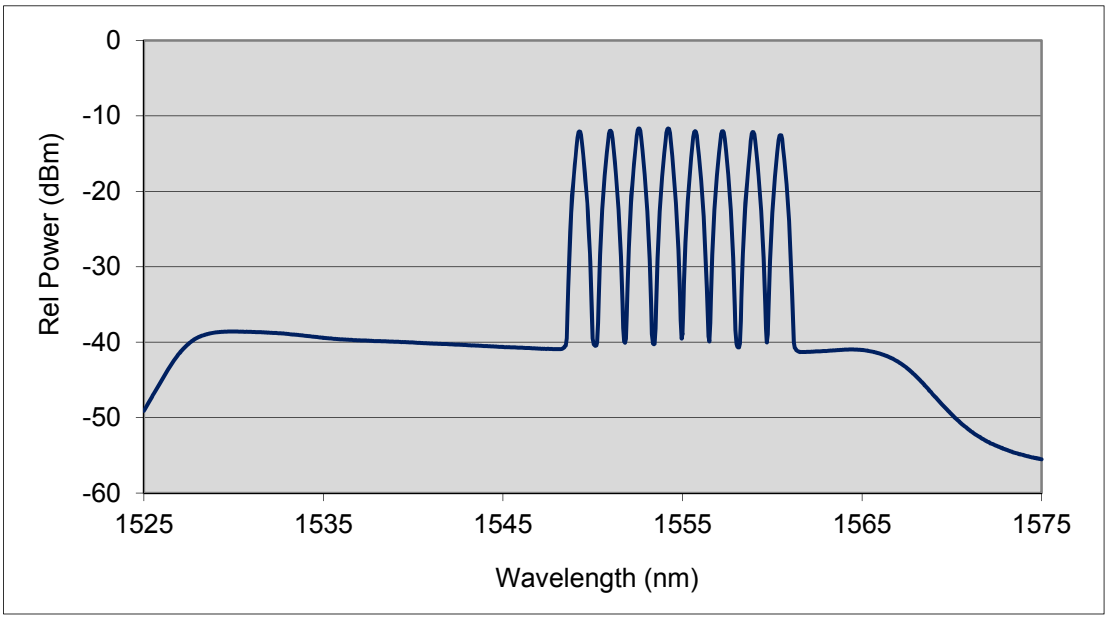


*Figure 2.6.4 – Example of Gain flattened EDFA Bandwidth with 8 WDM Channels.*

This band is from 1520nm to 1570nm and is known as the C-Band for telecommunication purposes. The central wavelength of this band is 1545nm whilst the peak gain is at 1532nm, as mentioned previously this band is adjacent to one of the lowest attenuation windows [40, 71, 72].

The typical output power of EDFAs are around +20dBm to +30dB, whilst the dual-pump configuration gives a flatter gain spectrum than with just co-propagation and counter-propagation, the gain spectrum is still heavily influenced by silica being amorphous along with any other dopants present within the fibre.

Each EDFA, whilst having a similar spectral shape, will have differences no matter how similar they are made, as variations in the pump powers will have an effect along with variations of the pump laser due to RIN (see Chapter 3, Section 3.1.3), and the effects of the medium they are passing through. The 1480nm pump wavelength has higher power lasers available, whilst there is also a requirement for the doped fibre to be longer to achieve high gain due to the smaller population inversion available compared to 980nm[45] as explained previously.

#### 2.6.1.2. Amplifier Gain in EDFAs

The gain of an amplifier is one of its most important aspects, as it is basically the measure of how much amplification a signal traveling through an amplifier will achieve. This relationship is generally linear until gain saturation occurs.

Gain saturation is the point where no matter how much power the signal has it will not receive an increase in amplification; in fact the opposite can be true, where a slight decrease happens due to noise generated in the amplifier (see ASE Section 2.5).
The Gain is a ratio of the powers of the input and output signals of a device, this can be represented as:

$$G = \frac{P_{out}}{P_{in}} \qquad \text{Eq. 2.6.1}$$

The actual gain of an optical amplifier is slightly more complex than equation 2.6.1 and is different due to the design and materials used, as well as the physics behind the reason for amplification.

The gain of an EDFA relates to a number of factors including the concentration of the Erbium dopant, the length of the doped fibre within the amplifier, the fibre core diameter and the pump powers. In some cases excited state absorption (ESA) will need to be taken into consideration depending on the pump wavelengths being used and the type of fibre, such as fluorosilica [40], but for 980nm and 1480nm pump wavelengths and silica fibre, excited state absorption can be ignored.

The relationship of all factors appropriate to determine the gain is described by:

$$G = \Gamma_S \, exp\left[\int_0^L (\sigma_S^e N_2 - \sigma_S^a N_1) dz\right] \qquad \text{Eq. 2.6.2}$$

The term $\Gamma_S$ denotes the confinement factor, or cross sectional area, which is related to the amount of doped fibre in the amplifier, and is therefore related to the active section of the fibre. Terms $\sigma_S^e$ and $\sigma_S^a$ are the emission and absorption density cross-sections at the signal wavelength, with $N_1$ and $N_2$ being the ion densities relating to the pump energy band and the signal, or metastable, band. The total ion density is $N_t = N_1 + N_2$. The term $L$ at the top integral limit is the total amplifier fibre length.

This shows in general that the gain increases exponentially with length, while the maximum gain is limited to the total ion density available and the relationship of the absorption and emission of photons with the signal wavelength. Along with noise factors such as ASE, these are the main relationships which affect the total available output power of the amplifier.

### 2.6.2. Raman Amplification

Raman Amplification uses the phenomenon known as Stimulated Raman Scattering or SRS to amplify optical signal.

SRS occurs when two or more signals at different wavelengths are put into a fibre which makes the power from the lowest wavelength transfer to the highest wavelength. In Raman Amplification this effect is used by having a

signal wavelength and a pump wavelength inserted into the same fibre which causes amplification of the signal wavelength.

The effect is similar to Spontaneous Raman Scattering and is due to the photons of the lower wavelengths having a larger amount of energy than those at the higher wavelengths. Due to the natural behaviour of photons the energy of the photons at lower wavelengths, thus higher energies, wants to decay towards the ground state. When these photons change in energy state they emit a photon at a higher wavelength than the original photon. This also produces an optical phonon, as not the all the energy departs from the atom or molecule, this phonon is the vibrational energy or frequency of the atom/molecule [40, 45, 56, 73].

For more detail on Raman Amplification see Chapter 3, Section 3.2.

## 2.7. System impairments: Linear Effects

Linear effects are those types of effects that have a linear relationship; such an example is the electrical current increase on a 1Ω resistor, with every 1V increase the current increases by 1A.
In the optical world, an example of such a relationship is dispersion, as it increases or decreases by the same amount per kilometre, a similar relationship is seen with distance and optical loss, which for silica fibre is a loss of 0.2dB/km.

### 2.7.1. Chromatic Dispersion

Chromatic dispersion is a linear process that causes light to spread out as it travels through an optical fibre. The cause of Chromatic Dispersion, or just dispersion, is down to two different types of reactions of light within the fibre; material dispersion and waveguide dispersion.

Material dispersion is induced by the reaction of light with the material the fibre is made from. This interaction is caused by the variation in the refractive index which changes depending on the wavelength of the light travelling through the fibre core. The wavelength dependent variability of the fibre core refractive index causes the light to travel at slightly different velocities, hence the spreading out of the pulse, which affects the group velocity of light pulses passing through the fibre; the effect is known as chirping, an example of which can be seen when light shines through a prism.

Waveguide dispersion is due to the ratio of light passing through the core and the cladding, of which up to 80% passes through the core, the rest through the cladding. Because the cladding is of a different refractive index to the core, the velocity of the light is greater in the cladding than the core, hence light that is recoupled from the cladding to the core, and vice-versa, causes pulse spreading. This type of dispersion can be limited by fibre design i.e. the diameter of the core, as shown in Figure 2.7.1, and also the core and cladding with respect to one another and the refractive index of the cladding can be chosen to limit light loss into the cladding from the core thus reducing attenuation as well as dispersion.

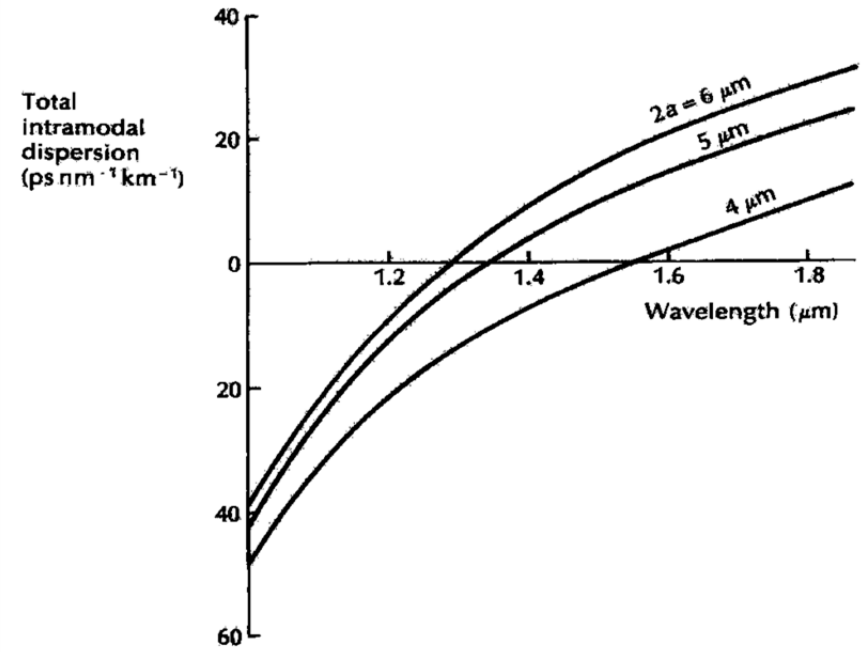


*Figure 2.7.1 – Intramodel Dispersion change with different fibre core diameters [74].*

The types of dispersion mentioned above are intramodel; this is the name for any type of dispersion that causes the group velocities, and therefore the

group velocity delay (GVD) to increase or decrease, this leads to temporal broadening of light pulses and it can also cause phase changes. An example of this is normal dispersion, where the velocities of the individual frequency components slow at the shorter wavelengths and increase in the longer wavelengths.

There is also intermodal dispersion, which is where individual modes of the group velocity have different values at the same frequency, this mainly affects multi-mode fibres. Since only single-mode fibres are dealt with in this thesis, this type of dispersion will be ignored.

To calculate the amount of dispersion in a fibre, the following equations can be used. Firstly, a definition of the group velocity can be written as:

$$V_g = \left(\frac{d\beta}{d\omega}\right)^{-1} \qquad \text{Eq. 2.7.1}$$

Where $V_g$ is the group velocity, $\beta$ is the propagation constant, and $\omega$ is the optical angular frequency. The propagation constant $\beta = \bar{n}\frac{2\pi}{\lambda}$ with $n_1 > \bar{n} > n_2$. Eq. 2.7.1 can be related to wavelength and refractive index by $V_g = \frac{c}{\bar{n}_g}$, where $\bar{n}_g$ is the group refractive index and when substituted gives:

$$V_g = \frac{c}{\bar{n} - \lambda\left(\frac{d\bar{n}}{d\lambda}\right)} \qquad \text{Eq. 2.7.2}$$

With $\bar{n}$ being the mode effective refractive index and $\lambda$ the wavelength of the optical pulse. To find out how much a pulse would broaden when propagating in an optical fibre the following can be used:

$$\beta_2 = \frac{d^2\beta}{d\omega^2} \qquad \text{Eq. 2.7.3}$$

This is known as the Group Velocity Dispersion or GVD parameter, and is useful to help calculate the dispersion.
The group dispersion can now be calculated using the dispersion parameter D, which is:

$$D = -\frac{2\pi c}{\lambda^2}\beta_2 \qquad \text{Eq. 2.7.4}$$

Eq. 3.1.4 shows that the spread of the pulse is related to the wavelength and the group refractive index through the propagation constant.
The group delay difference, which is the difference between the lowest and highest spectral components, is given by:

$$\Delta T = DL\Delta\lambda \qquad \text{Eq. 2.7.5}$$

Where, $D$ is the group dispersion, $L$ is the fibre length and $\Delta\lambda$ is the laser source spectral width. For the individual sections of dispersion we have the following two equations:

For Material Dispersion:

$$D_M = -\frac{2\pi c}{\lambda^2}\frac{dn_{2g}}{d\omega} = \frac{1}{c}\frac{dn_{2g}}{d\lambda} \qquad \text{Eq. 2.7.6}$$

Where $n_{2g}$ is the group refractive index of the cladding.

For Waveguide Dispersion:

$$D_W = -\frac{2\pi\Delta n}{\lambda^2}\left[\frac{n_{2g}^2}{n_2\omega}\frac{Vd^2(Vb)}{dV^2} + \frac{dn_{2g}}{d\omega}\frac{d(Vb)}{dV}\right] \qquad \text{Eq. 2.7.7}$$

Where $b = \frac{\bar{n}-n_2}{n_1-n_2}$ and $V = \frac{2\pi a}{\lambda}(n_1^2 - n_2^2)^{0.5}$, $V$ being the cut-off parameter regarding the number of modes available in a fibre, $n_1$ is the core refractive index, $n_1$ the cladding refractive index and $a$ is the core radius. For single mode fibres $V \leq 2.405$. The overall dispersion can then be found by:

$$D = D_M + D_W \qquad \text{Eq. 2.7.8}$$

The effect of dispersion on the bit-rate can be found using:

$$B \leq \frac{1}{4|D|\Delta\lambda L} \qquad \text{Eq.2.7.9}$$

For Broad-linewidths $\Delta\lambda$ is determined by the laser, while for Narrow-linewidths $\lambda = \frac{\Delta f\lambda^2}{c} = \frac{B\lambda^2}{c}$, which means the bit rate has to be smaller than the linewidth on the laser.

There are different orders of dispersion; Chromatic dispersion is 1st order whilst 2nd order is known as the dispersion slope. The dispersion slope is the change in dispersion with wavelength.
This can be summarised as:

$$S = \frac{dD}{d\lambda} \qquad \text{Eq. 2.7.10}$$

where $d\lambda$ is the wavelength difference of the maximum and minimum wavelengths for the fibre being used, while $dD$ is the difference in the dispersion between the maximum and minimum wavelengths. The dispersion slope, $S$, is measured in ps/nm$^2$*km.

The dispersion slope is especially important for systems using WDM, where it is desirable to have the same dispersion over all channels. A large dispersion slope will mean some channels are affected by dispersion more than others, an issue seen in the experimental results in Section 3.4.

#### 2.7.1.1. Dispersion Management

It is important that dispersion is controlled within optical transmission spans as its effects can degrade data to become unrecoverable depending on the fibre length and the data rate. The most common way is to use dispersion compensated fibre (DCF) to correct the relevant dispersion measured in ps/nm*km.

Dispersion in optical signals can be compensated for, but the amount of dispersion needs to be calculated beforehand as well as whether it is normal (positive) or anomalous (negative) dispersion [33]. Some examples of commercially available optical fibres are given in Table 2.7.1 with the typical values for attenuation and dispersion.

| ITU-T Standard | Fibre Type | Typical Attenuation value (C-band) | Typical Chromatic Dispersion value (C-band) | Dispersion Slope (C-Band) | Refs |
|---|---|---|---|---|---|
| | | [dB/km] | [ps/nm*km] | [ps/nm$^2$*km] | |
| G.652 | SMF-28 | 0.20 | +18.0 | +0.089 | [75] |
| G.652 | SMF-28 ULL | 0.18 | +18.0 | +0.092 | [8] |
| G.655 | LEAF (NZDSF) | 0.19 | +2.0 to +6.0 | na | [6] |
| G.654 | LEAF ULL | 0.16 | +20.4 | +0.06 | [9] |
| G.654 | LEAF-EP (NZDSF) | 0.20 | -3.0 | +0.12 | [9] |
| G.655 | TW-RS (NZDSF) | 0.25 | +2.6 to +6.0 | +0.05 | [76] |
| G.655 | TW-RS LWP (NZDSF) | 0.22 | +2.6 to +6.0 | +0.05 | [39] |
| G.655 G.656 | TW-Reach LWP (NZDSF) | 0.20 | +5.5 to +8.9 | +0.045 | [38] |
| G.654 | Z-Fiber | 0.17 | +18.5 | +0.055 | [10] |
| G.652 | DCF | 0.265 | -49 to -30 | -0.155 to -0.075 | [77] |
| G.652 | DCF | 0.20 | -97.7 | -0.328 | [*78*] |

*Table 2.7.1. – Optical Fibres and their Attenuation and Dispersion parameters.*

The fibres shown in Table 2.7.1 are a cross section of typical attenuation and dispersion parameters of optical fibres, most of which have anomalous dispersion. For more information on the ITU-T standards see references [79, 80].

Non-Zero Dispersion Shifted Fibre (NZDSF) and Non-Zero Dispersion fibre (NZDF) can be confused but are two different types of fibre, a type of NDSF is SMF-28 i.e. normal silica fibre. NZDSF has the wavelength at which dispersion is zero, moved to counteract the dispersion in fibres like SMF-28. Figure 2.7.2 shows measurements for typical fibres used in optical communications. It can

be seen that due to the large dispersion slope for SMF, that normal dispersion regimes must be used to combat the anomalous dispersion present.

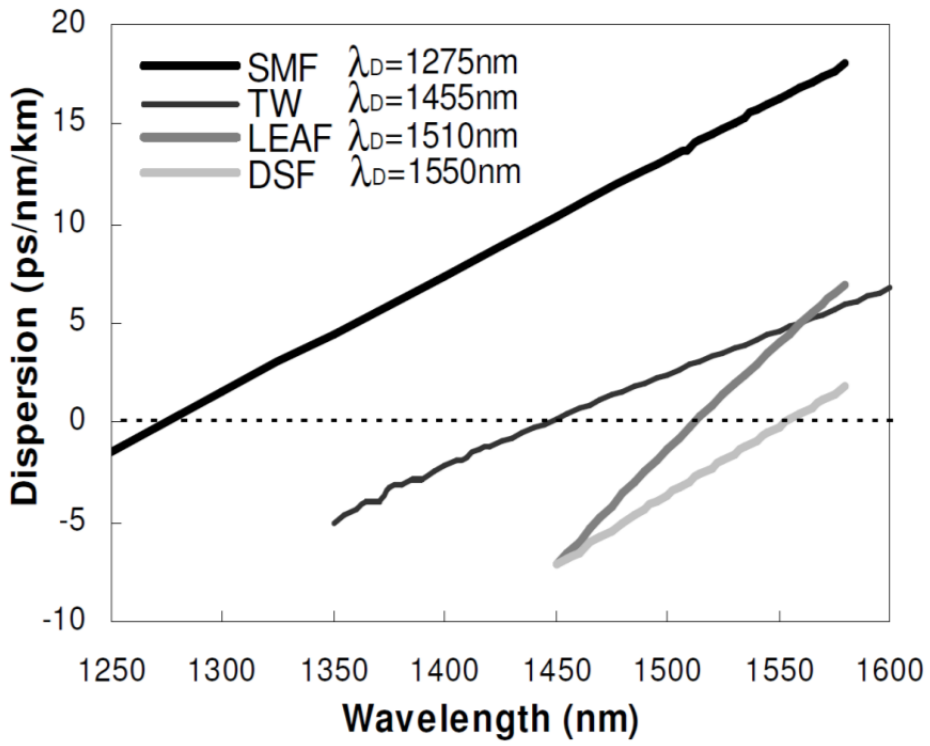


*Figure 2.7.2 – Dispersion parameter D versus wavelength for several commercial optical fibres [81].*

The wavelength at which the dispersion is zero separates the dispersion into two separate regions. The region below zero is the negative or normal dispersive region, while above zero it is known as the positive or anomalous region. The reason for the regions being normal or anomalous is down to how the light pulses travel through the fibre. For normal dispersion, the lower frequencies, or longer wavelengths, travel faster than the higher frequencies or shorter wavelengths, which is classed as normal behaviour for light as it propagates through a medium. In the anomalous region the opposite happens, the higher frequencies (shorter wavelengths) travel faster than the lower frequencies (longer wavelengths), this is therefore the opposite to how light normally propagates, and hence it is anomalous.

There are ways of making sure the dispersion has a minimal effect at the receiver and these usually involve Dispersion Compensating Fibres (DCF). As the name suggests, DCF compensates for the amount of dispersion that will be caused by a certain length of normal fibre, such as SMF-28. The DCF will be

chosen for its compensation figure, this is the amount of compensation needed for a stated length of normal SMF fibre, in SI units the compensation value is ps/nm-km. So for example a 1km length of SMF-28 has a dispersion of 16ps/nm, to compensate for that you need a 1km DCF with compensation of -16ps/nm. For normal dispersion you need to compensate with anomalous dispersion.

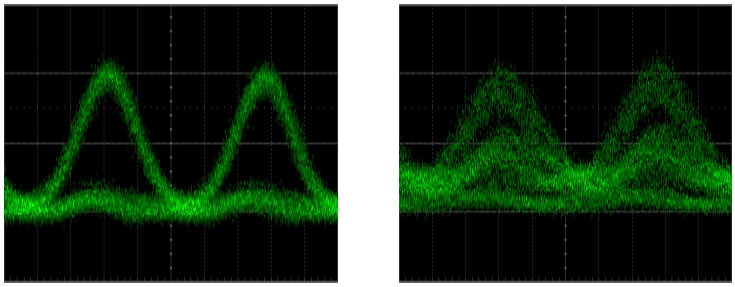

*(a)* *(b)*

*Figure 2.7.3 – Dispersion at 40Gbps with dispersion of 17ps/nm*km over a distance of 5km. (a) is at 0km (b) is at 5km [74].*

These fibres can be placed either before the fibre span, known as pre-compensation, or placed after the fibre span, or post-compensation. Either set-up has to be correctly managed to make sure that there is the right amount of dispersion compensation. If there is not enough compensation, the light will be in the anomalous region and still positive, meaning at the receiver the data is unreadable.

Figure 2.7.3 shows the eye diagrams of how an uncompensated signal degrades due to dispersion, with the dispersion being 17ps/nm*km. Having too much dispersion compensation will also have the same effect, but the spectral frequencies will be opposite.

Electronic Dispersion Compensating Modules (EDCM) are a type of dispersion compensation technology that is used instead of, or with, DCFs. The advantage of these types of device are that the dispersion correction which can be made is on a much smaller scale than with DCFs, they can be tuneable either within a continuous band or tuneable to a grid, such as ITU 50GHz and 100GHz grids, which was the type of EDCM used in Section 3.4. These modules can also be "active". In other words if the dispersion changes due to

different wavelengths being used e.g. in a WDM system, there will be a significant dispersion slope. An EDCM is able to be software controlled to track the changes in dispersion and correct as needed [82].

One of the disadvantages with EDCMs is that they use Array Wave Guides (AWGs) which channel optical power at discrete wavelengths. Due to the broad noise floor that passes through AWGs, averaging of the power can occur, which can limit these type of devices to signals that have higher powers and larger OSNRs (>20dB) as high attenuation is possible. This can lead to the dispersion not actually being the main issue, and therefore the device is compromised in how it works, meaning using DCF fibre may actually be a better choice for the system even if dispersion is a little worse.

### 2.7.2. Polarisation Mode Dispersion

Polarisation Mode Dispersion (PMD) is caused by an optical effect in fibres known as birefringence. Birefringence is caused by small defects in the circularity of the fibre core and leads to changes in the fundamental mode of the signal, which in turn affects the polarisation. These effects can be less than 1% of the total circularity of the fibre. Other causes of birefringence are bending and twisting of the fibre, flattening of the fibre and temperature differences, but obviously these effects vary throughout the fibre [33, 46]. The effect of birefringence on the state of polarisation (SOP) causes pulse broadening which is a greater problem at higher data rates as the pulse width of the signal decreases. It will also cause the polarisation to change as a signal travels through a fibre as each polarisation mode will have a different velocity. This results in a difference in propagation time, $\Delta\tau$, and causes the previously discussed pulse broadening. If we look at PMD in more detail, where there are two orthogonal polarisation modes, $v_1$ and $v_2$, the differential time delay $\Delta\tau_{pol}$ can be found between the two polarisation modes as it travels through a fibre of distance $L$. From this we can see that:

$$\Delta\tau_{pol} = \left| \frac{L}{v_1} - \frac{L}{v_2} \right| \qquad \text{Eq. 2.7.11}$$

PMD, unlike other dispersion effects, is not stable. The reasons for this have been described previously. What this means however is that at the output of the fibre a time varying fluctuation appears. This shows that PMD cannot be totally accounted for using Eq. 2.7.11, and a probabilistic method has to be used.
For long fibre lengths PMD can be calculated as a mean value of the differential group delay of the polarisation modes. Hence:

$$\left\langle \Delta\tau_{pol} \right\rangle \approx D_{PMD}\sqrt{L} \qquad \text{Eq. 2.7.12}$$

Where $D_{PMD}$ is the average PMD, which is measured in ps/$\sqrt{\text{km}}$, where typical values are between 0.1 and 1.0 [46, 83].

### 2.7.3. Rayleigh Scattering

Rayleigh scattering is caused by the density of the fibre not being completely homogenous throughout its length. This inhomogeneity causes some molecules of the material that the fibre is constructed from to be in clumps; this is due to the heating processes which play a part in the creation of optical fibres. These molecules are much smaller than the optical wavelengths of the laser light passing through the fibre, but there are enough collisions within these denser areas to cause light to be scattered in all directions and to deplete the amount of power available. This becomes more significant when the wavelength decreases as the relationship is proportional to $\lambda^{-4}$.
The loss attributed to Rayleigh scattering can be approximated by

$$\alpha = 1.7\left(\frac{0.85}{\lambda}\right)^4 \qquad \text{Eq. 2.7.13}$$

Where, $\alpha$ is the loss in dB/km and $\lambda$ the wavelength in μm.

As well as issues at shorter wavelengths, the potential for the laser beam coming into contact with higher density areas increases over long distances and this can have a significant impact by increasing the amount of scattering present. No wavelength shift is attributed to this type of scattering [73, 56].

This type of scattering is also known as Rayleigh-centre scattering, there is also Rayleigh-wing scattering, this occurs on the spectral wings of the signal rather than at the centre peak, this is caused by interactions with oxides within the fibre which have fluctuations of composition due to the creation process.

Rayleigh scattering can be measured in any direction, but it is the scattering measured in the same axis as the signal which can be an issue. The most problematic version of Rayleigh scattering is double Rayleigh back scattering as it significantly increases noise in a transmission span. This process occurs when a spontaneously emitted photon travelling in the forward direction, which in itself adds to the overall noise, is reflected by an atom and enables the photon to counter propagate. The photon then gets reflected again, hence the double back scattering, and once again travels in the co-propagating direction.

The issue here is when a distributed amplification scheme is in place, i.e. Raman amplification. The Rayleigh scattering interacts with the pump laser energy in counter and co-propagating direction, which then amplifies the overall noise and becomes a significant loss with distance, especially when the signal is of low power and is amplified along with the Rayleigh scattering noise. This noise can be construed as a type of crosstalk as it is wavelength dependent and is sometimes referred to as Rayleigh crosstalk [45].

Rayleigh scattering can be useful however. An example of which is when the loss in an optical fibre needs to be found. An Optical Time Domain Reflectometery (OTDR) trace is taken which uses the Rayleigh back scattering to record a trace showing the increasing loss as light travels through a fibre. The OTDR measures the time it takes for the Rayleigh back scattered light and shows it as a decreasing line [84].

In relation to Stimulated Raman Scattering, Rayleigh back-scattering can impact at high energies, which causes additional noise to occur within the system, limiting the energy available for SRS.

Both Rayleigh scattering and Brillouin scattering (Section 2.8.4) can have significant impacts in long-haul transmission spans and are partially related phenomena, but they can be minimised by using the right signal input powers to balance the potential scattering that could occur.

## 2.8. System impairments: Nonlinear Effects

All optical systems suffer from the effects of nonlinear phenomenon to one degree or another. The majority of the time these effects are unwanted and are minimised as much as possible, but these effects can be harnessed to create interesting and novel ways around problems transmitting optical data over long distances.

Three non-linear effects have already been mentioned, Brillouin scattering, Rayleigh scattering and Raman scattering. A summary of these effects is supplied in the subsections below:

### 2.8.1. Self-Phase Modulation (SPM)

Self-Phase Modulation (SPM) occurs due to the intensity dependency of the refractive index of optical fibre (also known as the Kerr effect) as shown by the following equation:

$$\Delta n = n_2 I \qquad \text{Eq. 2.8.1}$$

Where $\Delta n$ is the change of the refractive index, $n_2$ is the refractive index and $I$ the intensity of the light pulse [33, 85].

SPM causes a phase shift that is proportional to the intensity of the light pulse, consequently, due to the shape of the pulse (e.g. Gaussian) the intensity is different, and so the induced phase shift is also different when looking at different parts of the pulse, so it is therefore temporal. This phase shift causes the "chirping" of the pulse.

Chirp is when the frequencies inherent in the light pulse spread as the light travels through a fibre. Gradually the frequencies at the red end (lower frequencies) of the spectrum are travelling at a faster rate than those at the blue end (higher frequencies) of the spectrum, this then causes an increase in the pulse broadening effects relating to chromatic dispersion.
SPM occurs more with shorter pulses and therefore higher data rates, as well as systems using high transmitter powers, and so is an ever-increasing problem [45, 86].

### 2.8.2. Cross-Phase Modulation (XPM)

Cross-phase modulation (XPM) is the process where the interaction of two light waves in a fibre causes the phase of the first light wave to change. This phase change can be represented as a change in the refractive index, similar to SPM, by the following equation:

$$\Delta n = 2n_2 I \qquad \text{Eq. 2.8.2}$$

This equation is similar to the one representing SPM, except that there is an additional factor of 2. This factor represents the interaction of two beams of light in the same polarisation, if the polarisations of the beam are different by $\pi/2$, then the factor is 2/3 [85, 87].

XPM can be used in the wavelength conversion process, but this is not directly related to the Kerr Effect. In most cases it is a problem rather than a helping hand as it causes unwanted crosstalk in Wavelength Division Multiplexing (WDM) systems through the intensity fluctuation present in the Group Velocity Dispersion (GVD). It can also be affected by the amount of Polarisation Mode Dispersion (PMD) which is present in a system [88, 89].

### 2.8.3. Four Wave Mixing (FWM)

Four Wave Mixing is a non-linear process that occurs when a minimum of two beams of light, each with a different wavelength, interact and create scattered light at a wavelength different to the original beams of light. It is usually described as there being three frequencies propagating through a fibre, which then interact to create a fourth frequency.

The process is also phase dependent, and this interaction can make FWM a problem over larger distances when the phases are matched. If the phases are unmatched cancellation occurs and FWM is suppressed.

An example is two frequencies, $f_1$ and $f_2$ which interact, with $f_2$ being higher in frequency then $f_1$, creating two additional frequency components $f_3$ and $f_4$. This happens by:

$$f_3 = f_1 - (f_2 - f_1) = 2f_1 - f_2 \qquad \text{Eq. 2.8.3}$$

And,

$$f_4 = f_2 + (f_2 - f_1) = 2f_2 - f_1 \qquad \text{Eq. 2.8.4}$$

Hence we have $f_3$ lower in frequency than $f_1$ and $f_2$ while $f_4$ is higher in frequency than $f_1$ and $f_2$. We can therefore see that $f_3$ and $f_4$ are upper and lower sidebands, while in a three frequency interaction the resultant outcome is nine sidebands. These sidebands degrade the power of the main frequencies as they travel through the fibre until eventually becoming larger than the original frequencies.

FWM causes problems within WDM systems where crosstalk can occur between multiple channels and possible power differences. This issue can be reduced by having channels of unequal spacing, and yet this can cause other problems in itself.

There are actually many uses for FWM, such as pulse broadening effects in Supercontinuum Generation (which is a strong broadening of the light spectrum but not in the temporal domain), and in Phase Conjugation, where light of different phases causes an additional frequency to be created [90, 91].

### 2.8.4. Brillouin Scattering

Brillouin scattering is the process where light is scattered from acoustic phonons. While similar to optical phonons mentioned in section 3.2, acoustic phonons are vibrations which are related to the frequency of the atoms they are emitted from; they are in essence sound waves [73]. The process of the coupling of optical fields and acoustic waves is called electrostriction.

Electrostriction, or the elasto-optic effect, is caused by the change in the density of a dielectric, such as an optical fibre, under the influence of an electric field. An example of this is the electric field component of a high intensity laser. This process can cause dielectric materials to change in shape, but only slightly as this effect is only small [73, 92, 93].

Looking at the atomic level, the atoms are attracted towards the field because of the higher energy available; hence the material has a larger increase in density where the field is at its strongest. As a result this process changes the refractive index of a fibre and is one of the mechanisms that can cause non-linear refractive index, which in this case is related to the changes in density of the optical fibre structure.
This density increase affects how the phonons interact with the laser light by increasing the number of phonon-photon interactions, and therefore increases the number of potential scattering effects.

Phonons have thermal energies of around 0.024eV at room temperature, and so the energy can change dependent on the system temperature, i.e. the higher the temperature the greater their energy, which can have significant impacts on optical communications. Phonons are usually a greater problem at lower signal powers because the signal can be significantly impacted by

phonon scattering causing additional noise; at higher signal energies the phonons have less energy in comparison with the signal energy and therefore have less of an impact.

In relation to using Stimulated Raman Scattering, Brillouin scattering causes problems by interacting at lower energies and reducing the available energy for Stimulated Raman scattering to occur.

Brillouin scattering and Rayleigh scattering (Section 2.7.3) are partially related phenomena, but both can be minimised by using the right signal input powers to balance the potential scattering that could occur.

### 2.8.5. Raman Scattering

The phenomenon known as Stimulated Raman Scattering or SRS occurs when two or more signals at different wavelengths are put into a fibre which makes the power from the lowest wavelength transfer to the highest wavelength. An example of this is having a signal wavelength and a pump wavelength inserted into the same fibre which then causes amplification of the signal wavelength.

The effect is similar to Spontaneous Raman Scattering and is due to the photons of the lower wavelengths having a larger amount of energy than those at the higher wavelengths. Due to the natural behaviour of photons, the energy of the photons at lower wavelengths, thus higher energies, want to decay towards the ground state, so when these photons change in energy state they emit a photon at a higher wavelength than the original photon. This also produces an optical phonon as not all the energy departs from the atom or molecule, this phonon is the vibrational energy or frequency of the atom/molecule [40, 45, 56, 73].

For more detail on Raman Scattering see Chapter 3, Section 3.2.

# Chapter 3

# Ultra Long Raman Fibre based Amplification over Long Transmission Distances

## 3.1. Introduction

There are different types of Optical systems around the globe, ranging from long or ultra-long distance extending from hundreds of kilometres to tens of thousands of kilometres, many of which are submarine connections linking continents, e.g. North America to Europe under the Atlantic Ocean, through to Metropolitan networks which interconnect cities and areas together, and down to Fibre-To-The-Home (FTTH), which is the short link between a local exchange and a household or business and are usually only a few kilometres long.

The need to constantly improve these connections is tangible, but the additional costs in replacing network equipment needs to be limited as much as possible. The main costs involved are the fibre itself plus the cost of maintenance of devices within the transmission span, such as repeatered EDFA where physical amplifiers are placed within the span. Newer techniques used remote EDFA pumping, but this means replacing the usual silica SMF-28 type fibre with Erbium doped fibre.

Another issue is transparency; this is where the modulation format, signal wavelengths and phase information can pass through without having conversion to electronic means. In most cases it is now normal to have purely optical means rather than Optical-Electrical-Optical conversion, as the most common technique in long distance transmission is discrete EDFA amplification.

There are two broad categories which the techniques to improve received signal quality come under, these are Repeatered and Unrepeatered. The following discussion will be limited to the following Repeatered and Unrepeatered techniques:

- EDFAs and related technologies.
- Raman amplification, ultra-long Raman fibre lasers and quasilossless spans.

The discussion will include advantages and disadvantages of both repeatered and unrepeatered transmission techniques, especially effects that can cause problems in ultra-long fibre transmission (ULFT).
Experimental results relating to Raman Amplification can be found in Section 3.2.

Repeatered amplification consists of multiple EDFAs along the transmission span amplifying the signal as it travels through the fibre medium. These amplifiers are placed at stages where the attenuation of the fibre medium has not reduced the signal power so much, that, when the signal is amplified the noise floor is amplified by the same amount, thus reducing the OSNR of the signal over the length of the transmission span. Once the signal is passed through multiple amplifier sections this can lead to very low OSNR and high error counts at the receiver.

These repeatered sections mean higher infrastructure costs and an increase in system complexity. Unrepeatered sections therefore have advantages in these respects as the fibre has no need to be sectioned between amplifiers, and one span is virtually uninterrupted between transmitter and receiver.

Using repeatered EDFA configurations in transmission spans, such as those used in [17], can be utilised for transmission distances of thousands of kilometres. However the fibre between each EDFA can be classed as a span in its own right, so in fact repeatered transmission is lots of smaller spans placed together to make one large one. An example of this is shown in [16], where a 10Gpbs x 96 channel WDM system needs 130 repeaters to transmit a clear

signal which works out at one every 70km. This increases the cost of such installations, and if the technology used in the repeaters is too old it may be useable in the future for higher data rates and more complex modulation techniques. Therefore any change in the transmission infrastructure is costly, so the simplification and ease with which the infrastructure has the ability to be upgraded in the future, is an important consideration.

Gain flatness is also an issue, as with so many amplifiers in series each one will have some gain tilt, even if small, which will build up over the fibre span. For repeatered systems the only option is to include gain equalisers within the span to counteract the tilt, this obviously adds complexity [16]. Dispersion compensation is added to every span with a normal dispersion profile, then after every 10 repeater span sections anomalous dispersion is present, which when joined with the normal dispersion fibre equalises the dispersion. This dispersion compensation needs to be carried out every 70km [16].

EDFAs are still the main technology for long transmission spans, especially for submarine spans, and will be for the foreseeable future for spans of thousands of kilometres. Despite the additional cost of the amplifier sections, e.g. every 50km [17], using more efficient modulation formats such as Quadrature Phase Shift Keying (QPSK), along with Polarisation Division Multiplexing (PDM), over extremely long distances, as in [17], is a significant improvement over current technologies. However these same modulation formats can also be used in none repeatered schemes and can give similar improvements [16, 36, 37, 94, 95, 96].
Coherent Detection was also used in many experiments involving repeatered transmission as it provides better sensitivity than Direct-Detection receivers (see Chapter2 Section 2.5.1), but again, complexity and cost are the main issues against using those types of receiver.

High data rates in the region of 100Gbps can be comfortably transmitted using these techniques [17, 36, 37, 94, 95, 96]. Exotic fibres have also been used, such as in [36] where a 7-core fibre was used to increase the amount of data transmitted. The Q-Values for these configurations are between 11dB and 7dB.

Unrepeatered transmission spans use a variety of techniques to keep the signal OSNR at a level where the receiver enables the data to be successfully demodulated with a low number of errors, or low BER, to facilitate the recomposition of the transmitted data at the receiver. There are various ways to keep the signal at a sufficiently high OSNR so the data is readable at the receiver, such as: Remote Pumping of EDFAs; Ultra Low Loss Fibre (ULL), which can give fibre attenuation down to 0.162dB/km for Commercially available fibres; Large, Very Large and Ultra Large Effective Area Fibre which are known as LEAF fibres.

These techniques can also be used in combination to limit the attenuation and reduce the amount of amplification needed, such as [19, 20, 21, 22, 23, 24, 25, 35, 60, 61].

Remote Optical Pumping Amplifiers require the doping of optical fibre with Erbium at a point, or at points, along the transmission span where the OSNR is large enough that the amplification of the signal and the noise makes little difference at the receiver. If the points where the fibre has been doped are too far apart, the OSNR will be too low to be recovered at the receiver and provide good BER values.
This can be similar to repeatered spans, but the main use of ROPAs is at a distance of around 100km from the end of the transmission span to give a boost to the signal before it reaches the receiver. A single ROPA is more commonly used because it is cheaper than using multiple ROPAs, although that type of scheme would give a better balance to the OSNR over the transmission span, plus a single ROPA can be added close to the receiver equipment, usually in the same room, rather than replacing a whole transmission span. Experiments involving ROPAs are [18, 19, 20, 21, 22, 23, 24, 25].

Large Effective Area Fibre (LEAF) is a type of Non-Zero Dispersion Shifted Fibre (NZ-DSF) that trades off the reduction in non-linear effects that NZ-DSF gives, but with an increase in dispersive effects, although the dispersion is still less than with SMF-28. This compromise is partly due to its larger acceptance angle and therefore wider light cone compared to normal NZ-DSF. This wider

light cone allows more light to enter the fibre, which means that the light is distributed over a wider area therefore reducing the peak power and non-linear effects. However this same design of a large effective area increases the dispersive effects, but when compared with SMF-28 fibre they are still much lower [6, 9, 33].

Ultra Low Loss Fibre has dopants added to lower the normal attenuation of 0.2dB/km for Silica fibres, such as SMF-28, down to 0.16dB [9, 10] for commercial fibres, although figures of 0.148dB/km have been measured in the laboratory [7, 8, 10]. For more on optical fibres see Chapter 2 section 2.2.

Regarding the actual configuration for Raman amplification, the majority use simple Raman Amplification which relies on either 1$^{st}$ Order processes using 1455nm pumps, 2$^{nd}$ Order using 1365nm pumps, or 3rd Order using 1285nm pumps, to produce the Stoke shift wavelength at 1550nm [18, 24].

For other configurations, such as those used within this thesis, FBGs were utilised to create a laser cavity, with the FBG working at the 1$^{st}$ Stoke shift wavelength of 1455nm after being pumped at the 1365nm wavelengths [14], other examples of ULRFL are shown in [63].

There is also the consideration whether single or bi-directional pumping should be used. Single pumping can be either forward or backward; forward pumping has a lower noise profile whilst backward pumping gives a reduction in the effects of non-linearities. More on pump direction configurations can be found in Sections 3.2 and 3.3.1.
Examples of experiments using single pumping are found in [20, 23, 25, 61] whilst bi-directional pumping experiments can be found in [18, 19, 20, 28, 35, 58, 59].

All of these techniques can be used together to improve the received OSNR. Such configurations have been used in [25] where the average OSNR across all 64 channels was 10.6dB, at 0.1nm resolution, over a 468km span.

Apart from the experiments in this thesis which used SMF-28 fibre up to 320km, the maximum distance where SMF-28 was employed in a transmission system was 240km [29]; it was also used for sensor applications using 300km [63]. Other experiments using SMF-28 can be found in [94].

For other fibres the maximum distance was 601km [18] for 1 channel transmission, 574km with 4 channels using Enhanced Pure Silica Core Fibre (EPSCF), which is a type of LEAF and ULL combined; the experiment also used ROPA and 3$^{rd}$ order Raman pumping and gave a Q-value of 9.5dB with an OSNR of 5.8dB/0.1nm with 4 channels.

As with EDFA based amplification, there is a mix of using Coherent Receivers and Direct-Detection with Raman amplification techniques. For experiments involving Raman amplification configurations, the following papers used Coherent receivers [17, 20, 21, 22, 25, 58, 61], while Direct detection was used in [18, 23, 24, 35, 57]. More detail on these types of receiver can be found in Section 2.5.

There are also some experiments using hybrid Raman-EDFA configurations, [21, 58, 61, 64, 95] in which EDFAs can be physically repeatered, or Erbium doped fibre is used for the transmission span, whilst Raman pumping is also employed to generate additional gain.

## 3.2. Raman Amplification and Ultra-long Raman Fibre Lasers (ULRFL)

The process of Raman amplification is based on a phenomenon known as Stimulated Raman Scattering or SRS. SRS occurs when two or more signals at different wavelengths are put into a fibre, this makes the power from the lowest wavelength transfer to the highest wavelength. An example of this is having a signal wavelength and a pump wavelength inserted into the same fibre which causes amplification of the signal wavelength. Raman amplification can be used over a broad range of wavelengths, which is another advantage over other amplification types.

Raman amplification uses an effect similar to Spontaneous Raman Scattering (SRS) and is due to the interaction of photons with silica atoms that cause the photons to scatter but with less energy and at lower frequencies (higher wavelengths), this is because some of the photons energy is absorbed by the atom it has interacted with.

The difference between spontaneous and stimulated versions of Raman scattering are mainly down to the control of the Raman scattering process by use of a laser that has been generated with a limited range of wavelengths; the spontaneous scattering can occur at any wavelength and produce a photon with a random wavelength dependent on the atom the photon has interacted with. The presence of a pump laser aggregates the majority of the atoms to have similar energies, and therefore produce new photons of wavelengths within a known band. These photons will then produce more photons at ever higher wavelengths as the Raman scattering will continue to take place, and is only limited by the length of the optical medium that the light is travelling through; although in reality optical fibre is not lossless therefore absorption of these photons will occur, which means there is a limit to the length of the medium before other noise mechanisms take over [14, 15]. This process is described in more detail below.

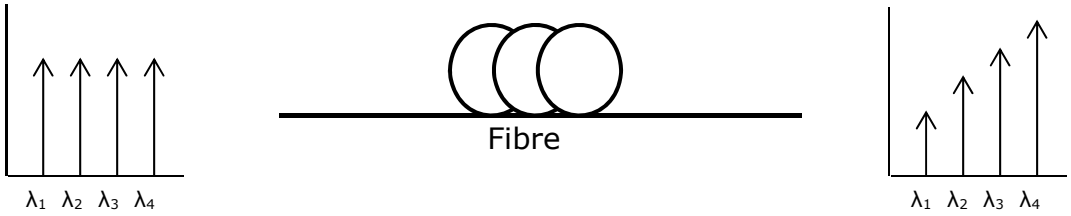


*Figure 3.2.1 – The effect of SRS through a typical fibre span.*

The energy of the photons at lower wavelengths, thus higher energies, wants to reduce towards the ground state, and so when these photons change in energy state they emit a photon at a higher wavelength than the original photon. This also produces an optical phonon as not all the energy departs from the atom or molecule, this phonon is the vibrational energy or frequency of the atom/molecule.

In SRS, this occurs when a photon hits an atom/molecule and starts the process described above.

A description of the physical process that causes the effect is detailed thus: When a photon of wavelength $\omega$ is absorbed by the transmission medium a photon with the wavelength $\omega_S = \omega - \omega_v$ is produced; where $\omega_S$ is the Stokes wavelength, $\omega$ is the wavelength of the initial photon and $\omega_v$ the excitation energy that was contained in the atom/molecule the original photon interacted with. The excitation state the atom is left in is $\hbar\omega_v$, where $\hbar$ is the Planck constant divided by $2\pi$, which is equal to $1.055 \times 10^{-34}$J.s, and relates the Planck Constant to radians and angular frequency [40, 56, 73].

The virtual or intermediary state (Ei in the diagram) is created by the absorption of the photon but this is not a stable energy level, while G, $E_1$ and $E_2$ are stable. Due to Ei being unstable, a photon is emitted at a higher wavelength but only with the energy that allows the atom/molecule to reduce to an energy state that is stable; hence a phonon is created at $E_1$. This phonon has a frequency determined by the material it belongs to, so for Silica this is 13.2THz calculated by $\omega_{Phonon} = (E_2 - E_1)/h$. This frequency is the materials resonant frequency [56, 73].

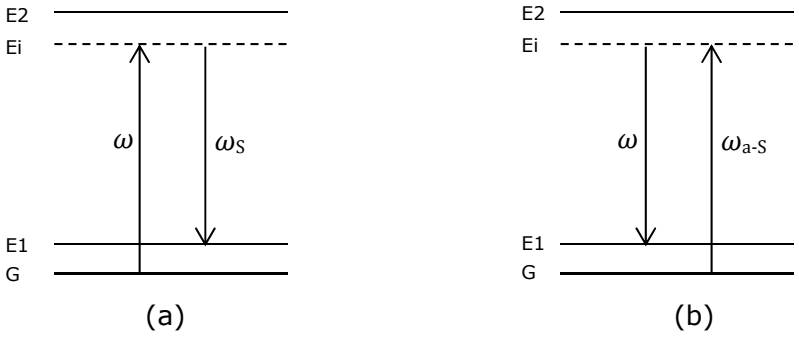


*Figure 3.2.2 – (a) Stokes and (b) Anti-Stokes scattering.*

Taking the resonant frequency and the frequency of the initial absorbed photon, the frequency of the emitted photon can be calculated by $\omega_{Emit} = \omega_{Absorb} - \omega_{Phonon}$. The Raman scattering effect is not fixed directly at 13.2THz but has a bandwidth of 6THz giving a range of 10THz to 16THz [56, 73]. Therefore the Raman Effect is generally broadband and can be effective up to 16THz (or 125nm in the 1550nm window) away from the original transmitted

frequency (or wavelength). The overall response is linear, but drops significantly around the 16THz [40].

For Raman amplification we take this effect and use it to increase the number of photons present in the fibre, hence amplification. Using a high powered pump at around 1450nm gives an amplified signal around 1550nm, which is useful for telecommunication applications.

SRS works for two or more wavelengths; consequently two different pumps can be used to generate even more amplification for a broader range of wavelengths, and can help towards creating a phenomenon known as Supercontinuum [27, 30, 99].

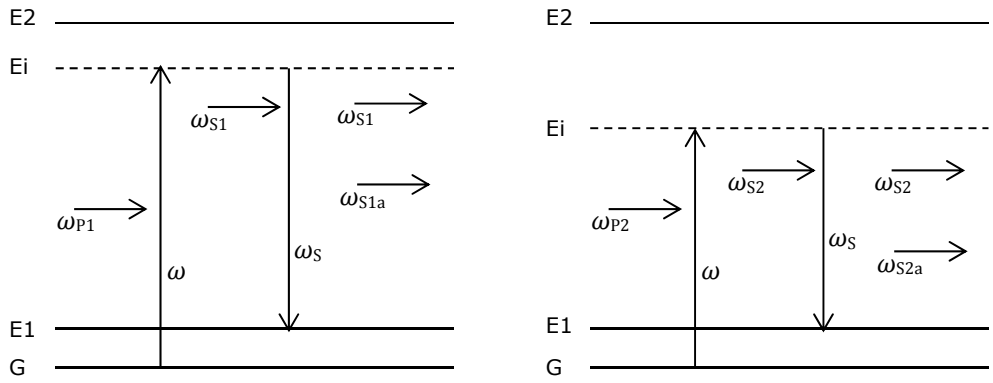


*Figure 3.2.3 – Multiple stimulated Raman scattering using 2 pumps.*

Figure 3.2.3 shows the configuration of the energy levels using two pumps, 1st pump P1 is a lower wavelength, whilst the 2nd pump, P2 is a higher wavelength [56].

Using the above properties, a technique using a forward pump and a backward pump into the transmission fibre can give good Ultra-long Transmission results, as shown in [18, 19, 20, 21, 22, 23, 24, 25, 27, 35, 57, 58, 59, 60]. Single pump configurations are still used due to their own individual advantages for example forward pumping is relatively low noise while backward pumping has a high tolerance to non-linear effects. This means for certain experimental setups forward or backward pumping may be used depending on the desired outcome; some examples are shown in [20, 21, 23, 25, 59, 61, 64, 98] of this type of usage. Using bi-directional pumps is a

compromise that realises the advantages of incorporating both directions within experimental configurations.

The basic setup is shown in Figure 3.2.4 and shows a signal being transmitted into a transmission span; first the signal passes through a 3dB coupler which has the forward pump laser introduced through the 2nd input. For a signal at 1550nm this pump laser would be set between 1450nm and 1460nm to get the 1st Stokes shifted wavelength.

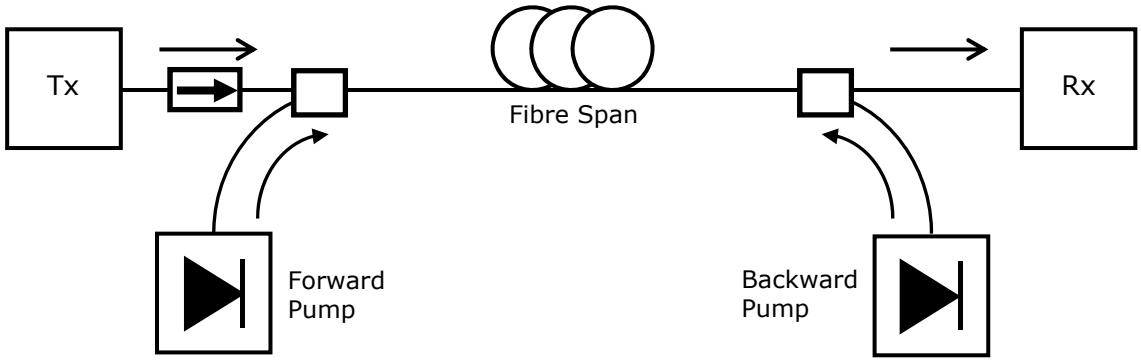


*Figure 3.2.4 – 1st Order Raman Amplification with dual pumping in a ULFL.*

The change in the signal power $P_S$, with regards to the pump power $P_P$, along the fibres longitudinal axis $z$, can be demonstrated using the following equations:

$$\frac{dP_s}{dz} = g_R P_p P_s - \alpha_s P_s \qquad \text{Eq. 3.2.1}$$

$$\pm \frac{dP_p}{dz} = \frac{\omega_p}{\omega_s} g_R P_p P_s - \alpha_p P_p \qquad \text{Eq. 3.2.2}$$

Where $g_R$ is the fibre Raman gain coefficient normalised with respect to the effective area of the fibre, $A_{eff}$. The attenuation coefficient for both signal and pump wavelengths is represented by $\alpha_s$ and $\alpha_p$ respectively and $\omega_s$ and $\omega_p$ are the angular frequencies of the signal and pump. $\pm$ is the representation of the co-propagation and counter-propagation of the CW input from the pump lasers. The first term on the right-hand-side of Eq. 3.2.1 represents the signal gain due to SRS with the second term representing the signal loss; for Eq. 3.2.2 the first term represents the depletion of the pump due to SRS and the second term the pump loss [100].

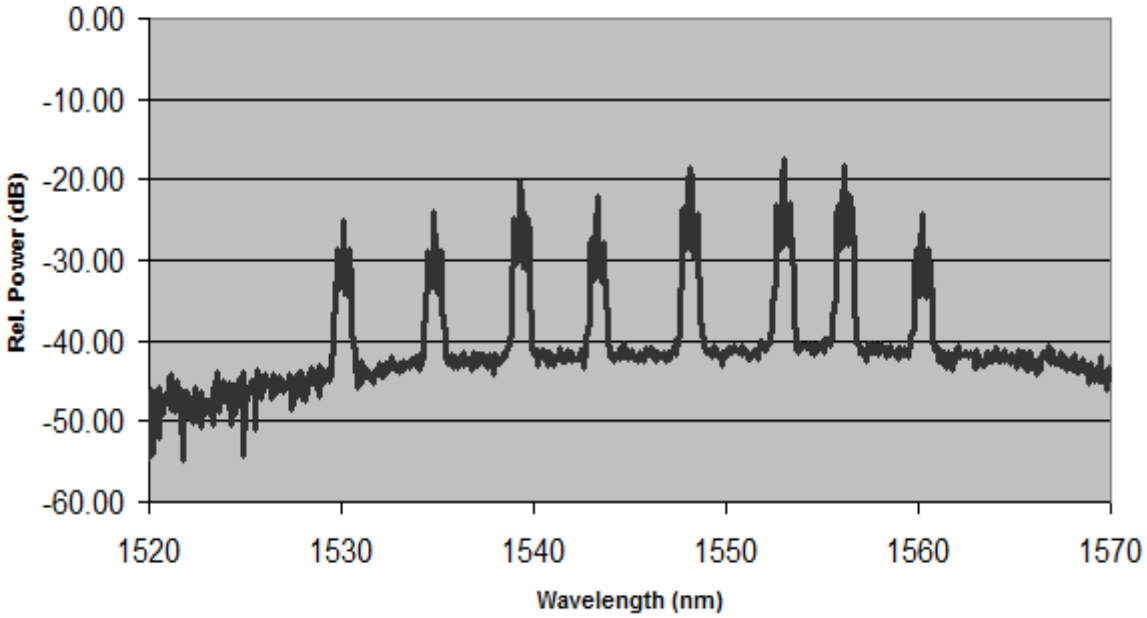


*Figure 3.2.5 – Gain bandwidth over C-Band using Raman Amplification.*

For the experiments in Chapter 3 of this thesis, Ultra-long Raman laser based amplification was used which is based on 2nd Order processes but utilises FBG's to create a laser cavity. This arrangement exploits the 2nd order process to create 1455nm wavelengths in the FBG from the 1365nm pump, which then creates Stokes wavelengths within the cavity which appear at 1550nm, hence causing gain at the signal wavelength.

In this case, the 2nd Order process required a similar setup to that shown in Figure 3.2.4, but with Fibre Bragg Gratings (FBGs) inserted after the high power couplers. The FBGs were inscribed for the wavelength 1455nm, which is 95nm below 1550nm wavelength of the signal. The reason for using FBGs in this way was to create  a double Stokes Shift by using Amplifiers in the 1365nm region to create a 1st order Stokes shift around 1455nm, which would then make a 2nd Stokes shift around 1550nm, with both FBG's having a bandwidth of 0.1nm.

The setup for this is shown in Figure 3.2.6. Isolators were included within the high power couplers, although it is shown separately in Figure 3.2.6.

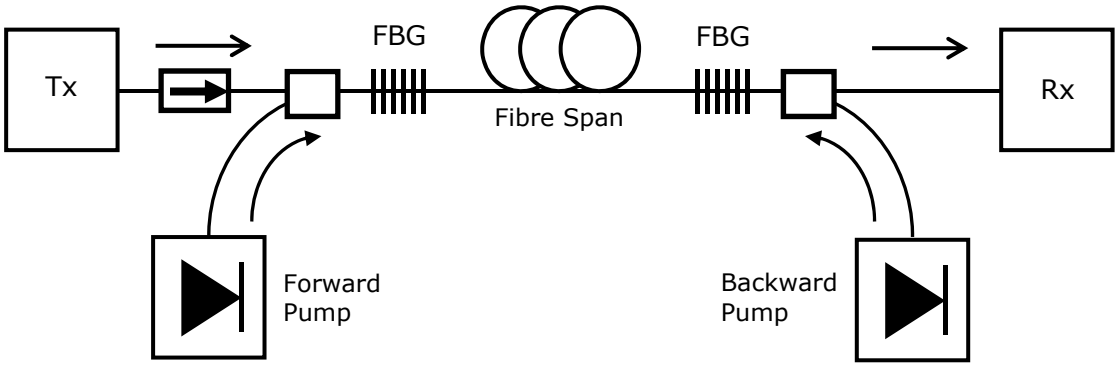


*Figure 3.2.6 – 2nd Order Raman Amplification with dual pumping using FBGs in a ULFL.*

The effect of Raman amplification, as described previously, is broad, with up to 125nm bandwidth from the central wavelength, which means the whole of the C-Band can be amplified using this technique, and therefore multiple channels can be amplified at the same time.

This configuration, shown in Figure 3.2.6, gives us in effect a Raman laser, as the FBGs act as a cavity with high reflectivity >95%, this allows the power to build up within the cavity to a certain point before it is released. This type of configuration was used in [14, 15, 26, 27, 28, 29, 30, 31].

Unrepeatered long distance amplification was investigated using distributed bi-directional Raman amplification [29], this showed a higher gain using b-directional pumping when compared with co-propagating and counter-propagating schemes. When compared to EDFA only schemes, it was shown that there were significant improvements of between 2 and 6 Log BER for a 240km span with post-compensation for the dispersion, using data rates of 2.5Gbps and 10gbps, respectively. Numerical model in [28] confirmed that 2nd order bi-directional Raman amplification gives a better OSNR up to 200km.

The essence of [14] was a numerical model that compared bi-directional Raman pumping with ULRFLs. This showed that ULRFL has a distinct advantage over regular bi-directional pumping in noise performance and gain excursion. It was also found that there existed a point where the noise from DRBS could cause a reduction in OSNR after 250km span lengths, and that

moderate input signal powers should be used rather than higher signal powers.

In [15] the model in [14] was put to the test with a ULRFL cavity of 270km, the longest laser cavity at that time. This showed that the balance of gain over loss was possible over very long distances creating a quasilossless span; this was investigated in [31], although this paper in effect used a repeatered technique by creating an 82km ULRFL cavity. Using this cavity, a signal was passed through 2500km of fibre using a recirculating loop with the ULRFL within the loop; the comparison was made with repeatered EDFA transmission and it showed that 6dB less input power was needed for the same received signal quality. However a quasilossless span can see an increase in non-linear distortions at low powers as explored in [30] but gives better results at higher powers for a true non-repeatered quasilossless span.

The results in [31] expanded on the notion of quasilossless spans, which led to the development of Supercontinuum generation as described in [27] where TW and highly non-linear fibre (HNLF) were used, where not only was a quasilossless span created but the gain was developed over a bandwidth of 200nm.

The summary of the results presented in section 3.4 of this thesis is shown in [26].

### 3.2.1. Advantages and Disadvantages of Raman Amplification and Ultra-long Raman Fibre Lasers (ULRFL)

There are two measures that can be used so that Raman Amplification can be proven to be superior to EDFA. These are the Noise Figure and Gain Flatness.

The Noise Figure (NF) is the ratio of the OSNR at the input and the OSNR at the output; this shows how much the signal is degraded by an amplifier such as an EDFA. In the context of Raman amplification, the Noise Figure is the equivalent noise figure that would need to be measured at the receive end of

the transmission span by an amplifier without Raman amplification present, but which would be obtainable with the same OSNR as if Raman amplification was present.

For the equivalent EDFA based system:

$$NF_{sys} = NF_{eq}\alpha_s L \qquad \text{Eq. 3.2.3}$$

While with Raman pumping within the span instead:

$$NF_{sys} = NF_R \qquad \text{Eq. 3.2.4}$$

Because:

$$NF_{eq} = \frac{NF_R}{\alpha_s L} \qquad \text{Eq. 3.2.5}$$

Where $\alpha_s L$ cancels out when Eq. 3.2.5 ($NF_{eq}$) is placed in Eq. 3.2.3 and therefore confirms the validity of Eq. 3.2.4.

The above equations show the total system Noise Figure, $NF_{sys}$, is a combination of attenuation and fibre length giving the total loss of the transmission span plus the amplifier Noise Figure: $NF = \frac{SNR_{in}}{SNR_{out}}$. Thus under Raman conditions there would be little or no loss over the transmission span and can be classed as quasi-lossless.

At the other end of the scale is a signal with a total loss through the span before being amplified. This would mean the signal would be almost unrecoverable at the receiver, as the OSNR would be very low due to the ASE in the system being amplified along with the low signal, therefore more ASE is generated and this lowers the OSNR even more. This then gives an increase in the NF.

In Raman amplification the Gain is, in effect, evenly distributed throughout the fibre span, as in a repeatered span, but using no discrete amplified sections to achieve this, plus higher signal power is maintained along the length of the

span. It was also found in [98] that gain flattening in Raman amplification can be helped by the use of broader linewidth Raman pumps.

The Gain Flatness of an amplifier or a system is the product of multiple wavelengths being amplified, with one or more wavelengths being amplified to a greater extent when compared to other wavelengths. Due to there being a limited amount of Gain from the amplifier it means some wavelengths consequently receive less gain than other wavelengths; these wavelengths are the shorter wavelengths, whilst longer wavelengths receive more gain.
An amplifier with high gain flatness is one where all wavelengths receive the same, or nearly the same, amount of gain, i.e. the gain is spread equally amongst all wavelengths passing through the amplifier.

To reduce the gain difference between wavelengths in EDFA based systems, lossy elements are placed in the amplifier path to reduce the power of those wavelengths which receive the most gain, and therefore spread the gain more equally over the bandwidth of the amplifier. The total gain will be limited by the lowest gain wavelength which is obviously worse for an amplifier with a highly tilted gain. The disadvantage of this is it reduces the amount of gain in the system, and therefore the maximum output power of the amplifier.

The wavelength dependent profile of the gain, when signals are being amplified, is also known as the Noise Figure Tilt. As described above NFT is the difference between the wavelength with the highest gain and the wavelength with the lowest gain. Which means the greater the difference in the achievable gain the larger the NFT. The NFT is also reliant on the amount of ASE, and this is greater at lower gain wavelengths and therefore affects the overall NFT.

Multipath Interference is when photons hit an atom or molecule in the fibre and they are reflected backwards in the opposite direction to the signal photons. These photons can then collide with another atom or molecule and travel in the forward direction again, co-propagating with the signal. This effect is known as Double Rayleigh Backscattering (DRB).

DRB can travel in many directions, but those scattered photons that are co-linear with the signal, can have a degrading effect through the addition of noise. One example of this is when DRB travels through an amplifier; due to its inherent mechanism it travels through two lots of gain as, in effect, the amplifier will see two separate photons. The direction of travel through the gain medium does not matter in these instances thus additional ASE is observed at the receiver.

The mechanism, explained above, occurs throughout the fibre length and is entirely random; this apparent randomness is due to where denser areas appear within the fibre material (as mentioned in Section 2.8.4). This can have two effects; firstly intensity of the signal can fluctuate, and secondly small changes in phase can become apparent. Both of these when multiplied many times can have major issues at the receiver.

Pump Noise Transfer is the process where the fluctuations of the Raman amplification, which occur at less than 1ps intervals, combine with pump frequencies that are lower than 1THz and cause intensity fluctuations in the power of the signal. Relative Intensity-to-Noise transfer is the measurement of this phenomenon and is described in more detail in Section 3.3.

Bi-directional pumping reduces the Multi-Path Interference (MPI) penalty by reducing the amount of Double Rayleigh Backscattering (DRB) and as such the gain excursion is reduced. A lower noise figure can be achieved compared to just counter-propagation [102, 103].

Turning to ultra-long Raman fibre lasers (ULRFLs), the main advantages of this type of distributed Raman amplification over lumped Raman amplification are two fold; in that the power profile is flatter with the gain profile closely matched with the span loss, and also the noise performance is improved compared to non-ULRFL based techniques [14, 15, 30, 31].

Some experimental measurements showing the power distribution for different fibre span lengths are shown in Figure 3.2.7. It can be seen that the longer the distance the larger the change in the power distribution. This is caused by

the gain excursion through the fibre span which changes with distance, as the gain from the forward pump starts to decrease after ~35km and only increases again around 85km. This power distribution change is seen as a peak when the signal sees the gain from the forward pump, it then reduces in gain as it travels through the fibre. The measured power is reduced by half out around ¾ of the way through the fibre. The signal then begins to interact with the gain from the backward power and thus gives a lossless output.

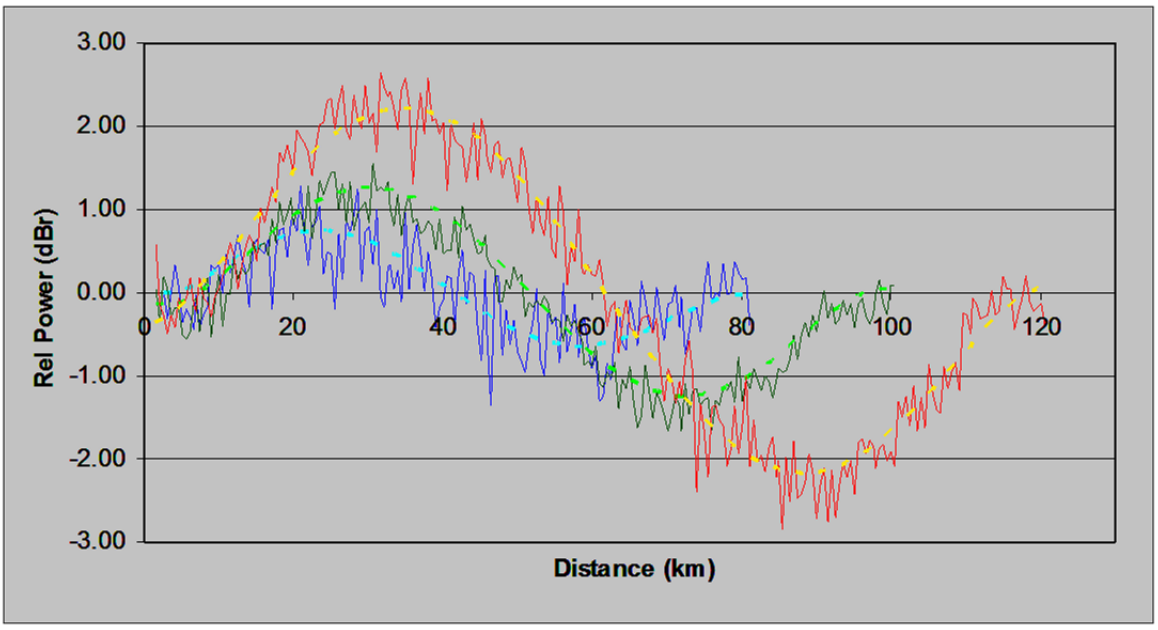


*Figure 3.2.7 – Power distribution of ULRFL for span lengths of 80km, 100km and 120km. Sixth order polynomial fits also shown.*

It can be seen that the power excursion at the different span lengths ~1.5dBr for 80km, ~2.5dBr for 100km and is ~4dBr at 120km. The fit shown is a statistical fit calculated via a $6^{th}$ order polynomial which shows the overall response of power over distance with the noise removed.

The power change through the fibre span was measured using the optical time-domain reflectometery (OTDR) technique which measures the amount of reflected power from the light transmitted into the fibre. For very long lengths beyond 150km this technique cannot be used as the loss in the fibre, due to absorption, is too great to get full measurements, hence why no OTDR traces at 240km and 320km distances have been included.

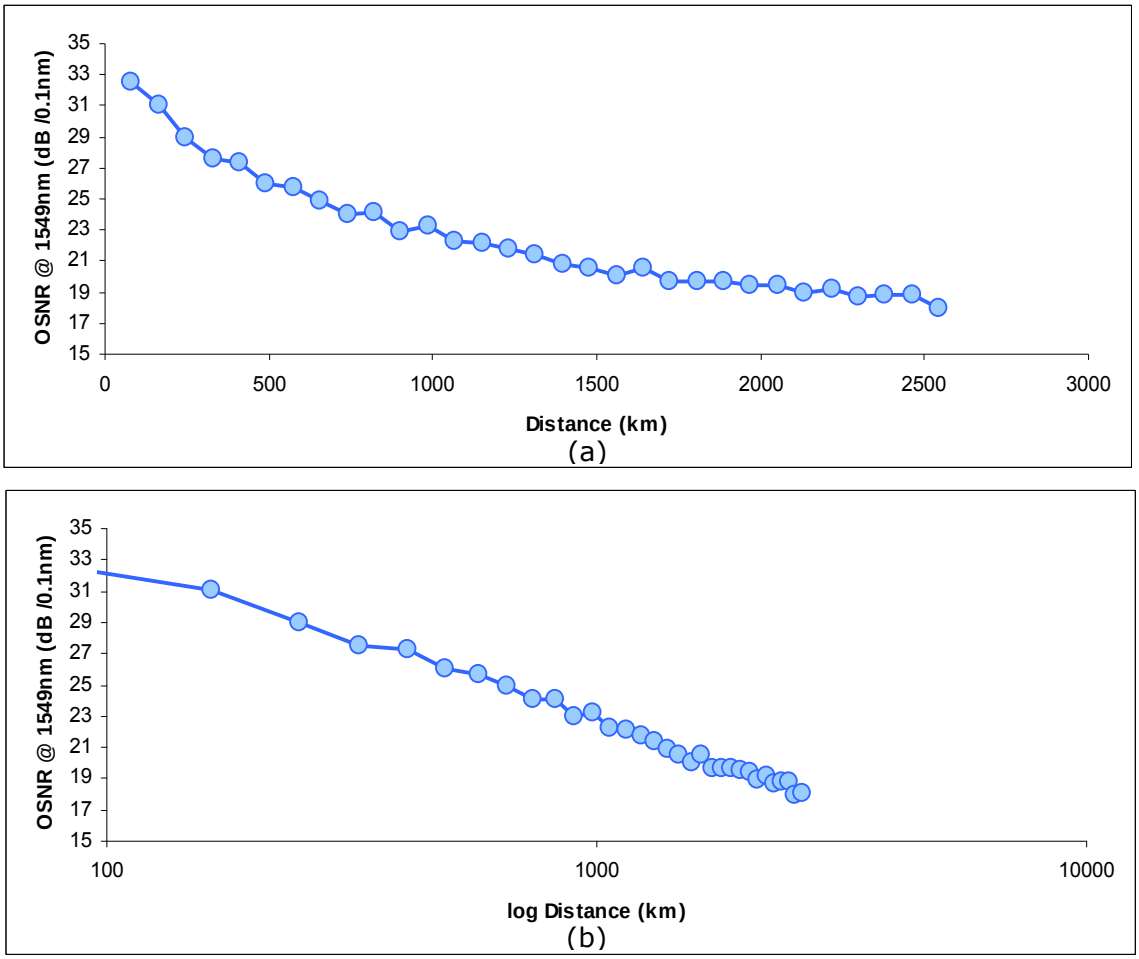


*Figure 3.2.8 – OSNR vs transmission distance (Linear (a) and Log (b)) using a recirculating loop with a length of 101km.*

The distribution of the noise over the length of the fibre is shown in Figure 3.2.8 with OSNR measured against fibre distance. This shows that the main reduction in OSNR due to noise occurs within the first 500km after which the OSNR continuous to decrease in an exponential fashion. It shows that if the noise can be controlled and minimised near the beginning of the fibre span, then the OSNR will have a less significant reduction overall when using an ULRFL. These measurements used a recirculating loop with a span of 101km up to 2600km, similar to [31].

### 3.3. Relative Intensity-to-Noise (RIN) Transfer

Relative Intensity-to-Noise transfer, or RIN, is the measurement of the total amount of noise generated by a laser. This noise can be described as fluctuations between the pump laser and the signal. These fluctuations are caused by spontaneous emission within the laser cavity, as well as thermal noise and shot noise, depending on the type of laser used; i.e. semiconductor lasers or fibre-based lasers. The fibre based lasers are not affected by thermal and shot noises directly only indirectly through the pump laser used, which is quite often semiconductor based. Large RIN is usually found in low-quality laser sources and can cause significant degradation of signals, similar in effect to ASE.

There are a number of RIN measurement techniques. The most common technique is direct measurement via a pump-probe method in which a laser pulse, with known characteristics, is passed through a Raman amplifier whilst a pump laser is injected, either to study forward pumping behaviour, or backward pumping behaviour, depending on the setup; both studies occur whilst the Raman amplifier is in an undepleted state.

The output of the amplifier is connected to an electrical spectrum analyser using a photodetector to detect the resulting pulse intensity. In this process the RIN transfer is seen as a change in the modulation frequency on the analyser.

Although this measurement technique seems simple, there are issues that need to be overcome to get a true reading of the RIN:

- Calibration of the spectrum analyser to measure random noise instead of sinusoidal waves. Typically 2 dB is added to the noise floor, but this can depend on how the spectrum analyser is setup.

- DC component of the photocurrent needs to be accounted for in the photodiode, this is usually corrected as part of the calibration of the spectrum analyser.

- The photo diode must operate within the unsaturated linear region, as noise within the photodiode builds up at saturation, making it harder to measure the RIN in the system.

- The timing jitter within the signal needs to be known to remove this from affecting the RIN measurements as RIN and timing jitter are correlative.

Once these issues are corrected for, it can be agreed that the measurements are accurate within typical error margins [73, 104].

Within the rest of this section, RIN is considered from the point of view of Raman amplification, with examples of RIN shown, and a summary of the reasons for some of the configurations used within Raman amplified systems is given.

Initially backward Raman pumping was the main option when Raman amplification was used due to the low noise and small amount of gain excursion. The gain excursion is defined as a transient gain error which includes a gain offset, or the difference in the maximum and minimum of the average power as it travels through a fibre.
The use of bidirectional pumping has benefits over single direction pumping when used with long span lengths, benefits such as higher gain and lower noise, when compared with EDFA based amplification.

One major issue however is due to the fast gain dynamics of the Raman amplification process, which is in the order of femtoseconds (fs). The RIN present on the pump laser couples efficiently with the signal when forward pumping is used. To minimise the RIN signal transfer, low noise pump lasers with broad line-widths can be used; examples of these pumps are spectrally

broadened DFBs (SB-DFBs) [102] and inner-grating-stabilized multimode (IGM) lasers [102].

The type of lasers which are useful in Raman amplification have to achieve both low RIN and a sufficiently broad line-width, as it allows Forward, Backward and Bidirectional pumping by minimising the Raman gain ripple, whilst boosting the possible gain available from the Raman Amplifiers and giving a flattened gain spectrum [101].

The amount of laser noise transferred to the signal will depend upon the wavelength of the laser noise, plus the configuration of the Raman pumps needs to be taken into consideration. The configurations for Raman amplification are: single co-propagating, single counter propagating, bi-counter-propagating and bi-co-propagating [102].

The total RIN, in dB, can be calculated using the RIN of the pump and the signal, hence:

$$RIN_T = 10log\left(\frac{RIN_s}{RIN_p}\right) \qquad \text{Eq. 3.3.1}$$

Where, $RIN_s$ represents the signal RIN, $RIN_p$ is the RIN from the pump laser source, and $RIN_T$ is the total system RIN.

The direction of the pump laser can affect the amount of RIN transferred from the pump wavelength to the signal wavelength, as well as having other positive and negative effects (see section 3.1). With Forward pumping the noise is less than with backward pumping, but vis-à-vis, the effects from non-linearities are reduced with backward pumping.

The difference in the Group Velocity Dispersion (GVD) of the pump and signal is called "walk-off"; it is dependent on the starting condition of the light from both the pump and the signal, plus the inherent dispersion of the fibre used. The walk-off is something that needs to be considered when calculating the RIN as it affects the interaction between pump and signal.
If the pump and signal do walk-off then the coupling of the intensity noise reduces with increased walk-off as the walk-off averages the RIN.

The corner frequency for co-propagation is 1-100MHz, and is calculated using $f_c = \frac{\alpha_p}{2\pi D \Delta\lambda}$ or $f_c = \frac{\alpha_p}{2\pi S \left|\frac{\lambda_s - \lambda_p}{2}\lambda_0\right|(\lambda_s - \lambda_p)}$, where $S$ is the dispersion slope and $\lambda_0$ is the zero-dispersion wavelength of the fibre. The corner frequency is the frequency where the 3dB point of a filter is measured. This shows that RIN transfer, due to walk-off, acts like a low-pass filter, because as the frequency of the intensity noise increases the RIN transfer decreases. The same effect applies to the increase in dispersion, pump-signal wavelength separation and the effective length of the fibre, whilst a similar outcome can occur if the fibre attenuation decreases.

With regard to RIN in non-zero dispersion fibres, if the zero-dispersion wavelength is between the pump and the signal wavelengths then there is a reduction in walk-off, which leads to an increase in the RIN corner frequency and hence the RIN transfer. In the worst case scenario the zero dispersion wavelength is exactly half way between the pump and signal wavelengths, thus there is no walk-off and the RIN transfer is at its most efficient. For forward pumping Raman amplifiers the worst choice of fibre would be NZDSF as its non-zero dispersion wavelength is around 1550nm.

For the backward pumping case, the signal encounters an ever strengthening pump from its forward direction, which means the walk-off is not the most important factor, but instead the fibre attenuation takes precedence.

Compared to the forward or co-propagating case, the corner frequency of the counter-propagating case depends on the fibre attenuation only, this results in lower RIN transfer. The RIN for the counter-propagating case is less, as the corner frequency is in the 1kHz range and can be calculated using $f_c = \frac{\alpha_p V_g}{4\pi}$, whilst for co-propagation it is in the 1-100MHz range [102, 105, 107].

The presence of low dispersion can significantly increase the sensitivity to RIN for fibres types such as NZDSF and SMF-28. When using either of these types of fibre, the pump-RIN would have to have a value of $<-130$ dB/Hz, even for a single amplifier. The issue of RIN transfer would be worse if low dispersion fibres are used, especially if the zero-dispersion wavelength is half-way

between the pump and signal wavelengths, as discussed in Section 3.3.1 [102, 105, 107].

For Bidirectional pumping the RIN transfer occurs mainly in the forward-pumping direction, so the RIN from backward pumping can be ignored.

For 2nd Order Raman amplification the RIN is increased compared to 1st Order Raman amplification, but the other noise mechanisms are decreased [109, 110].

Some experimental work was carried out into the potential degradation due to RIN, with the Q-value measured at 10dB in [105], this showed that forward pumped amplification was much more sensitive to RIN than backward pumped amplification with a penalty difference of 50dB between them, which means to avoid pump-RIN transfer penalties a maximum pump RIN of <-120dB/Hz for forward pumping, and -70dB/Hz for backward pumping, is needed to avoid an increase in RIN. If there is more than one amplifier then the RIN will build up linearly with each additional amplifier.

### 3.3.1. RIN Measurement and Suppression techniques

In the previous section it was shown how significant RIN can be when looking at the direct causes of some issues within transmission systems. There are a number of ways to try and supress RIN and improve the performance of optical transmission systems.

The suppression of RIN within lightwave systems is a difficult but important consideration. The majority of RIN is from the laser sources used within optical systems, so the majority of suppression techniques are concentrated in this region. The RIN of a laser can be reduced by operating laser diodes with stabilised injection current, and also through laser design which minimises external noise susceptibility and quantum fluctuations [104].

One such technique to reduce RIN in lasers is Laser Cavity Injection (LCI), this is the process of injecting the light from one laser into the cavity of another laser. This process reduces the RIN by inhibiting unwanted modes, whilst promoting the wanted modes. The use of a polarisation controller to control the polarisation of the light entering the laser cavity enhances the control by minimising one polarisation, and hence reduces the build-up of RIN by half, in addition to the reduction of unwanted modes [111].
A similar technique of RIN suppression to LCI is via Self-Injection Locking (SIL), where the light from the laser is injected, via a circulator, back into the laser cavity rather than using a separate laser. This increasingly promotes the wanted modes over those unwanted modes by way of a feedback process. RIN suppression was around 20dB/Hz [112, 113].
Both LCI and SIL, as described above, have been used in DFB lasers, whilst a similar technique has been explored in semiconductor lasers [114].

Turning to Raman systems, as discussed previously in Section 3.3, it is stated that in co-propagating regimes the higher frequency RIN >10MHz is reduced whilst the low frequency RIN is increased. In counter-propagating systems, owing to the opposite directions of pump and signal, the RIN is reduced due to the averaging out of the resultant pump and signal combination.

It is difficult to implement any feedback loop derivatives, such as SIL, in Raman cavities due to their length, so alternative methods need to be used. One such method is to reduce RIN in $2^{nd}$ order RFLs, where the $1^{st}$ and $2^{nd}$ order wavelengths are produced via low power semiconductor lasers. It was found that by matching the frequency of the $2^{nd}$ order laser current fluctuation, via the modulation of the $1^{st}$ order laser by the same frequency, it stymies the RIN transfer between $1^{st}$ order pump laser and the signal and achieves a RIN transfer reduction of -20dB over a bandwidth of 10MHz [115].

Other techniques for Raman based systems include the use of a double cavity, in which the Stokes wavelengths are produced, at specific powers. This set-up produces a lower RIN because there is a low amount of RIN transfer from one cavity to another and therefore between different order Stokes wavelengths, this also smooths the output of the Raman fibre laser (RFL) [116].

Also developed was the suppression of RIN at the 1st Stokes wavelength, which would decrease the potential for RIN transfer to 2nd order wavelengths even further than in [116]. This technique uses a point which allows the clamping of the 1st order output power to around 1.2W, meaning the resultant 2nd order wavelength has little RIN transfer due to the lack of fluctuations in the 1st order wavelength as a result of power clamping [117].

Another technique which builds upon the ones already mention for RFLs includes a type of feedback, but it is not a SIL-type feedback. This technique uses a small signal that is modulated according to the information given by the negative feedback loop to control electronics. The signal is of the same wavelength as the 2nd Stokes wavelength. The frequency of modulation does not have to be resonant with the RIN, but close to the typical frequencies, which means there is a greater amount of pump power available than with the other techniques [118].

Another RIN suppression technique relates to the use of the intensity modulator, this is a device present in pretty much all optical transmission systems. Typically an additional modulator is added to correct for amplitude fluctuations using a tap to couple light to a photodiode, which indicates an offset when compared to a reference voltage. This offset is then used to change the modulation current, and hence cancel out the RIN [119].
In this design the additional modulator is not needed as the feedback is used to slightly adjust the modulation that supplies the data to the light wave to supress the RIN, and also reduces the additional insertion loss within the system. This technique can also reduce phase noise in certain circumstances. As with previous experiments, a bandwidth of 10MHz was used to measure the RIN [120].

A Similar technique, as described here, used a Semiconductor Optical Amplifier (SOA), and by controlling the injected current, which controls the amount of gain supplied by the SOA, when the amplifier is at saturation, the RIN can be reduced [121, 122, 123].

There is also a suppression technique which relates to the improvement of noise rejection at the receiver. It is standard within the design of coherent receivers due to the reduced complexity in using a MZI and one photodiode, instead of beam splitters and four photodiodes. The technique which is applied at the receiver consists of a coherent receiver, where the Local Oscillator (LO), used to demodulate the incoming signal, has RIN which could be transferred to the incoming signal. The MZI is the main reason for the RIN suppression, as long as the FSR is equal to twice the Intermediate Frequency (IF). The IF is the difference between the signal and LO frequencies. The frequency difference between the LO and the RIN means that within the MZI, the signal and LO power is coupled to the wanted output, whilst the LO RIN is transferred to the opposite output, where it is discarded. The reduction in photodiodes meant there is less shot and thermal noise to be transferred as well [124].

It can be stated that, overall, to achieve low RIN within optical systems, the pump lasers used in Raman amplification techniques, need low RIN.
Pump lasers such as FBG-FP lasers typically have RIN of -120dB/Hz, whilst those with a narrow line width, such as DFBs, can achieve RIN of -160db/Hz. Narrow linewidths however cause an increase in SBS, and can therefore negate the RIN improvement by causing system noise elsewhere, therefore a pump laser need low RIN, plus a linewidth that is not narrow enough to cause SBS, yet narrow enough to reduce the system RIN. Pump lasers which can lead to low system RIN are the Inner-Grating Multimode lasers (IGMs) and Spectrally Broadened Distributed Feedback laser (SB-DFBs) [100, 125].

Other more general effects can also be used to contribute significantly to the reduction in RIN, such as having low fibre dispersion, which limits the increase in RIN purely by limiting the dispersion of the light, also balanced receivers which reduce RIN by, in effect, “seeing” more signal than noise i.e. higher OSNR.

## 3.4. Experimental Results

The experiments into unrepeatered transmission were reduced to two main experiments, both of which used Raman amplification and an ultra-long fibre span; one was at 240km and the second at 320km. A further experiment of around 400km was not completed due to time constraints and equipment issues.

The experiments and their results are shown and discussed in the following sections:

- Section 3.4.1 – 240km ultra-long transmission.
- Section 3.4.2 – 320km ultra-long transmission.

These results are shown and analysed in the sections mentioned above, then conclusions made from them in Section 3.5.

The channels that were used during the transmission experiments are shown in Figures 3.4.1 to 3.4.2 and Tables 3.4.1 to 3.4.2 as follows:

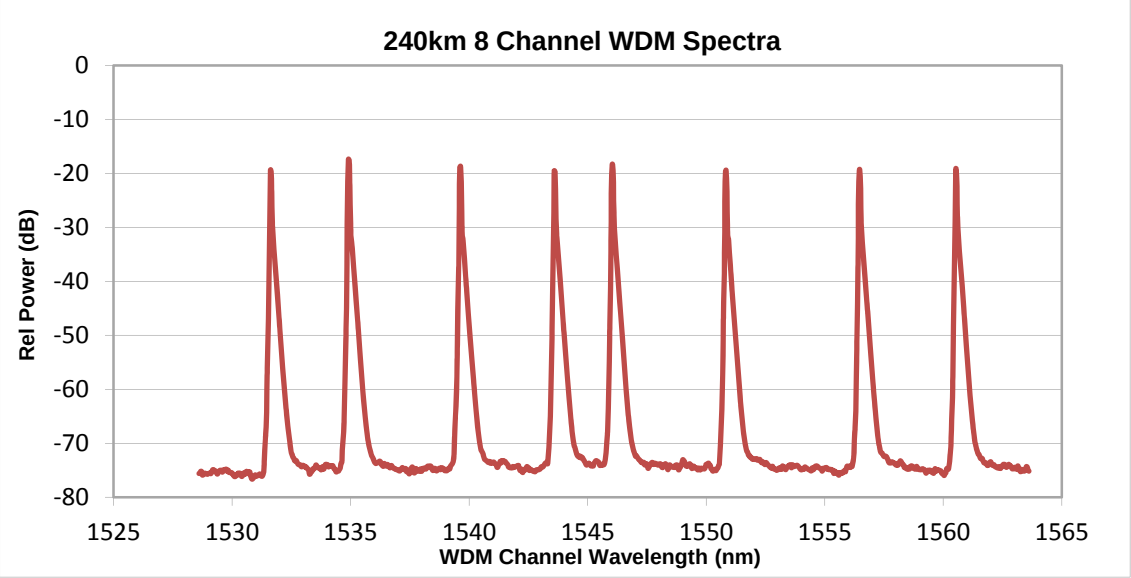


*Figure 3.4.1 – Transmitted WDM Channel wavelengths for 240km experiments.*

| Channel | Wavelength (λ) |
|---|---|
| 1 | 1531.62 |
| 2 | 1534.91 |
| 3 | 1539.64 |
| 4 | 1543.59 |
| 5 | 1546.04 |
| 6 | 1550.84 |
| 7 | 1556.47 |
| 8 | 1560.53 |

*Table 3.4.1 – Transmitted WDM Channel wavelengths for 240km experiments.*

The channel spacing is within the ITC 50GHz grid, although not at the central wavelength of each 50GHz channel, with an approximate average 500GHz channel separation between channels. The non-uniformity of the channel spacing is down to the laser sources available for the experimental configuration at 240km. The channels were also chosen to give a general indication of the response across the majority of the C-Band, which runs from 1530nm to 1565nm and is the normal medium for modern telecommunications.

This is due to superior amplifiers and a useful amount of naturally anomalous dispersion at these wavelengths.

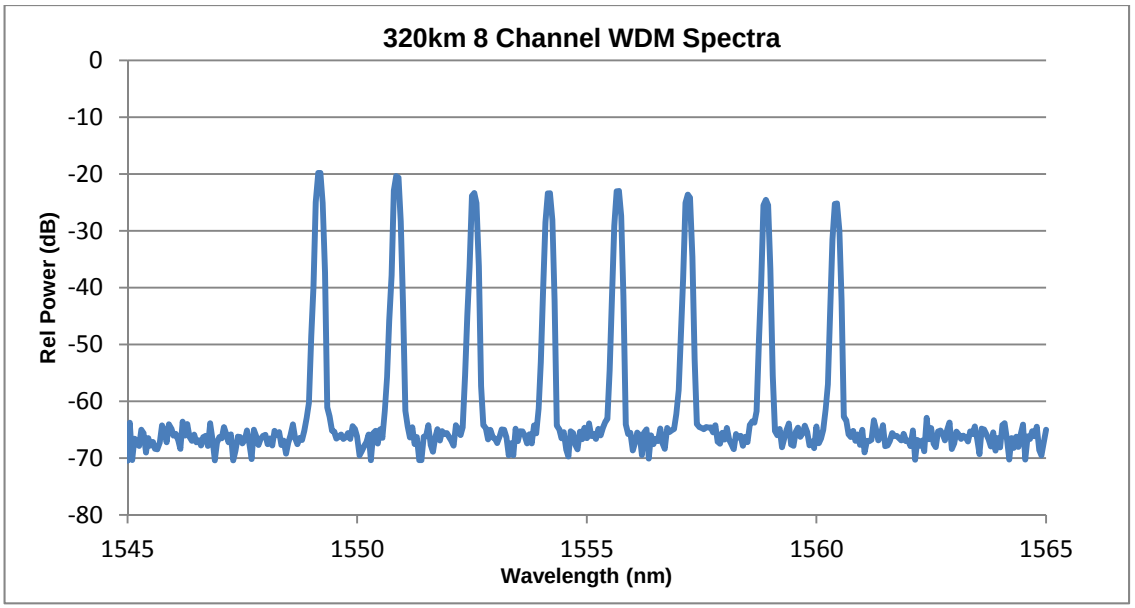


*Figure 3.4.2 – Transmitted WDM Channel wavelengths for 320km experiments.*

| Channel | Wavelength (λ) |
|---|---|
| 1 | 1549.30 |
| 2 | 1550.92 |
| 3 | 1552.52 |
| 4 | 1554.13 |
| 5 | 1555.75 |
| 6 | 1557.36 |
| 7 | 1558.98 |
| 8 | 1560.61 |

*Table 3.4.2 – Transmitted WDM Channel wavelengths for 320km experiments.*

These channels were chosen to be within the ITU 50GHz Grid, as described in Chapter 2 Section 2.1.2, which gives a separation between the channels of 200GHz so as to minimise ISI and Crosstalk. The spectral width at 42.7Gbps is 0.342nm, whilst the 50GHz Grid gives a channel spacing of 0.40nm; this gives a difference of 0.058nm, or ±0.029nm either side of the signal pulse.

The wavelengths used for the 320km experiments used a narrower bandwidth; this was due to problems with correcting dispersion over the whole bandwidth of the channel wavelengths used for the 240km experiments at the longer fibre span length.
The problem was there was not enough Raman gain over the larger bandwidth of 30nm used for the 240km experiments, owing to the extra losses experienced with the additional fibre to make the span 320km. This issue required a reduction in the bandwidth, which gave an increase in the possible gain due to the average power being increased when using a narrower bandwidth.

The Raman amplification used was $2^{nd}$ order Raman amplification, which uses FBGs at either end of the transmission span; this technique was described in section 3.1.3. The power variation over the transmission span is less using $2^{nd}$ order Raman amplification with a variation of 2.72dB with bi-directional amplification, with $1^{st}$ Order amplification having an approximately 11dB bi-directional variation. This meant the population depletion in $2^{nd}$ order amplification should be less, giving the potential for additional overall gain when compared to $1^{st}$ order setups.

Single direction pumping obviously gives a larger variation over the whole transmission span when compared to bi-directional pumping [20, 21, 23, 25, 59, 61, 64, 98, 99].

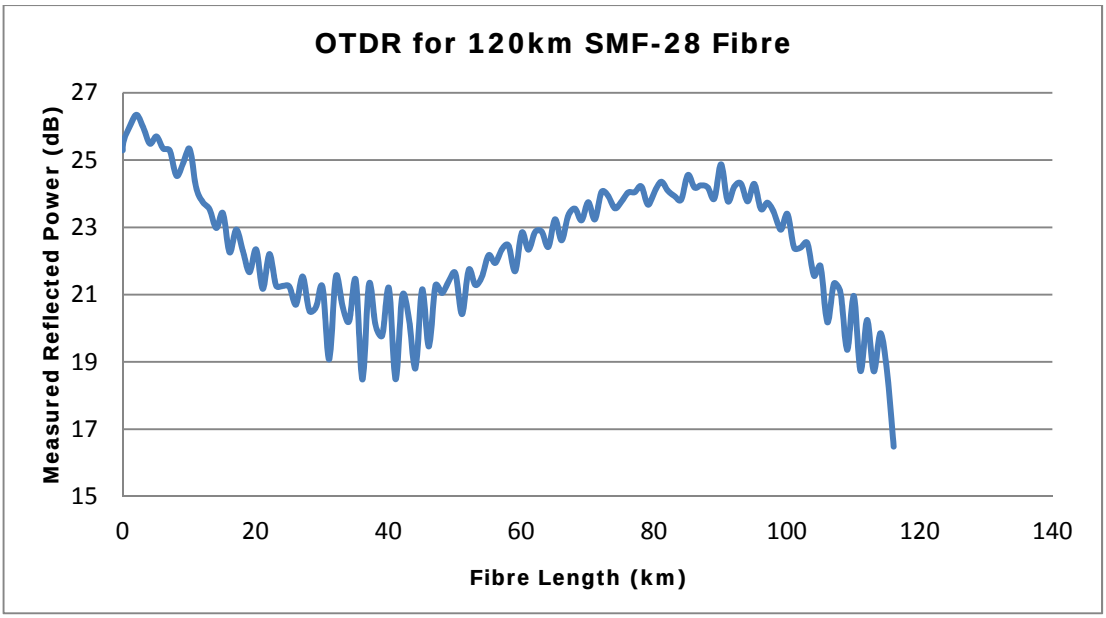


*Figure 3.4.3 – An OTDR measurement from a 120km span.*

For the 240km and 320km configurations, the total fibre span loss was measured using the Optical Time-Division Reflectometery (OTDR) technique [90], and came out as 48.3dB for 240km and 67.1dB for 320km. An example of an OTDR trace is shown in figure 3.4.3 which is over a 120km span, this shows how much of the power is reflected.

The power used in the Raman pumps at 240km was 1.4W (31.46dBm) for the forward pump and 1.25W (30.97dBm) for the backward pump. For the 320km experiment the forward and backward Raman pump powers were 1.85W (32.67dBm) and 1.4W (31.46dBm) respectively.

The forward and backward powers basically "tilt" the Raman gain, which is useful when one end of the spectrum has channels with a greater peak power than those at the other end, therefore by changing the power output of the Raman pumps this can be equalised. However other problems can emerge as noise mechanisms appear when the pump power is too low or too high. When the pumps powers are too low there isn't enough power to create the Stoke wavelength(s), so any light from the pumps appears as noise.

In the reverse situation where the pump powers are too high, the amplified signal is increased to a level that causes the light to back scatter, and it therefore becomes part of the noise caused by Brillouin Scattering and Double Rayleigh Back-Scattering.

All spectra and OSNR measurements were taken using a 0.1nm bandwidth on the Optical Spectrum Analyser (OSA).

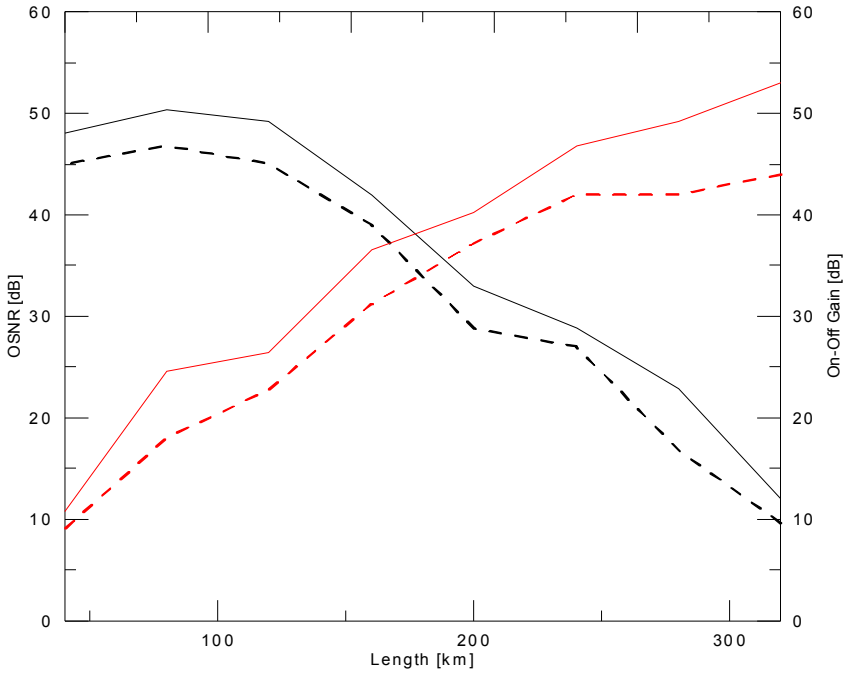


*Figure 3.4.4 – The relationship of OSNR (black line) and On-Off Gain (red line) with distance. Solid lines represent best case scenario and dashed line the worst [24].*

Figure 3.4.4 shows experimental results [26] for OSNR and On-Off Raman Gain as they change with distance. This shows that for 240km the OSNR should be between 26dB and 30dB, whilst for 320km the OSNR could be as low as 9dB and as high as 12dB. These measurements were taken with Raman pumping only. The OSNR and On-Off Gain results in Figure 3.4.4 will be tested in the following experimental sections.

DPSK receivers are a common type of receiver used in optical transmission systems. This is due to DPSK being a modulation technique that gives a potential 3dB improvement and double spectral efficiency when compared to OOK. There are a number of different detection techniques that could have been used for DPSK, but the two main types of receiver which were considered

were Direct-Detection and Coherent receiving. Due to its simplicity Direct-Detection was chosen for these experiments. For detail on modulation techniques see Chapter 2 Section 2.4.2, and for Optical Receivers see Chapter 2 Section 2.6.

### 3.4.1. 240km Ultra-long Transmission

Carrying out an experiment at 240km was for proof of concept before going onto longer transmission spans. Simulations had previously been carried out [14, 108] for up to 300km comparing both 1st order bi-directional Raman amplification and 2nd order bi-directional Raman amplification, with the 2nd order using FBGs as per the experiments in this chapter. It was found that 2nd order Raman amplifier had a smaller Nonlinear Phase Shift of 1.80 compared to 2.31 for 1st order, and a reduced difference in power variation was also found for the same OSNR values [15, 99].

Experimental investigation into using FBGs in a 1st order Raman amplifier to create an ultra-long fibre laser were carried out in [15] to confirm whether there was a limit to the length of a laser cavity. The limit was found to be around 270km, although the experimental investigation went up to 303km. The Rayleigh backscattering was found to cause the signal to degrade significantly due to the intra-cavity modes becoming indistinguishable, therefore reducing the effect of the mode reflections from the FBGs within the cavity; as a result, after being amplified, the noise is increased thus rendering it almost impossible to recover the signal at the receiver.

In this experiment 2nd Order Raman amplification is used in an Ultra-long Raman Laser which should decrease the nonlinearity seen within the fibre cavity [126]. Referring back to the simulations in [14] they dictate an improved resilience to nonlinearities along with added OSNR improvements, and a slight increase in amplification of the signal at around 1550nm. Each FBG was reflective of >95% of the light within the fibre cavity.

Using ULRF in unrepeatered Raman amplification, which in essence becomes a quasi-lossless span [14, 27, 30], means the gain across the total length of the transmission fibre span should equalise the total loss of the span. The setup for this experiment involved creating a span of 240km of SMF-28 fibre, with 240km of DCF to compensate for the dispersion. A Transmit-side and a Receive-side were constructed using EDFA's and DCF's on either side of the transmission span, as explained in section 3.2.

A transmitter was setup to transmit 8 channels, with the wavelengths as shown in Table 2.4.1; these were then passed through a multiplexer and then a data modulator, which modulated data that consisted of a PRBS $2^{31}$-1, using RZ-DPSK modulation. In total this gave an 8x42.7Gbps output, and a total capacity of 341.6Gbps.

RZ was used instead of NRZ because the ability to recover the clock rate with RZ is less complex. DPSK was used because it has a number of advantages over other modulation techniques. It has a 3dB improvement in sensitivity over ASK modulation and XPM effects on the differential phase are limited, it is also comparatively easy to demodulate compared to other types of phase shift keying. For more on modulation see Chapter 2 Section 2.4.2.

As well as RZ-DPSK modulation, RZ-ASK modulation was used for the 240km experiments. ASK is a much simpler type of modulation requiring a transmitter that uses a single data modulator to encode the transmitted data using the signal amplitude. These amplitude changes can be directly detected by a photodiode. Using RZ requires an additional pulse carver as described in Section 2.4.

The modulated data was then passed to a Pre-Amplifier which was a dual pumped Gain Flattened (GF) EDFA. The signal was directed through 160km of DCF to effectively pre-chirp the signal and then through a Booster Amplifier, this was also a GF-EDFA but with three pumps for additional power amplification, before it was sent through the transmission span. This was the Transmit-side.

The signal was then sent through the 240km transmission span, where Raman amplification would take place (Raman Amplification is described in more detail in Section 3.1.3) and a quasi-lossless span generated.
The Raman pumps were set at 1.4W (31.46dBm) for the Forward pumping, and 1.25W (30.97dBm) for the backward pumping powers.

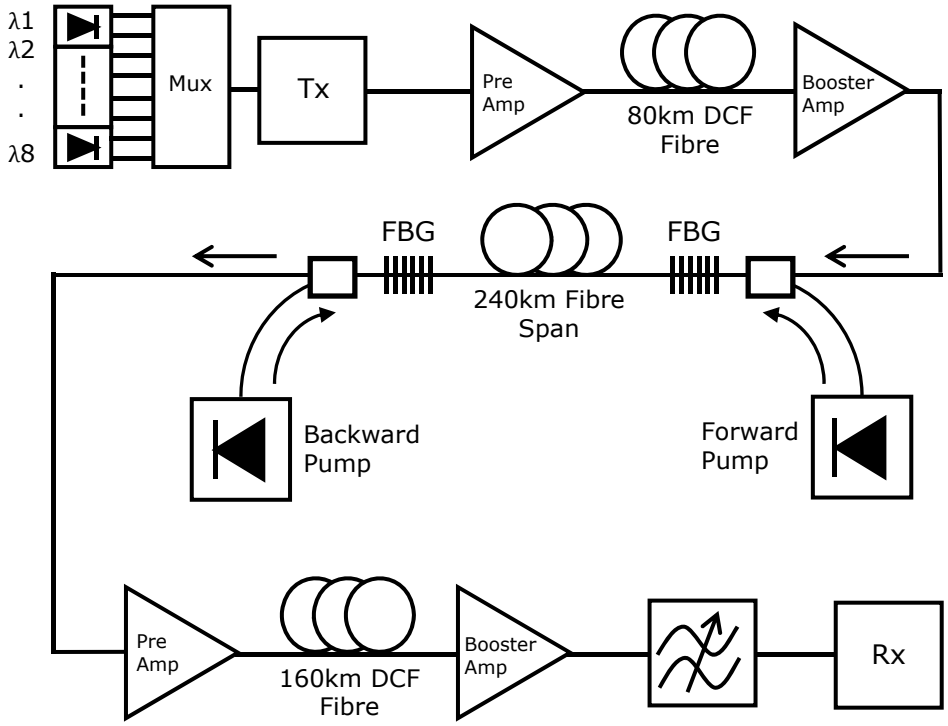


*Figure 3.4.5 – System setup for 240km 8-Channel WDM Transmission.*

Once the signal had passed through the transmission span the loss was measured and came out at 48.3dB, consistent with 0.2dB/km for SMF-28. The signal on the Receive-side passed through a GF-EDFA Pre-Amplifier, and then through 80km of DCF, plus an additional 2.5km DCF-LEAF[†], before finally passing through a second GF-EDFA Booster Amplifier.

[†]An explanation for using the additional small amount of DCF-LEAF is as follows: The lowest amount of DCF available was 5km, but this amount of fibre was insufficient for complete correction of the dispersion for the whole span. A DCF for Low Effective Area Fibre (LEAF) was used for "tuning" the dispersion compensation in small 2.5km amounts of fibre. The need for this additional fibre was due to the type of DCF fibre used. The length of the 80km DCF fibre reel used for the fibre span compensation was set for use within the L-Band

(1565-1625nm); this meant the $L_{eff}$ within the C-Band (1520-1565nm) was approximately 82km, hence the need for additional dispersion compensation using small amounts of DCF-LEAF.

The addition of 2.5km of DCF actually meant using 10km of DCF-LEAF, but due to the dispersion compensation of 4ps/nm for DCF-LEAF, the effective length of the fibre for compensating SMF was 2.5km, as SMF-28 is 16ps/nm. Consequently to achieve 10km of SMF compensation 40km of DCF-LEAF would have to be used. This did not compensate for the dispersion in full as the lower two channels were still affected, but it was as close as possible using the fibre available.

The asymmetric split of using 80km pre fibre span, and 160km post fibre span, existed due to having only 80km lengths of DCF available, so the only splits available for pre/post fibre span were 240km/0km; 160km/80km; 80km/160km; and 0km/240km. Through trial and error, we found that 80km/160km gave the best dispersion compensation compared to the other DCF configurations.

The resulting signal was then sent through a tuneable filter which was used as a wavelength demultiplexer. The receiver consisted of a Delay Line Interferometer (DLI) where the two outputs were attached to two photodiodes, one on DATA and the other on $\overline{\mathrm{DATA}}$. For more detail on DLIs see Chapter 2 Section 2.5.3.

A Clock Recovery module was used to control the temporal drift in the system. The CR took 30% of the signal using a 70%/30% optical splitter which allowed the data rate to be properly measured at the receiver and for the received bits to be in the correct sequence.

Figure 3.4.6 shows eye diagrams of each channel measured at the receiver after 240km transmission, with 80km of SMF-28 and two modules of LEAF, one of 5km and the other of 2.5km, which gave a total of 87.5km of fibre.

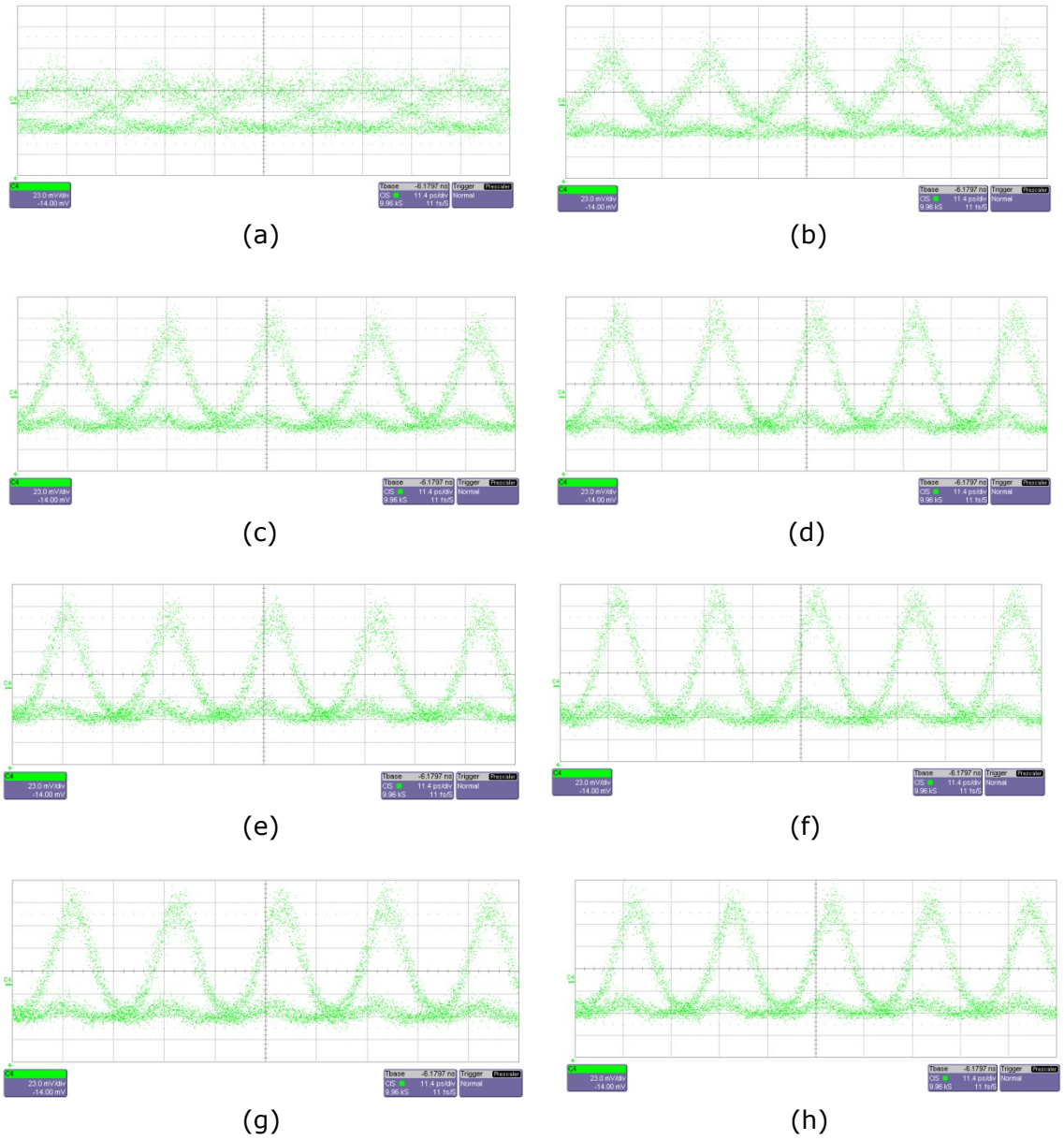


*Figure 3.4.6: - Eye diagrams showing received signals from Ch1 (a) to Ch8 (h) after 240km transmission span with 160km DCF before transmission span and 87.5km DCF after transmission span.*

Channel 1 has a significantly closed eye and Channel 2 also has a reduced opening when compared with channels 3 to 8. It wasn't known if this was due to too much dispersion compensation or not enough, so the amount of fibre was decreased to 85km.

Figure 3.4.7 shows the eye diagrams for the 8 WDM channels received after 240km transmission, with 80km of SMF-28 and 5km of LEAF to compensate for the dispersion.

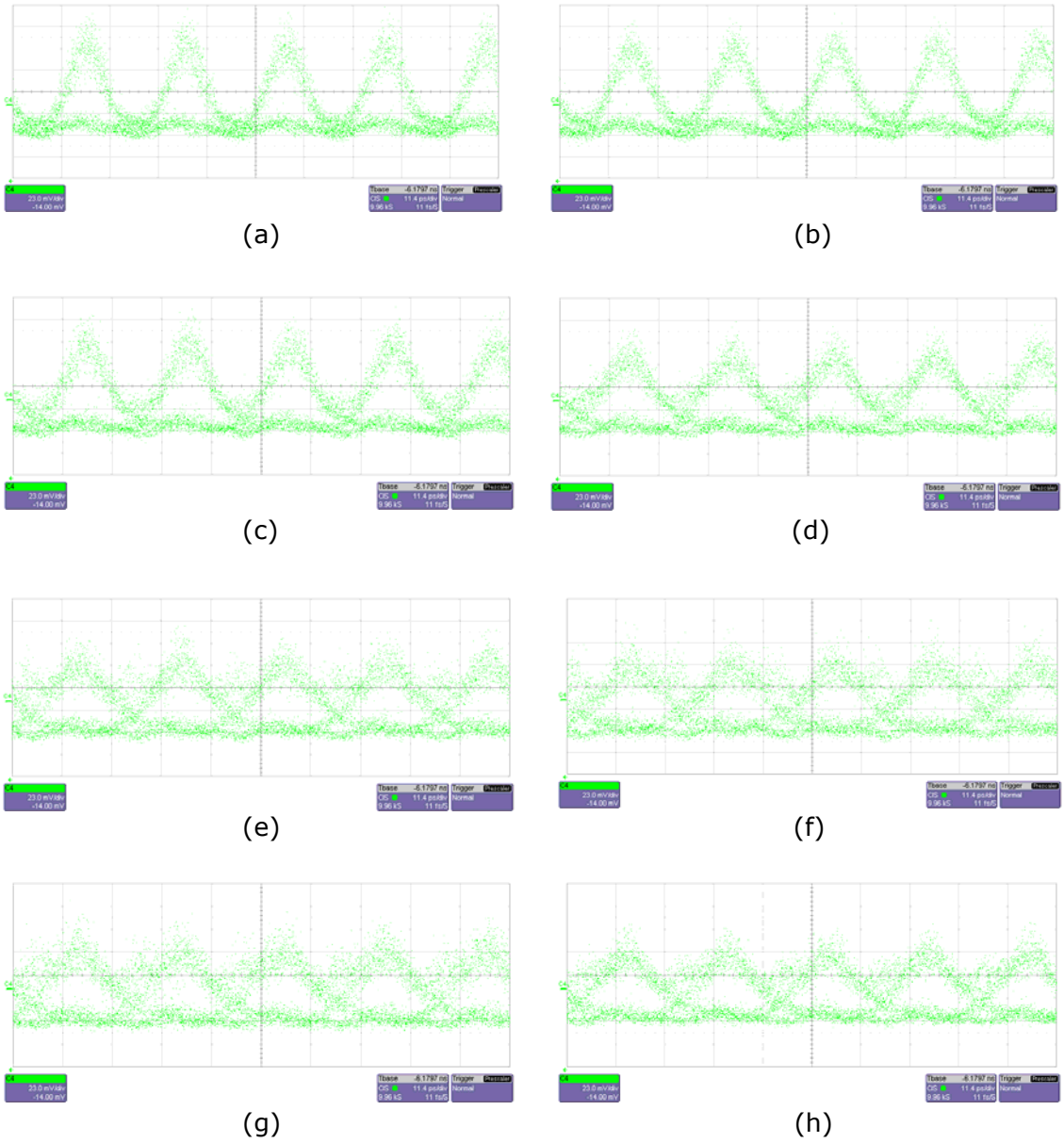


*Figure 3.4.7: - Eye diagrams showing received signals from Ch1 (a) to Ch8 (h) after 240km transmission span with 160km DCF before transmission span and 85km DCF after transmission span.*

Compared to the diagrams in Figure 3.4.6, Channels 1 and 2 are improved with Channel 1 significantly so, but channels 3 to 8 are comparatively degraded. Because the overall results for the transmission system was more important than individual channels, it was decided that the 80km+5km was the better "average" as Q-values could be measured from all 8 channels, even though the Q-values were lower overall.

The received data for both ASK and DPSK modulation formats are shown in Figure 3.4.8 showing the improvement due to using DPSK over ASK; both measurements used direct-detection and balanced receiving. A 2dB to 3dB improvement can be seen apart from on channels 1 and 2, where gain tilt and dispersive effects limited the expected improvement.

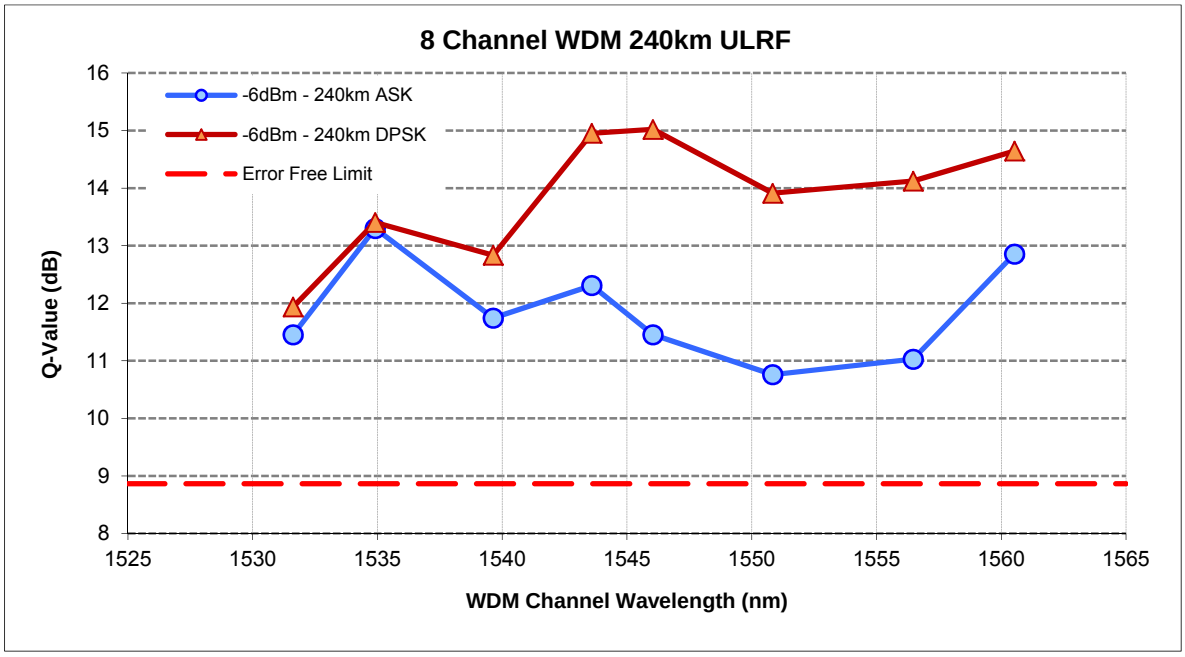


*Figure 3.4.8 – 240km 8-Channel WDM Transmission Results for 42.7Gbps RZ-ASK and RZ-DPSK modulation.*

The red dotted line is the limit below which Forward Error Correction (FEC) could not be used to obtain any usable data.
The results show that for all WDM channels FEC would not be needed.

Channel 6 at 1553.4nm is the closest to the line at around 11dB, and is 2dB above the FEC limit [26]. The FEC limit is equal to 8.86dB Q-Value or $3x10^{-3}$ BER. The FEC limit that is being used is a hard decision 2$^{nd}$ generation limit with an overhead of 7%. See Chapter 2 section 2.1.3 for more details on FEC limits.
These results are comparative to those using ROPA techniques where Q-Values of between 7dB and 12dB were measured and OSNRs of 7dB to 15dB [18, 19, 20, 21, 22, 23, 24, 25]. Only [22] had higher OSNR and that was using Digital Signal Processing.

The spectra in Figure 3.4.9 is that of the initial input into the WDM before modulation takes place (shown in red), and the output of the system just before entering into the receiver (shown in blue). The reduction in the peak power and increase in noise floor is apparent, and is partially caused by the linear effects of ASE and attenuation due to the fibre length (as described in Chapter 2 Section 2.3.1).

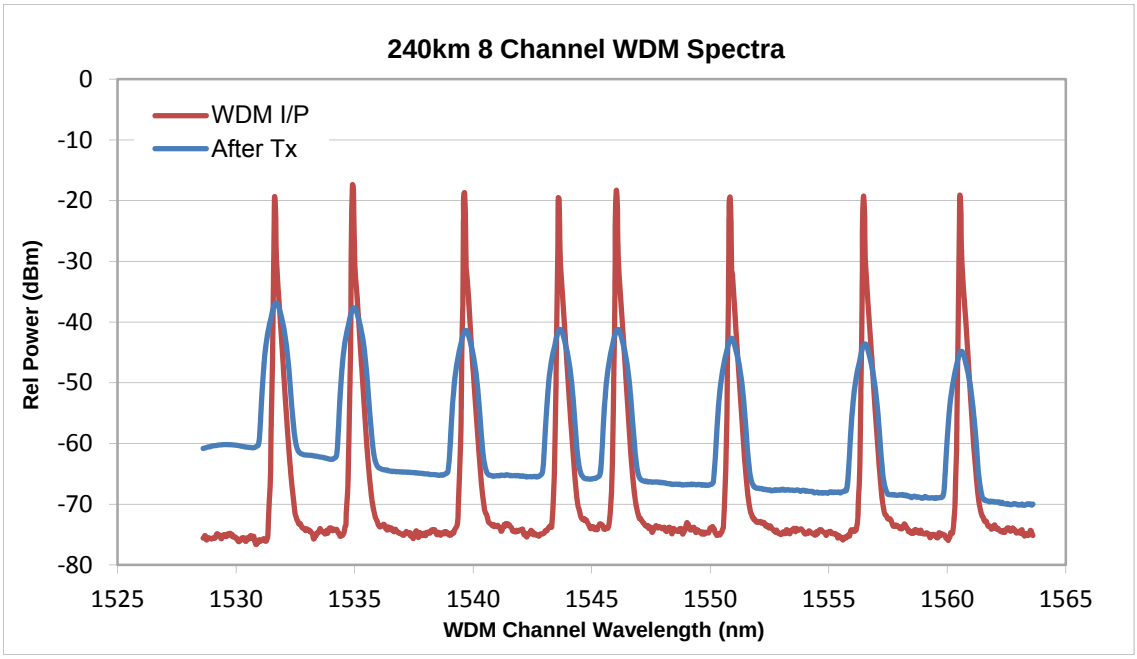


*Figure 3.4.9 – 240km 8 Channel WDM 42.7Gbps RZ-DPSK transmit and receive Spectra.*

Dispersion was an issue, and was not matched completely because the dispersion compensation could only be tuned to within 2.5km using DCF fibre. This meant that the transmit power had to be increased for the first three channels, namely 1531.62nm, 1534.91nm and 1539.64nm, to try and achieve a decrease of the BER at the receiver. This obviously meant additional noise was apparent on these channels which, with the high attenuation over the length of the fibre, also affected the gain flattening within the EDFAs present on the receive path, hence the slight tilt seen in the spectrum. This is a generally recognised problem which causes capacity issues, as explored in [23], although a Remote Optically Pumped Amplifier (ROPA) is used and the experiments are at lower data rates than used here, the same issues are still apparent, if not more so [18, 19, 20,21, 22, 23, 24, 25, 35, 57, 58, 59, 60, 61, 64, 98].

### 3.4.2. 320km Ultra-long Transmission

The actual setup for the 320km experiments was the same as that used for the 240km experiments, apart from using a longer transmission span and adding the appropriate amount of DCF for dispersion compensation. In this case the DCF used for dispersion compensation was symmetrical, with 160km before and after the transmission span; this was because the 80km DCF reels could be split equally. The setup is shown in Figure 3.4.10.

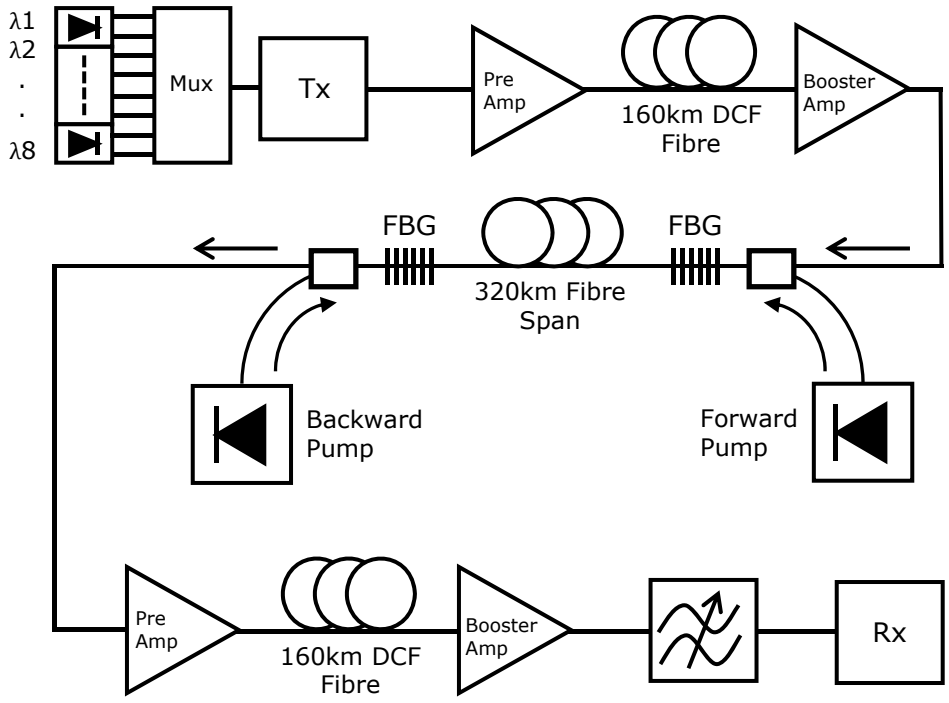


*Figure 3.4.10 – System setup for 320km 8-Channel WDM Transmission.*

With the longer transmission span a higher original input power of +3dBm was required to compensate for the reduction in the amount of Raman gain obtainable. Furthermore, the attenuation was approximately 64dB (at 0.2dB/km for SMF-28) for 320km compared to 48dB for 240km, which meant the span was not quasi-lossless.

The downside is that this combination creates additional noise in the system and lowers the OSNR. The Raman pumps had to be increased in power to 1.85W (32.67dBm) and 1.4W (31.46dBm) for forward and backward pumping respectively due to the attenuation increase mentioned above. These values

are not far off those simulated for 300km, 32.4dBm and 33.4dBm, in [14]. The drawback was an increase in the instance of Raman backscattering, which reduced the population in the fibre, hence the reason why both the input power and the Raman pumps were increased.

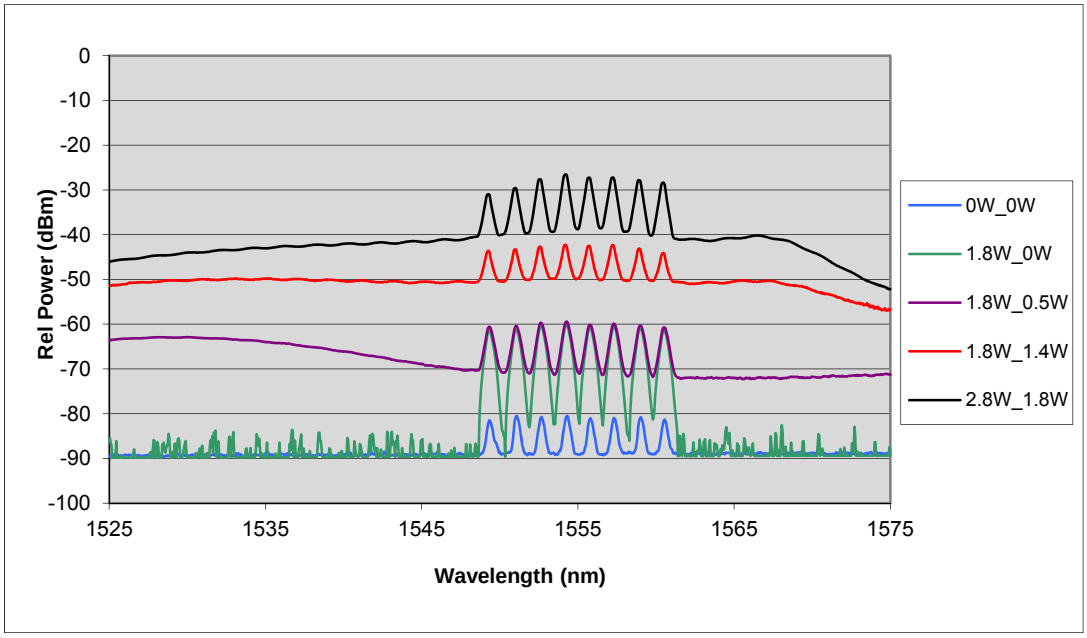


*Figure 3.4.11 – The output from the transmission span with different Forward and Backward Raman pump powers.*

Due to the increase in power there is also a rise in the uncontrolled processes of spontaneous Brillouin and Rayleigh back scattering. Figure 3.4.11 shows how the output power changes with the increase or decrease of the backward pump power. For the BER measurements, the forward pump power was fixed at 1.85W and the backward pump power at 1.4W as the gain spectrum is flatter therefore requiring less pre-emphasis at the input to the transmission span. If there is a gain tilt the channels can have different output powers. This can be fairly extreme at the end of the Raman spectrum, so when, as an example, the higher wavelengths have an OSNR of 25dB the lower ones can have an OSNR of 5dB or even disappear totally due to there not being enough gain at that wavelength.

Due to the increased loss, dispersion and the need for higher pump powers increasing DRBS, the wavelengths used for 320km experiments were of a narrower bandwidth consistent with the ITU 200GHz grid. This reduced the variation of the gain, OSNR and dispersion slope.

There are no ASK results for this distance as it was not possible to achieve error free transmission at this distance.

The problems with dispersion which were discovered for the 240km experiments were also present at 320km, and due to the tighter arrangement of the WDM channels in the 1549nm to 1560nm range, because of lower output power, a tuneable dispersion compensator was tried.

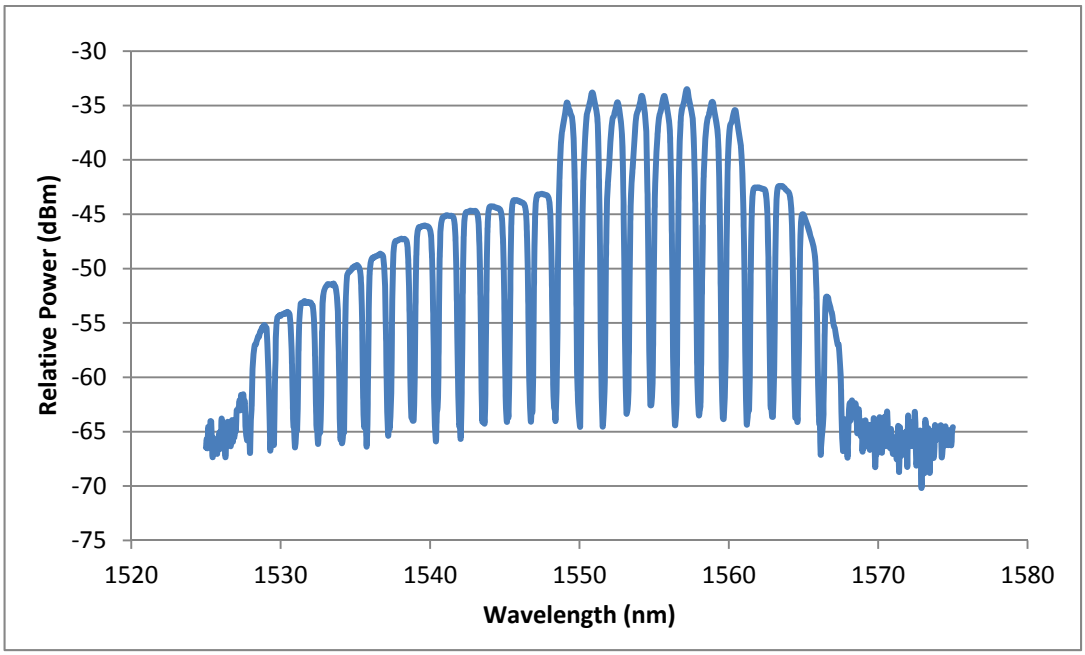


*Figure 3.4.12 – The measured spectral output from a TeraXion Tuneable Dispersion Compensation Module (TDCM) [127].*

A TDCM works by electronically adjusting the refractive index by heating of the waveguides through the device with thin-film devices. An AWG is used to demultiplex wavelengths into channels that fit into the 50GHz grid. For more on TDCMs please see Section 2.7.1.1.

As can be seen in Figure 3.4.12, there were 25 channels, and each channel has light coming through due to the broadband noise present from ASE and DRBS, which meant that there was an effective reduction in the OSNR of the WDM channels after the TDCM, so although it was effective in compensating for the dispersion, the problems caused by the broadband noise being channelled by the device afterwards outweighed the initial enhancement.

The dispersion compensation of the TeraXion TDCM was +/-1200ps/nm*km and had a dispersion resolution of 5ps/nm*km [127].

Figure 3.4.13 shows the initial WDM signal input to the transmission span and the difference in the output of the fibre span with and without Raman amplification. This difference can be measured and is known as the On-Off Gain. From the results in Figure 3.4.13 it can be seen that the On-Off Gain is in the range of 50dB, which is exactly as shown in the experimental results in Section 3.4, Figure 3.4.4.

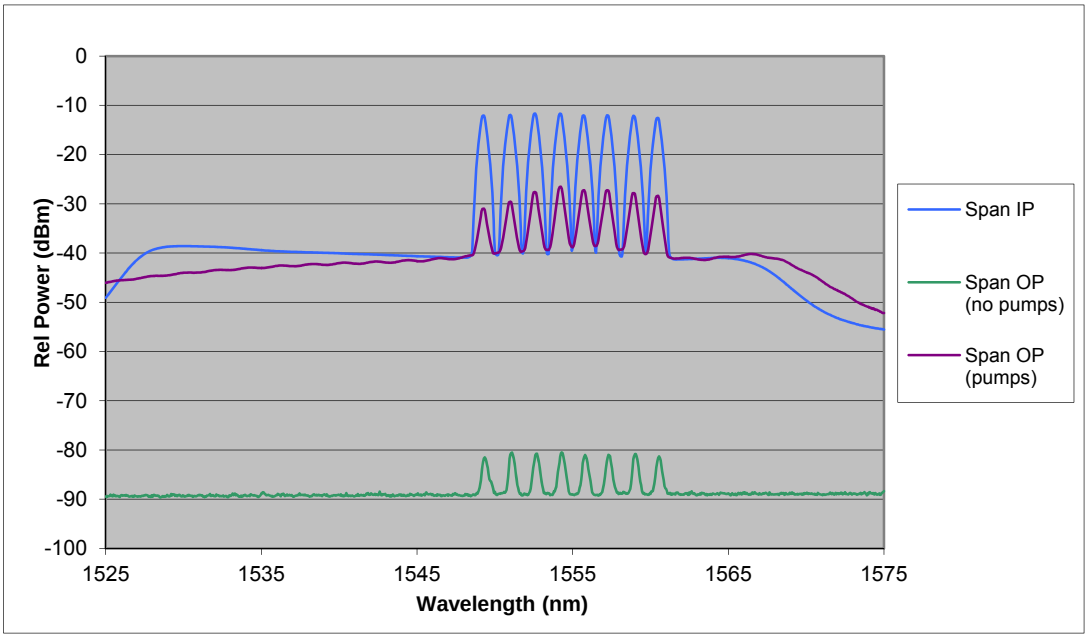


*Figure 3.4.13 – The input into the transmission span and the output with Raman pumping on and Raman pumping off.*

The measured OSNR is slightly low by about 2dB from the previously measured OSNR at 320km, whilst the On-Off Gain is just above the centre of the expected gain value.

In Figure 3.4.14 the results show a fairly similar Q-Value across all 8 channels. The key reason for this is that the channels are tightly spaced and are only present within a 12nm bandwidth, thus concentrating the power over a small band. This also meant that the dispersion compensation could be kept the same for all channels transmitted through a distance of 320km as the variation with using a wider bandwidth is not a problem, unlike with the

240km transmission results in Figure 3.4.8 which show a worse Q-Value for both ASK and DPSK on Channel 1 compared to other WDM channels.

The biggest issue at 320km distance was the significant increase in noise relating to ASE and DRBS compared with 240km. This appears to be attributable to where the light from the backward pump starts to cause gain in the fibre, which appears to be after 280km and leaves 30km of further signal loss, which is enough to drop the OSNR from 26dB down to 15dB, a drop of 11dB compared to 3dB at 240km.

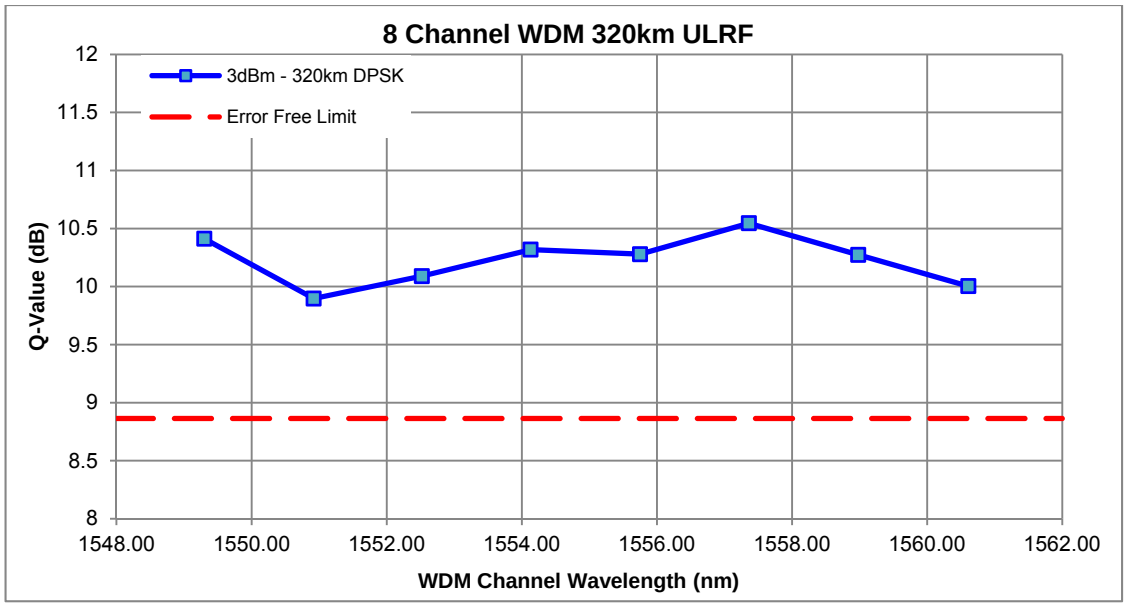


*Figure 3.4.14 – 320km 8-Channel WDM Transmission Results for 42.7Gbps RZ-DPSK modulation.*

The major downside of these experimental results is that the amount of power necessary to achieve results at 320km is required to be significantly higher than with the 240km results, as the additional fibre meant an increase in attenuation and also led to a significant impact from Rayleigh back scattering. As shown by [18] there is a physical limit to just purely Raman transmission above 250km without using alternative techniques [25, 35] or finding a simple way to reduce the DRBS.

The spectra shown in Figure 3.4.15 shows the initial 8-channel WDM signal, the blue graph, with the corrected transmit powers for each channel which were set to achieve an overall flatness at the receiver, as is displayed by the output from the transmission span, shown as the red graph. Each channel was

also pre-emphasised to give each channel a similar OSNR of 7dB at the receiver.

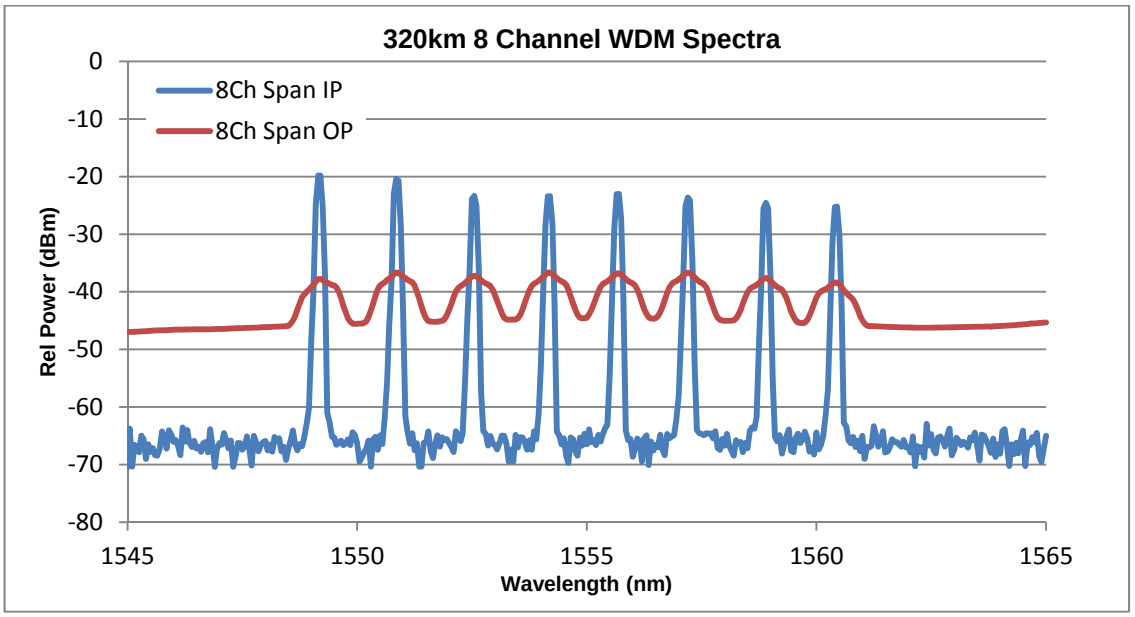


*Figure 3.4.15 – 320km 8-Channel WDM 42.7Gbps RZ-DPSK Spectra with pre emphasis on Channels 1 and 2.*

The resultant reduction in power is around 15 to 20dB, although the noise floor has increased by around 20dB also, which is giving around 5dB of power relative to the noise floor at the receiver.

## 3.5. Conclusions

From the experimental results in Section 3.4, it can be concluded that for 240km spans there is the potential for the exploitation of ULRF within current long haul fibre networks, such as MANs, as either a replacement for EDFA or as part of a hybrid Raman-EDFA amplification scheme. For extremely long spans in the thousands of kilometres EDFA is still the best choice

For 320km spans the results were not as encouraging, as nonlinear effects such as DRBS built up to significantly degrade the WDM channels, giving OSNRs of 7dB and Q-Values of 10-10.5dB, although this is within the FEC limit. If FEC were added the signal could be improved by as much as 2dB, and

with a larger FEC header, such as 3rd generation FEC with 20% overhead, the error rate could be improved even further.

When compared to other experimental techniques such as ROPAs, the length of the transmission span is smaller than for many of these types of experiment. The advantages are that the Q-value for both the 240km and 320km experiments are in the same region as these other systems, with a minimum of 9.9dB for the 320km span with DPSK, whereas for the 240km span the minimum was 10.8dB for ASK and 11.9dB for DPSK. The high Q-values were 15dB for the 240km span using DPSK and 13.3dB using ASK, whilst the 320km span using DPSK was 10.5dB.

There was however a problem with dispersion which led to Channels 1 to 3 being compromised, especially with DPSK when compared with ASK, where the channels were within 1dB of each other. Channels 4 to 8 had a difference of 2dB or wider, which was as expected [52].
If it had been possible to control the dispersion minutely the improvement overall would have been expected to be around 2dB to 3dB per channel.

For 320km this was slightly mitigated by using a narrower bandwidth for the WDM channels, hence all channels were within 0.6dB of each other.
More work needs to be done to investigate if the degradation at longer distances due to DRBS, which causes the lasing within the ULRFL cavity to reduce significantly, can be inhibited, and therefore the transmission of WDM channels over a wider bandwidth made possible.

As well as DRBS, RIN could also be a factor for the increase in noise, as the forward pumps in both experimental setups were higher than the backward pumps, thus RIN transfer could occur to a greater extent.

Through the experimental work undertaken it can be considered that ULRFL amplification techniques show the potential for improving the performance of transmission spans, particularly those with existing infrastructure, as it has been shown that normal silica based fibre, such as SMF-28, can be used with

such a system. This would mean that no additional cost would be incurred by the need to replace fibre with types of LEAF or ULL fibres.

There is still further work to be done however, at distances greater than 250km, to improve the noise figure and reduce the significant degradation from nonlinear effects such as DRBS.

In conclusion, the use of ULRFL to upgrade existing infrastructure using data rates up to 42.7Gbps, utilising fibre span lengths below 320km, along with the employment of simple direct-detection, has been shown. In future work the impact of using receiver types with greater complexity could be investigated. Particular types that could be considered are coherent receivers, which can give significant improvements when compared with direct-detection, this could therefore enable the use of ULRFL over much greater distances.

There are a number of potential avenues for future work, but each brings an increase in the issue already seen. As an example a greater number of WDM channels could be tested using this approach, but unless there is tight dispersion control and a reduced amount of excursion in the gain profile, positive results greater than 320km are unlikely. Moreover, as the fibre span distance is increased, the gain bandwidth is reduced, along with the OSNR, so coherent receivers would not necessarily give an improvement in these circumstances. Higher data rates >100Gbps would also need to be considered, but this brings its own difficulties with an increased likelihood of cross-talk due to ISI, a need for very tight dispersion compensation, and higher average power per bit slot, means there is a potential for lower OSNR values; this indicates higher gain over the transmission span would be required, which would bring its own problems with noise mechanisms such as RIN transfer and DRBS effecting an increase in system noise as a result of higher initial Raman pump powers.

# Chapter 4

# Offset Wavelength Filtering

## 4.1. Introduction to Offset Filtering Theory

The improvement of received signals is an important factor for optical networks. This improvement can be specifically determined as a reduction in bit-error rates (BER), and/or an increase in OSNR, for the received signals. There are many different approaches which can be incorporated into optical systems to help recover the transmitted signal. Most methods involve using amplification and more efficient modulation, but there are also methods to improve the quality of the received signal at the receiver.

Optical Filtering and optical attenuation are two major problems within optical transmission networks. Attenuation occurs via a signal travelling through a transmission fibre span; this loss accrues within the optical fibre due to its inherent physical properties, as discussed in Section 2.2.
Filtering is caused by passive and active devices within the transmission system. As light travels through these devices there are numerous filtering events, which, due to the inherent design of these devices, reduce the signal quality at the receiver. This is especially clear within WDM systems using devices such as add/drop multiplexers and cross connects, this is because as the signals come across the filtering effects caused by passing through each device, a decrease in the signal amplitude occurs; after multiple passes through these types of devices there is a high potential for the OSNR to decrease to very low levels, and therefore significantly lower the received BER. One such technique identified to help signal recover from this significant impairment is known as asymmetric, or offset, wavelength filtering.

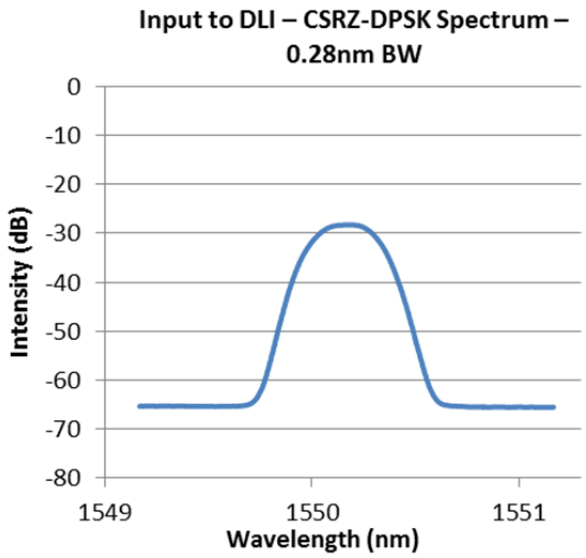


(a)

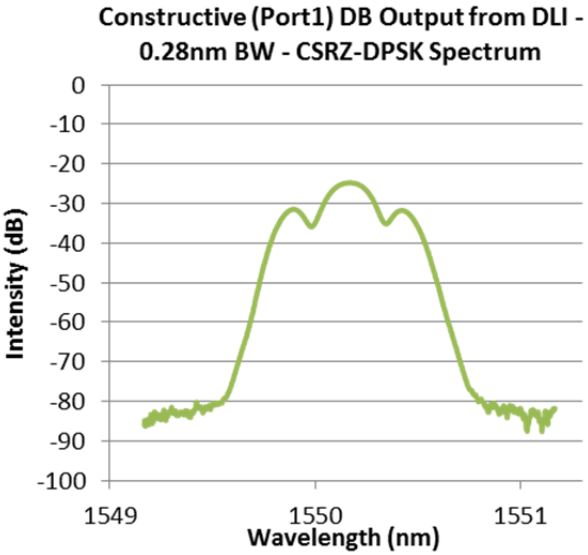


(b)

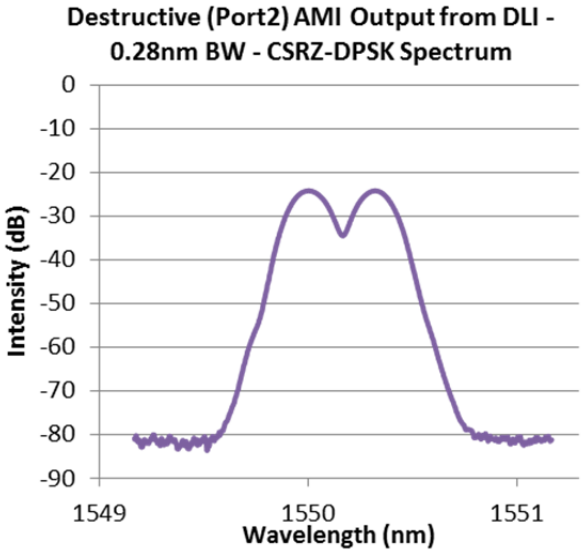


(c)

*Figure 4.1.1 – (a) Input spectra into DLI; (b) Output spectra from Constructive port of DLI; (c) Output of Destructive port of DLI.*

Offset wavelength filtering is all about the improvement of the quality of the received signal after transmission through networks with tight optical filtering (TOF), where a series of devices cause a filtering effect on the signal as it travels through a network, thus decreasing the bandwidth of the signal as well as reducing the signal power due to insertion losses. Another technique called Band-Limited Filtering (BLF) could be used, but this uses a filter on both sidebands of the signal (Double Side Band (DSB)) whilst Offset Filtering uses a single filter on a Single Side Band SSB or Vestigial Side Band (VSB). The advantage of this technique is that only part of a signal needs to be filtered because for offset filtering, second side bands and the carrier are unneeded

although in VSB a small portion of the second side band is visible, but this gives a wider bandwidth; this was studied in [128].

Each received signal will have issues such as Inter Symbol Interference (ISI) and an increase in Amplified Spontaneous Emission (ASE). This is due to Optical Repeating within the transmission line reducing the signal quality. Insertion Loss is also a factor. Whenever light encounters an optical device, such as an amplifier or a filter, some of the light is absorbed as it enters and then travels through the device. This is known as Insertion loss and is the actual fixed loss in the device due to its physically inherent properties. This insertion loss increases the total loss within the system and therefore helps reduce receive power.

These types of issues are especially relevant in Wavelength Division Multiplexing (WDM) and Demultiplexing (WDD), where multiple channels are combined or divided according to their wavelength. Crosstalk is one of the causes related to ISI along with Chromatic Dispersion; these are very important issues to control. Crosstalk occurs when a portion of $\lambda_1$ is measured at the output for $\lambda_2$, this can affect the quality of the received signal by introducing additional noise and can potentially corrupt the 1's and 0's and change the Threshold Level. The cause is mainly due to the laser source wavelength and the channel wavelength not matching up completely [56].

An important subject is the applicability of BER and Q-Value for optical transmission system measurements.
BER is an absolute measurement which takes into account the threshold level and bitrate over a certain time period. This means for low BER such as $10^{15}$ measurement times need to be exceedingly long.
The Q-Value on the other hand is a statistical measurement and can therefore approximate the BER considering the noise variance on logical 0 and logical 1, as well as the threshold value.
The statistical properties of the signal information are imperative for Q-Value calculations and are approximated as Gaussian distributions. If the signal distribution is non-Gaussian then the Q-value cannot be calculated. Q-value gives a better understanding of the relationship between the eye-opening of a

signal eye diagram and the BER [110]. The relationship of BER and Q-value are explained in more detail in section 4.2.

DPSK has advantages over modulation formats such as PSK due to its simplicity and ease of demodulation, plus its sensitivity is superior when compared to other modulation types [52, 129].
All measurements within this chapter were taken using a DPSK receiver, with more information relating to this type of receiver available in Chapter 2 Section 2.5.

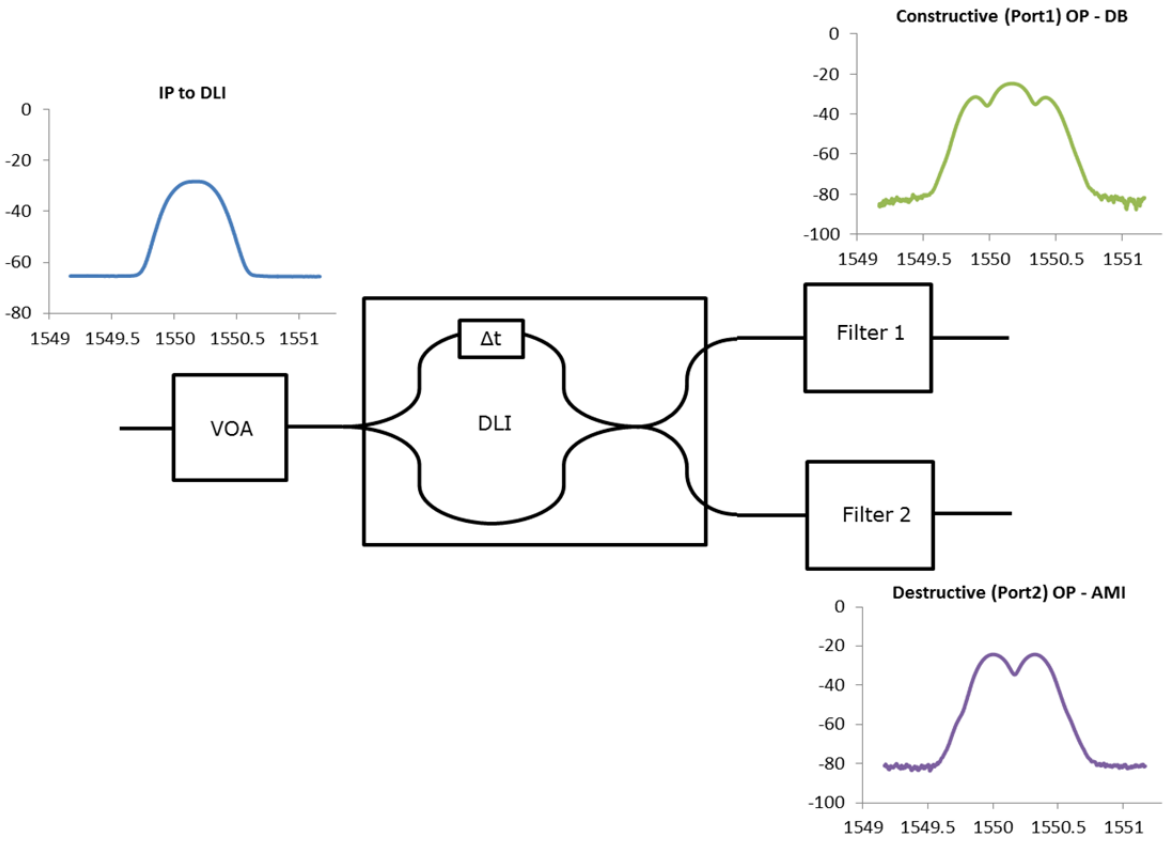


*Figure 4.1.2 – Diagram showing the typical setup of DLI and Filters detailing the cause of improved signal quality when using offset filtering.*

Offset or Asymmetric filtering enhances the received signal by using the destructive port of the DLI, used in DPSK demodulation, to improve the overall Q-value. The mechanism taking place is that each demodulated DPSK output from the DLI is in effect two different modulation formats, Duobinary (DB) and Alternate Mark Inversion (AMI); where AMI is basically the spectral inverse of DB, where DB has one peak AMI has two with a null between them. By "detuning" a filter on the destructive output port the filter can be centred on

one of the AMI peaks, therefore in effect demodulating to a DB signal rather than an AMI, making both DLI output DB and improving the overall output of the received signal.

Figure 4.1.2 shows the representation of a DLI, with measured spectra for the input and outputs of the DLI. The shape of the spectra from the constructive and destructive ports, show the expected outputs of Duo-binary (DB) from Filter 1 and Alternate Mark Inversion (AMI) from Filter 2.
This effect can be seen in the single ended results shown at the beginning of the experimental section 4.6 and was simulated in [32]. More on the modulation formats used and generated as part of the system are in Section 4.3.

Offset filtering has been used previously in [130], but those experiments used Amplitude modulation formats and lower data rates of 10Gbps, although WDM transmission was also considered. Data rates of 40Gbps have been used in some other experiments, as in [131]. Positively, all the experimental results discussed here show that offset filtering is a useful technique when implemented to improve received signal quality.
Offset filtering can also be part of dispersion control, where it has been demonstrated that improved Q-values at higher dispersion rates are achievable [32, 130, 131, 132, 133, 134, 135].

## 4.2. Optical Filters and Filter Shapes

Filters, optical or otherwise, are defined as devices which allow only a certain band of wavelengths to pass through. This control of frequencies or wavelengths is useful in many ways, the main use being filtering noise from signals. The filter is tuneable if it is able to choose different wavelengths; this property can be used for demultiplexing certain signals when a number of them are present. Filters are useful for equalising the gain and filtering out noise, and can therefore improve SNR in a specific bandwidth as the filter averages out the noise over a smaller bandwidth, rather than the larger bandwidth apparent before the filter.

There are also some devices that are not filters but respond to signals in similar ways to filters. Examples of these are optical switches, modulators, optical cross-connects, AWGs and multiplexers. The filtering effect of these types of devices, especially within a network where these devices are cascaded, is of interest with regards to the experiments in this thesis.

### 4.2.1. Optical Filter Types

There are many types of optical filters, but the main types used in optical communications are those based on diffraction of light through a prism or the absorption of wavelengths outside of the wanted bandwidth

Most modern filters are based on either fibre or waveguide technologies. These can contain structures such as Gratings which allow only certain wavelengths, using diffraction, to interfere wavelengths with different phases; those wanted wavelengths will have constructive phases and transmit, while those with destructive phases get reflected.

The most important characteristics of a filter are as follows:

- The centre wavelength is the mean wavelength between the filter band edges.

- The peak wavelength is the wavelength at which attenuation is lowest, but this does not always match with the centre wavelength. The attenuation wavelength and centre wavelengths are most closely matched at 1550nm bandwidths when compared with other transmission bands.

- The Nominal wavelength is the wavelength which the manufacturer designed the filter to be used at; the actual centre wavelength is usually slightly different to this due to variations in the manufacturing process.

- The bandwidth of the filter is the space between the edges of the filter shape, but it is totally dependent on where you measure the width from. In many manufacturers data sheets this is measured at 3dB down (-3dB) from the filter band peak, additionally the 1dB or 30dB bandwidth are sometimes quoted.

A maximum and minimum can also be mentioned if there is a high polarisation dependency of the filter.

Some key factors that a filter should adhere to are a low insertion loss, have polarisation independent loss i.e. low Polarisation Dependent Loss (PDL), and be insensitive to temperature variations, or at least have extremely low sensitivity that generates a wavelengths shift smaller than the wavelength spacing in the WDM system being used.

As will be explored in this chapter, a flat pass-band is needed when used within a network due to the cascading of devices causing a narrowing of the bandwidth, and as described previously, a sharp edge or skirt on the filter will limit crosstalk in WDM systems and is known as the isolation of the filter.

Filters using gratings are very useful, the main types of gratings used in these filters being Fibre Bragg Gratings, a type of reflective grating, and Long-period Gratings, which are transmission gratings.
FBGs can be used as notch filters, or bandstop filters, as they reflect unwanted wavelengths. The reflected light will however travel back towards the source, so isolation and absorption of the reflected wavelengths must be part of any filter design using FBGs. To calculate the wavelength, which will be reflected by a certain FBG, the following equation can be used

$$\lambda_0 = 2n_{eff}\Lambda \qquad \text{Eq. 4.2.1}$$

Where $\Lambda$ is the grating period, $n_{eff}$ is the effective refractive index of the waveguide the FBG is in and $\lambda_0$ is the Bragg wavelength.

Long-period Gratings can be used as bandpass filters as they reflect unwanted wavelengths into the cladding, which is extremely lossy, thus allowing the wanted wavelengths(s) to pass through.

The wavelength which will be transmitted can be calculated using:

$$\lambda = \Lambda\left(n_{Core-eff} - n_{Clad-eff}^{P}\right) \qquad \text{Eq. 4.2.2}$$

Where $n_{Clad-eff}^{P}$ is the effective refractive index of the cladding. This depends on the pitch of the grating as to which cladding modes will propagate and give the appropriate effective refractive index. $\lambda$ is the resulting transmitted wavelength.

In addition to their use in filters, FBGs are also employed in Add/Drop devices such as circulators and cross-connects. These devices are used to switch channels and they can also be incorporated as part of a dispersion compensation regime, which is why such devices need to be included in system wide filtering processes.

Long-period Gratings are used within EDFAs as filters and to flatten the gain profile (see Section 2.6.1). Both types of grating can have multiple gratings placed within a device to accept or reject different wavelengths, and hence can be used as multiplexers and demultiplexers, such as AWGs. However AWGs usually use different lengths to multiplex or demultiplex wavelengths.

Another type of filter, using partially reflective mirrors with up to 99% reflectivity, are known as Etalons or Fabry-Perot Etalons, as they use the same setup as a laser cavity in Fabry-Perot Lasers. These devices use partially reflective mirrors which are at a fixed distance to create a cavity. The cavity has a length which, for certain wavelengths, is equal to half of those wavelengths, and because the cavity is reflective this means the whole wavelength is equal to the reflection off both mirrors in the cavity, or 2L.

Smaller fractions of the wavelength, i.e. a quarter, 1/8$^{th}$, 1/16$^{th}$ etc., can also create a standing wave, but the interference patterns are weaker as the number of cycles of the wavelength within the cavity increase. This leads to

only one main wavelength, or a narrow band of wavelengths, plus some of the lower energy harmonics relating to the wavelengths, being transmitted. All other wavelengths are strongly attenuated. This type of filter is an example of a narrowband filter. A simplified diagram of the design of a Fabry-Perot cavity is shown in Figure 4.2.1.

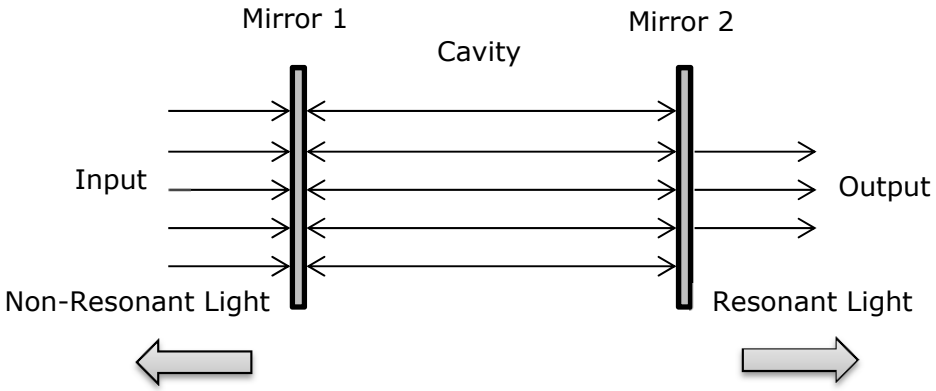


*Figure 4.2.1 – Diagram showing structure of a Fabry-Perot cavity.*

A similar type of filter to the etalon is a type of interferometer in which at least one of the mirrors is able to move away, or towards, the other mirror at the opposite end of the cavity. This will then allow the filter to be tuneable for different wavelengths, where the limits on the wavelengths which can be allowed through the filter, depend on how far apart the mirrors are. If too far away additional loss will mean a significant degradation of the signal power on top of the insertion loss, too close and the optical power may be too high and the majority of wavelengths may be passed through rather than reflected, meaning additional noise in the system.

One type of filter using FP cavities is the thin-film multi-cavity filter; this uses thin film technology to change the refractive index, and therefore the wavelength dependence of the mirrors at either end of the cavity, which creates tuneability in a different way.

Free Spectral Range is the separation between two peaks at which resonance occurs, an example of which could also be said to be two successive passbands, and is given by:

$$FSR = \frac{\lambda^2}{2nd} \qquad \text{Eq. 4.2.3}$$

Where, $\lambda$ is the wavelength of the resonant peak, $n$ is the refractive index of the material between the mirrors and $d$ is the distance between the mirrors. From the FSR the Finesse, or how accurate the filter is at accepting or rejecting wavelengths, can be calculated using:

$$Finesse = \frac{FSR}{FWHM} \qquad \text{Eq. 4.2.4}$$

Where, FWHM is the Full-Width Half-Maximum of the filter shape. FWHM is used because it represents the mean energy in the pulse over its mean width. Therefore it can be stated the higher the Finesse, the narrower the filter passband and the sharper the edges of the passband.

Another way to define Finesse is using the reflectivity, R, of the mirrors, as shown in Eq. 4.2.5.

$$Finesse = \frac{\pi\sqrt{R}}{1-R} \qquad \text{Eq. 4.2.5}$$

The finesse of the filter is increased when the number which is calculated is higher.

A couple of major factors affecting the finesse is the reflectivity of the mirrors, where the less reflective the mirrors the broader the spectral width of the transmission peak, due to more wavelengths being transmitted. Absorption within the filter is another major cause of the decrease in Finesse as this lowers the available energy and causes the filter peaks to reduce in sharpness; this is due more to the absorption of light by the mirrors than other means.

Filters within a system can be cascaded; this has the effect of increasing the amount of filtering by the narrowing of the passband, and is in effect what happens when there are a number of devices which act as filters in a system. The ultimate width of the narrowed passband is the bandwidth at the point where the FSR coincides, and is the lowest common FSR between the filters. The narrowing in turn increases the Finesse and the FSR is also increased. Where the FSR does not coincide with the bandwidth, the overall passband is much narrower, because the FSR is much larger than when the FSR coincides.

Acousto-Optic Tuneable Filters (AOTFs), also known as Bragg Cells [136], are very versatile because they can select multiple wavelengths at the same time. This allows them to be used as crossconnects allowing different wavelengths to be passed through at the same time, which is useful when using WDM channels. A similar technology is used in lithium niobate modulators [137]. The operation of AOTFs is carried out by using the properties of an acoustic wave to create an FBG within a waveguide. This process happens by using birefringent material to make a waveguide, the density of which can be altered in a periodic manner by using an acoustic wave generated by an acoustic transducer, such as those using the piezoelectric effect. This wave travels in the opposite direction to the light wave which only contains the lowest polarisation states, or modes, due to the waveguide material. Polarisation can be seen as Transverse Electric and Transverse Magnetic modes, TE and TM, of a wave. The acoustic wave, through its interaction with the medium, changes the refractive index of the waveguide which effects the polarisation of the light. This is the same effect as an FBG, so in effect a temporary FBG has been created within the waveguide. This allows the light to be transferred from one polarisation, TE, to another, TM, by way of the Bragg condition.

This specific condition can be found by:

$$\frac{n_{TM}}{\lambda} = \frac{n_{TE}}{\lambda} \pm \frac{1}{\Lambda} \qquad \text{Eq. 4.2.6}$$

Where $n_{TM}$ and $n_{TE}$ are the refractive indices relating to the relevant polarisation modes, $\lambda$ is the wavelength the mode conversion occurs at, and $\Lambda$ is the period of the grating. The general term for the Bragg condition can be found in Eq. 4.4.1. A polariser is used at the end of the waveguide to choose the desired mode.
Another way to remove the polarisation dependence of the filter is to use couplers, or a Mach-Zhender Interferometer, with polarisers at the input to split the polarisation into its two modes, which are then converted, as previously mentioned, and then recombined.

When using AOTFs as wavelength crossconnects instead of a filter, the only difference is due to sending more than one acoustic wave into the device

simultaneously through the separate arms. This allows wavelength switching at the two output ports.
For a basis on the theory of Bragg grating based optical filters see [138].
Mach-Zhender Interferometers can also be used as filters, and their operation is discussed in Section 4.3.

### 4.2.2. Waveshapers, including Wavelength Selective Switches

Waveshapers are devices which are used to manipulate optical signals. These devices are based on Wavelength Selective Switches (WSS), but have additional programmable elements which can be used to change the phase, width, and even the shape of an optical pulse.
WSS's are devices that, as their name suggests, select wavelengths and switch them onto output ports of the devices, this is very useful in wavelength multiplexed systems and are usually a part of Random Optical Add/Drop Multiplexers (ROADMs) which are used as optical system switches.

A typical WSS is comprised of the following devices: diffraction gratings, cylindrical mirror, Liquid Crystal on Silicon (LCoS) multi-pixel sensor and a polariser, plus focusing optics.

The operation of the Finisar WSS [139] is as follows: light is passed from the input fibre and through a polariser, which separates the orthogonal polarisation states and fixes them to the same state as accepted by the diffraction grating. The light is then reflected off the cylindrical mirror towards the grating.
Once at the grating, only light close to the Littrow incidence i.e. the angle at which dispersion is maximised with minimum path deviation, is passed through. This light is dispersed and reflected back towards the mirror and onto the LCoS sensor. The dispersed light lands on different parts of the sensor after it has passed back through the imaging optics; this is therefore analogous to each channel, depending on the ITU grid selected.

The LCoS sensor is programmed via embedded software. This allows a range of functions to be chosen, such as the selection of different frequency grids, the central frequency of each channel, the bandwidth, the phase, and the amplitude, to be selected and measured and also to be manipulated, e.g. using the phase and amplitude details and creating a function in software which works like a virtual Delay Line Interferometer, as seen in the experiments in Section 4.4. This works because each channel is isolated from the others on the LCoS sensor using the frequency grid pattern.
The light returned from the LCos sensor is steered to a particular output port. The port can be chosen, again using software, to control the beam steering at the LCoS sensor [139].

An example of the Waveshapers multifunction approach is shown in the experiments in Section 4.4, these use the Waveshaper to create a DLI and also filter responses on each output. The Waveshaper was programmed using MATLAB script.

### 4.2.3. Optical Filter Shapes

The ideal filter shape is a square filter because all wanted frequencies are allowed through with no attenuation and all other frequencies rejected with total attenuation. In practice this does not happen and all filters, no matter how square, are an approximation of a square filter. This allows some unwanted frequencies through with very low energy, but also reduces the energy of those wanted frequencies near the edge of the filter shape.

There are issues however with square shaped filters as the sharp edges of a filter of that shape can cause significant harmonic frequencies to occur. This causes energy from the fundamental frequency to be transferred to frequencies beyond the bandwidth of the filter, and as the harmonics are caused by the filter, they appear after the filter and therefore reduce the spectral efficiency of the filter.

A balance therefore needs to be made with a filter designed to limit the unwanted frequencies, but also not cause a large transfer of energy to the harmonic frequencies.

The most typical filter shape used are Gaussian or Super-Gaussian in shape, this is due to a Gaussian distributions similarity to actual filter designs and the shape of signal pulses are also generally Gaussian in shape, unless otherwise amended into other possible shapes such as triangular, saw or square.

A Gaussian distribution is represented by the following equation:

For Intensity distribution: $I = I_o e^{-2r^2/\omega^2}$ Eq. 4.2.7

Where $e$ = 2.718 is the base of the natural logarithm. And because $e^0 = 1$, $I_o$ is therefore the intensity of the light at the centre of the beam, $r$ is the radius of the distribution (where $r = 0$ at the centre of the distribution), and $\omega$ is the "flatness" at the top of the distribution [56].

An example of a Gaussian shaped filter is shown in Figure 4.2.2, which has normalised intensity and relative frequency.

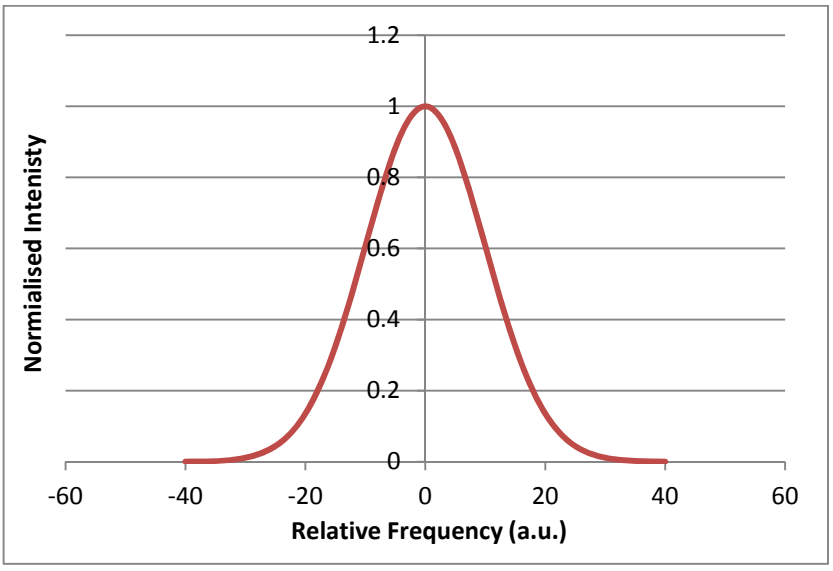


*Figure 4.2.2 – Example of a Gaussian pulse with an 80GHz bandwidth.*

The filter shape in Figure 4.2.2 can be called a 1st order Gaussian filter shape, as the top of the filter shape becomes flatter it becomes known as a higher order Gaussian filter, such as 2nd or 3rd order and can be calculated using:

$$F_G(\Delta f) = exp\left(-\frac{ln2}{2}\left(\frac{2(\Delta f - f)}{\nu}\right)^{2n}\right) \qquad \text{Eq. 4.2.8}$$

Where $F_G(\Delta f)$ is the Gaussian filter output, $f$ is the central frequency of the filter with $\Delta f$ being the frequency offset of the filter, $\nu$ is the bandwidth of the filter at 3dB and $n$ is the order of the Gaussian filter.

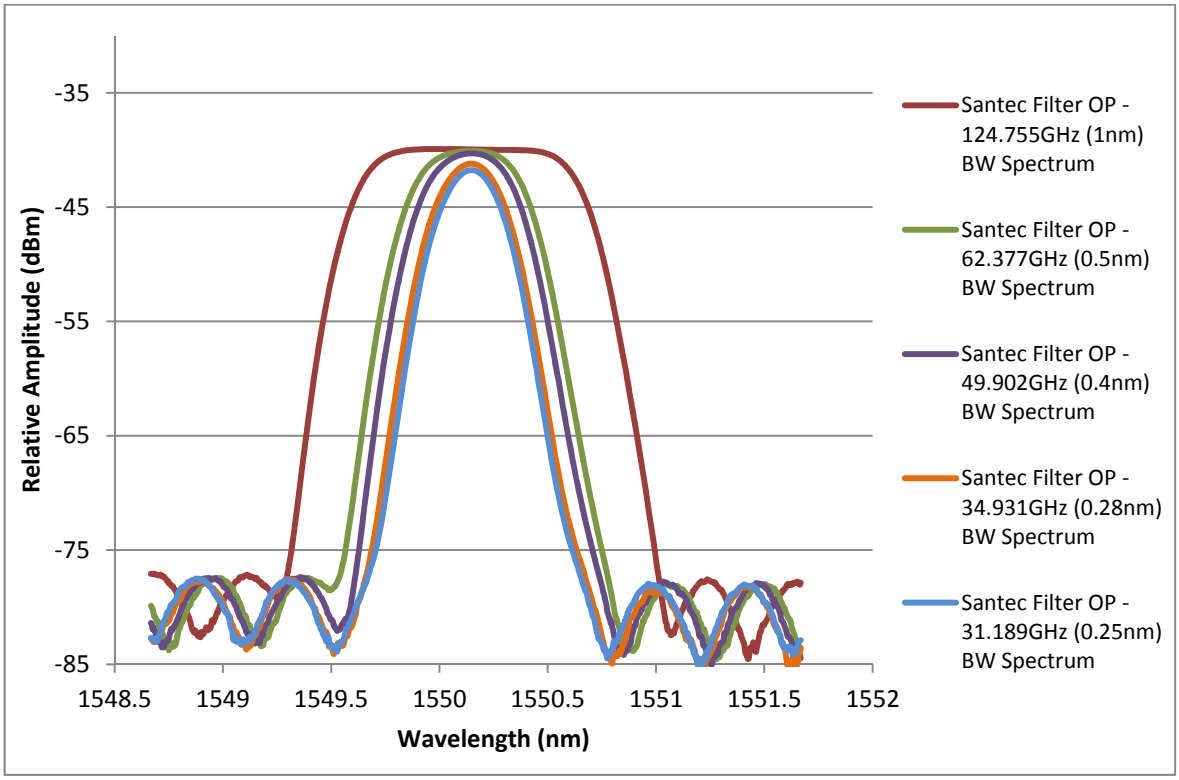


*Figure 4.2.3 – Measurements of Bandpass shapes of Santec OTF-950 Bandpass Filter for bandwidths from 0.25nm to 1nm; each bandwidth measured via ASE passing through the filter.*

The measurements shown in Figure 4.2.3 are from the Santec OTF-950 filter [120] used in the experiments in Section 4.4. These show a fairly square top at wider bandwidths >1nm which is equivalent to a 3rd order, or super Gaussian filter, while those <1nm represent a response closer to 1st or 2nd order Gaussian distributions.

Investigation into filter shapes relating to this topic were carried out in [32, 132, 133] and found that a 3rd Order Gaussian filter shape was the most reliable fit for the physical filters to be used, as per the measurements described previously.

In the first set of experiments, physical Santec filters were used, whilst in the additional experiments, Waveshapers were used.

To try and confirm whether the filter shapes were the same, we took bandwidth measurements via an optical spectrum analyser, using the method of passing ASE though the filter, so as to simplify the measurements without modulation issues if actual signals were used.

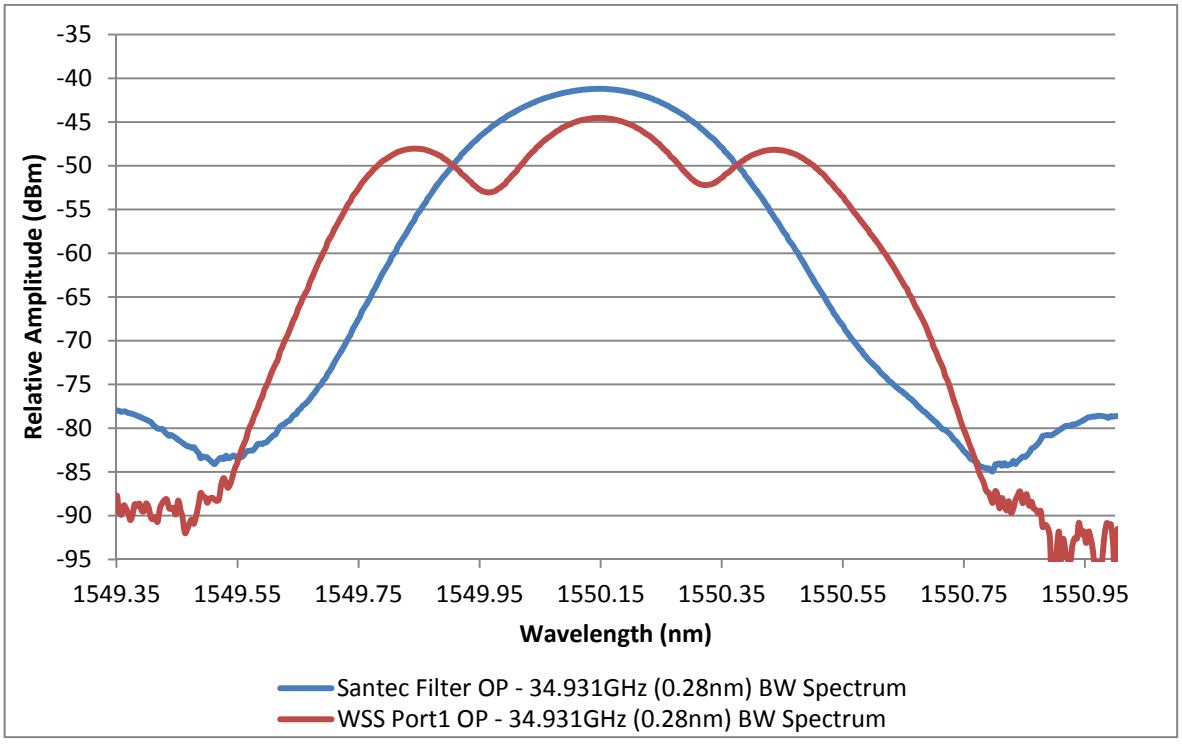


*Figure 4.2.4 – Bandwidth used: 35GHz (0.28nm); Measurements of Bandpass shape of Santec OTF-950 Bandpass Filter (Blue) and Finisair Waveshaper programmed Filter (Red); each bandwidth measured via ASE passing through the filter.*

Figure 4.2.4, shows the physical Santec Filter shape, a typical Gaussian of around 2$^{nd}$ order, whilst the Waveshaper Filter is steeper, which is indicative of a 3$^{rd}$ or even 4$^{th}$ Order Gaussian filter, although the top is not flat as would be expected with higher orders, but this is because of the way the Waveshaper works. The Waveshaper is in essence a Wavelength Selective Switch (WSS) and has many channels available, of which three are shown here, but it is a programmable device so we can select the wanted channels only. However, due to how the WSS has to be programmed, the comb of channels is visible at all times, unless a notch filter is designated, which is what we have here.

The problem is that this comb effect means it is difficult to find out whether this shape is actually Gaussian within the channel, which would actually make the filter a lower order if using the middle channel and similar in shape to the top of the Santec Filter, or that the shape we see in Figure 4.2.4, which could have potentially undesirable effects, is the actual filter shape. How it would affect the offset filtering processes with these other channels visible, if not actually in use, are questions that will need to be answered in future detailed work.

## 4.3. Interferometers - Mach-Zehnder and Michelson Types

The Interferometers used in the experimental setups are of two types, Michelson, where there is one input and one output, and Mach-Zhender where there can be one or two inputs, and two outputs.

Mach-Zehnder Interferometers (MZI) are constructed using two 3dB couplers interconnected through two paths of differing lengths, this allows a wide range of uses, such a multiplexing and switching due to constructive and destructive signal outputs.

Firstly a single directional coupler should be considered, where $P_0$ is a single input into the upper fibre of the coupler, and there are two outputs, $P_1$ and $P_2$, representing the power of the upper and lower fibres respectively. The equation below describes the power coupled from the upper fibre into the lower fibre.

$$P_2 = P_0 \sin^2(\kappa d) \qquad \text{Eq. 4.3.1}$$

With $\kappa$ being the coupling coefficient and *d* the length of the coupling region.

Using conservation of power (for identical core fibre):

$$P_1 = P_0 - P_2 = P_0\left[1 - \sin^2(\kappa d)\right] = P_0 \cos^2(\kappa d) \qquad \text{Eq. 4.3.2}$$

Hence the phase of the upper fibre is 90° ahead of the lower fibre. The same can be shown for an MZI, which is basically two couplers connected back-to-back but with one arm slightly longer than the other to create a known phase difference [40]. The basic theory of a MZI can then follow on from the above. The propagation of light though a MZI can be represented by the matrix below:

$$M_{Coup} = \begin{bmatrix} \cos \kappa d & j \sin \kappa d \\ j \sin \kappa d & \cos \kappa d \end{bmatrix} \qquad \text{Eq. 4.3.3}$$

This basically shows that the lower fibre arm lags the upper fibre arm by 90°, and with 3dB couplers being involved, $2\kappa d = \pi/2$, so therefore we have:

$$M_{Coup} = \frac{1}{\sqrt{2}} \begin{bmatrix} 1 & j \\ j & 1 \end{bmatrix} \qquad \text{Eq. 4.3.4}$$

We then have a phase shift relative to each of the arms to consider due to either a difference in the length of the arms ($\Delta L$), or a difference in the refractive index (where $n_1 \neq n_2$) with $\Delta L = 0$.

The phase difference is given by:

$$\Delta\phi = \frac{2\pi n_1}{\lambda} L - \frac{2\pi n_2}{\lambda} (L + \Delta L) \qquad \text{Eq. 4.3.5}$$

Considering the above with respect to $\Delta L$ we can see that Eq. 4.3.5 can be reduced to:

$$\Delta\phi = \kappa \Delta L \qquad \text{Eq. 4.3.6}$$

Where $\kappa = \frac{2\pi n_{eff}}{\lambda}$.

This can now be represented in matrix form as:

$$M_{\Delta\phi} = \begin{bmatrix} e^{(j\kappa\Delta L/2)} & 0 \\ 0 & e^{(-j\kappa\Delta L/2)} \end{bmatrix} \qquad \text{Eq. 4.3.7}$$

We can now see the output of the MZI with the combination of Eq. 4.3.3 and Eq. 4.3.7 in the following equation:

$$M_{Out} = M_{Coup} \bullet M_{\Delta\phi} \bullet M_{Coup} = \begin{bmatrix} M_{11} & M_{12} \\ M_{21} & M_{22} \end{bmatrix} = \begin{bmatrix} \sin \kappa \Delta L/2 & \cos \kappa \Delta L/2 \\ \cos \kappa \Delta L/2 & -\sin \kappa \Delta L/2 \end{bmatrix} \quad \text{Eq. 4.3.8}$$

The equations above [40] show that the following occurs: a signal is put into the Input, which then meets the first coupler. Here the signal is split into two, with half the power going into either arm. However, we also get a phase change relating to both arms i.e. this means the upper arm leads the lower arm by a phase shift of $\pi/2$ with respect to the upper arm.

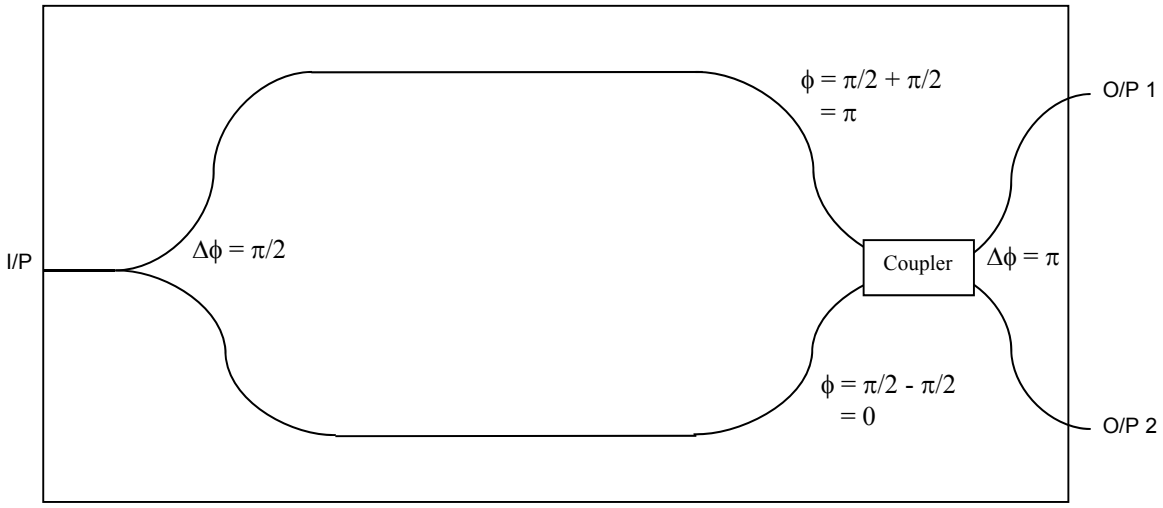


*Figure 4.3.1 – Basic diagram of a Mach-Zehnder Interferometer (MZI) with phase changes.*

At the second coupler there is again a phase change, therefore we have the following: $\frac{\pi}{2} + \frac{\pi}{2} = \pi$ for the upper leg $\frac{\pi}{2} - \frac{\pi}{2} = 0$ for the lower leg, so there is an overall $\pi$ phase shift which equals to constructive interference at output 1 and destructive interference at output 2.

## 4.4. Experimental Results

These experiments were carried out to find out whether the theoretical basis for improvements in the received signal using offset filtering [32, 132, 133, 134] could be confirmed. Experiments were designed, using different filter configurations, to see whether the theoretical improvements could be shown to be real and significant for each simulated configuration, and to see if the improvements are consistent for filter placement within the receive path and whether they have a significant impact in signal quality. All experiments

included in this chapter were back-to-back measurements; no transmission experiments were carried out.

The receiver used was a type of Direct-detection, with clock recovery used in certain where indicated within this section. Both single ended detection with one photodiode, and balanced receiving using two photodiodes, were used. Balanced detection has fibres attached to the photodiodes that are of equal length, this is to minimise the time delay between the pulses when they arrive at each of the diodes. This time delay can cause timing jitter and decreases the quality of the received signal, so needs to be as small as possible.

Different duty cycles, ranging from NRZ-DPSK to 33% RZ-DPSK modulation, were also used to see whether the theoretical improvement due to offset filtering was the same across different formats.

The amount of filtering used in these experiments is analogous to the Strong filtering regime. In an optical system or network, this would indicate that there are a number of cascaded filters or devices that can cause filtering effects, as discussed in section 4.1. These devices produce concatenation of the filtering effect, hence narrowing the bandwidth of the system considerably and consequently a significant amount of filtering is apparent. In Weak filtering regimes there are a small number of filters, or devices acting as filters, this means the filtering effect is small within a system or network.

For filter configurations using one filter on the destructive port, the RZ-DPSK signal is demodulated using the DLI thus creating a Duobinary (DB) output on the constructive port and an Alternate Mark Inversion (AMI) output on the destructive port. The destructive port is used because the spectrum of the AMI has a double peak; hence offsetting the filter on the destructive port will in essence create a duobinary output.

The reason that DB and AMI are created from the DPSK modulated signal, when demodulated using a DLI, is due to the offset in length between the two arms of the DLI. This difference in length of 1-bit creates a phase difference. When the original DPSK modulated input signal is interfered with the delayed version of itself, it produces a DB output on the constructive port since it is an

additive effect, and AMI on the destructive port which is a subtractive effect, for this reason a peak appears on the DB spectra whilst a dip appears on the AMI spectra, both at the centre frequency of the original input signal.

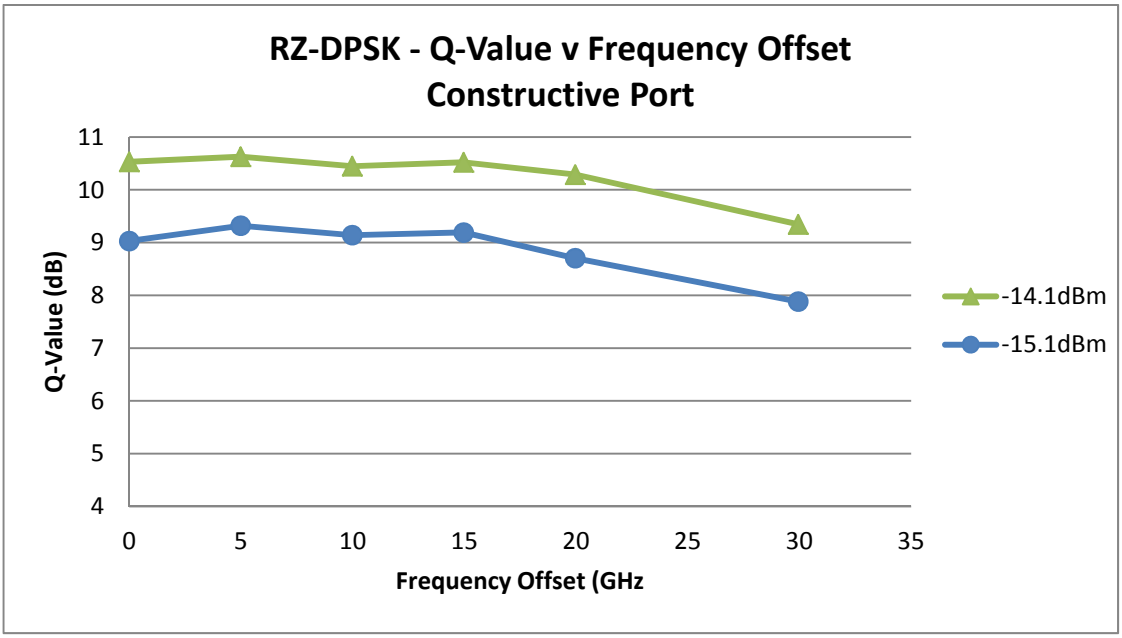


*Figure 4.4.1 – Single Ended: DLI Constructive Port. Filter1 with a 35GHz (0.28nm) Bandwidth with offset changed.*

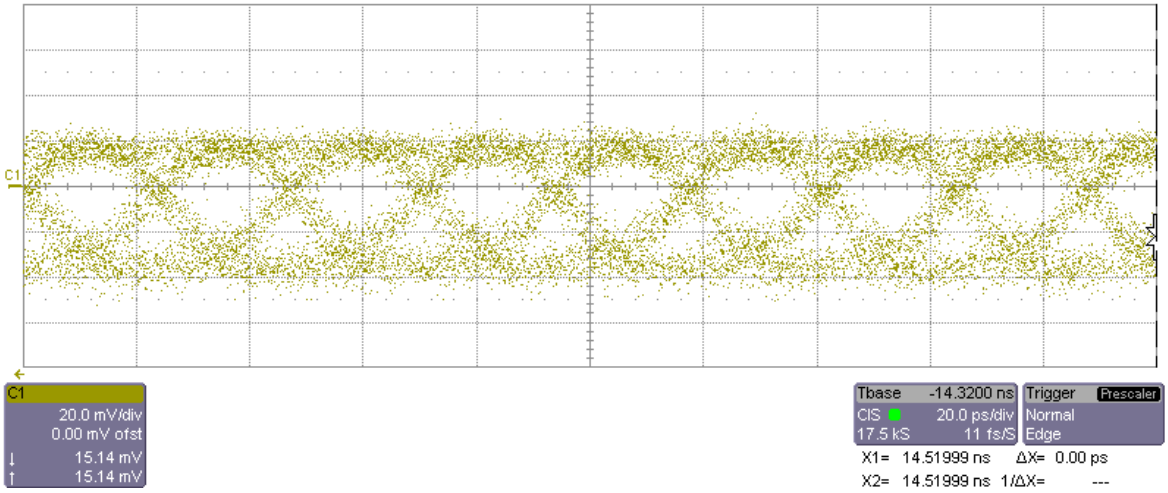


*Figure 4.4.2 – Eye Diagram showing the output of the DLI Constructive port; Filter1 with a 35GHz (0.28nm) Bandwidth.*

The improvements indicated by the simulations would give a relative improvement of between 1dB and 5dB [32, 132, 133, 134] dependent on filter placements. More detail is given in the individual configuration sections.

Before taking measurements with different configurations both outputs from the DLI were measured separately with single ended detection to record the base result from offsetting the filter frequency.

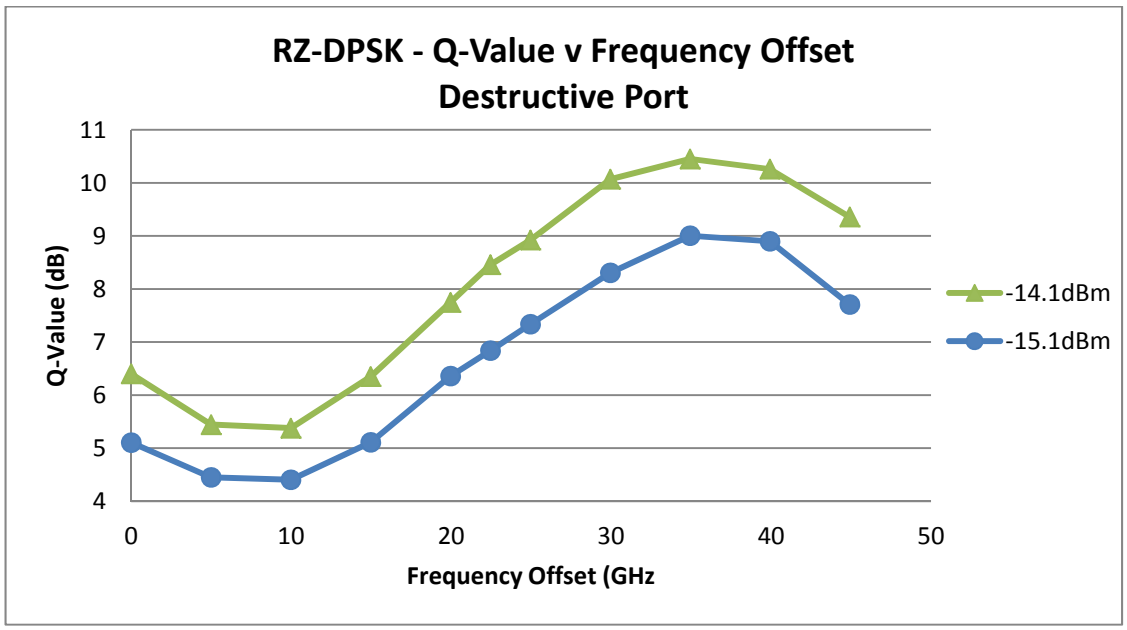


*Figure 4.4.3 – Single Ended: DLI Destructive Port. Filter1 with a 35GHz (0.28nm) Bandwidth with offset changed.*

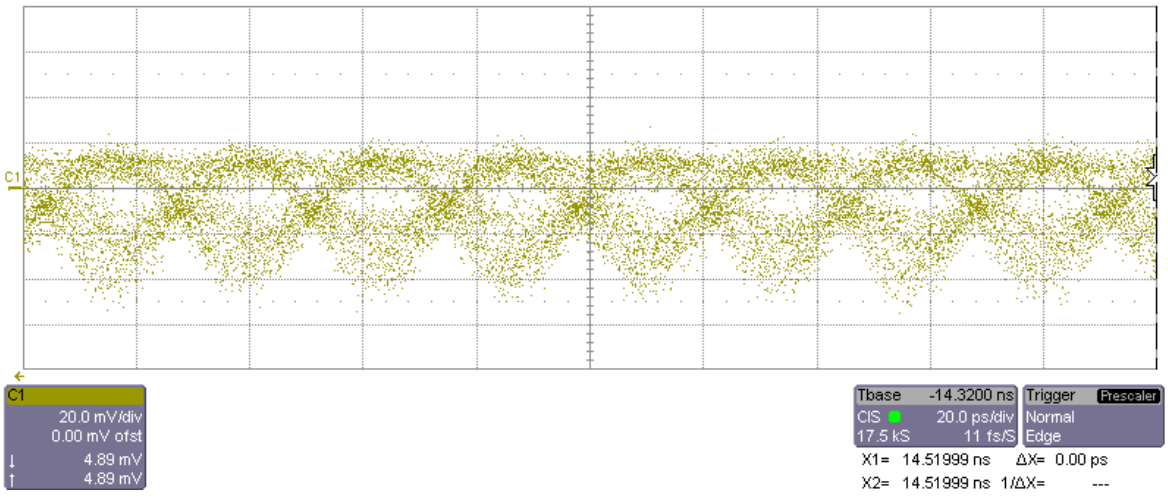


*Figure 4.4.4 – Eye Diagram showing the output of the Destructive port; Filter1 with a 35GHz (0.28nm) Bandwidth.*

This setup simply used one filter, with each output connected through the filter and measured in turn; both filters were set to a bandwidth 35GHz (0.28nm). The results from single ended receiving are shown in Figures 4.4.1 and 4.4.3 for Constructive and Destructive ports respectively, while Figures 4.4.2 and 4.4.4 show the relevant eye diagrams of the constructive and destructive

outputs. This gave an indication that improvements in the output were possible and that by using balanced receiving it could be possible to improve on these results depending on the configuration.

The configurations are grouped into three subsections; single filter configurations, dual filter configurations and three filter configurations.
Each subsection has a number of different configurations using the number of filters stated, apart from the three filter configuration where the only configuration tested was with one filter (Filter 3) used before the DLI, with the other two filters (Filters 1 and 2) placed on each output of the DLI.

Unless otherwise stated, all measurements were taken with the OSNR at 20dB (with a 0.1nm resolution bandwidth).

### 4.4.1. Single Filter Configurations

The first configurations consisted of a single filter placed either before the Delay Line Interferometer (DLI) in the receive path, or in the receive path on the destructive output of the DLI. This was to try and prove that the theory for offset filtering would work experimentally.

With the single filter two measurement techniques were used, balanced receiving and single ended receiving; Balanced receiving using two comparable photodiodes connected to the SHF Error Analysers DATA and $\overline{\mathrm{DATA}}$ inputs. Single ended receiving using destructive and constructive ports individually to compare their outputs.

BER measurements were taken using the SHF Error Analyser and converted in Q-Values, as it is easier to compare like-for-like as all simulated results were in Q-values. Q-values take into account the variance of the received noise powers of a logical 1 and a logical 0, with 0 generally having a lower variance [40] see Section 4.2 for the theoretical basis.
Some previous work had been done with a single filter before the DLI but no frequency offset was carried out on the filter [140].

#### 4.4.1.1. Single Filter before the Delay Line Interferometer (DLI)

The first configuration was the simplest in construction, with a single filter placed between the Transmit Amplifier and the DLI on the Receiver side of the configuration. This combination is also known as pre-filtering.

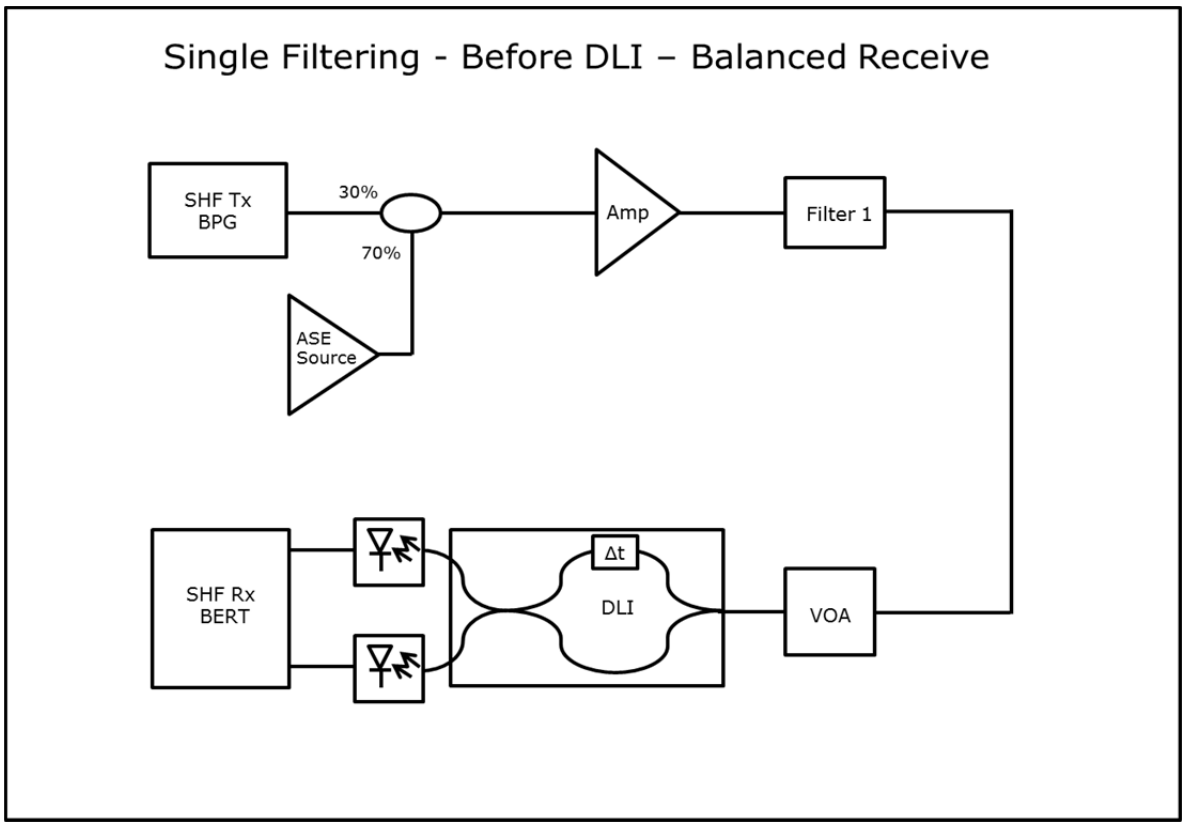


*Figure 4.4.5 – Single Filter before DLI with Balanced Receive.*

The configuration shown in Figure 4.4.5 is the single filter configuration with the filter placed before the DLI. This gives an example of the filtering seen in a short transmission span where some attenuation of the signal occurs, but the overall signal is improved by removing the ASE built up over the span. The data is in DPSK modulation format which is created by passing the initial PRBS $2^{31}$-1 data through an MZI that has a 1-bit delay. This creates a Phase Shift in one path compared to the other. The data is then either passed through a second modulator to give RZ data or the modulator is switched off, which gives NRZ data.

The ASE source is supplied via an EDFA with tuneable drive current connected to the 70% port of the coupler, while the data signal is sent through the 30%

port. The combined signal and noise is sent through another EDFA to boost signal power before it enters the filter.

The filter is of a typical 3rd order Gaussian shape [32, 132, 133, 134]. After the filter a Variable Optical Attenuator (VOA) is used to control the signal power going into the DLI, the DLI then decodes the DPSK modulation format into simple ASK, with Constructive and Destructive outputs connected to two separate photodiodes, which convert the received optical signal into an RF signal for the SHF Bit Error Rate Test-set (BERT) to read the errors based on the decision threshold of the receiver.

The results shown over the next few pages are mainly for proof of concept, and show whether investigations into further configurations were worthwhile.

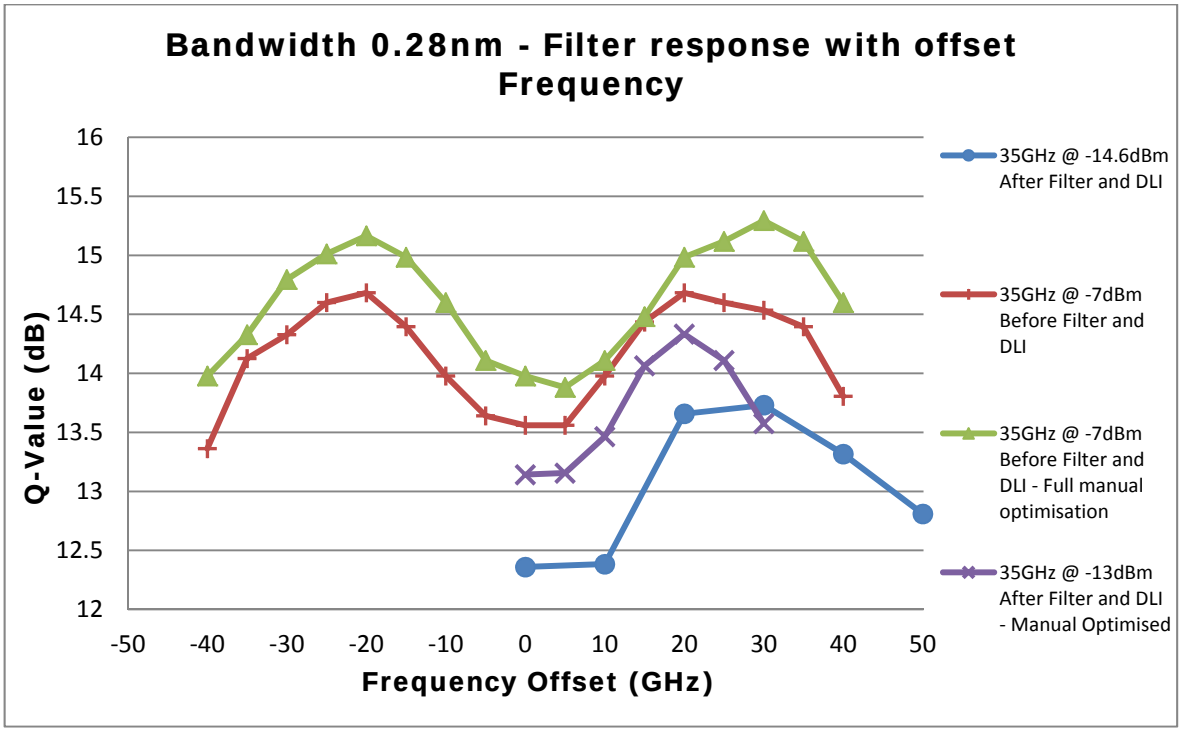


*Figure 4.4.6 – Q-Value change with Frequency offset, using 42.7Gbps RZ-DPSK modulation and fixed bandwidth of 35GHz (0.28nm).*

The results shown in Figure 4.4.6 illustrate the Q-value measured with respect to the frequency offset of the filter. The centre frequency of the filter was set at 193.402THz (λ = 1550.1nm) as this was the frequency where the intensity peak of the laser was highest.

For the first measurement the BER was taken every 2.5Ghz (λ = 0.12nm) from -40GHz to +40GHz, with one measurement carried out up to +50GHz; this gave a wide enough band to see whether any of the improvements indicated by the simulations could be measured, and if there was an improvement indicated, what was the amount of Q-value improvement.

It can be seen that, in general, as the filter is offset, an improvement in the received Q-value is apparent with an increase of ~1.5dB after 20GHz to 30GHz offset. This result is in line with those predicted by the simulations [32, 132, 134].
One result was only measured to 30GHz, but it dips before the others suggesting there is still some issue with repeatability; this seems mainly down to system stability.

The results shown in Figures 4.4.7, 4.4.8 and 4.4.9 show the Constructive and Destructive outputs of the DLI for filter bandwidths of 0.26nm, 0.28nm and 0.32nm. This was to demonstrate whether the improvement seen was consistent over different bandwidths or whether the improvement disappeared and therefore only existed at 0.28nm.

All graphs show the results at two different receive powers, indicating that there is some consistency in the measurements even when the receive power is changed.
The results show, as expected, that the destructive port does exhibit an improvement with an offset of 8GHz to 30.5GHz with a Q-value of just above 12dB for 0.32nm and slightly higher for 0.28nm, whilst the Q-value was around 13.5dB at 0.26nm.

We can compare these results to those in [141] where a similar setup was used, but the filter before the DLI was not offset which gave a worse performance on the destructive port, as expected, compared to that of the constructive port. We have proved here that, by offsetting the filter, an improvement is realised using single ended or balanced receive.

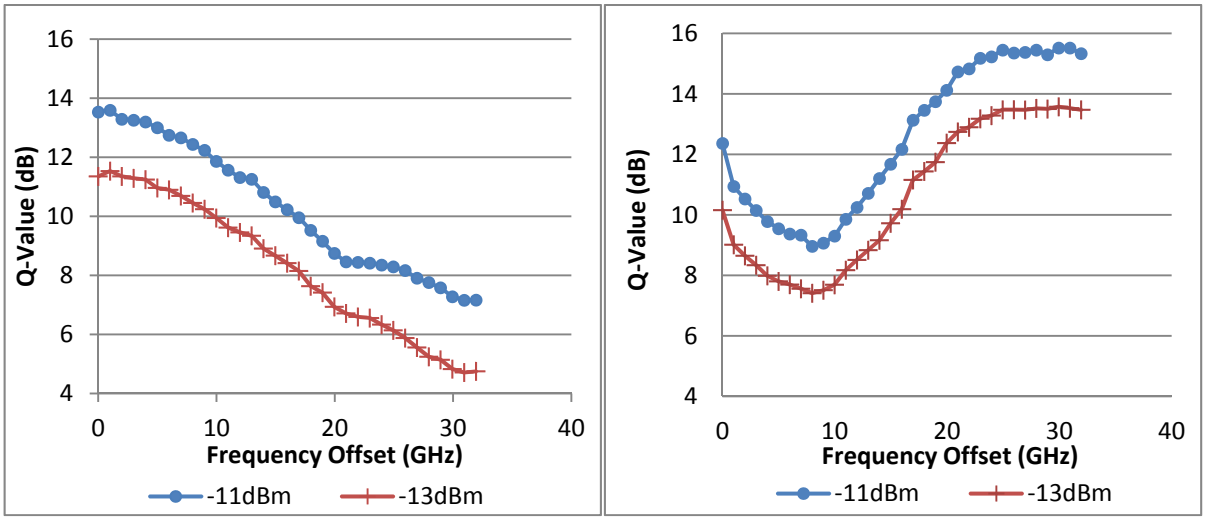


*(a)* *(b)*

*Figure 4.4.7 – 32.5GHz (0.26nm) BW: (a) Constructive Port (b) Destructive Port.*

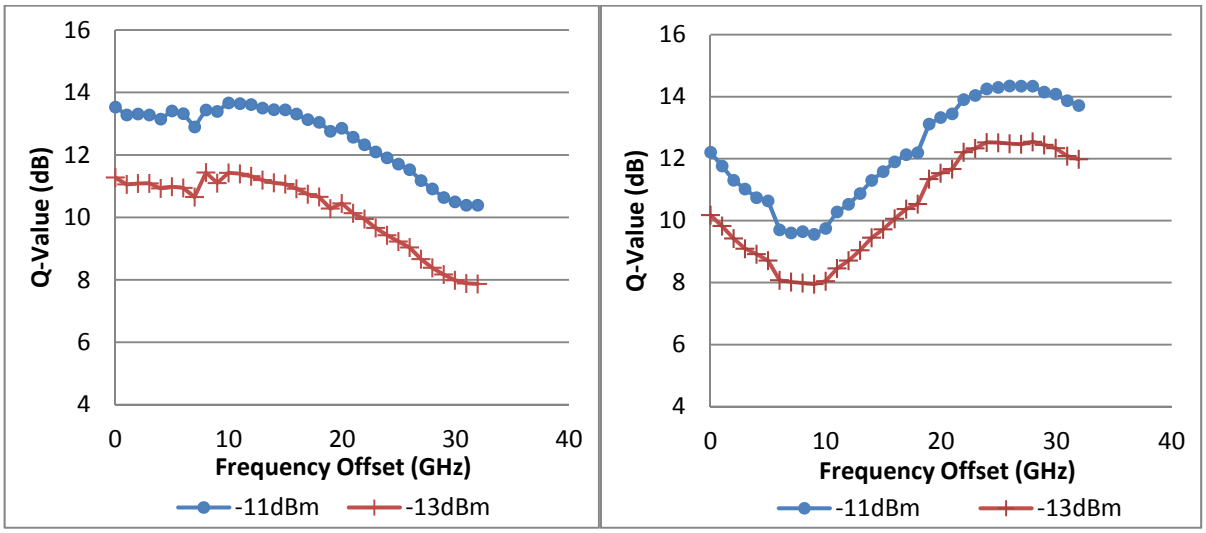


*(a)* *(b)*

*Figure 4.4.8 – 35 GHz (0.28nm) BW: (a) Constructive Port (b) Destructive Port.*

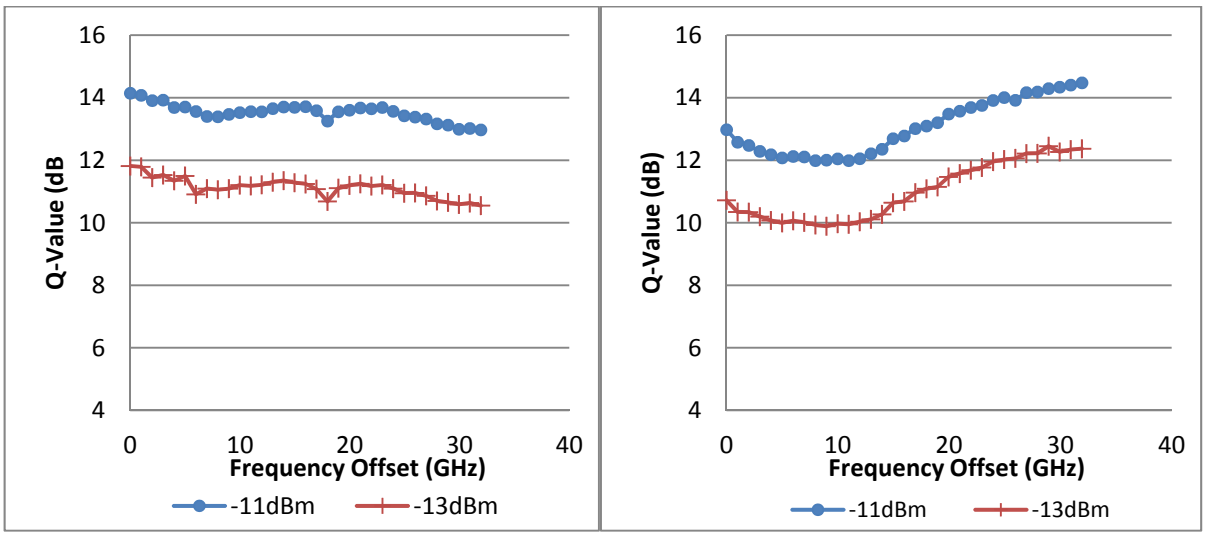


*(a)* *(b)*

*Figure 4.4.9 – 40GHz (0.32nm) BW: (a) Constructive Port (b) Destructive Port.*

The conclusion for using one filter before a DLI is that an improvement of about 2dB can be gained, at an offset of 8GHz to 30.5GHz at a data rate of 42.7Gbps using RZ-DPSK modulation.

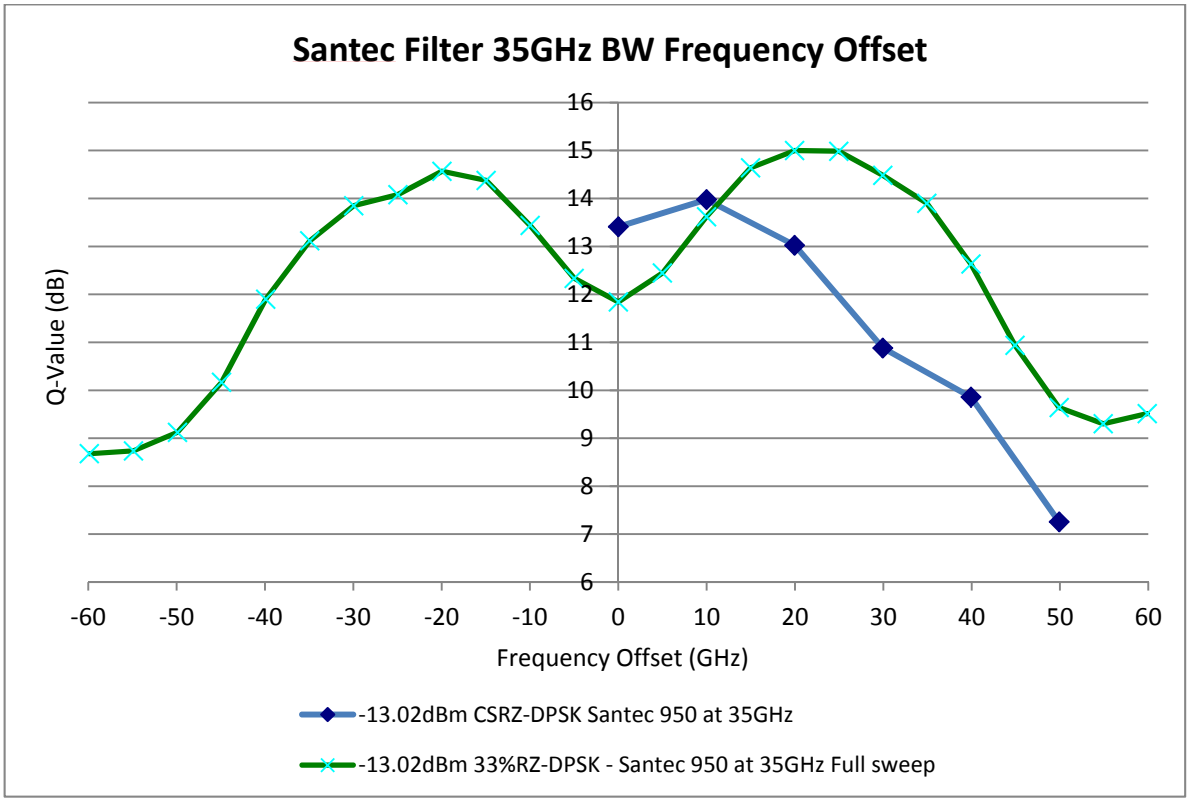


*Figure 4.4.10 – Q-Value change with Frequency offset for 42.7Gbps 33%RZ-DPSK and CSRZ-DPSK.*

The single filter result using 33%RZ-DPSK, from negative to positive offset, was repeated using a Waveshaper for comparison purposes; these results can be seen in Figure 4.4.10. Also shown is CSRZ-DPSK, which confirms that only limited improvement is expected with this modulation format in the strong filtering regime [134, 141, 142, 143].

The Waveshaper was used for the completion of experiments for both 2 and 3 filter configurations, and can be seen in Sections 4.5 and 4.7

#### 4.4.1.2. Single Filter after the Delay Line Interferometer (DLI)

In this experimental setup, as shown in Figure 4.4.11, a single filter was placed on the destructive port of the DLI with a balanced receiver.

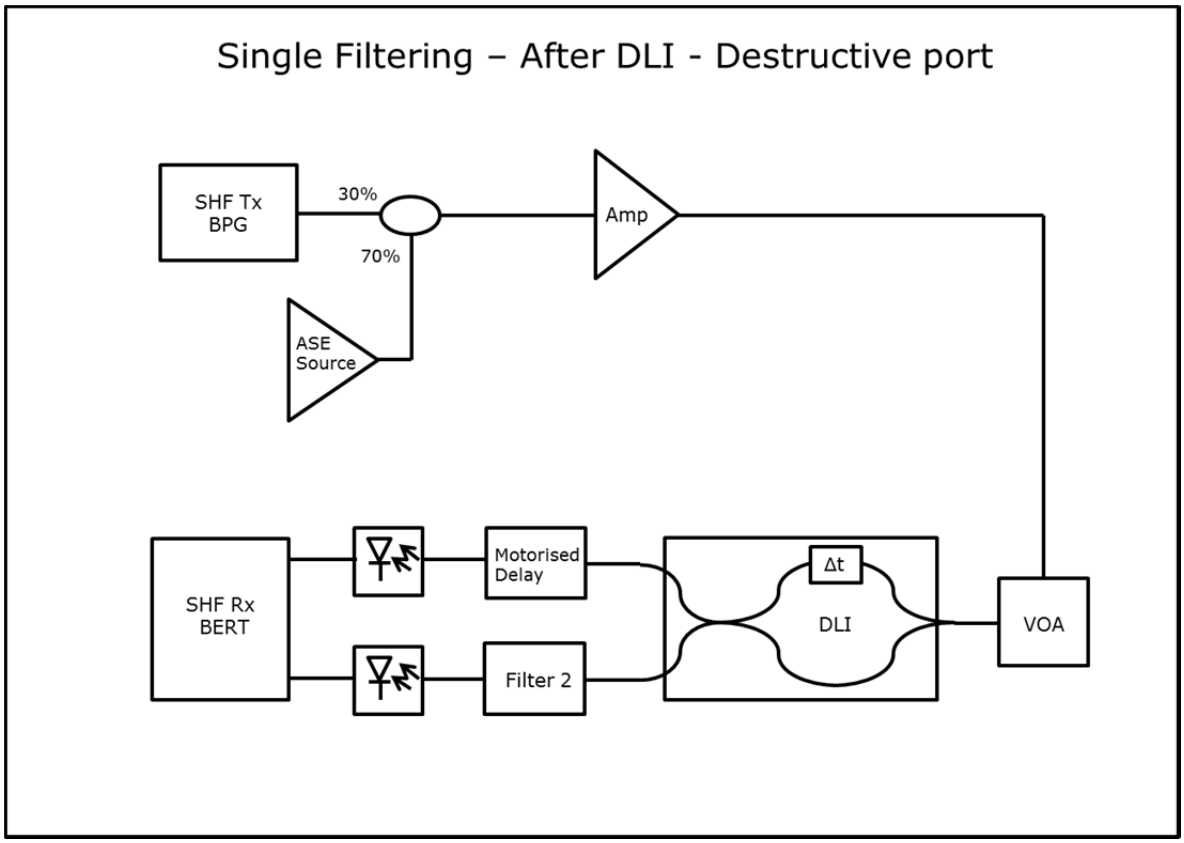


*Figure 4.4.11 – Single Filter after the Destructive port of the DLI with Balanced Receive.*

For comparison different modulation formats were used to see if any sensitivity improvements were maintained, improved, or became worse, whilst using the same physical setup.
The modulation formats used were all DPSK using the following bit slot duty cycles; RZ with 33% duty cycle, CSRZ (equivalent to 67% RZ) and NRZ (100% duty cycle).

The results are shown in Figure 4.4.12 for two different received powers and Figures 4.4.13 and 4.4.14 with three different received powers. This was purely down to the measurements for RZ-DPSK modulation not being recorded to a receive power as low as -16dBm.

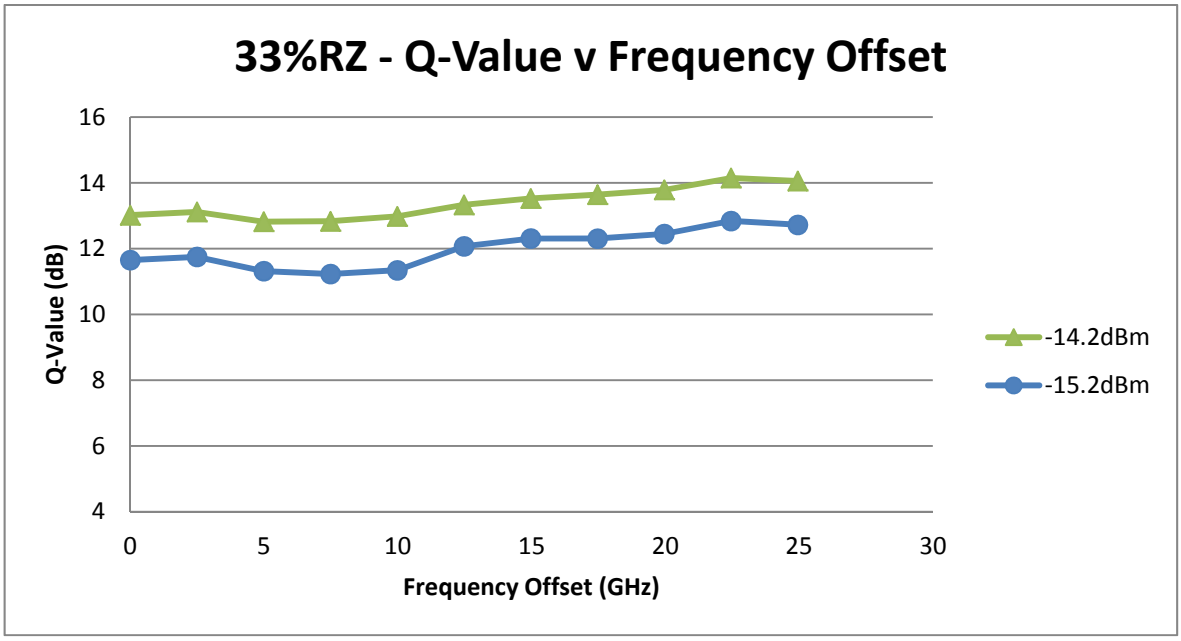


*Figure 4.4.12 – 35GHz (0.28nm) BW: Return-to-Zero Modulation (RZ).*

Figure 4.4.12 shows the case for 33%RZ-DPSK modulation with the filter being offset up to 25GHz. The results of two separate received powers are shown to see if there was any dissimilarity when different transmitted powers were received. The resulting graphs show there is a slight improvement of about 1dB in the Q-value when the frequency offset is close to 23GHz.

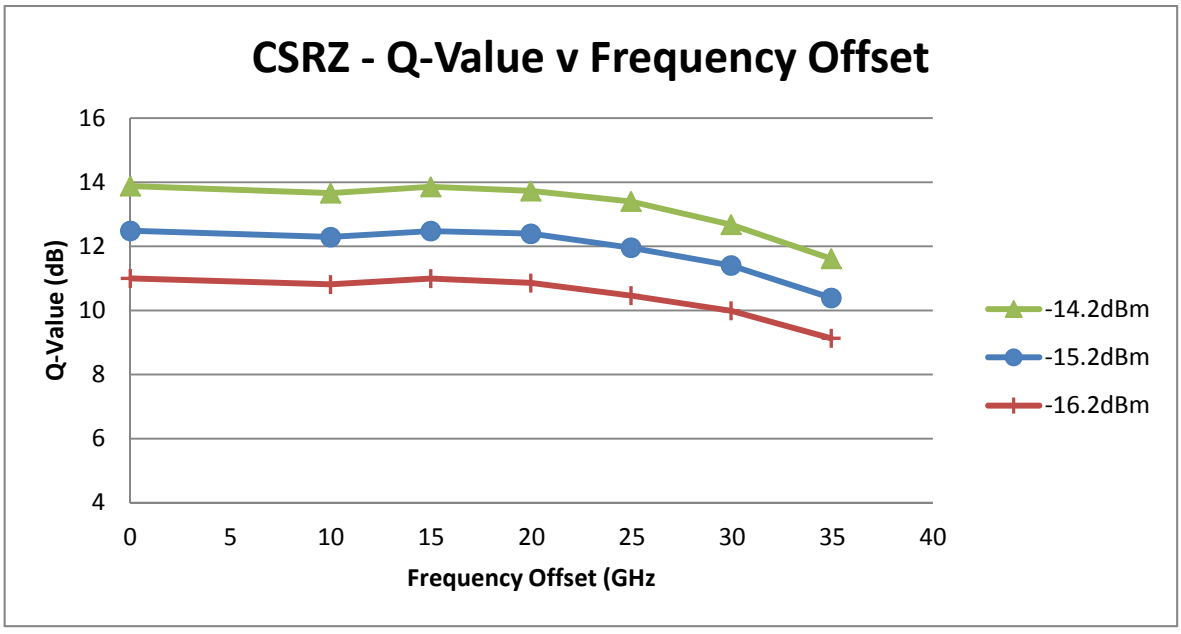


*Figure 4.4.13 – 35GHz (0.28nm) BW: Carrier Supressed Return-to-Zero Modulation (CSRZ).*

For the results shown in Figure 4.4.13, the modulation format was CZRZ-DPSK, which is the same as 67% RZ-DPSK. The format had been used

previously and had shown no improvement [32], so it was important to repeat the measurements to confirm the original findings.

The results show a slight degradation of performance until 12GHz, where performance picked back up slightly, but then degraded again after 17GHz until there was a 2dB-2.5dB drop at 35GHz. This confirms results from previous simulations [32, 132, 134].

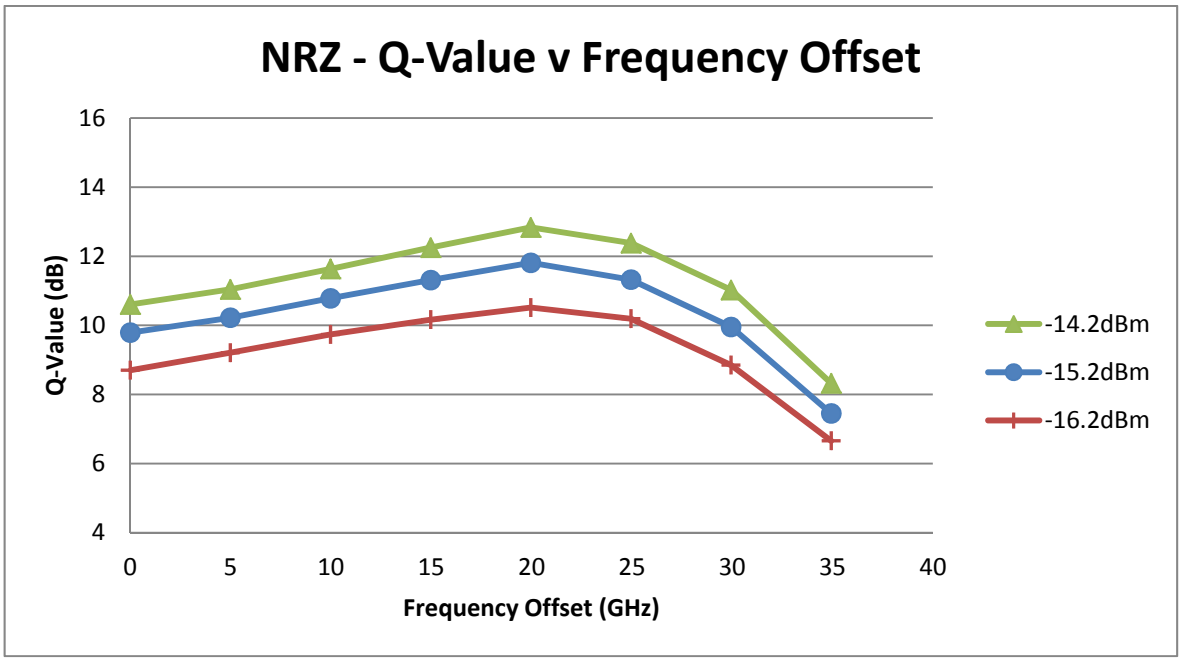


*Figure 4.4.14 – 35GHz (0.28nm) BW: Non-Return-to-Zero Modulation (NRZ).*

Figure 4.4.14 shows the results for NRZ-DPSK; these show an improvement of 1.5dB-2.25dB; however the peak improvement is 1dB lower than for RZ-DPSK and the Q-value at zero offset is 2dB-2.25dB below RZ-DPSK. This seems to be due to more noise on the NRZ eye diagram when compared to the RZ eye diagram creating an increase in ISI, where the difference in the noise is due to the RZ format being more resilient to ISI, this is due to its shorter pulse widths when compared to NRZ.

Comparing the three different modulation formats, 33% RZ-DPSK, CSRZ-DPSK and NRZ-DPSK, we can see that CSRZ-DPSK shows no improvement, only a comparable result at 15GHz as with the result at 0GHz, after which the Q-value drops by 2.2dB at 35GHz.

In section 4.4.1.1, it was shown that there was improvement using 33%RZ-DPSK of ~3dB, where CSRZ showed almost none. There have been experiments using CSRZ that have reported slight improvements which used "pre-filtering", namely measurements were taken using a single filter which was offset prior to the DLI or receiver [143], but this occurred within weak filtering conditions where bandwidths of >50GHz were used.
The reason for this absence of improvement in strong filtering conditions (<50GHz) using CSRZ is related to the fact that the demodulation of the signal by the DLI has a 1-bit delay for the DPSK demodulation. This 1-bit delay causes the phase changes, related to the CSRZ format, to be different when compared to the phase of the original signal; so while this would not affect the data, it would affect the resulting spectrum by creating a small amount of carrier, therefore causing a flattening of the DLI output and no improvement after the DLI.

The measurement results using 33% RZ-DPSK showed an increase of 1dB over a 25GHz offset, which is explained via the AMI to DB conversion, and also owing to this duty cycle of 33% being less robust to narrow filtering when compared to CSRZ as it has a broader spectrum. Therefore, narrow filtering will have more of an effect, and a greater improvement from the offsetting of the AMI port should be seen, as establish in Figure 4.4.13.

Turning to NRZ-DPSK modulation, an improvement of 2.2dB at 20GHz is shown in Figure 4.4.14, which again can be explained via the AMI to DB conversion and the broader spectrum. However, there is a comparative loss at 20GHz between NRZ and the RZ formats, with 33% RZ and CSRZ being 0.9dB higher.

The above difference can be explained because of the averaged power over the bit slot, which for both RZ formats gives a higher peak power, thus less signal loss. Also, due to the lower duty cycles, the RZ formats have a higher tolerance to fibre non-linearity compared to the higher duty cycle NRZ.
In general NRZ is inferior in receive sensitivity terms than RZ, which accounts for the ~1dB difference in maximum Q-Value, thus can be up to 3dB lower in general due to a lower peak power per bit slot. However, NRZ has other

advantages such as simpler transmitter design which leads to lower system costs.

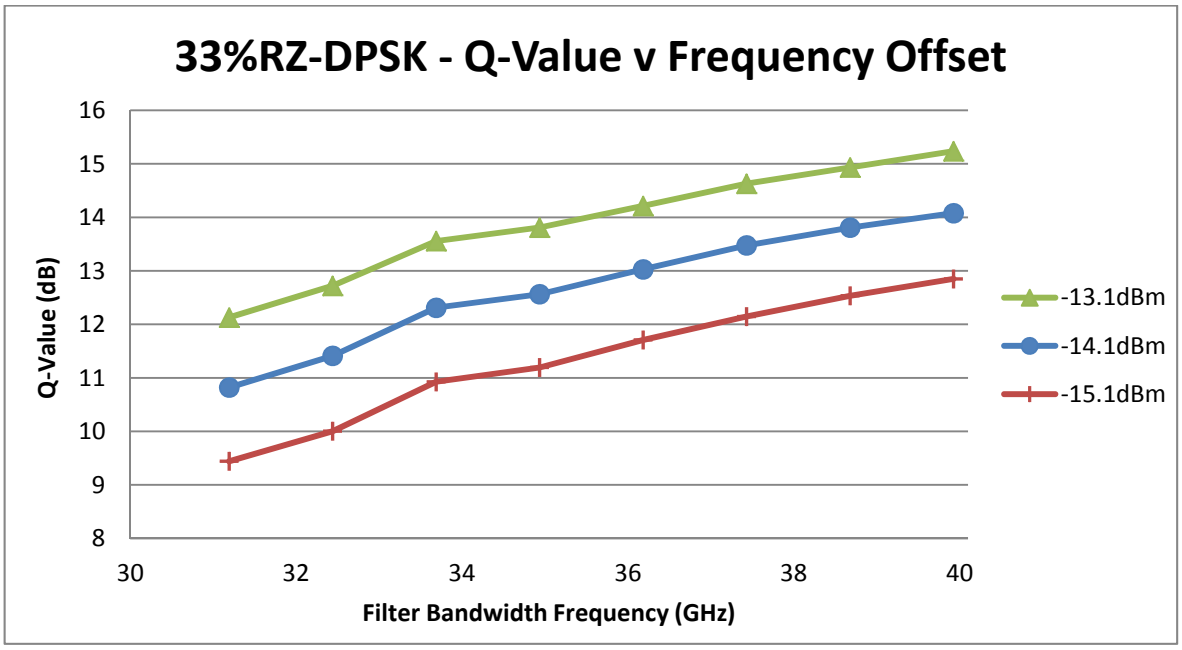


*Figure 4.4.15 – Using RZ-DPSK Modulation, Q-Values measured for different Filter Bandwidths with no filter offsets.*

Figure 4.4.15 shows the Q-Values calculated for three different receive powers across a range of bandwidths, from 32GHz to 40GHz with an offset set at 0GHz. As expected, it shows a general deterioration with tighter filtering, but flattens out slightly between 33.7GHz and 35GHz before the general trend resumes. This may be caused by some frequency dependent loss within the filter as the effect also seems to be present at the half-wavelengths of these frequencies.

If the results are compared with the simulations and previous experimental results in [32] there is a slight difference in the number of bandwidth measurements which were taken; 33GHz to 35GHz for the simulations and 31GHz to 37.5GHz for the experimental case in [32], whilst the measurements were taken over 31GHz to 40GHz in the experimental case in this section in Figure 4.4.15. The general trend is similar, with an increase in Q-values by ~3dB, and also the slight improvement at 33.7GHz (0.27nm) is seen in the experimental results, Figure 7.5 in [32]. The results in Figure 4.4.15 need to be repeated with different offset frequencies for the same filter bandwidth changes.

### 4.4.2. Two Filter Configurations

The use of two filters meant that a number of additional configurations were available. The first configuration was to keep one filter in between the DLI destructive output and the receiver.
As with all configurations, the frequency offset of the filter that was nominally called Filter 2, was changed first and then Filter 1 was adjusted, with Filter 2 either being kept at the frequency offset which gave the maximum output, or at zero offset.

#### 4.4.2.1. One Filter before the DLI and one Filter after the DLI

For this configuration only CSRZ-DPSK modulation was used. CSRZ-DPSK is similar to 67% RZ-DPSK as the temporal pulse of CSRZ is the same as having a 67% RZ duty cycle. This is because of the broad spectrum of CSRZ, which is caused by its generation using DLI and half-bit rates.

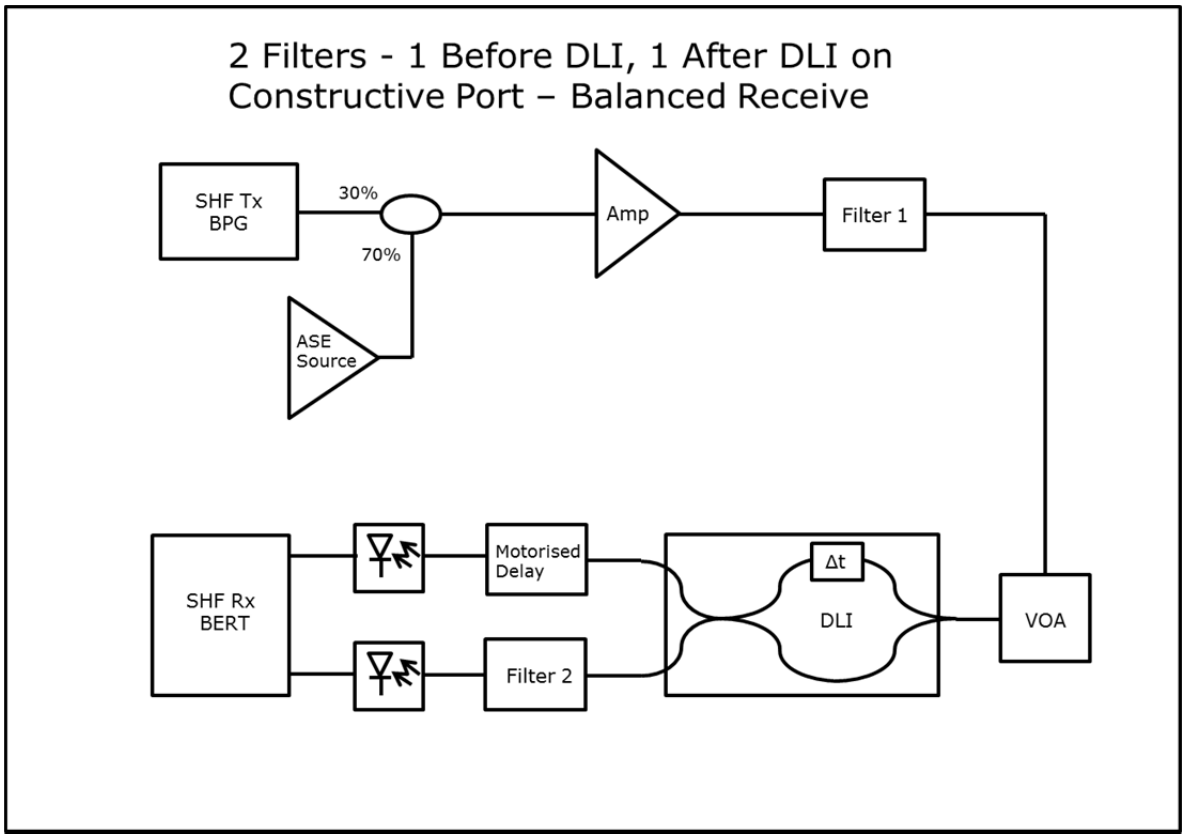


*Figure 4.4.16 – Single Filter before DLI and single filter after the Destructive port of the DLI with Balanced Receive.*

CSRZ modulation was selected as this was the worst case scenario from the previous experiments with one filter, due to having no visible improvement, which can be seen in Section 4.4, specifically in Figure 4.4.13 within that section. Any noted improvement using CSRZ-DPSK would therefore indicate the potential for even larger improvements using other the modulation techniques of 33%RZ-DPSK and NRZ-DPSK.

The configuration shown in Figure 4.4.16 is of two filters. One filter is placed before the DLI, as in section 4.4.1.1, and the second is placed after the Destructive output of the DLI, as in section 4.4.1.2.

No simulation work was carried out for this configuration.

The output on the Constructive side had fibres lengths calculated with the correct delay to match the addition of the filter and its connected fibres, between the DLI output and photodiode at the receivers, so that the partially demodulated output for each side is measured at the same bit slot.

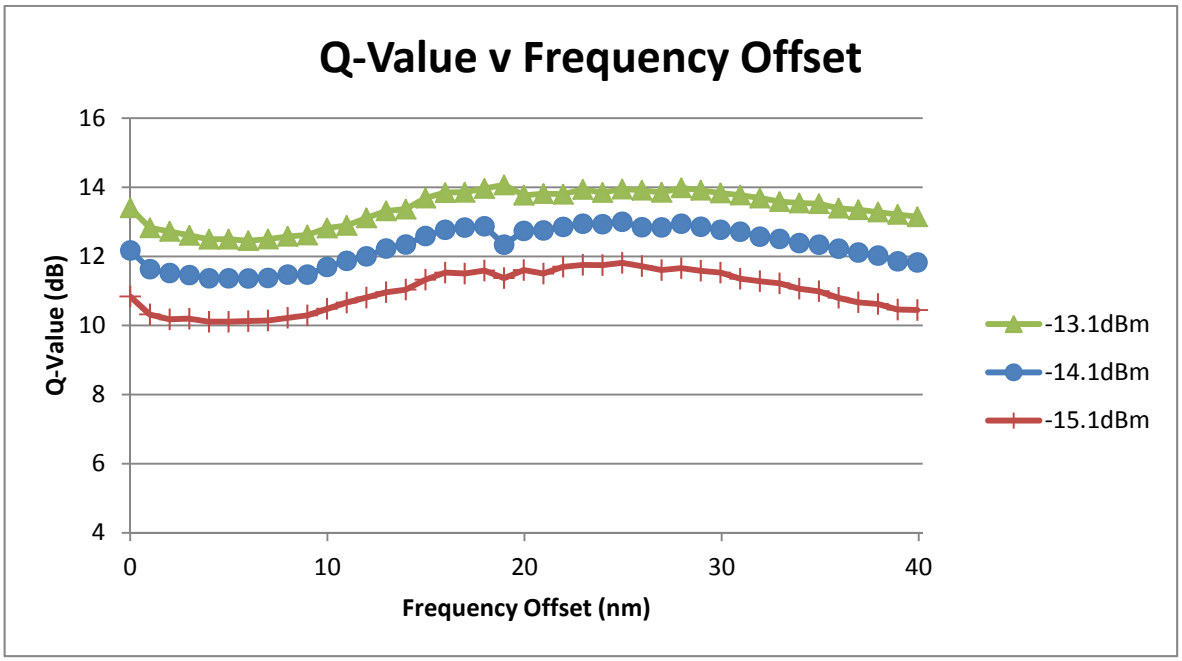


*Figure 4.4.17 – 35GHz (0.28nm) BW: one filter before DLI and one on the DLI Destructive Port. 42.7Gbps CSRZ-DPSK modulation*

The results shown in Figure 4.4.17 show a slight improvement at 17-18GHz offset, apart from at a receive power of -13.1dB where the highest Q value is seen at 19GHz with an improvement of 0.6dB.

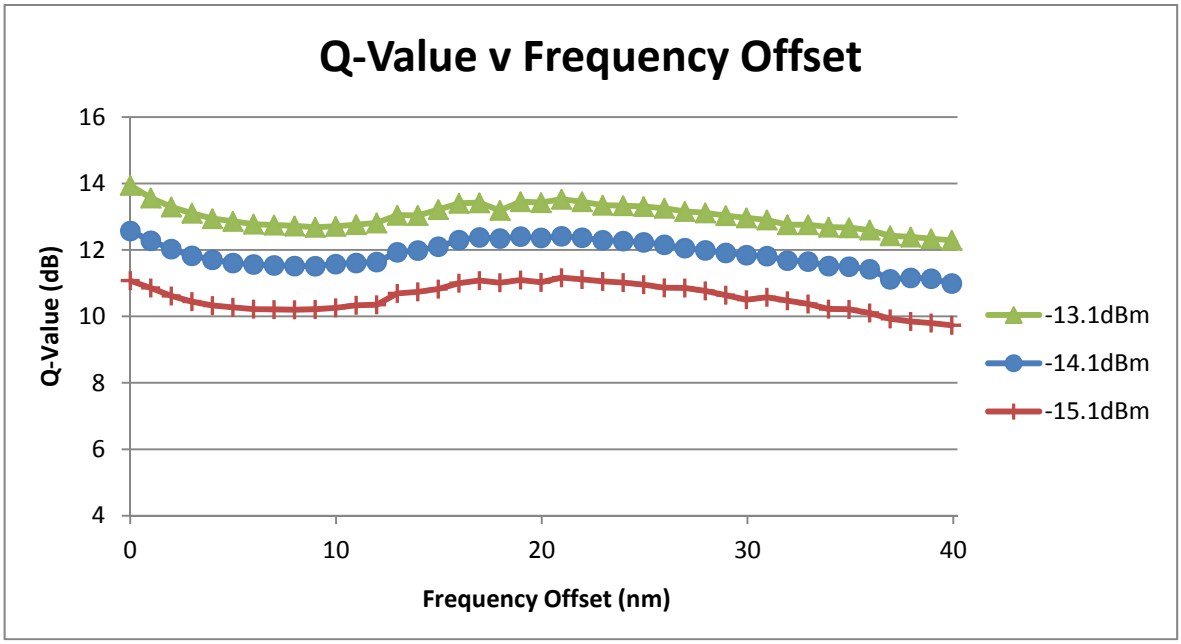


*Figure 4.4.18 – 35GHz (0.28nm) BW: one filter before DLI and one on the DLI Destructive Port. 42.7Gbps CSRZ-DPSK modulation – Measurements repeated.*

Unfortunately at the lower receive powers there is a decrease in Q-value imparted by a small dip in the graph. The reason for this is unknown, but could be down to variations in the balanced receive detection point due to equipment temperature drift, which meant the correct balance point wasn't reached when measured and recorded. There could also be an issue relating to this offset frequency being close to the half-wavelength of the filter bandwidth, the bandwidth being 35GHz. Some form of SPM may be present, causing the peak of the AMI signal to change in the spectral domain.

A similar response is seen with the change in bandwidth measurements in Figure 4.4.15 between 33.7GHz and 34.9GHz, in one of the filters before the DLI which may be explained by some wavelength dependent loss being present at those frequencies, which would also affect their half-wavelengths.

Owing to the graphs showing different results at 19GHz for the three receive powers measured, the results were repeated. This time they showed no improvement over that recorded at 0GHz offset, even though the graphs were of similar shape, so it was concluded that there was some sort of system issue between these and the original BER measurements. This could be down to temperature drift during the time interval between the first and second measurements, or a software issue.

#### 4.4.2.2. Two Filters before the DLI

Using two filters in series before the DLI maximises the attenuation and filtering effects, which is similar to a transmission line with high data rates passing through it; in this instance 42.7Gbps.

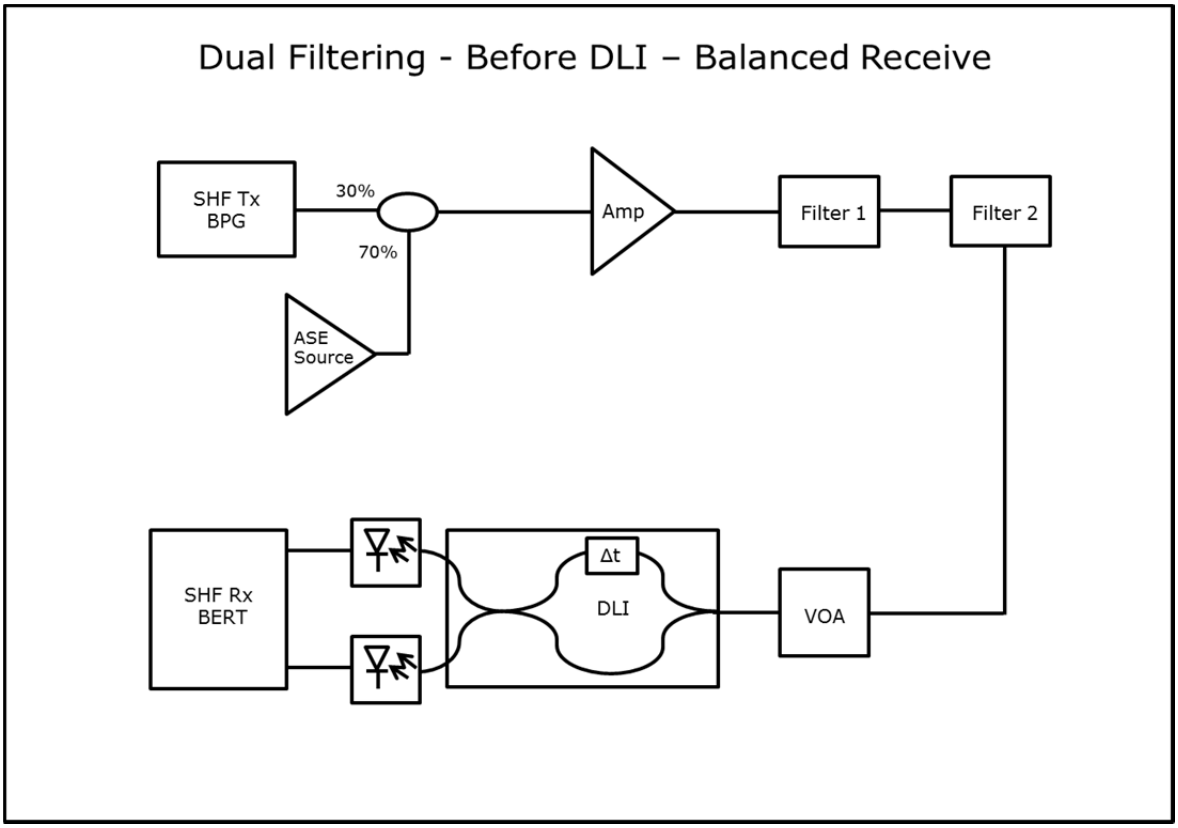


*Figure 4.4.19 – Two Filters before DLI with Balanced Receive.*

In section 4.4.1.1 there was one filter placed before the DLI which showed some improvement. Adding a second filter will reduce the receive power but there will still be an improvement in Q-values, as seen in the previous configurations.

No simulated results were carried out for this configuration.

Figure 4.4.19 shows the configuration with the two filters before the DLI. Each filter started with a bandwidth of 35GHz (0.28nm) and 0GHz offset, where filter 2 was changed and filter 1 kept at the initial starting condition and BER measurements taken. We took measurements at three different bandwidths;

35GHz (0.28nm), 40GHz (0.32nm) and 50GHz (0.40nm), to see how much effect the change in bandwidth had.

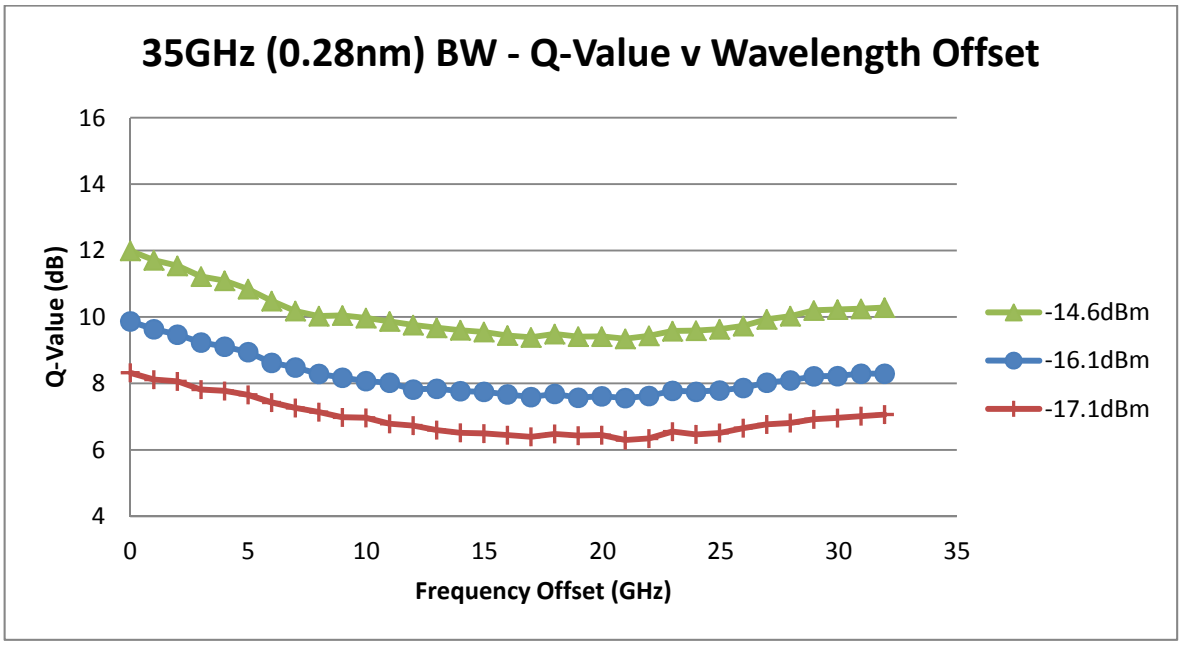


*Figure 4.4.20 – 35GHz (0.28nm) BW: two filters before DLI; 42.7Gbps CSRZ-DPSK modulation.*

We see for Figure 4.4.20 there is no improvement with frequency offset over no offset, although there is a slight upward trend at the last few measurements past 31GHz offset.

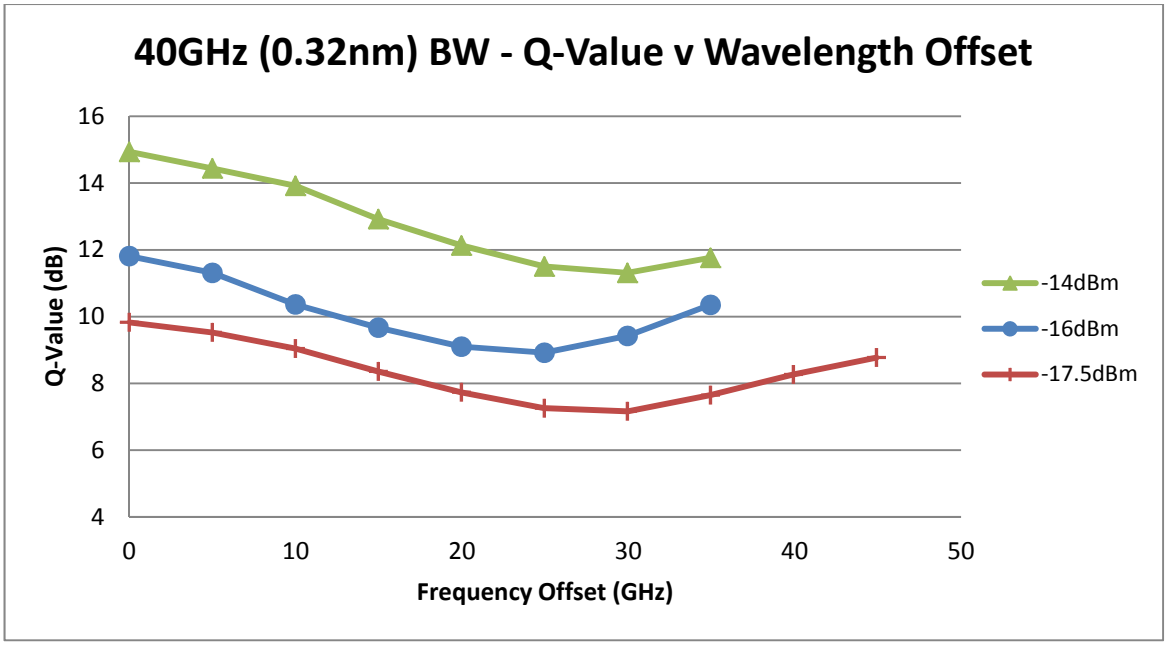


*Figure 4.4.21 – 40GHz (0.32nm) BW: two filters before DLI; 42.7Gbps CSRZ-DPSK modulation.*

In Figure 4.4.21 we see again that there is no improvement up to 0.35nm offset compared to 0nm offset, although as with the previous results, there was a slight upward trend near the end of the measurements, but, there is a slight deviation at -16dBm receive power where the return gradient starts earlier than for -14dBm and -17dBm.

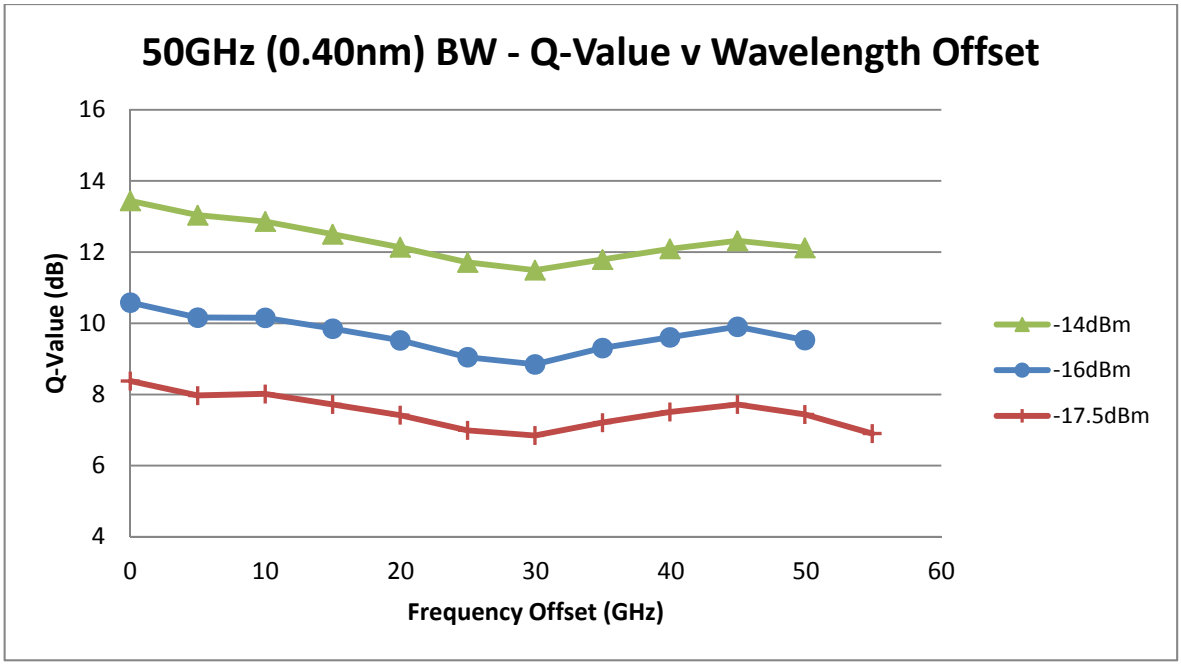


*Figure 4.4.22 – 50GHz (0.40nm) BW: two filters before DLI; 42.7Gbps CSRZ-DPSK modulation.*

For the widest bandwidth of 50GHz in Figure 4.4.22, we see there is less degradation overall, but no improvement is seen when compared with the results for the previous bandwidths. The reason for this could be that the amount of filtering apparent reduces the signal power too much, so that any offsetting gives a minimal improvement in the first filter, but this is not seen by the second filter due to the extra loss, hence no improvement is seen.

#### 4.4.2.3. Two Filters after the DLI using Physical Filters

This configuration was an important benchmark for confirming the simulations as described in [32]. The results should show an improvement of 2dB when compared to non-offset filtered measurements within a 50GHz grid.

The configuration shown in Figure 4.4.23 has two filters after the DLI, one on the Constructive port and the second on the Destructive Port; these were initially set at 35GHz (0.28nm) bandwidths with no offset. Then Filter 2 had its offset changed up to a value of 22.5GHz (0.18nm).

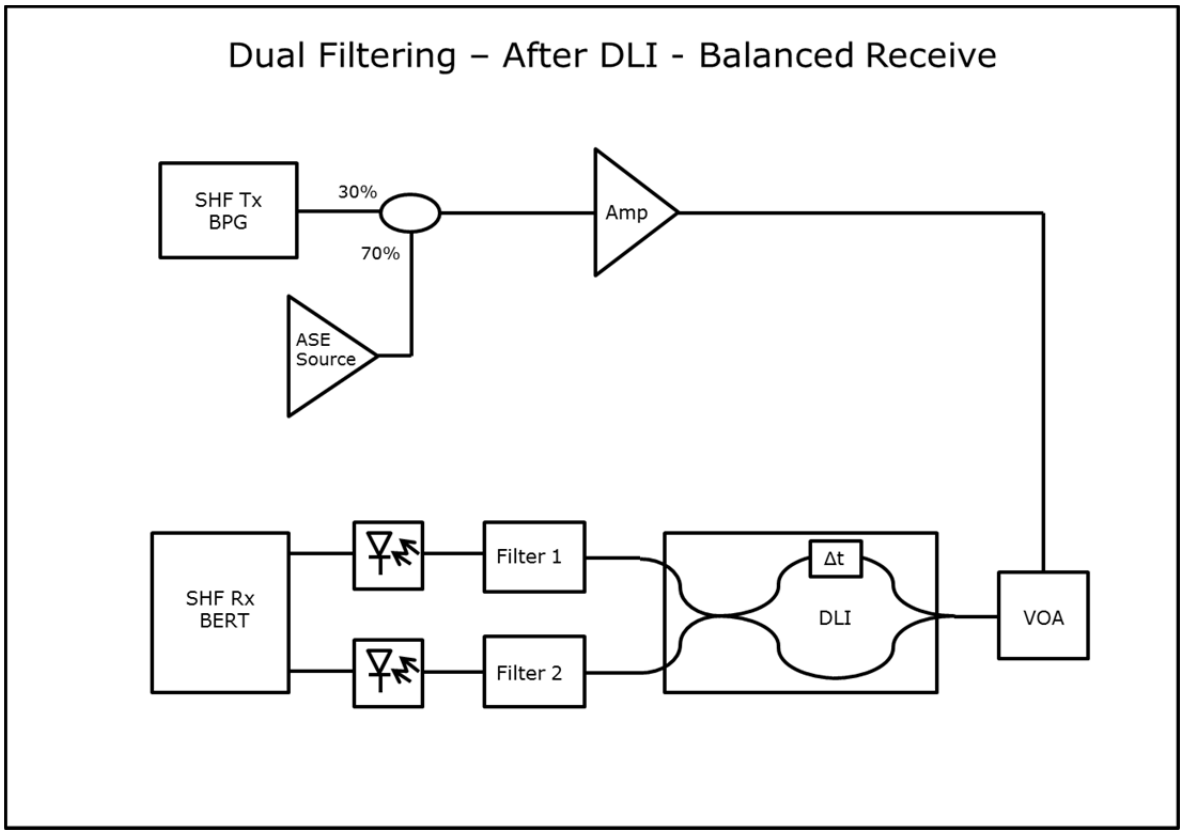


*Figure 4.4.23 – Two filters after DLI, Filter 1 after the Constructive port and Filter 2 after the Destructive port. Balanced Receive.*

After measurements were taken at 1GHz steps, the offset with the lowest BER was set. Filter 1 was then changed in the same manner, up to 22.5GHz, to see if any additional improvement was seen.

The results shown in Figure 4.4.24 are for the first case, which is where the offset of Filter 2 was changed. They show a general decrease in Q-value up to 6GHz offset, at this point the Q-value starts to increase in value, apart from a small dip at 13GHz. This is equal to the point where the half-wave of the filters central frequency is found.

After this point the gradient increases to 20GHz, which was where the highest Q-value occurred. At the point of highest Q-value, the measurements were stopped as after this, according to simulations, there should be a decrease in

Q-value due to being past the optimal frequency for Q-value improvement within the 50 GHz bit slot [32].

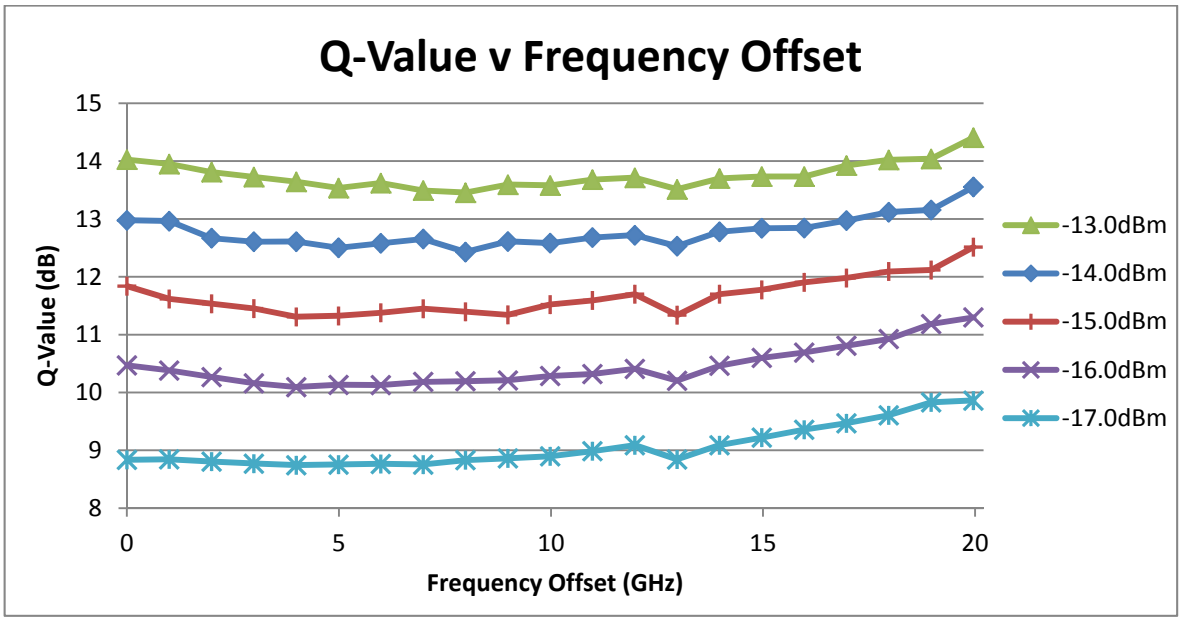


*Figure 4.4.24 – 35GHz (0.28nm) BW: Filter1 after Constructive port with offset fixed at 0GHz; Filter2 after Destructive port with offset changed; 42.7Gbps CSRZ-DPSK modulation.*

We can see in Figure 4.4.24 that there is an improvement at 20GHz using offset filtering, but it is only around 0.5dB compared to the measurements at the 0GHz offset for the filtered Carrier.

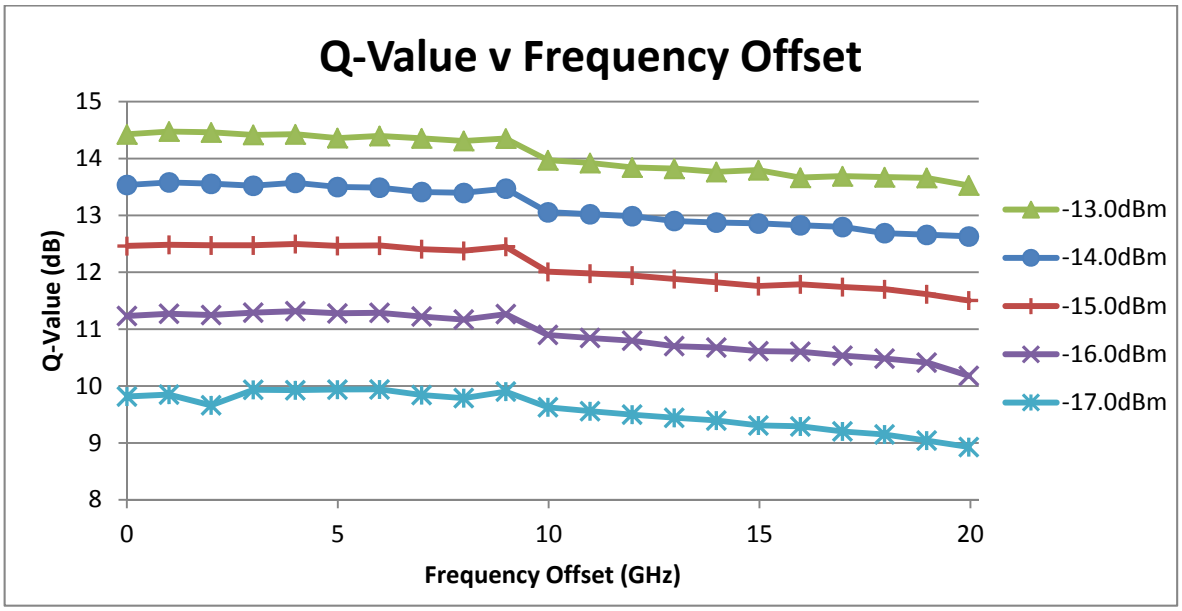


*Figure 4.4.25 – 35GHz (0.28nm) BW: Filter1 after Constructive port with offset changed; Filter2 after Destructive port with offset fixed at 20GHz; 42.7Gbps CSRZ-DPSK modulation.*

Next, Filter 2 was fixed at 20GHz and Filter 1 was offset from 0GHz to 20GHz, this was to see if any additional improvement could be found. The results are shown in Figure 4.4.25, and apart from a very small improvement around 1GHz, the Q-Value decreases slowly until 9GHz offset where there is a slight peak in the Q-value, which is 0.5dB lower than at 1GHz offset. After this point it decreases by 0.5dB and then steadily decreases even further.

As can be seen, having the second filter offset, as well as Filter 1, shows no significant improvement when compared to no offset in Filter 2.

Overall, this configuration does show an improvement. In the case where there is no offset for filter 1, but an offset of 20GHz for filter 2, an improvement of between 0.4dB and 1.1dB was measured depending on the received power, with the highest relative improvement at -17dBm. This is an interesting finding and could be useful for systems with low received power.

#### 4.4.2.4. Two Filters after the DLI using a Waveshaper (WSS)

The previous results in section 4.4.2.3, used CSRZ-DPSK, and show a potential improvement, or at least a recovery, appearing at 20GHz frequency offset. Due to time limitations, this was not fully explored at the time. When time became available to be able to repeat these experiments, only one physical filter was accessible, so it was decided to look for an alternate way to achieve the same setup without them. The alternative was to use a Waveshaper, which is a device that can be programmed to replicate switching and filtering actions; more on how Waveshapers work can be found in section 4.2.2.

Due to time constrains it was decided to use 33%RZ-DPSK after comparing with CSRZ-DPSK, as seen in Figure 4.4.10 in Section 4.4.1.1, as it could potentially show a greater improvement than with CSRZ-DPSK, and would be quicker confirmation of improvements using the Waveshaper.

The setup is shown in Figure 4.4.26 and is the same as Figure 4.4.23, apart from the Filters and the DLI replaced directly with the Waveshaper.

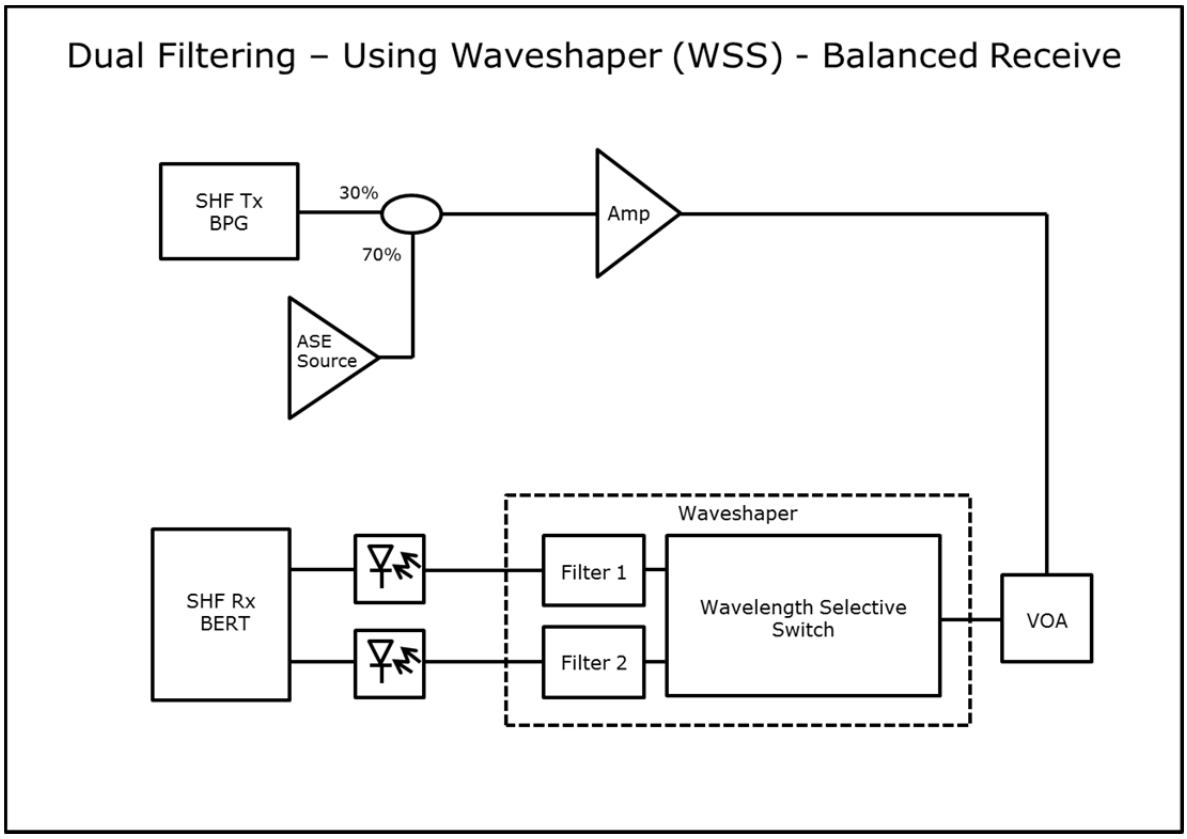


*Figure 4.4.26 – Two filters after WSS, Filter 1 after the Constructive port and Filter 2 after the Destructive port. Balanced Receive.*

The DLI and the filter responses were programmed using Matlab. This allowed the variables of the filters to be changed, whilst the output from the DLI remained at its most efficient. The variables which could be changed were the centre frequency, the bandwidth, and the offset, and also whether one, or both filters, were "on" or "off"; the "on" selection meant they were included in the system whilst the "off" selection in effect removed them from the system, allowing the pure DLI output to be measured. For this configuration both filters were on, i.e. the light was passed through an emulated bandpass filter before travelling to the output, rather than directly to the output with no filter emulation present; this is the off condition. The filter shapes were set to be 3$^{rd}$ Order Gaussian as the best fit.

For completion of the results from this configuration, the measurements were taken out to an offset of 60GHz so as to cover any potential points of interest. As can be seen in Figure 4.4.27, there are three distinctive lines. These are the measurements taken from Filters 1 and 2, which were changed alternately i.e. whilst the one is offset, the other is fixed, hence the blue and green lines.

The brown/pink line represents the offsetting of both filters together to the same offset frequencies.

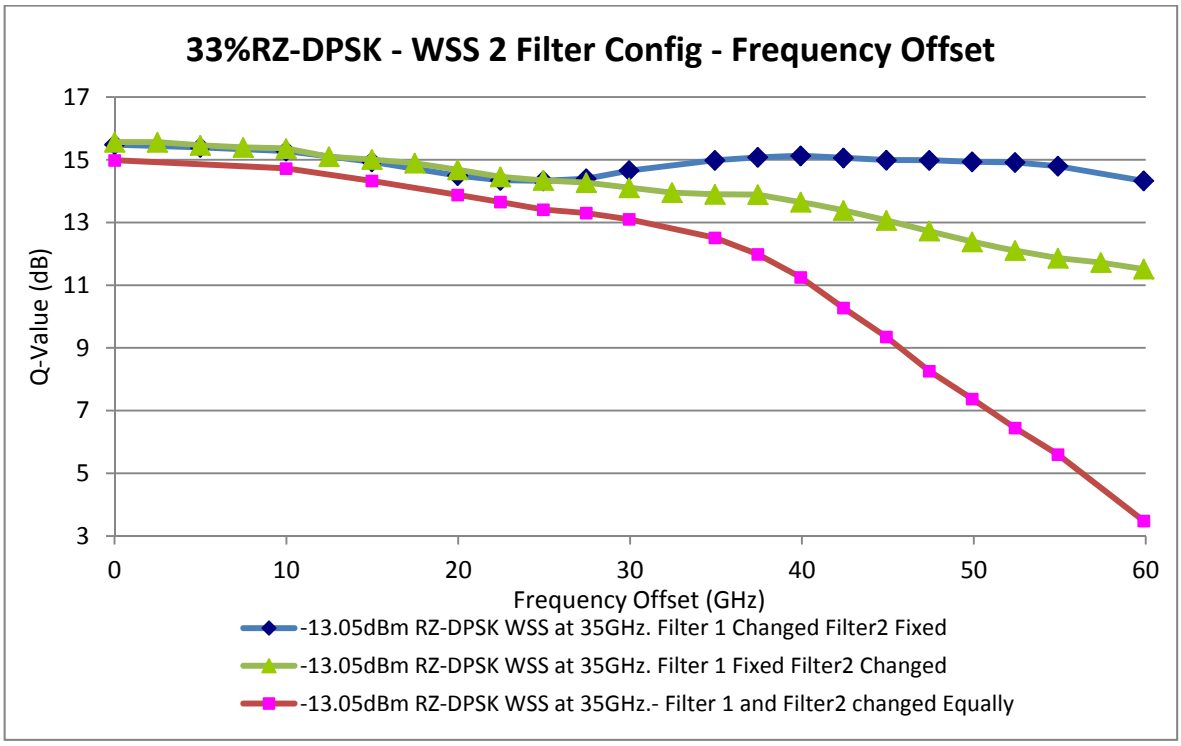


*Figure 4.4.27 – 35GHz (0.28nm) BW: Filter1 after Constructive port; Filter2 after Destructive port; Filter1 offset changed when Filter2 offset fixed (Blue) and Filter2 offset changed when Filter1 offset fixed (Green); Both Filters changed equally (Brown/Pink).*

First looking at the blue line, where Filter1 was offset and Filter2 fixed at 0GHz, we can see there is no improvement indicated at 20GHz, which is the opposite of what was seen in the CSRZ-DPSK results shown in Figure 4.4.24. However, at 35GHz offset, the same frequency as the filter bandwidth, we see a recovery which peaks at 40GHz, but this is still 0.36dB below the peak at 0GHz. The green line represents Filter1 fixed at 0GHz and Filter2 offset; this shows a general trend of a decrease in Q-value with increasing offset.

One reason for no noticeable increase in Q-value at 20GHz may have been down to the length of time it took for the original measurements to be taken, resulting in a slight drift in the system output, whilst the BER test-set used is not dynamic and is set around a fixed point.
Another reason may be that the filter shapes generated by the Waveshaper are not a close enough match to the physical filters used originally, as the

flatness of the filter can make a difference in its response to an incoming signal.
Looking at the pink/brown line, we can see that when both filters are offset at the same time, the quality of the output decreases, which indicates that there is no improvement to be garnered by offsetting both with large offsets.

In conclusion, from the latest results shown in Figure 4.4.27 we can see that there is a recovery after 35GHz when filter 1 is offset which Filter2 fixed, but no improvement was achievable. This could be due to the Waveshaper filter shapes not being close enough to the physical filters used previously. The 33%RZ-DPSK result is unlike the CSRZ-DPSK results in Figure 4.4.24, where an improvement was seen after 20GHz, and shows the potential differences depending on the modulation type used.
The repetition of the CSRZ-DPSK had been planned, but unfortunately there was limited amount of time with the Waveshaper, so the three filter configurations were prioritised. Further investigation should therefore be carried out into the measurements using CSRZ-DPSK.

### 4.4.3. Three Filter configuration

The three filter configuration involves one filter before the DLI, and one each on the Constructive and Destructive output ports of the DLI. For the measurements in this section only Filter 2, placed at the output of the DLIs destructive port, was offset.
The ultimate aim of trying the three filter configuration experimentally is to confirm the results of the simulations in [32].

#### 4.4.3.1. Three Filter configuration using Physical Filters

According to the simulation results there was expected to be an improvement of between 2dB and 4.7dB for an OSNR of between 15dB and 22dB [32, 133, 134]. For these measurements we used an OSNR of 20dB (0.1nm resolution). The expected improvement was down to the crossover of the Destructive port

to DB from AMI, at the same time the highest peak on the Constructive port is apparent. This gave the best balanced output.

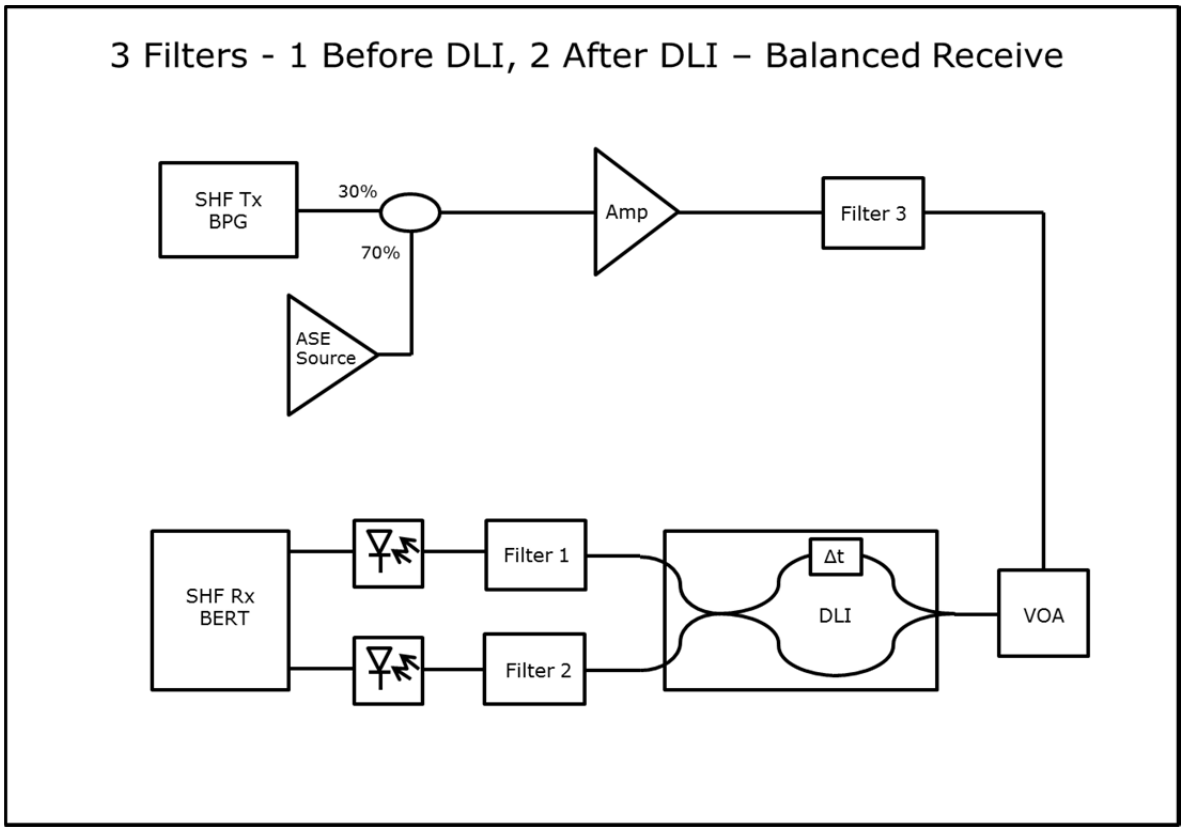


*Figure 4.4.28 – Three Filters: one before the DLI, Filter 3; two after the DLI; Filter 1 after the Constructive port and Filter 2 after the Destructive port of the DLI. Balanced Receive.*

The simulations used an offset of up to 20GHz (0.16nm) for offset measurements, but up to 30GHz (0.24nm) for the filter bandwidth graph (Figure 4.4.15). This showed an increase in Q-values for wider bandwidths, as expected, for the 1 filter configuration as shown in Figure 4.4.11 in section 4.4.1.2.

The configuration in Figure 4.4.28 shows no improvement over the measured range, however there is a recovery beyond 24GHz which starts to flatten out after 51.9GHz, but this is still 2dB less than at 0GHz offset. This result may therefore only be of interest in strongly filter regimes which use a large amount of offsetting, where wavelength or frequency offsetting of the laser or other devices are used.

The simulations in [32] predicted that after 3GHz of offset on Filter 2 that a slight increase of ~1dB should be present, followed by a decrease of 2dB after 12GHz, with a steady decrease to a loss of 4dB to 5dB by 20GHz. This is the furthest that the simulated measurements go to. This seems to tie in with the measurements seen in Figure 4.4.29, although we see a decrease of ~7dB at 20GHz. The highest Q-value in the simulations came where Filter 1, on the constructive port, was offset by around 8GHz, and Filter 2 was then offset by 5GHz.

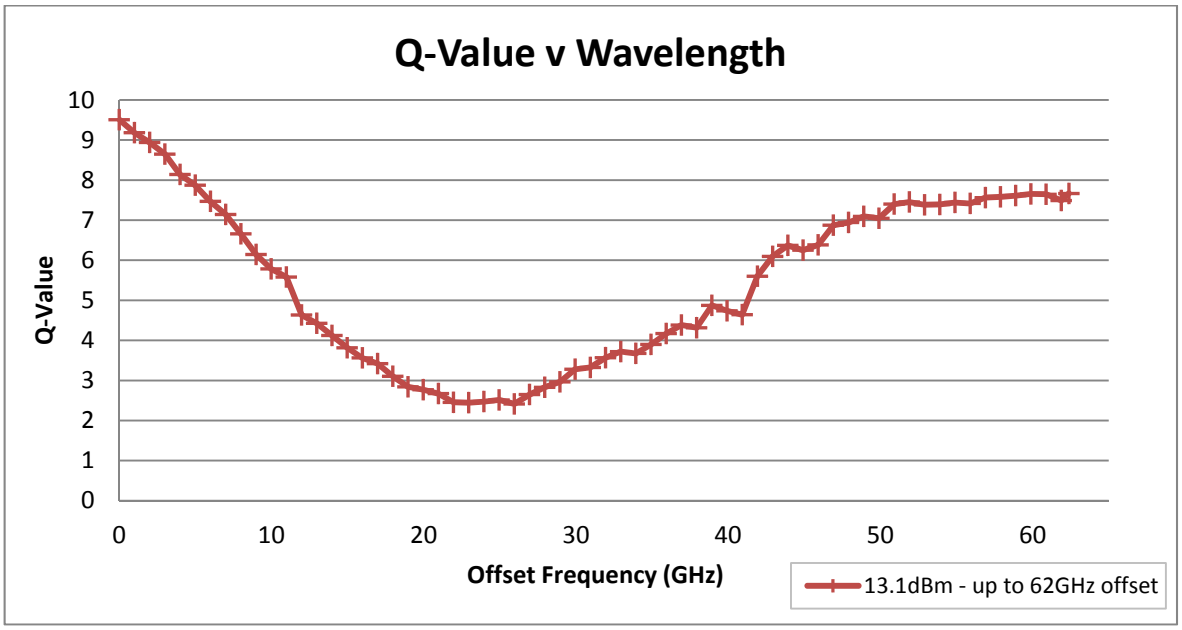


*Figure 4.4.29 – 40GHz (0.32nm) BW: Filter 1 and Filter 3 fixed at 0GHz, Filter 2 offset changed up to 62GHz (0.5nm); 42.7Gbps CSRZ-DPSK modulation.*

The result in Figure 4.4.29 needs to be repeated with appropriate offsets on both filter 1 and 2 at the DLI outputs to see whether the simulated result can be confirmed. This would also discover if there were any imbalances present in the receiver or the DLI that caused the loss at 20GHz, but otherwise the result seems to confirm the simulation, as seen in Figure 7 of [134] and in [32].
A simulation extending out to offsets around 60GHz to confirm the above result needs to be carried. In the next section a CSRZ-DPSK simulation was carried out, but only to an offset of 20GHz, and can be viewed in Figure 4.4.35. Time constraints limited the repetition of this experiment and also a more in-depth inquiry into this configuration. In essence, future work would include all filters being offset with respect to one another, and then all of the

filters offset at the same time to completely cover any unexpected issues and/or improvements.
In Section 4.4.3.2, we used a Waveshaper to complete some of the experimental work not carried out above.

#### 4.4.3.2. Three Filter configuration using Waveshaper (WSS)

Here we repeat and extend the 3 Filter configuration experiments using a Waveshaper to replicate the DLI and both filters after the DLI. Filter 1 was a standalone Santec Filter as previously.

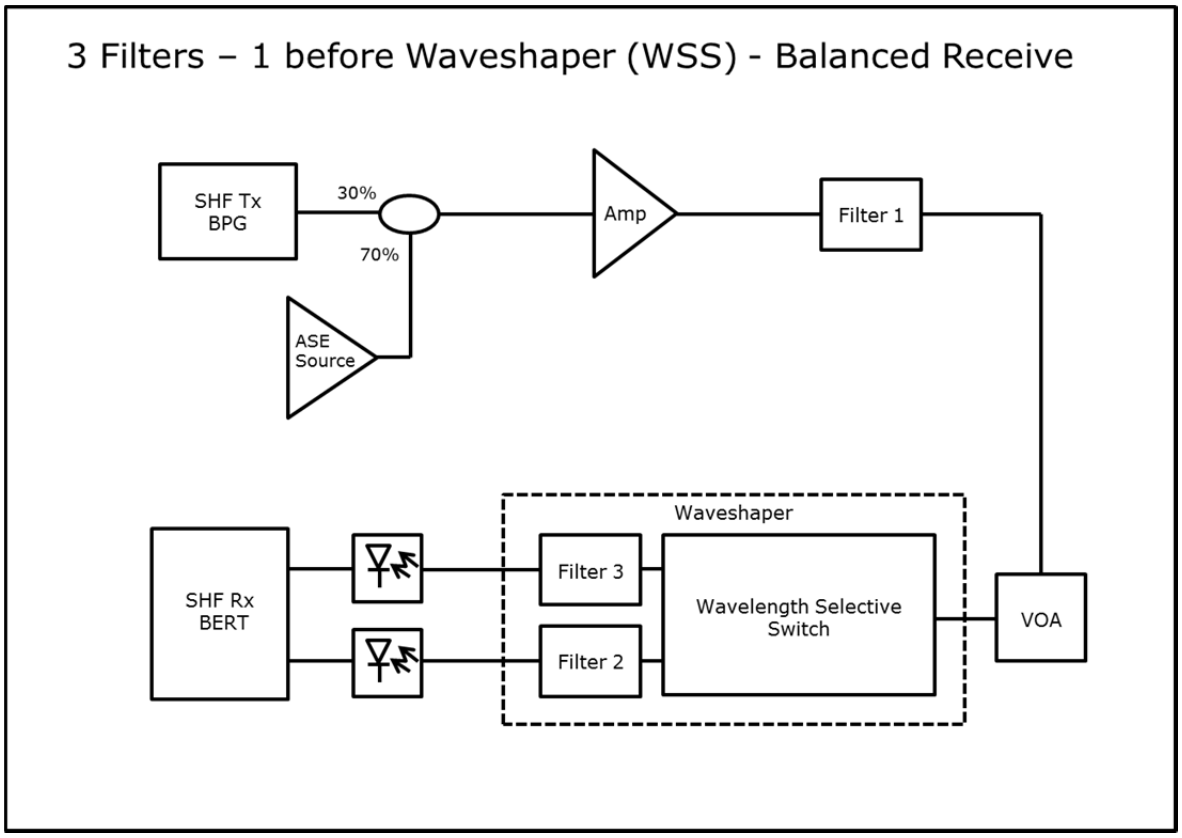


*Figure 4.4.30 – Three Filters; One before the Waveshaper and Two filters within the Waveshaper; Filter 1 after the Constructive port and Filter 2 after the Destructive port. Balanced Receive.*

We programmed the Waveshaper using MATLAB script which enabled the process of the DLI and to change the filter shapes, bandwidths, and frequency offset from the central frequency for each filter. The filters could be changed together, or separately.

As with the two filter configuration, we first offset Filter2 and fixed Filter3 at 0GHz, and then swapped the Filter situation for fixed and offset. Filter3 was then used as the offset filter from 0GHz to 60GHz offset, whilst Filter2 was fixed at a certain offset frequency. This was repeated up to an offset of 60GHz. Those Filter2 frequencies were: 0GHz, 9.980GHz, 19.961GHz, 29.941GHz, 39.921GHz, 49.902GHz and 59.882GHz.
Filter1 was kept fixed for all measurements and increased the amount of filtering in the system, causing an attenuation of 3dB.

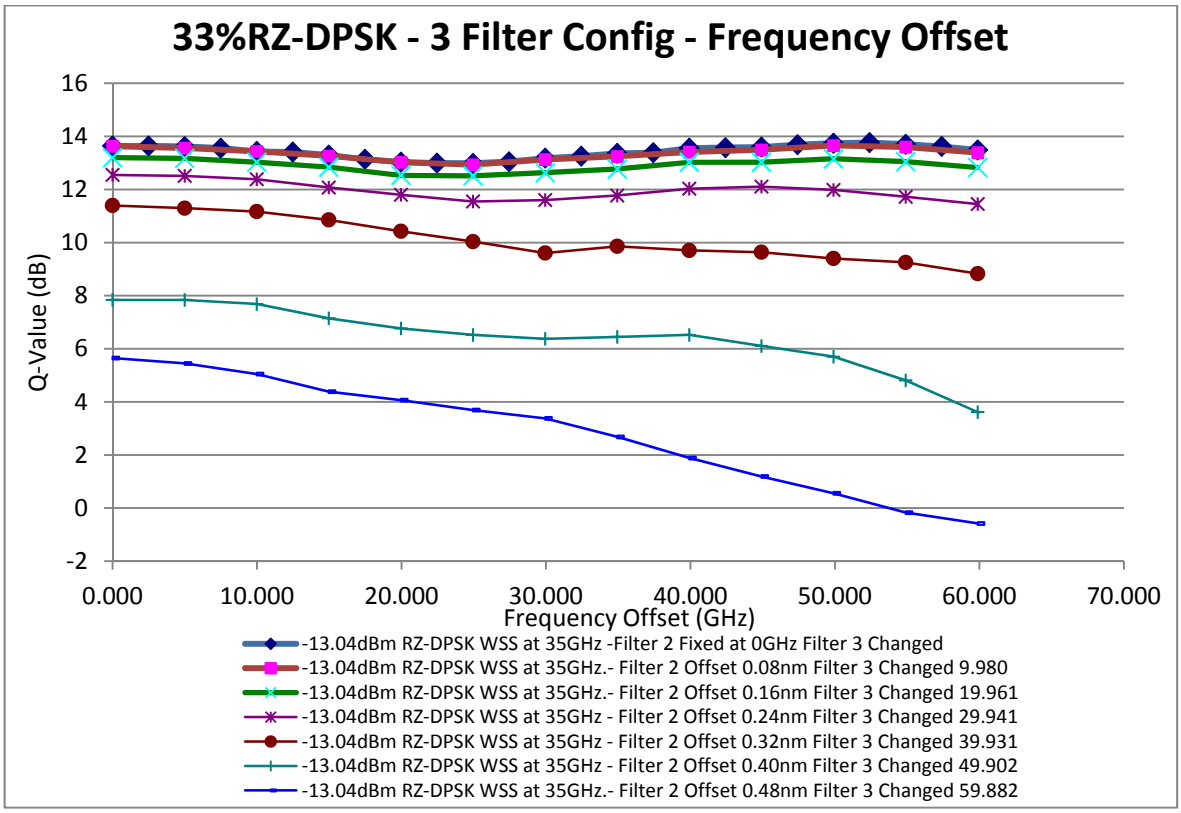


*Figure 4.4.31 – 35GHz (0.28nm) BW: Filter1 after Constructive port; Filter2 after Destructive port; Filter1 offset changed when Filter2 offset fixed (Blue) and Filter2 offset changed when Filter1 offset fixed (Green); Both Filters changed equally (Brown/Pink).*

As we can see in Figure 4.4.31, the general trend shows a very small improvement of 0.13dB after Filter 3 was offset by 52.4GHz, with Filter2 at 0GHz offset. From there on in, the Q-value decreases as Filter2 is increasingly offset, leading to a large drop of over 6dB at an offset of 60GHz for Filter3. Within this area the potential for any measured improvement, or recovery, is reduced after 40GHz.

This process is better shown on the contour plot show in Figure 4.4.32, as the two "peaks" are easily visible, whilst the signal degradation is complete at the low point near 60GHz.

The 33%RZ-DPSK modulation format is a good proxy for the 50%RZ-DPSK format, as previous results show [134, 144] although 50%RZ-DPSK has the best improvement, 33%RZ-DPSK was not far behind, so could also still be useful.

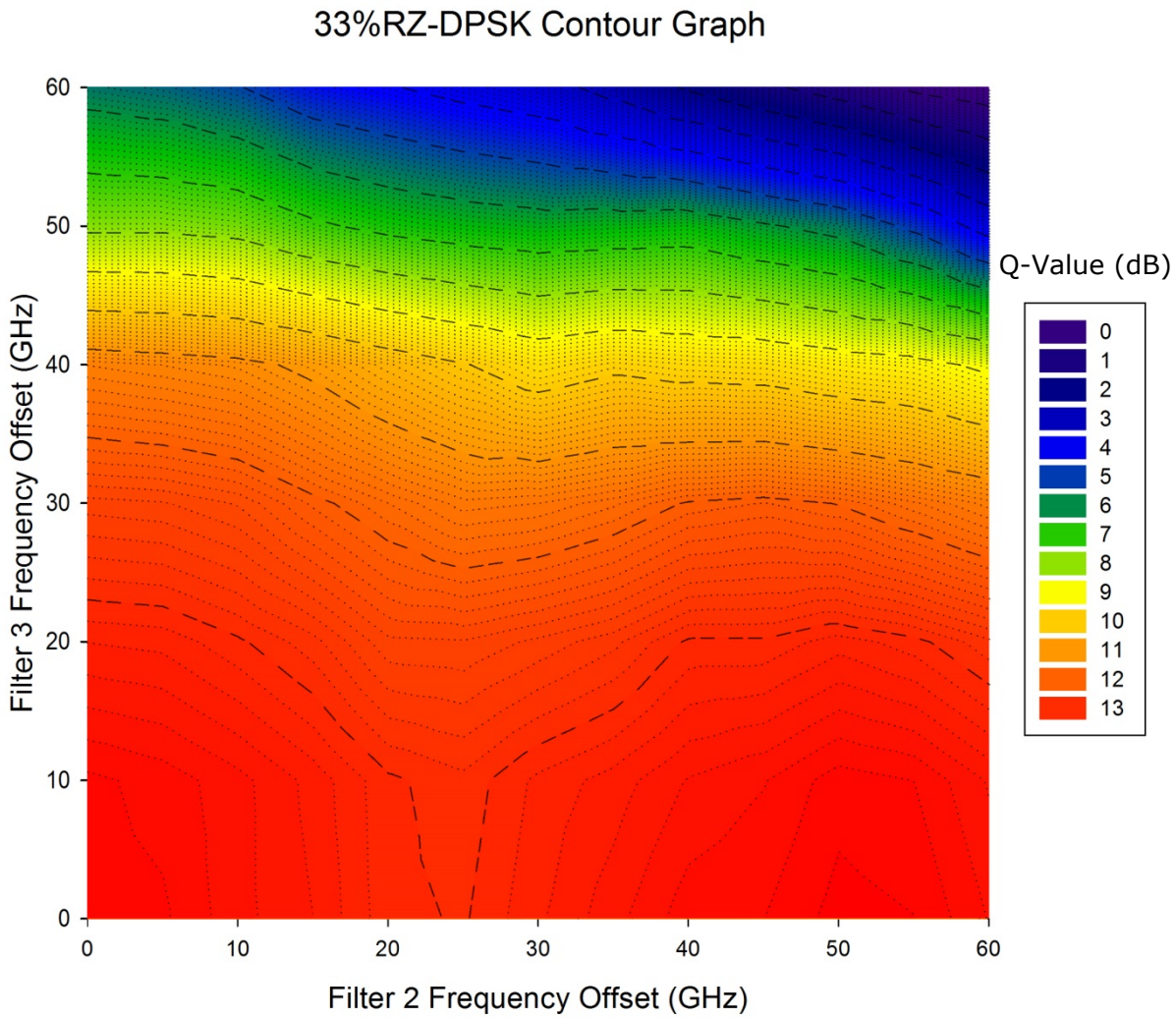


*Figure 4.4.32 – 35GHz (0.28nm) BW: Contour plot showing result of offsetting Filter 2 (Constructive port) and Filter 3 (Destructive port) whilst passing through 33%RZ-DPSK modulated data.*

Although there is only a very small improvement, the confirmation of the procedure and configuration has been shown, especially when compared with the simulation results showing the expected outcomes. This could be due to

issues with the Filter shapes as discussed in Section 4.2 and shown in Figure 4.2.4.

We repeated the measurements for the CSRZ-DPSK modulation format. No improvements were expected due to the simulation output and also previous work as in [134, 143, 144, 145].

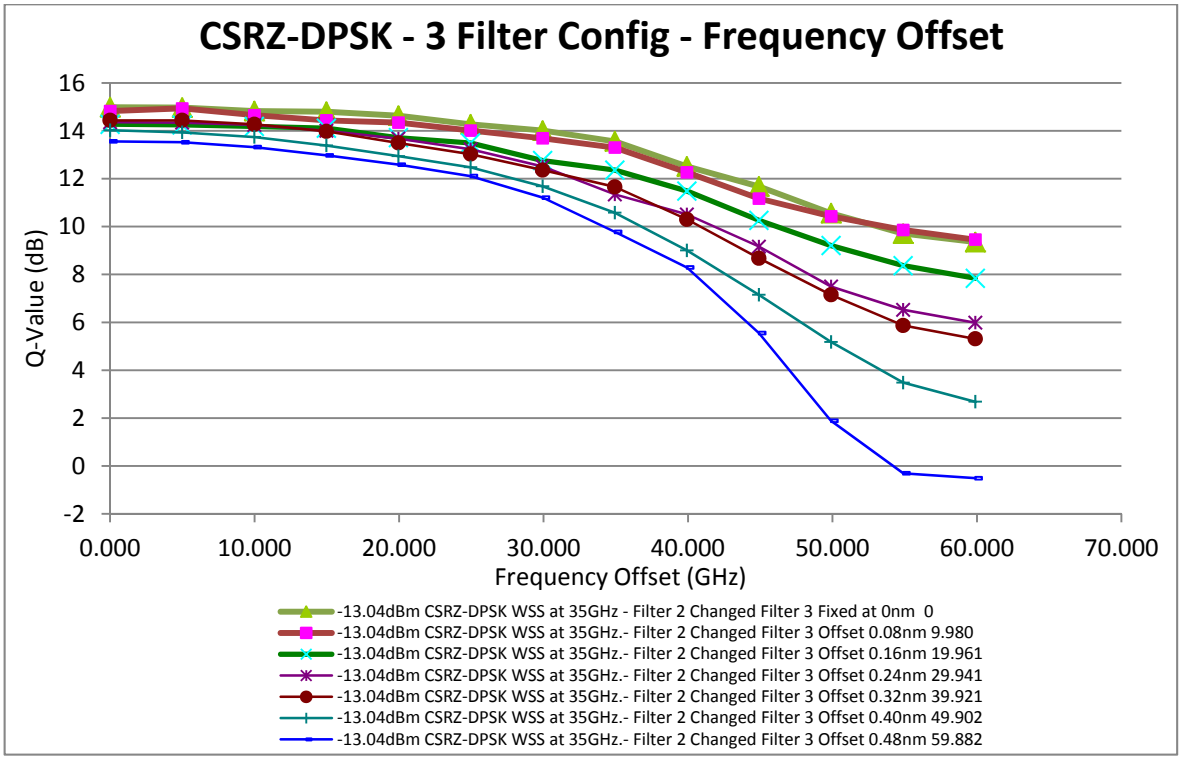


*Figure 4.4.33 – 35GHz BW: Filter1 after Constructive port; Filter2 after Destructive port; Filter1 offset changed when Filter2 offset fixed (Blue) and Filter2 offset changed when Filter1 offset fixed (Green); Both Filters changed equally (Brown/Pink).*

With these measurements, Filter2 was changed while Filter3 was fixed at the following frequency offsets; 0GHz, 9.980GHz, 19.961GHz, 29.941GHz, 39.921GHz, 49.902GHz and 59.882GHz. This measurement process was chosen due to the measurements being easier to record as very low Q-values were present at the furthest end (60GHz offset) of the measurements, which made it difficult to record the measurements where Filter2 was fixed at 60GHz and Filter3 adjusted, as seen with the measurements in Figure 4.4.31; a series of low Q-values had to be recorded, which took more time due to the software used; swapping the order of which of the Filters were changed, as explained above, made this easier.

We see in Figure 4.4.33 that as Filter2 is changed, the Q-value reduces considerably after 25GHz.

If we look at the measurements in the opposite direction i.e. Filter3's offset against Filter2, there is a steady decrease. At 0GHz the decrease is only 1.27dB, while at 60GHz the decrease is almost 10dB. A small upward tick seen when Filter2 is offset by 5GHz and Filter3 was offset by 10GHz. This may be the representation of the high point of the peak, if we compare the experimental results with the simulation results for CSRZ-DPSK in Figure 4.4.35, but the value of the improvement is relatively small in practice.

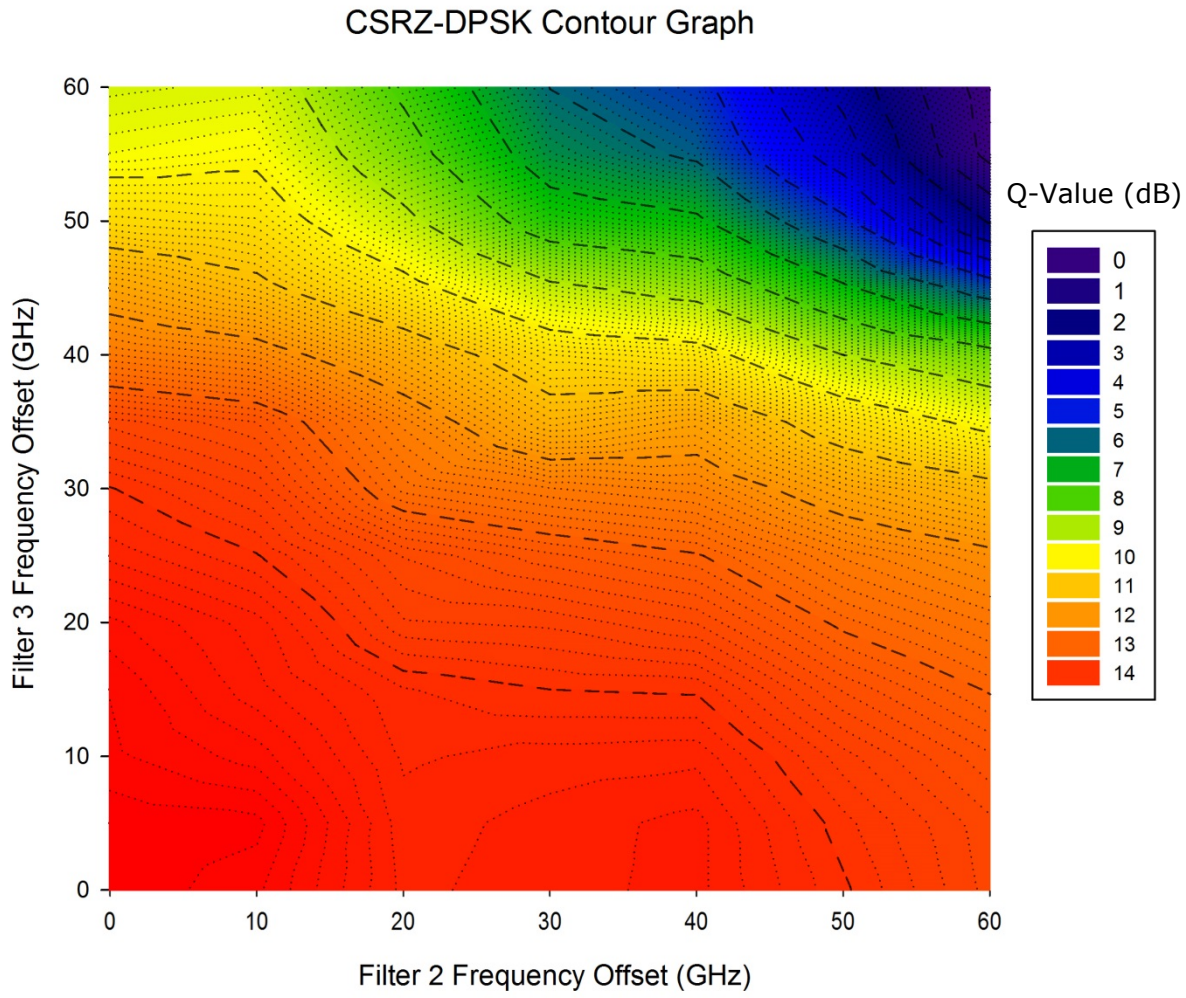


*Figure 4.4.34 – 35GHz (0.28nm) BW: Contour plot showing result of offsetting Filter 2 (Constructive port) and Filter 3 (Destructive port) whilst passing through 33%RZ-DPSK modulated data.*

If we look at the contour plot, we see the peak performance is at 0GHz. For CSRZ-DPSK, this is as expected. There is a slight recovery around 40GHz,

similar to 33%RZ-DPSK, but no improvement, unlike 33%RZ-DPSK where there was a slight improvement here.

The Q-values do degrade at a greater pace after 20GHz, so by 60GHz offset, the level seen is at 0.5dB. The peak, however, does spread out past 10 GHz by 5GHz, which could suggest that there is a potential for improvement within this area, as seen with the simulation results for CSRZ-DPSK in Figure 4.4.34, which show a peak at 4.5GHz by 8GHz, and the relative shape of the contour lines is similar. A contour plot with measurements taken at a higher resolution, ideally every 1GHz, would have to be taken to revel whether that is the case. Again, some of these issues could be due to differences with the Filter shapes as discussed in Section 4.2 and shown in Figure 4.2.4.

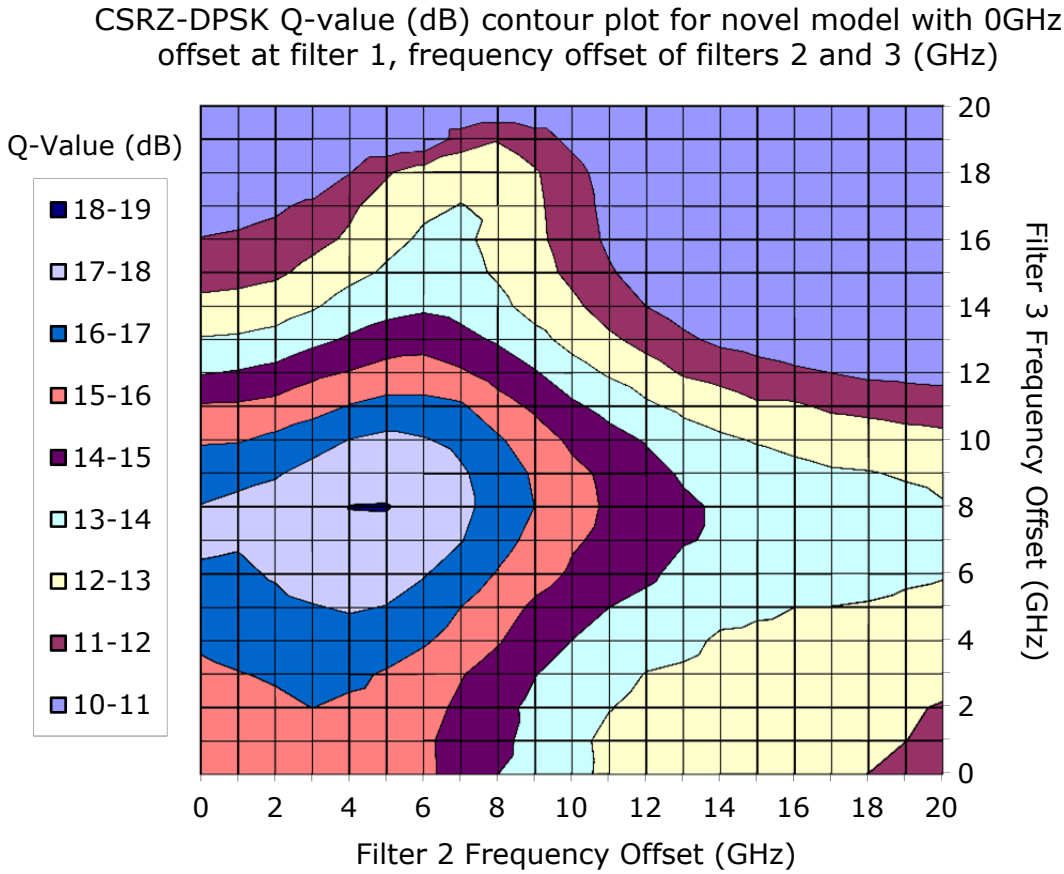


*Figure 4.4.35 – Simulation at 35GHz (0.28nm) BW: CSRZ-DPSK 3 filter configuration. Frequency offset of both Filter2 (Destructive Port), Filter 3 (Constructive Port).*

If we look at the simulation separately, there is a peak when the offset of Filter2 is 4.5GHz, and Filter3 is offset by 8GHz. This region is very small, which indicates the peak is only just above 18dB in value. The reason for a

peak here is the offsetting of the destructive port, which has an effective AMI signal on it, basically "sees" one of the double peaks of the AMI spectrum, as shown earlier in the Chapter in Figures 4.2.1 and 4.2.2, but also in the DLI there is a vestigial on the Constructive port, which together gives this improvement [134, 144].

Due to the unavailability of an appropriate transmitter to generate 50%RZ-DPSK modulation, it meant that, unfortunately, no measurements using 50%RZ-DPSK were able to be taken, this means only simulation results are available as can be seen in Figure 4.4.36.

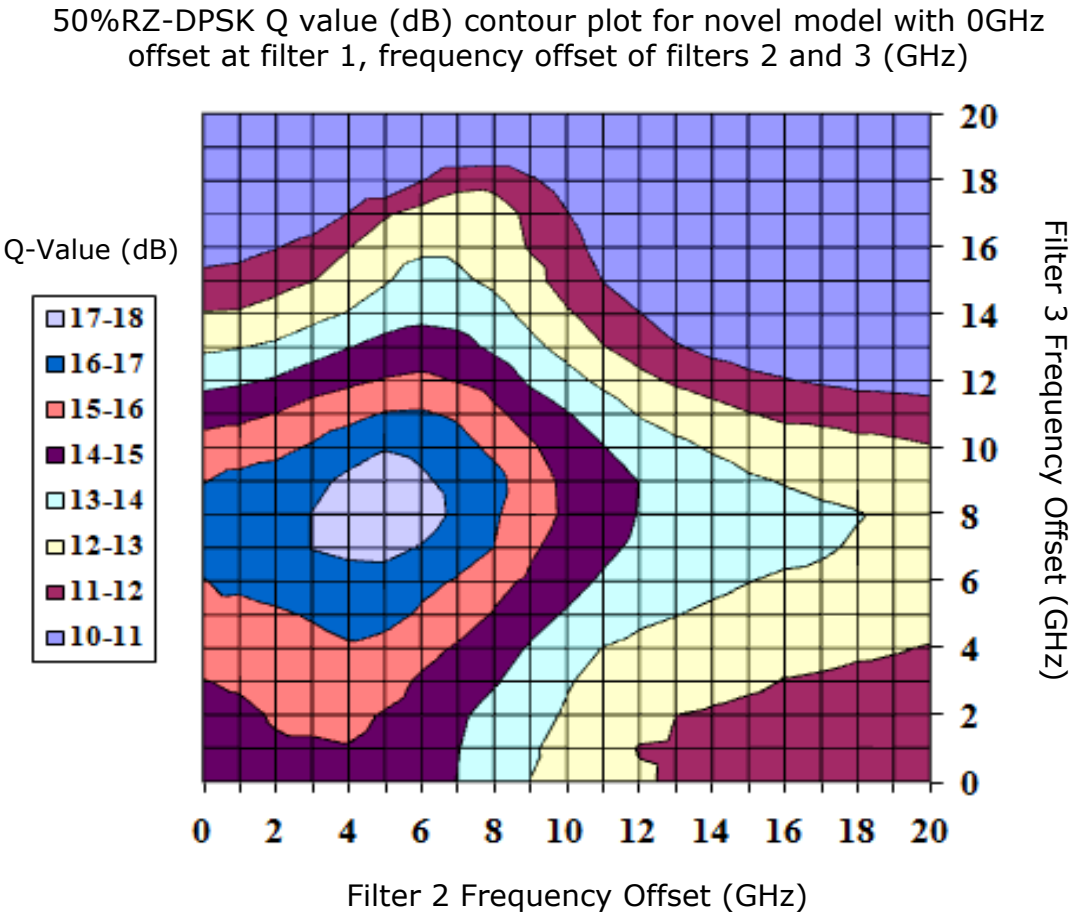


*Figure 4.4.36 – Simulation at 35GHz (0.28nm) BW: 50%RZ-DPSK 3 filter configuration. Frequency offset of both Filter2 (Destructive Port), Filter 3 (Constructive Port).*

However, from these simulations it can be inferred, taking into account the comparisons of the measurements for 33%RZ-DPSK and CSRZ-DPSK and their relevant simulation results, to suggest that actual measurements using

50%RZ-DPSK, under ideal conditions, should see an improvement of ~3dB, when Filter 2 is set with a 5GHz offset and Filter 3 with an 8GHz offset.

The improvement seen within the simulation in Figure 4.4.36 is a result of the way AMI and DB interact when they are formed from 50%RZ-DPSK, in which a vestigial, or "left over", part of the AMI double peak causes a spectral peak that is higher than with other RZ-DPSK formats [132, 133, 140, 144].

## 4.5. Conclusion

From the results of the different offset filtering configurations, we can conclude the following:

The use of one filter before a DLI, as in section 4.4.1.1, has demonstrated that by offsetting the filter, an improvement is seen using a single ended receiver or a balanced receiver, as was reported in [134, 143] and was in line with those predicted by the simulations [32, 132, 134]. The improvement of the received Q-value was found to be in the region of 2dB, and was gained using an offset of 25GHz to 31GHz with RZ-DPSK modulation at a data rate of 42.7Gbps. It was also found that if the filter before the DLI was not offset, a decrease in performance was recorded on the destructive port when compared to the constructive port. This was as expected and reported in [132, 134, 142].

In Section 4.4.1.2, different modulation techniques were compared, these being 33% RZ-DPSK, CSRZ-DPSK and NRZ-DPSK.

The best relative improvement was seen with NRZ-DPSK, shown in Figure 4.4.13. This increased by 2.2dB from 0GHz to 20GHz, but when compared to RZ and CSRZ formats there was a reduction of 0.9dB. The true peak output was 12.8dB. The measurements in Figure 4.4.12, for CSRZ-DPSK, showed no improvements, only degradation after 20GHz, and 50% RZ showed an improvement at 25GHz of 1dB, this has been shown previously in [32, 142]. The peak output was 13.8dB. The results for 33% RZ-DPSK, Figure 4.4.11,

showed a relative improvement of 0.9dB after 25GHz and the best peak output of 14dB.

The reason for the lack of increase when using CSRZ-DPSK modulation is because the demodulation process of the signal by the MZI requires a 1-bit delay for the DPSK demodulation, this causes the phase changes related to the CSRZ format to be different to those phases transmitted initially. Whilst this would have no effect on the transmitted data, it would affect the resulting received spectrum by creating a small amount of carrier to appear, therefore causing a flattening of the spectral output and no improvement after the DLI.

In section 4.4.1.1 CSRZ-DPSK had been used in "pre-filtering", namely before the DLI or receiver, where results have shown an improvement [143].
In situations where cascaded filtering appears over a transmission link [145], CSRZ-DPSK has also been proved to show little improvement, which is consistent with the findings here.

The results using 33% RZ-DPSK shows an increase of 1dB over 25GHz offset, this is explained via the AMI to DB conversion on the destructive port, and owing to this duty cycle having a broader spectrum compared to CSRZ-DPSK, narrow filtering has a greater affect. Therefore a larger improvement from offsetting the AMI should be realised, as can be seen in Figure 4.4.11.

For NRZ-DPSK a relative improvement of 1.5dB to 2.2dB was seen at the offset of 20GHz. However, this relative improvement is 1dB lower than for RZ-DPSK. This could be due to a greater amount of noise inherent within the NRZ format when compared to RZ, thus creating an increase in ISI. The difference between NRZ and RZ can be explained by the amount of power averaged over the bit slot, which for both RZ formats gives a higher peak power and thus less signal loss. Also because of the lower duty cycles of the RZ formats, these have a higher tolerance to fibre non-linearity compared to higher duty cycle formats, such as NRZ.

For the two filter configuration in section 4.4.2.1, this involved placing one filter before the DLI and one on the destructive port of the DLI. The result

from this experiment was mixed. The first set of results showed an improvement of between 0.6dB and 0.8dB at 18GHz, for a received power of -13.1dBm and -15.1dBm. This was encouraging and was supported by the one filter experiments on the destructive port of the DLI.
However, a dip in the received power was noted at 19GHz for -14dBm and -15.1dBm received powers. Because this frequency is close to the half wavelength of the filter bandwidth of 35GHz, it is assumed there are some issues that may be produced by SPM causing the peak of the AMI signal to change in the spectral domain.

A similar response can be seen with the bandwidth measurements with one filter before the DLI in Figure 4.4.14, where, with the change in bandwidth at 33.7GHz to 34.9GHz, a slight change in the linear response is seen. This may indicate some frequency or wavelength dependent loss is present at this frequency range which would also affect their half-wavelengths.

The measurements described above were repeated. This time they showed no offset improvement over that recorded at 0GHz with a -13.1dBm received power. An actual degradation of 0.4dB at 17GHz was measured, although as previously, a dip appeared around 18GHz but this time it only occurred on the -13.1dBm power measurement. For the -14dBm, a decrease of 0.2dB at 17GHz is apparent compared to 0GHz, whilst for -15dBm there is no difference between 0GHz and 17GHz.

Other issues, such as temperature drift during the time interval between the first and second measurements, or system or software issues, could also play a part in these noted differences.

For the two filter configuration before the DLI, seen in Section 4.4.2.2, no measured improvement was seen. It is assumed that this result is caused by additional loss, meaning the improvement seen by offsetting Filter 1 would be lost due to attenuation. When Filter 2 was offset, the signal had been attenuated to a level where offsetting gave a negligible result.

The two filter configuration in section 4.4.2.3 uses an individual filter on the constructive and destructive ports of the DLI. This allows potential for the signal quality to be improved by changing the offset of both filters to induce the lowest BER, or highest Q-value.

It is known that offsetting the destructive port will achieve a comparative improvement for that output, accordingly it was expected that some improvement would be seen. The greatest improvement on the destructive port (using Filter 2) was an offset of 20GHz, which gave an improvement of between 0.4dB and 1.1dB depending on the received power.

For the constructive port (Filter1) the offset frequency that gave the best output was found to be 0GHz. This is not a huge surprise, as shown in the previous sections. In general the constructive port will only get worse as the filter is offset away from the central peak, however, sometimes the filter may not be exactly on the central peak, and so offsetting the constructive port may be worthwhile.
The highest relative improvement on the destructive port was found at -17dBm with an increase of 1.1dB. This is an interesting finding and could be useful for systems with low received powers.

In Section 4.4.2.4, where a Waveshaper was used as a comparison with the actual physical filter used in Section 4.4.2.3, we can see that the improvement at 20GHz is not present and we do not see any improvement until 30 GHz offset. This suggests that either there was an issue with the original measurements, or that this could be due to the physical filter shapes and the Waveshaper filter shapes having slight differences.

For very tightly filtered systems, such as the three filter experiments in section 4.4.3.1, no notable improvement was realised when offsetting the filters.
With no offset i.e. 0GHz offset, a Q-value of 9.5dB was measured, when filter 2 was offset, there was the start of a recovery after 24GHz, where the Q-value was 2.47dB until an offset of 51.9GHz where the Q-value of 7.45dB was recorded and did not increase significantly afterwards. The reason for this was that the filter on the constructive port, Filter1, was not offset, so when we

compare to Figure 7 in [133] it can be seen that Filter1 was at 0GHz and so no improvement should have been expected.

In Section 4.4.3.2, the three filter configuration was repeated using a Waveshaper to simulate the filters on the destructive and constructive ports of a DLI, where the Waveshaper were also programmed with a DLI. A separate Santec 950 optical filter was deployed before the input to the Waveshaper. As with the previous experiments with physical filters, Filter1, the Santec Filter, was fixed with a Bandwidth of 35GHz and no offset, while Filter2 and Filter3, which were within the Waveshaper, were offset up to 60GHz to cover the range seen with the incomplete experiment in Section 4.4.3.1.

In these experiments, we compared three different modulations to see how they performed in the narrow filtering regime; these were 33%RZ-DPSK, 50%RZ-DPSK and CSRZ-DPSK. NRZ-DPSK was not repeated due to the previous results showing an improvement significantly below the other modulation types.

For all the measurements included in Section 4.4.3.2 a lower resolution of 4.5GHz had to be used to achieve them due to time constrains, rather than a higher 1GHz resolution as hoped.

For 33%RZ-DPSK a slight improvement was seen around 50GHz, but this was only about 0.5dB, there was potential for an improvement peak to appear between filter offsets of 5-10GHz. No simulation results were available for this modulation type, but from other results [132, 133, 134], it is suggested that 33%RZ-DPSK should show improvements over CSRZ-DPSK, but they would not be as good as with 50%RZ-DPSK.

When we then look at CSRZ-DPSK results, there was no improvement, although an additional peak did appear around 37GHz, but this was much lower than at 0GHz. This was partially expected as it had been proven [132, 133, 134, 144] that CSRZ-DPSK gives only slight improvements at bandwidths of 35GHz, unlike at bandwidths of around 50GHz, where it can give significant improvements.

Comparisons with the simulation results are limited, as those results only go as far as 20GHz, but they still show a potential small improvement around 5-10GHz. Simulations showed there may have been scope for significant improvement, but previous experimental and simulation results have proved to be lower.

Unfortunately for 50%RZ-DPSK, no transmitter capable of producing this modulation type was available, only the simulation results have been included for a general overview. The simulation results show a significant improvement of around 3dB to 4dB when Filter2 is offset at 5GHz and Filter3 offset of 8GHz. No details are available past 20GHz as the simulations were limited to that amount of offset. When taken as a whole with the experimental and simulation results for 33%RZ-DPSK and CSRZ-DPSK, we can assume with some confidence that there would be some improvement, but whether it would be as marked is unknown until actual experimental validation takes place.

The fact the filter shapes resulting from the Waveshapers did not match those of the Santec filters, and the filter shapes used in the simulations potentially had lower order Gaussian shapes when compared to the actual filters used, could be limiting factors for the measurements, and therefore by inference, the simulation comparisons, as discussed in Section 4.2. This means the attainment of an acceptable and comprehensive conclusion for this section cannot be made.

In general we can conclude the following:

Using one filter on the destructive port to offset the central wavelength, whilst leaving the constructive port set at 0GHz offset (either with or without a filter), can give an increase in the Q-value for the received signal of up to 2dB. This could have some impact within those systems that have strongly filtered regimes.

When two filters are applied on each output of the DLI, an extra bit of flexibility can be added to a system by the fine tuning of the peak outputs of both ports to secure the best signal quality.

It has been seen that for certain filtering regimes offset filtering could be a useful technique for increasing the quality of the received signal, especially at low powers, further work needs to be done by using these techniques with long-haul transmission spans to see if any improvements could be measured that would indicate a simple way to improve current systems.

The findings within this chapter are of interest to those systems that have strong filtering regimes, i.e. those systems that have either cascaded and/or multiple devices that cause filtering of transmitted signals, such as add-drop multiplexers, wavelength switches and cross-connects, as well as filters. The use of offset filtering could improve the received signals in these systems by 1dB or 2dB when using either pre-filtering for ASK or DPSK modulation techniques, or offset the destructive port of a DLI when using only DPSK. Another way of achieving similar results is to offset the laser source instead of offsetting filters; however this may cause excessive cross-talk.

For very narrow filtering (<0.25nm bandwidth), offsetting the filter is limited as this technique depends on using broader spectral pulses and finding the peak performance within that spectral band, which for long haul transmission spans and complex systems with multiple switches may indicate a significant block for its suitability. This inference is supported by results in [141].

The use of Waveshapers in lieu of physical filters needs more work, as the comparison of the filter shapes from both Waveshapers and physical filters showed there was a significant difference, which could explain the lack of high Q-Value improvements in the experiments compared to the simulation results.

More complex modulation systems, such as DQPSK and Polarisation modulation techniques, should also be investigated as these types of modulation can improve the received signal considerably, while the effect of the type of offset filtering detailed in this chapter, on these modulation formats, is unknown in practice. Coherent detection could also be used instead of direct-detection.

Offset filtering, whilst shown to be an interesting effect, may not be suitable for networks with a vast selection of cascaded devices, or those using long-haul transmissions due to the very narrow filtering that occurs, but may be useful for short to medium haul systems and systems with some cascaded devices within a 50GHz grid. For systems with broad filtering (>1nm bandwidth) these techniques will not work.

The next step would be to use offset filtering in conjunction with an ULRFL over long distance spans. A similar experiment has been carried out in [124] with pre-filtering and using 2 forward pumping spans and 1 backward pumping span within a recirculating loop of 360km.
The proposed system would differ by using the ULFRL and the two filter "tuning" technique on both DLI outputs. This would create a novel transmission system and confirm whether or not both offset filtering, and ULRFL, could work in the field as part of a tightly filtered long haul transmission system.

Although we have shown proof of concept, future higher resolution measurements of 1GHz, with either physical filters, or better fitting filter shape using Waveshapers, should be carried out to demonstrate whether the improvements seen can be better pinpointed and improved upon.

# Chapter 5

## Conclusions

This thesis is concluded by comparing the main objectives with the resultant outcomes. The overarching aim was to provide evidence that there are new ways to use current techniques to improve the transmission of optical signal over long distances with as little loss as possible, and secondly to confirm whether simulated results, pointing towards a possible simple way to improve the received signal at the receiver, could be confirmed.

First we tackle the transmission objectives.
Our aim here was to prove that long distance transmission could be improved by the use of Ultra-long Raman Fibre Lasers (ULRFLs) over a single unrepeatered span, instead of using other amplification techniques over unrepeatered and/or repeatered spans. The use of standard transmission fibre, such as SMF-28, was also a priority, rather than using large effective area fibres such as LEAF or TrueWave, or special ultra-low loss fibres. Experiments using non-SMF-28 fibres can be found in the following references [19, 20, 21, 22, 23, 24, 25, 35, 60, 61].

The experimental work was planned to build on previous work where an ULRFL cavity of 270km was developed creating a quasilossless span [15], and simulations in [14] found that ULFL had an improved noise figure and a better gain profile when compared to bi-directional $1^{st}$ order and $2^{nd}$ order Raman amplification. Bi-directional pumping [18, 19, 21, 28, 35, 58, 59] has been advantageous compared to single pumping [20, 23, 25, 61] for some time. Other examples of ultra-long transmission experiments can be seen in the following [22, 24, 27, 57, 60,].

| Un-repeatered Transmission Distance (km) | Total Transmission Distance (km) | Number of Channels and Data Rate (Gb/s) | Modulation Type | Transmission Technique | Fibre Types Used | Refs |
|---|---|---|---|---|---|---|
| 100 | 100 | 1x640 | RZ-OOK | WTC | SMF | [97] |
| 240 | 240 | 1x10 | NRZ-OOK | Backward RP | SMF-28 | [29] |
| 298 | 298 | 20x10 | WDM Ethernet | Bi-direction RA + EDFA | NZDSF | [59] |
| 300 | 300 | 1x107 | RZ-DQPSK | Bi-direction RA | NZDSF | [57] |
| 300 | 300 | 8x112 | TI-PDM-RZ-QPSK | Forward RP + Coherent Rx | NZDSF | [58] |
| 300* | 300* | N/A* | CW* | ULRFL* | SMF-28* | [63]* |
| 320 | 320 | 8x43 | WDM RZ-DPSK | ULRFL | SMF-28 | [26] |
| 440 | 440 | 64x43 | PDM-RZ-BPSK | 3rd Order Backward RP + ROPA | EPSCF | [20] |
| 444 | 444 | 8x120 | PDM-NRZ-QPSK | DRA+ROPA No DA | PSCF | [21] |
| 462 | 462 | 4x100 | PDM-QPSK | Bi-Dir RP + ROPA + RTP + Coherent Rx | EPSCF + ULL-LEAF | [22] |
| 468 | 468 | 10x43 | NRZ-DPSK | Bi-Dir DRA + ROPA | PSCF | [19] |
| 468 | 468 | 64x43 (33GHz Spacing) | PDM-RZ-BPSK | RFL for ROPA | EPSCF + ULL-LEAF | [25] |
| 505 | 505 | 32x12.3 | WDM | Dual λ RP + ROPA | PSCF | [23] |
| 525 | 525 | 4x10 | WDM | 3rd Order CRP + ROPA | EPSCF | [24] |
| 574 | 574 | 4x10 | WDM-RZ-DPSK | 3rd Order Bi-RP + ROPA | ULL-LEAF | [18] |
| 601 | 601 | 1x10 | WDM-RZ-DPSK | 3rd Order Bi-RP + ROPA | ULL-LEAF | [18] |

***Table acronyms:***

*CRP: Cascade Pumping; DA: Discrete Amplification; DRA: Distributed Raman Amplification; EPSCF: Enhanced Pure Silica Core Fibre; MC: Multicore; MCF: Multicore Fibre; QL: Quasilossless; RA: Raman Amplification; R-EA: Raman EDFA Amplification; RFL: Raman Fibre Laser; ROPA: Remote Optical Pump Amplification; RP: Raman Pumping; RTP: Real Time Processing; TI: Time Interleaved; WTC: Wavelength Transparent Conjugation.*

** This configuration was tested as a strain sensor only, not as a communications system.*

*Table 5.1 – Summary of unrepeatered long-distance transmission experiments.*

Table 5.1 shows a summary of unrepeatered transmission results, while Table 5.2 shows a summary of results for repeatered transmission; both tables illustrate the usage of a range of different techniques. The inclusion of repeatered transmission results is to show a comparison with the lengths of unrepeatered systems, with the actual lengths of unrepeatered fibre sections used within repeatered systems.

| Un-repeatered Transmission Distance (km) | Total Transmission Distance (km) | Number of Channels and Data Rate (Gb/s) | Modulation Type | Transmission Technique | Fibre Types Used | Refs |
|---|---|---|---|---|---|---|
| 50 | 9000 | 80x100 | PDM-QPSK | EDFA | PSCF | [17] |
| 55 | 6160 | 40x128 | PDM-QPSK | MC-EDFA | 7-Core MCF | [94] |
| 80 | 7040 | 72x100 | PDM-QPSK | Hybrid R-EA + Coherent Rx | LEAF | [64] |
| 82 | 2500 | 1x43 | RZ-ASK | QL Span | SMF-28 | [31] |
| 100 | 100 | 1x640 | RZ-OOK | WTC | SSMF | [97] |
| 100 | 7200 | 16x112 | PM-QPSK | EDFA | ULL-LEAF | [61] |
| 100 | 11400 | 40x112 | PM-QPSK | Backward RA | ULL-LEAF | [61] |
| 200 | 6000 | 32x112 | PM-QPSK | Hybrid R-EA | ULL-LEAF | [61] |
| 200 | 1000 | 40x43 | NRZ-DPSK RZ-DQPSK | EDFA | ULL-SMF | [98] |

***Table acronyms:***

*CRP: Cascade Pumping; DA: Discrete Amplification; DRA: Distributed Raman Amplification; MC: Multicore; MCF: Multicore Fibre; PSCF: Pure Silica Core Fibre; QL: Quasilossless; RA: Raman Amplification; R-EA: Raman EDFA Amplification; RFL: Raman Fibre Laser; ROPA: Remote Optical Pump Amplification; RP: Raman Pumping; RTP: Real Time Processing; TI: Time Interleaved; WTC: Wavelength Transparent Conjugation.*

*Table 5.2 – Summary of repeatered long-distance transmission experiments with unrepeatered sections stated.*

The biggest advantage of using an ULRFL is the comparative flatness of the gain when compared to bi-directional 2$^{nd}$ order Raman pumping, since the cavity is the whole transmission medium rather than just a section. This limits the gain excursion and therefore the power profile is flatter over the transmission length. ULRFL were also used in [14, 15, 26, 27, 29, 31, 63].

Numerical modelling of Raman pumping, including 2$^{nd}$ and 3$^{rd}$ order, single and dual, including co and counter propagating, can be found in [28, 30. 35].

The most common technology currently used is EDFA, due to its ease of use within current systems, but on its own it is limited to repeatered systems, or short-haul (<100km) unrepeatered systems. Examples of their use in repeatered system are in [17, 94, 98].

A technology that is increasingly being used is Remote Optically Pumped Amplification (ROPA), which consists of a piece of fibre doped with a gain material such as Erbium, these are usually placed at the centre of the transmission span for ROPA only amplification, or placed near the end of the transmission span when ROPA is used with other amplification techniques, as this give a gain boost at the far end of the transmission span, examples of this are [20, 21, 22, 23, 25].

There are those systems which use a combination of EDFA and Raman amplification, such as in [59, 61], where the EDFA is used as a pre-amplifier prior to the Raman section. This aspect is different to their usage within the experiments in Section 3 of this thesis, where the EDFAs were used for balancing out the losses within the dispersion compensation sections. In [59] negative dispersion NZDSF fibre was included within the actual transmission span rather than within the transmitter or receiver sections as in Section 3. The EDFA and Raman Amplification combination could potentially make available a higher overall system OSNR, thus allowing longer transmission spans, with or without repetition. The unrepeatered transmission lengths were between 200-300km with OSNRs of 15.5dB (after 27x200km repeaters) and 27.5dB.

The majority of the longer transmission experiments use Raman pumping, although there are different configurations. These configurations are Forward Raman pumping, Backward Raman pumping and bi-directional Raman pumping.

The longest unrepeatered transmission span was identified as 601km in [18], this system used 3$^{rd}$ Order Bi-directional Raman Pumped Amplification (RPA) as well as ROPA situated 146km from the end of the transmission span, the transmission rate was at 10Gbps using RZ-DPSK modulation. This system also

used ULL-LEAF, which had an attenuation of 0.162dB/km, compared to normal SMF-28 whose attenuation is nominally 0.2dB/km. The Q-value averaged around 9.5dB.
If we compare with those results using special fibre types, we can see an improvement over standard SMF of up to 0.05dB, which can add up to a significant reduction in the system loss over hundreds of kilometres of fibre, this can also realise higher gain profiles when using Raman amplification techniques. The cost of replacing SMF-28 with speciality fibre would be a major undertaking in any current installation, which is why those techniques that can be implemented within current fibre stock are important, hence using Raman amplification, and specifically ULRFLs. The use of speciality fibres can be found in [18, 22, 24, 25, 57, 58, 59, 61, 64, 94].

The modulation type and the amount of channels used are also important, with phase based modulation, such as DPSK and QPSK, showing the best results, although this is balanced by the increase in complexity of the transmitter and receivers. The number of channels used can also have an impact as there is only so much gain available, which is why multi-bit transmission is important in WDM systems. The maximum number of channels used was 64 at 43Gbps for 468km unrepeatered transmission, and 80 at 100Gbps for repeatered transmission (50km unrepeatered length) [17, 25].

In Chapter 3 we used Raman amplification over the distances of 240km and 320km using ASK and DPSK modulation formats. We found that it was possible to receive signals over this distance with a good enough recovery, this would mean Forward Error Correction could be used in the receiver to further improve the received signals from the transmission system.

When looking at the 240km results, it was found the amount of dispersion present on channels 1 to 3 caused a significant reduction in the received signal quality of around 4dB, which is significant over very long distances and actually erased the expected improvement between ASK and DPSK. This problem could not be overcome due to the inability to optimally tune the dispersion compensation for all channels. A bandwidth of 30nm was used for these measurements, which is close to the total bandwidth of the C-band. 8-

channels were transmitted here with an average 500GHz separation, which means many more channels could be transmitted using the appropriate grid spacing.

For the experimental results at 320km, the bandwidth of the WDM channels was reduced to 11nm, giving a channel spacing of 200GHz. This reduction in bandwidth was because the Raman pump power required for a 30nm bandwidth was unachievable. The increase in the length of the span meant the gain spectrum was narrower, the consequence of which was that a much narrower channel bandwidth at the Ramen gain peak had to be used. Outside of the narrower bandwidth the OSNR was too low to achieve error-free transmission.
The actual measurements for the 320km span were fairly flat across the range with Q-Values only differing by 0.5dB (10-10.5dB) with an OSNR of 7dB. This significant reduction in OSNR when compared with the 240km experimental results, was caused not only by the extra 20dB loss due to the increase in fibre length, but also by nonlinear effects such as DRBS, which built up because the gain over the span was not enough to compensate for the significant degradation of the WDM channels. The Q-value measurements, however, were still beyond the 7% FEC limit.

The work in Chapter 3 using ULRFL has to be compared to other techniques used in long-haul systems. The alternative systems include the use of devices such as EDFAs, including hybrid Raman-EDFA configurations [21, 59, 61, 64, 98], and ROPAs [18, 19, 20, 21, 22, 23, 24, 25], some of which include the requirement to use specific fibre types, such as ultra-low loss (ULL) fibre and/or doped fibre (used in ROPAs) to achieve the improvement, rather than only using the already existing standard fibre systems.
The techniques installed in transmission systems are those which balance cost, compatibility with existing infrastructure, and which give the greatest improvement within the system. However, for new system installations ULRFLs are unlikely to be considered as systems using ROPAs and ULL fibres would be a significantly better choice due to the long term benefits. ULRFL may still be considered for current system installations, but only for long-haul systems

using higher loss fibre, although older short and medium-haul transmission spans could also gain some benefit.

It is clear from these results that there is still further work to be done at distances greater than 250km to improve the noise figures and reduce the significant degradation from nonlinear effects, such as DRBS, when transmitting over SMF-28 type fibres.

The second task was to see whether using filters within the transmission path could improve the received signal in a strongly filtered system, the results of which appear in Chapter 4.

To see whether the improvements predicted by previous simulation results or experimental work [32, 129, 130, 132, 133, 134, 135, 142, 143, 144, 145, 146, 147, 148, 149, 150, 151] were achievable, or repeatable, back-to-back measurements were taken using different configurations. These configurations consisted of the following: one filter only, two filters or three filters.
The various configurations were analogues of different types of tight optical filtering found in optical systems, and to show how, by offsetting filters at certain places within a system, a potential way to improve the received signal could be establish.

Pre-filtering was a simple example of strong filtering before the receiver, where a 35GHz filter bandwidth was used to try and match the type of narrow-band filtering seen when using channels within the 50GHz grid, whilst placing filters after the DLI, or "post-filtering", was an attempt to see how the outputs from the DLI, after demodulating a DPSK signal, could be used to improve received signals.

An amalgamation of "pre" and "post" filtering was used to confirm some simulated results [32, 132, 133, 134] and this showed that up to 5dB of improvement could be found.

The highest improvement using this setup was around 2.2dB, under half of the predicted value, although the results showed the model and the general theory behind the offset filtering effect could be confirmed.

Other configurations were also tried, such as two filters before the delay line interferometer, and a three filter setup which had one filter prior to the DLI and one filter on each output of the DLI (the constructive and destructive ports). In the first situation no improvement in the received signal was measured, whilst in the latter case there was also no improvement, but the results may fit with the simulation [32, 133] where only one filter was offset on the destructive port, however the model had both filters offset, which means both the experimental setup and the simulation need to be rechecked.

Additional experiments were carried out using a Waveshaper. This device was used for comparison purposes with the physical Santec filters used in the previous experiments. The Waveshaper was programmed to process the input signals as a DLI, and was also programmed with two "post" filters on each arm which allowed their bandwidth and frequency offsets to be independently altered. A physical "pre" filter was placed prior to the Waveshaper input.
The Waveshaper therefore permitted the emulation of the two filter configuration, one on each arm of the DLI "post" filtering, and the three filter configuration, this was the same as the two filter configuration mentioned but with the addition of a "pre" filter before the DLI.

The Waveshaper confirmed that offset filtering is viable using programmable devices to emulate physical filters; however it was found that the programmed filter shape did not closely match the filter shape of the original physical filters, which is an issue that will need more investigation.

For the offset filtering measurement using the Waveshaper, the greatest improvement was with 33%RZ-DPSK, of around 0.5dB, but no simulation was available for comparison.
For CSRZ-DPSK there is some potential for improvement, unfortunately the measurement resolution was too low for certainty, but it could be as high as 3dB-4dB with a 5GHz by 8GHz (Filter2 by Filter3) offset, as shown by the

simulation results. Only simulation results were available for 50%RZ-DPSK, these showed the potential for an improvement of 3dB to 4dB.
All of the Waveshaper measurements used a resolution of 5GHz, which was found to be too coarse; this suggests the experiments should be repeated at 1GHz resolution to seek experimental confirmation with the simulations.

It has been shown that offset filtering is a technique which should be looked into further, although these results were limited to back-to-back only. In general the majority of the results from simulations have been confirmed, where they have not, more work needs to be carried out to see if the issues are system related or inherent to the filters and/or configurations used.

Although we did not use the offset filtering technique over long distances, only back-to-back configuration were used, we ascertained that it was possible to simply enhance the signal and reduce the error count by increasing the measured Q-values by up to 2.2dB, and have succeeded in finding some simple configurations which could be used in the real world for a comparatively small additional cost. We also found that the use of programmable devices such as Waveshapers, to emulate DLI and filters, is a potential alternative and/or addition to physical filters.

Further work, which could not be completed in time for this thesis, included incorporating both the long-distance Raman amplification, with the offset filtering, in order to investigate the possibility of improvements in received signal quality in tightly filtered long-haul transmission systems.

It has been seen that for certain filtering regimes offset filtering could be a useful technique for increasing the quality of the received signal, especially at low powers. Further work, to utilise these techniques within long-haul transmission spans, should be carried out, to see whether there are any measurable improvements that could indicate a simple way to improve current systems.

Offset filtering has been shown to be an interesting effect, although it may not be 100% suitable for networks with a vast selection of cascaded devices or

those using long-haul transmissions due to the very narrow filtering that occurs, the use of devices such as Waveshapers may change this. However, offset filtering may be useful for short to medium haul systems and systems with some cascaded devices within a 50GHz grid. For systems with broad filtering (>1nm bandwidth) these techniques will not work.

In conclusion, it has been shown that both ultra-long Raman fibre lasers (ULRFL), and offset filtering, are interesting techniques which could be easily installed into current optical systems, giving a noteworthy improvement to systems which have suffered some degradation in signal quality over time. However, the findings for both techniques are somewhat limited to specific systems requirements, such as legacy systems that need to recover some of their original performance. In the near future there is some doubt that either technology would be utilised within brand new installations, although in the longer term, ULRFL is the more likely candidate to be considered due to its flexibility and potential.

# Publications

1. Murray, N.J. Olubodun, O.A. Harper, P. Doran, N.J. (2013). Performance Enhancement of Partial-42.7Gbps DPSK via an Asymmetrical Receiver Design. 15th International Conference of Transparent Optical Networks. Cartagena, Spain. 23rd-27th June 2013.

2. Olubodun, O.A. Murray, N.J. Harper, P. Doran, N.J. (2013). Performance Evaluation of Strongly Filtered Asymmetric 42.7Gbps Coherent 50% RZ-BPSK System. 15th International Conference of Transparent Optical Networks. Cartagena, Spain. 23rd-27th June 2013.

3. Olubodun, O.A. Murray, N.J. Harper, P. Doran, N.J. (2013). Performance Enhancement of Asymmetric Filtered 40Gb/s Carrier Suppressed Return to Zero Differential Phase Shift Keying Receiver in a 50GHz Grid. IET Optoelectronics Journal, vol. 7, issue. 1, February 2013. Pages 14-19.

4. Rosa, P. Harper, P. Murray N.J. Ania-Castañón, J.D. (2012). Unrepeatered 8 x 40Gb/s Transmission Over 320km SMF-28 Using Ultra-long Raman Fibre Laser Based Amplification.
   IN: European Conference on Optical Communications. 38th. Amsterdam 16-20 September 2012.

# Bibliography


1. Maiman, T.H. (1960). Stimulated Optical Radiation in Ruby. Nature, Vol. 187, No. 4736. Pages 493-494.

2. Nelson, D.F. Boyle, W.S. (1962) A Continuously Operating Ruby Optical Maser. Journal of Applied Optics. Vol. 1, Issue S1. Pages 99-101.

3. K.C. Kao. The Nobel Prize in Physics 2009. Nobel Foundation. 6th October 2009 [Online]. Available from: http://www.nobelprize.org/nobel_prizes/physics/laureates/2009/press.html [Accessed 24th February 2013].

4. Kao, K.C. Hockham, G.A. (1966). Dielectric-fiber surface waveguides for optical frequencies. Proceeding of the IEE. Vol. 113 No. 7. Pages 1151 to 1158.

5. Kapron, F.P. Keck, D.B. Maurer, R.D. (1970). Radiation Losses in Glass Optical Waveguides. Applied Physics Letters. Vol. 17, No. 10. Pages 423 to 425.

6. Corning LEAF Optical Fiber Production Information. (Dec 2012). Corning Inc. New York.

7. Li, M-J. Nolan, D.A.(2008). Optical Transmission Fiber Design Evolution. Journal of Lightwave Technology, Vol. 26, No. 9, May 1, 2008. Pages 1079 to 1092.

8. Corning SMF-28 ULL Optical Fibre. (2011). Corning Inc. New York.

9. Corning Vascade Optical Fibres Product Family. (2010). Corning Inc. New York.

10. Z-Fiber. (2010). Sumitomo Electric Lightwave Corp. North Carolina.

11. Mears, R. J. Reekie, L. Jauncey, I. M. Payne, D. N. (1987). Low-Noise Erbium-Doped Fibre Amplifier Operating at 1.54μm. Electronics Letters. Vol. 23 No. 19. Pages 1026 to 1028.

12. Raman, Sir C.V. The Nobel Prize in Physics 1930. Nobel Foundation. 10th December 1930 [Online]. Available from: http://www.nobelprize.org/nobel_prizes/physics/laureates/1930/press.html [Accessed 24th February 2013].

13. Landsberg, G.; Mandelstam, L. (1928). A new phenomenon in which light scatters in crystals (Eine neue Erscheinung bei der Lichtzerstreuung in Krystallen). Springer. The Science of Nature (Die Naturwissenschaften). Vol. 16, Issue 28. Pages 557 to 558.

14. Ania-Castanon, J.D. and Turitsyn, S.K. (2008) Unrepeatered Transmission Through Ultra-long Fibre Laser Cavities. Optics Communication. Issue 281. Pages 5760-5763.

15. Turitsyn, S.K. Ania-Castanon, J.D. Babin, S.A. et al. (2009). 270km Ultra-long Raman Fibre Laser. Physical Review Letters. Issue 103. Pages 133901-1 to 133901-3.

16. Yoneyama, K. Sakuyama, H. Hagisawa, A. (2010). Construction Technology for Use in Repeatered Transoceanic Optical Submarine Cable Systems. NEC Technical Journal. Vol. 5, No. 1. 2010. Pages 41 to 45.

17. Salsi, M. et al. (2010). 80×100-Gbit/s transmission over 9,000km using erbium-doped fibre repeaters only. European Conference on Optical Communications. 36th. Torino 19-23 September 2010.

18. Bissessur, H. Bousselet, P. Mongardien, D.A. and Brylski, L. (2010). Ultra-long 10Gb/s Unrepeatered WDM Transmission up to 601km. Optical Fiber Conference and National Fiber Optic Engineers Conference. San Diego 21-25 March 2010.

19. Puc, A. Chang, D. Pelouch, W. Perrier, P Krishnappa, D. Burtsev, S. (2009). Novel Design of Very Long High Capacity Unrepeatered Raman Links. European Conference on Optical Communications. 35th. Vienna 20-24 September 2009.

20. Bousselet, P. Bissessur, H. Lestrade, J. Salsi, M. Pierre, L. Mongardien, D. (2011). High Capacity (64x43Gb/s) Unrepeatered Transmission over 440km. Optical Fiber Conference and National Fiber Optic Engineers Conference. Los Angeles 6-10 March 2011.

21. Chang, D. Pelouch, W. McLaughlin, J. (2011). 8x120Gb/s Unrepeatered Transmission over 444km (76.6dB) using Distributed Raman Amplification and ROPA without Discrete Amplification. ECOC Technical Digest, paper Tu.3.8.2, 2011.

22. Bissessur, H. Bousselet, P. Mongardien, D. Boissy, G. Lestrade, J. (2011). 4x100Gb/s Unrepeatered Transmission over 462km Using Coherent PDM-QPSK Format and Real-Time Processing. ECOC Technical Digest, paper Tu.3.8.3, 2011.

23. Bakhshi, B. Richardson, L. and Golovchenko, E.A. (2009). Ultimate Capacity Limitations in Repeater-less WDM Transmission up to 505 km. Optical Fiber Conference and National Fiber Optic Engineers Conference. San Diego 22-26 March 2009.

24. Labrunie, L. et al. (2005). 4 X 10 Gb/s WDM Unrepeatered Transmission over 525 Km with Third-Order Cascaded Pumping. European Conference on Optical Communications. 31st. Glasgow 25th-30th September 2005.

25. Bousselet, P. Mongardien, D. Etienne, S. Bissessur, H. (2012). 64 x 43 Gb/s Unrepeatered Transmission over 468 km Using PDM-RZ BPSK with 33 GHz Spacing. OFC/NFOEC Technical Digest, paper OTu2A.5, 2012.

26. Rosa, P. Murray, N.J. Harper, P. and Ania-Castañón, J.D. (2012). Unrepeatered 8 x 40Gb/s Transmission Over 320km SMF-28 Using Ultra-long Raman Fibre Laser Based Amplification.
IN: European Conference on Optical Communications. 38th. Amsterdam 16-20 September 2012.

27. El-Taher, A.E. Ania-Castañón, J.D. Karalekas, V. Harper, P. (2009). High efficiency supercontinuum generation using ultra-long Raman fiber cavities. Optics Express, Vol. 17, No. 20, September 2009. Pages 17909 to 17915.

28. Tong, Z. Wei, H. Jian, S. (2004). Investigation and optimization of bidirectionally dual-order pumped distributed Raman amplifiers. Optics Express, Vol. 12, No. 9, May 2004. Pages 1794 to 1802.

29. Kunarajah, E.A. Rochat, E. Simeonidou, D. (2003). Distributed bi-directional fibre Raman amplifiers. Fiber-based Component Fabrication, Testing, and Connectorization. Editors: Pruneri, P. Dahlgren, R.P. Sanger, G.M. Proceedings of SPIE, Vol. 4943. Pages 91 to 99.

30. Ania-Castañón, J.D. (2004). Quasi-lossless transmission using second-order Raman amplification and fibre Bragg gratings. Optics Express. Vol. 12, No. 19. September 2004. Pages 4372 to 4377.

31. Barker, L. El-Taher, A.E. Alcon-Camas, M. Ania-Castanon, J-D. Harper, P. (2009). 42.6Gb/s RZ-ASK transmission over 2500km using quasi-Lossless transmission spans. IN: European Conference on Lasers and Electro-Optics 2009 and the European Quantum Electronics Conference. CLEO Europe - EQEC 2009. IEEE.

32. Olubodun, O. (2011). High Speed Optical Phase Modulated Signalling with Offset Filtering in a 50GHz Grid. PhD Thesis. Swansea: Swansea University.

33. Ramaswami, R. & Sivarajan K.N. (2002). Optical Networks: A practical perspective. San Francisco. Morgan Kaufmann Publishers.

34. Neilson, D.T. (2006). Photonics for Switching and Routing. IEEE Journal Of Selected Topics In Quantum Electronics. Vol. 12. Issue No. 4.

35. Gunning, F.C.G. et al (2012). All-Optical OFDM and Distributed Raman Amplification: Challenges to Enable High Capacities and Extend Reach. 14th International Conference on Transparent Optical Networks. Coventry 2-5 July 2012, paper We.B1.3.

36. Aoki, Y. et al. (2012). Next-Generation 100 Gb/s Undersea Optical Communications. IEEE Communications Magazine, February 2012. Pages S50 to S57.

37. Bhandare, S. Joshi, A. Becker, D. (2010). Optical Coherent Receiver With a Switchable Electrical Dispersion Compensator for 10 Gb/s DPSK Transmission up to 300 km of SSMF in Metro Optical Networks. Journal of Lightwave Technology, Vol. 28, No. 1, January 1, 2010. Pages 47 to 58.

38. OFS TrueWave REACH Low Water Peak (LWP) fiber. (2005). Furukawa Electric North America, Inc. USA.

39. OFS TrueWave RS Low Water Peak (LWP) Fiber. (2012). OFS FITEL, LLC. USA.

40. Keiser, G. (2000). Optical Fibre Communications. 3rd Edition. Singapore. McGraw-Hill Companies, Inc.

41. Single-Mode Fibers [online]. Available from: http://www.rp-photonics.com/single_mode_fibers.html [Accessed 18th February 2013].

42. Taylor, N and Grochocinski, J. (2002). The Impact of Fibre Effective Area on Systems using Raman Amplification. Corning Inc, New York.

43. PureAdvance® Single-Mode Fiber. (2012). Sumitomo Electric Lightwave Corp. North Carolina.

44. Kweon, G. (2002). Noise Figure of Optical Amplifiers. Journal of the Korean Physical Society. Vol. 41, No. 5. November 2002. Pages 617 to 628.

45. Agrawal, G.P. (2002). Fibre-optic Communication Systems. 3rd Edition. New York: John Wiley & Sons.

46. Bates, R.J. (2001). Optical Switching and Networking Hand Book. New York. McGraw-Hill Companies, Inc.

47. Raffaelli, C. et al. (2008). Photonics in Switching: Architectures, systems and enabling technologies. Computer Networks, 52, (2008), Pages 1873 to 1890 [online]. Available from: http://www.journals.elsevier.com/computer-networks [Accessed 18th February 2013].

48. Greenfield, D. (2002). The Essential Guide to Optical Networks. New Jersey. Prentice Hall PTR.

49. Kerr Effect [online]. Available from http://www.rp-photonics.com/kerr_effect.html [Accessed 28th October 2012].

50. ITU Grid Specification. BaySpec, Inc. [Online]. Available from: http://www.ece.queensu.ca/Current-Students/Undergraduate/Course-Homepages/ELEC-486/files/ITU-DWDM.pdf [Accessed 16th February 2013].

51. Winzer, P.J. Essiambre, R-J. (2006). Advanced Modulation Formats for High-Capacity Optical Transport Networks. Journal of Lightwave Technology. Vol. 24, No. 12. Pages 4711 to 4728.

52. Ho, K-P. (2005). Phase Modulated Optical Communication Systems. New York: Springer Science+Business Media LLC.

53. Haykin, S. (2001). Communication Systems. 4th Edition. New Jersey: John Wiley & Sons.

54. Gibson, J.D. Bhargava, V.K. Fair, I.J. (2002). The Communications Handbook: Chapter 13 - Forward Error Correction Coding. CRC Press. Boca Raton, Florida.

55. Forward Error Correction (FEC) [Online]. Available from: http://www.olson-technology.com/mr_fiber/FEC.htm [Accessed 6th March 2013].

56. Palais, J.C. (2005). Fibre Optic Communications. 5th Edition. New Jersey: Pearson Prentice Hall.

57. Du M., Yu, J. and Zhou, X. (2008). Unrepeatered Transmission of 107Gb/s RZ-DQPSK over 300km NZDSF with Bi-directional Raman Amplification. Optical Fiber Conference and National Fiber Optic Engineers Conference. San Diego 24-28 February 2008.

58. Xie, C. and Raybon, G. (2011). Unrepeatered Transmission over 300km NZDSF using 8x112Gb/s Time-Interleaved RZ-PDM-QPSK with Coherent Detection and Forward Raman Pumping. Optical Fiber Conference and National Fiber Optic Engineers Conference. Los Angeles 6-10 March 2011.

59. Karasek, M. Vojtech, J and Radil, J. (2010). Transmission of 20x10 GE Channels over 298km of NZ DSF with EDFA Assisted Bi-directional Raman Amplification. 12th International Conference on Transparent Optical Networks. Munich 27 June – 1 July 2010.

60. Bissessur, H. (2011). State of the Art in Non-repeatered Optical Transmission. ECOC Technical Digest, paper Tu.3.8.1, 2011.

61. Downie, J.D. (2012). 112 Gb/s PM-QPSK Transmission Systems With Reach Lengths Enabled By Optical Fibers With Ultra-Low Loss And Very Large Effective Area. Proceeds of SPIE 8284, Next-Generation Optical Communication: Components, Sub-Systems, and Systems, 828403.

62. Markow, A. (2005). Summary of Undersea Fiber Optic Network Technology and Systems. Terremark Worldwide, Inc. Miami, Florida. The David Ross Group, Inc. New Jersey.

63. Martins, H. Marques, M.B. Frazão, O. (2011). 300 km-ultralong Raman fiber lasers using a distributed mirror for sensing applications. Optics Express. Vol. 19, No. 19. September 2011.

64. Charlet, G. et al. (2009). 72x100Gb/s transmission over transoceanic distance, using large effective area fiber, hybrid Raman-Erbium amplification and coherent detection. Optical Fiber Conference and National Fiber Optic Engineers Conference. San Diego 22-26 March 2009.

65. Verly, G.P. (2002) Design of a Robust Thin-Film Interference Filter for Erbium-Doped Fiber Amplifier Gain Equalization. Applied Optics, Vol. 41, No. 16, 1 June 2002. Pages 3092 to 3096.

66. Ghoniemy, S. Mahmoud, S. (2007). Performance Optimization of Thin Film Optical Interference Filters For Optical Communication Systems. 2007 (1st) IEEE International Conference on Signal Processing and Communications (ICSPC 2007), 24-27 November 2007, Dubai, United Arab Emirates.

67. Segawa, T. (2008). High-Speed Wavelength-Tunable Optical Filter Using Cascaded Mach–Zehnder Interferometers With Apodized Sampled Gratings. IEEE Journal of Quantum Electronics, Vol. 44, No. 10, October 2008.

68. Ling, B et al. (2004). Acousto-optic Tunable Filters: Fundamentals and Applications as Applied to Chemical Analysis Techniques. Progress in Quantum Electronics, Issue 28 (2004), Pages 67 to 87.

69. Harumoto, M. Shigehara, M. Suganuma, H. (2002). Gain-Flattening Filter Using Long-Period Fiber Gratings. Journal Of Lightwave Technology, Vol. 20, No. 6, June 2002.

70. Au, J. Bardot, T. Bouslimani, Y. Hamam, H. (2006). Optical Fiber Components Obtained by Refraction Index Modulation and Geographical Formulation. IEEE Canadian Review, Spring 2006.

71. Optical Fibre Loss and Attenuation [online]. Available from: http://www.fiberoptics4sale.com/wordpress/optical-fiber-loss-and-attenuation/ [Accessed 15th February 2013].

72. Harper, P. (2012). Loss in Optical Fibre. Lecture notes, Aston University (unpublished).

73. Boyd, R.W. (2003). Nonlinear Optics. 2nd Edition. San Diego: Academic Press.

74. Harper, P. (2012). Dispersion in Optical Fibre. Lecture notes, Aston University (unpublished).

75. Corning SMF-28e Optical Fibre. (2007). Corning Inc. New York.

76. TrueWave RS Fiber. (1998). Lucent Technologies Inc. USA.

77. Thorlabs Dispersion Compensating Fiber - DCF-38. (2012). Thorlabs, USA.

78. Aston Institute of Photonic Technologies. (2013). DCF Summary, Laboratory Spreadsheet. Aston University (unpublished).

79. Barbieri, A. (2002). A Guide to Select Single Mode Fibers for Optical Communications Applications. San Jose, USA. Cisco Systems, Inc.

80. Cisco Systems. (2008). Fiber Types in Gigabit Optical Communications – White Paper. Cisco Systems, Inc.

81. Aston University, Aston Institute of Photonic Technologies, database from photonics laboratory, 2010.

82. Singer, A.C. Shanbhag, N.R. Bae, H-M. (2008). Electronic Dispersion Compensation - An overview of optical communications systems. IEEE Signal Processing Magazine. November 2008. Pages 110 to 130.

83. Agrawal, G.P. and Qin, L. (2004). Effects of Polarization-Mode Dispersion on Cross-Phase Modulation in Dispersion-Managed Wavelength-Division-Multiplexed Systems. Journal of Lightwave Technology. Vol. 22. Issue No. 4. Page 977-987.

84. Corning Engineering Services Department. (10th February 2009). OTDR Testing Basics. Applications Engineering Note 134, Revision Issue. Hickory, North Carolina. Corning Cable Systems LLC.

85. Black, U. (2002). Optical Networks: Third Generation Transport Systems. New Jersey. Prentice Hall PTR.

86. Self-Phase Modulation [online]. Available from: http://www.rp-photonics.com/self_phase_modulation.html [Accessed 28th October 2012].

87. Neilson, D.T. (2006). Photonics for Switching and Routing. IEEE Journal of Selected Topics in Quantum Electronics. Vol. 12. Issue No. 4.

88. Tricker, R. (2002). Optoelectronics and Fibre Optic Technology. Oxford. Newnes.

89. Cross-Phase Modulation [online]. Available from: http://www.rp-photonics.com/cross_phase_modulation.html [Accessed 28th October 2012].

90. Hunter, D.K. (2005). Delay-Line Storage in Optical Communications Switching. ECOC 2005 Proceedings. Vol. 5. Symposium Mo 4.1.2.

91. Four Wave Mixing [online]. http://www.rp-photonics.com/four_wave_mixing.html [Accessed 29th October 2012].

92. Melloni, A. Frasca, M. Garavaglia, A. Tonini, A. Martinelli M. 1998. Direct measurement of electrostriction in optical fibers. Optics Letters. Vol. 23, No. 9, May 1998. Pages 691 to 693.

93. Thevenaz, L. Kueng, A. Nikles, M. Robert, P. 1998. Electrostrictive Non-linearity in Optical Fibre deduced from Brillouin gain Measurements. OFC '98 Optical Fiber Communication Conference and Exhibit. Technical Digest Conference Edition 1998 OSA Technical Digest Series. Vol.2, San Jose, CA, USA, February 22, 1998. Pages 253 to 254.

94. Takahashi, H. et al. (2013). First demonstration of MC-EDFA-repeatered SDM transmission of 40 x 128-Gbit/s PDM-QPSK signals per core over 6,160-km 7-core MCF. Optics Express, Vol. 21, No. 1, 14 January 2013. Pages 789 to 795.

95. Yamazaki, E. et al. (2011). Mitigation of Nonlinearities in Optical Transmission Systems. Optical Fiber Conference and National Fiber Optic Engineers Conference. Los Angeles 6-10 March 2011. Paper OThF1.

96. Rashed, A. N. Z. (2012). Transmission Capacity Improvement of Ultra Wide Wavelength Division Multiplexing (UV-WDM) Submarine Fiber Cable Systems for Long Haul Depths. International Journal of Advanced Research in Computer Science and Electronics Engineering (IJARCSEE) Volume 1, Issue 10, December 2012. Pages 9 to 17.

97. Huo, B.P.P. etal. (2011). Transmission of 640Gbps RZ-OOK Channel over 100km SSMF by Wavelength Transparent Conjugation. Journal of Lightwave Technology. Vol. 29, No. 4. February 2011. Pages 516 to 523.

98. Gleeson, L.M. (2010). 43Gbit/s NRZ-DPSK and RZ-DQPSK transmission over 1000km of G.652 ultra-low-loss fibre with 200km amplifier spans. Optical Fiber Conference and National Fiber Optic Engineers Conference. San Diego 21-25 March 2010.

99. Alcon Camas, M. (2011). Applications of Ultra-long Raman fibre lasers in photonics. PhD Thesis. Birmingham: Aston University.

100. Headley, C. and Agrawal, G.P. (2005). Raman Amplification in Fiber Optical Communication Systems. London: Elsevier Academic Press.

101. Kobtsev, S.M. Pustovskikh, A.A. (2003). Gain-Flattened Wideband Raman Amplifier with Broad-Linewidth Pumps approximating Continuous-Spectrum Pump. 5th Pacific Rim Conference on Lasers and Electro-Optics. CLEO/Pacific Rim. 15-19 December 2003.

102. Headley, C. and Agrawal, G.P. (2005). Raman Amplification in Fiber Optical Communication Systems. Oxford: Elsevier Academic Press.

103. Islam, M.N. (2004). Raman Amplifiers for Telecommunications: Physical principles, Volume 1. New York. Springer-Verlag New York Inc.

104. Intensity Noise [online] http://www.rp-photonics.com/intensity_noise.html [Accessed 27th January 2014].

105. Fludger, C.R.S. Handerek, V. Mears, R.J. (2001). Pump to Signal RIN Transfer in Raman Fiber Amplifiers. Journal of Lightwave Technology, Vol. 19, No. 8, August 2001.

106. Pakarzadeh, H. Zakery, A. (2011). Numerical modelling of the pump-to-signal relative intensity noise transfer in two-pump fibre optical parametric amplifiers. Pramana – Journal of Physics. Vol. 77, No. 4. October 2011.

107. Bristiel, B. Jiang, S. Gallion, P. Pincemin, E. (2006). New model of noise Figure and RIN transfer in fiber Raman amplifiers. IEEE Photonics Technology Letters, Vol. 18, No. 8, April 15 2006.

108. Keita, K. Delaye, P. Frey, R. Roosen, G. (2006). Relative intensity noise transfer of large-bandwidth pump lasers in Raman fiber amplifiers. Journal of the Optical Society of America, B, Vol. 23, No. 12, December 2006.

109. Alcón-Camas, M. Ania-Castañón, J.D. (2012). RIN transfer in 2nd-order distributed amplification with ultralong fiber lasers. Optics Express, Vol. 18, No. 23, November 2010. Pages 23569 to 23575.

110. Alcón-Camas, M. Ania-Castañón, J.D. (2010). Relative intensity noise transfer in high-order distributed amplification through ultra-long fiber cavities. Photonics North 2010. Proceedings of SPIE, Vol. 7750. Pages 775017-1 to 775017-8.

111. Spiegelberg, C. Geng, J. Hu, Y. Kaneda, Y. Jiang, S. (2004). Low-Noise Narrow-Linewidth Fiber Laser at 1550nm. Journal of Lightwave Technology, Vol. 22, No. 1, January 2004.

112. Zhao, Y.J. Wang, Q.P. Chang, J. Ni, J.S. Wang, C. Sun, Z.H. Wang, P.P. Lv, G.P. Peng, G.D. (2012). Suppression of the intensity noise in distributed feedback fiber laser by self-injection locking. Laser Physics Letters 9, No. 10, 739–743.

113. Yeh, C.-H. Chow, C.-W. Pan, C.-L. (2011). Utilizing erbium fiber ring scheme and Fabry-Perot laser diode for stable and wavelength-tunable laser in single-longitudinal-mode output. Laser Physics Letters 8, No. 2, 130–133.

114. Csörnyei, M. Berceli, T. Marozsák, T. (2005). All-optical intensity noise suppression for solid-state and semiconductor lasers. Journal of Telecommunications and Information Technology, February 2005.

115. Mermelstein, M. D. Brar, K. Headley C. (2003). RIN Transfer Suppression Technique for Dual-Order Raman Pumping Schemes. IEEE Photonics Technology Letters, Vol. 15, No. 10, October 2003.

116. Krause, M. Renner, H. (2004). Double-cavity Raman fibre lasers with suppressed pump-to-Stokes transfer of low-frequency RIN. Electronics Letters 27th May 2004 Vol. 40 No. 11.

117. Sun, G. (2005). Output-power-clamped Raman fibre laser with suppression of low-frequency RIN transfer from pump sources. Electronics Letters 14th April 2005 Vol. 41 No. 8.

118. Zhou, Y. Sun, G. (2011). Suppression of pump-to-Stokes relative intensity noise transfer in Raman fiber laser by injection of modulated signal. Optik - International Journal for Light and Electron Optics Vol. 122, Issue 14, July 2011, Pages 1219–1221.

119. A. Yariv, H. Blauvelt, and S.-W. Wu. (1992). A reduction of interferometric phase-to-intensity conversion noise in fiber links by large index phase modulation of the optical beam. Journal of Lightwave Technology, Vol. 10, No. 7, Pages 978–981, Jul. 1992.

120. Nelson, C. W.. Hati, A. Howe, D. A. (2008). Relative Intensity Noise Suppression for RF Photonic Links. IEEE Photonics Technology Letters, Vol. 20, No. 18, September 15, 2008.

121. Zhao, M. Morthier, G. Baets,R. (2002). Analysis and Optimization of Intensity Noise Reduction in Spectrum-Sliced WDM Systems Using a Saturated Semiconductor Optical Amplifier. IEEE Photonics Technology Letters, Vol. 14, No. 3, March 2002.

122. Yamatoya, T. Koyama, F. Iga, K. (2000) Noise suppression and intensity modulation using gain-saturated semiconductor optical amplifier. Technical Digest of Integrated Photonics Research 2000, Canada, Pages 72–74.

123. Kim, S-J. Han, J-H. Lee, J-S. Park, C-S. (1999). Suppression of intensity noise in 10Gbit/s spectrum-sliced incoherent light channel using gain-saturated semiconductor optical Amplifiers. Electronics Letters 10th June 1999 Vol. 35 No. 12.

124. Pedersen, R. J. S. Ebskamp, F. (1993). New All-Optical RIN Suppressing Image Rejection Receiver with Efficient Use of LO and Signal Power. IEEE Photonics Technology Letters, Vol. 5, No. 12, December 1993.

125. Espindola, R.P. Bacher, K.L. Kojima, K. Chand, N. Srinivasan, S. Cho, G.C. Jin, E. Fuchs, C. Milner, V. Dautremont-Smith, W.C. (2002). Penalty-free 10 Gbit/s single-channel co-pumped distributed Raman amplification using low RIN 14xx nm DFB pump. Electronics Letters 31st January 2002, Vol. 38, No. 3, Pages 113-115.

126. Barker, L. (2011). Dispersion Management of Optical Transmission Systems. PhD Thesis. Birmingham: Aston University.

127. TeraXion Compact Tuneable Dispersion Compensation Module (CTDCM). (2011) Data Sheet: SPEC-007-201107-2.0. TeraXion, Inc.

128. Tsuritani, T. Agata, A. Morita, I. Tanaka, K. Edagawa, N. (2001). Performance comparison between DSB and VSB signals in 20 Gbit/s-based ultra-long-haul WDM systems. Optical Fiber Communication Conference. Anaheim, CA, USA. 17-22 March 2001. Paper MM5.

129. Lefrançois, M. Houndonougbo, F. Fauconnier, T. Charlet, G. Bigo, S. (2007). Cross comparison of the nonlinear impairments caused by 10Gbit/s neighboring channels on a 40Gbit/s channel modulated with various formats, and over various fiber types. Optical Fiber Conference and National Fiber Optic Engineers Conference. Anaheim, CA, USA. 25-29 March 2007. Paper JThA44.

130. Yan, L-S. Wang, Y. Zhang, B. Yu, C. McGeehan, J. Paraschis, L. Willner, A.E. (2005). Reach extension in 10-Gb/s directly modulated transmission systems using asymmetric and narrowband optical filtering. Optics Express, Vol. 13, No. 13, 27 June 2005. Pages 5106 to 5115.

131. Yan, L-S. Yu, C. Wang, Y. Lo, T. Paraschis, L. Shi, Y. Willner, A.E. (2005). 40-Gb/s Transmission Over 25 km of Negative-Dispersion Fiber Using Asymmetric Narrow-Band Filtering of a Commercial Directly Modulated DFB Laser. IEEE Photonics Technology Letters, Vol. 17, No. 6, June 2005. Pages 1322 to 1324.

132. Olubodun, O. Doran, N. (2011). Characterization of asymmetric filtered 40 Gb/s RZ-DPSK system-strong filtering considerations. Elsevier. Optics Communications 284. Pages 5259 to 5262.

133. Olubodun, O. Doran, N. (2011). Performance Improvement of Asymmetrical Filtered 40GB/s RZ-DPSK Receiver Design - Strong Filtering Considerations. 16th European Conference on Networks and Optical Communications. Newcastle-upon-Tyne. 20th-22nd July 2011.

134. Olubodun, O.A. Murray, N.J. Harper, P. Doran, N.J. (2013). Performance Enhancement of Asymmetric Filtered 40Gb/s Carrier Suppressed Return to Zero Differential Phase Shift Keying Receiver in a 50GHz Grid. IET Optoelectronics Journal, vol. 7, issue. 1, February 2013. Pages 14-19.

135. Lyubomirsky, I. Qui, T. Roman, J. Nayfeh, M. Frankel, M.Y. Taylor, M.G. (2003). Interplay of Fiber Nonlinearity and Optical Filtering in Ultradense WDM. IEEE Photonics Technology Letters, Vol. 15, No. 1, January 2003. Pages 147 to 149.

136. AOTF and AOTF-DUAL systems - Acousto-Optic Tunable Filter systems for Fianium supercontinuum sources. Data sheet v1.2. Fianium UK Ltd.

137. Acousto-Optic Modulators [Online]. Available at: http://www.rp-photonics.com/acousto_optic_modulators.html [Accessed 15th March 2013].

138. Song, G.H. (1994). Theory of symmetry in optical filter responses. Journal of the Optical Society of America A, Vol. 11, No. 7, July 1994. Pages 2027 to 2037.

139. Finisar, (2008), White Paper - Programmable narrow-band filtering using the WaveShaper 1000E and WaveShaper 4000E , Finisair Corporation.

140. Santec OTF-950 Wavelength & Bandwidth Tunable Filter v1.6. (2007). Santec Optical Instruments, Santec Corporation, Japan.

141. Binh, L.N. Huynh, T.L. Lam, H.Q. 2006. Optical filtering effects in hybrid 40Gbps and 10Gbps DPSK DWDM long-haul optical transmission. Optical Transmission, Switching, and Subsystems IV, Proc. of SPIE Vol. 6353, Pages 635318-1 to 635318-11.

142. Winzer, P.J. Chandrasekhar, S. Kim, H. (2003). Impact of Filtering on RZ-DPSK Reception. IEEE Photonics Technology Letters. Vol. 15, No. 6. June 2003.

143. Tanaka, K. Morita, I. Edagawa, N. (2001). Study on Optimum Pre-filtering condition for 42.7Gbps CSRZ-DPSK signal. Optical Fibre Communication Conference. Los Angeles, CA, USA. 23-27 February 2004. Paper TuF2.

144. Zhu, Y. Hadjifotiou, A. (2004). Nonlinear tolerance benefit of modified-CSRZ DPSK modulation format. Electronics Letters, Vol. 40, No. 14, 8th July 2004.

145. Morita, I. Agata, A. Edagawa, N. (2003). Study on optimum optical pre-filtering condition for highly spectral-efficient ultralong-haul transmission using 40Gbit/s CS-RZ signal and all-Raman repeaters. Optical Fibre Communication Conference. Atlanta, GA, USA. 23-28 March 2003. Paper FE4.

146. Strasser, M.M. Pfennigbauer, M. Pauer, M. Winzer, P.J. (2001). Experimental verification of optimum filter bandwidths in direct-detection (N)RZ receivers limited by optical noise. San Diego, USA. The 14th Annual Meeting of the IEEE. Lasers and Electro-Optics Society (LEOS). $12^{th}$-$13^{th}$ November 2001. Paper W K5.

147. Winzer, P.J. Pfennigbauer, M. Strasser, M.M. Leeb, W.R. (2001). Optimum Filter Bandwidths for Optically Preamplified NRZ Receivers. Journal of Lightwave Technology. Vol. 19, No. 9. September 2001. Pages 1263 to 1273.

148. Zong, L. Veselka, J. Sardesai, H. Frankel, M. (2009). Influence of Filter Shape and Bandwidth on 44 Gb/s DQPSK Systems. JWA17. Optical Fiber Conference and National Fiber Optic Engineers Conference. San Diego. 22-26 March 2009.

149. Malouin, C. Bennike, J. Schmidt, T.J. (2007). Differential Phase-Shift Keying Receiver Design Applied to Strong Optical Filtering. Journal of Lightwave Technology. Vol. 25, No. 11. November 2007.

150. Roudast, I. Antoniadesl, N. Wagnert, R.E. Habibyt, S.F. Stern, T.E. (1997). Influence of filtered ASE noise and optical filter shape on the performance of a WADM cascade. ECOC 97,22-25 September 1997, Conference Publication No. 448. Pages 143 to 146.

151. Lizé, Y.K. Christen, L. Wu, X. Yang, J-Y. Nuccio, S. Wu, T. Willner, A.E. Kashyap, R. (2007). Free spectral range optimization of return-to-zero differential phase shift keyed demodulation in the presence of chromatic dispersion. Optics Express. Vol. 15, No. 11. May 2007. Pages 6817 to 6822.